U.PORTO

FEUP FACULDADE DE ENGENHARIA
UNIVERSIDADE DO PORTO

Optimization and Control of TMB, SMB and SMBR units

Dissertation presented to the
Faculty of Engineering of the University of Porto
for the degree of Doctor in Chemical and Biological Engineering

by

Idelfonso Bessa dos Reis Nogueira

Supervisor

Doctor Ana Mafalda Ribeiro
Prof. José Miguel Loureiro

SRE CM *ASSOCIATE LABORATORY*
LABORATORY OF SEPARATION AND REACTION ENGINEERING
LABORATORY OF CATALYSIS AND MATERIALS

Laboratory of Reaction and Separation Engineering
Department of Chemical Engineering
Faculty of Engineering of the Univerisity of Porto
Porto, Portugal

June 2018

Abstract

The general objective of this thesis is to study the dynamics of True Moving Bed (TMB), Simulated Moving Bed (SMB) and True Moving Bed Reactor (TMBR) while addressing the inherent problems of those units due their dynamics with application of a TMBR for the synthesis of n-Propyl Propionate. The first two processes are characterized by being able to promote continuous separation of complex mixtures, such as chiral compounds. The last one, as a further development of the first two, is characterized by being able to promote reaction and separation simultaneously and continuously.

Due to the complex dynamics of those units, a series of problems are found in this field, such as process control, inference of their main properties, units design and optimization. In this way, in the present thesis, first a method based on Gram-Schmidt Orthogonalization to analyze the impact of the operating variables in the dynamic response of a TMB unit was proposed, concomitantly with a characterization of the dynamic system behavior. The results showed that the recycling flow rate is the operating variable with the greatest impact for a TMB used to separate bi-naphthol enantiomers. The step perturbation analysis showed the consistency of the proposed method and that some process variables perturbations result in a system inverse response for the recovery performance indicator.

Then, the orthogonalization method was applied to two SMB units, with four and eight columns, and an analysis of the transient behavior of the units was done. The results were compared with the ones obtained for a TMB unit. The results show that the TMB/SMB equivalence is valid only

for conditions that do not violate the regeneration/separation regions and that the transient behavior of the four columns SMB can resemble more the TMB.

Then, the control problem of a TMB unit was addressed, through the development of a novel strategy to identify transfer functions of TMB/SMB and its application on classical linear model predictive controllers (MPC). Therefore, it was proposed a modification in the MPC prediction, that consists in a strategy based on a switching system where the most adequate transfer function is employed in the controller to overcome the problems related with the process dynamic behaviour. The results show that the used methodology enables the easy identification of transfer functions at the process optimal operating point and that the MPC can control the process in both the servo and regulator problem cases. It is also showed that the transfer function identified can be applied in the control of a SMB unit with four columns, under its optimal conditions.

The inference problem was addressed by the development of a system composed by two Artificial Neural Networks working concomitantly with an offline measurement, named Quasi-Virtual Analyser (Q-VOA) system. The development of the Q-VOA was presented and the system was simulated in order to evaluate its efficiency. The results showed that the Q-VOA is capable of reducing the system errors and keep the prediction closer to the process true responses, when compared with the simple VOA system, which is based solely on model predictions. Furthermore, the results showed the efficiency of the measurement system even under the presence of non-measured perturbations.

For the design and optimization of TMB units a novel improved Self-Organizing Hierarchical Particle Swarm Optimization with Time-Varying Acceleration Coefficients with Mutable Searching Region (HPSO-TVAC-MSR) was proposed together with an adapted method to define the operating variables confidence region. This methodology presented better results when compared with the traditional method, the Triangle Theory. The main advantage of the proposed methodology is the possibility to track the possible operating regimes of the unit while meeting a given requirement.

The next step of this thesis had the focus on the production of the n-Propyl Propionate in a TMBR unit. Therefore, a series of experimental studies of the ProPro reaction system separation in a chromatographic fixed bed unit packed with Amberlyst 46 were performed. The adsorption equilibrium isotherms and the corresponding Langmuir model parameters were determined. A phenomenological model to represent the process was developed and validated through the experimental data. Meanwhile, it was proposed the characterization of the uncertainties of all steps and its extension to the model prediction. The results showed that the model predicted with precision the breakthrough experiments. Furthermore, the uncertainty evaluation was an important tool allowing the parameters estimation and model validation to be done with a low number of experiments while leading to high precision predictions.

Then, it was proposed the study of the production of n-Propyl Propionate in a Fixed Bed Adsorptive Reactor, with the development of a phenomenological model to represent this process and its validation through laboratory experiments in a lab-scale unit. The results showed

that the model was able to predict with precision the Fixed Bed Reactor experimental data. Paving the way to the development of a TMBR unit for the synthesis of the ProPro.

Finally, it was investigated a novel route of synthesis of n-Propyl Propionate through a TMBR unit packed with Amberlyst 46 resin with the application of the HPSO-TVAC-MSR to the TMBR unit design and optimization. The results demonstrated that the unit is capable of producing n-Propyl Propionate with high purity and conversion, over 99%. Furthermore, the productivity associated with low eluent consumption and operation at significant low temperature provide evidence that the SMBR may be an efficient and competitive route for the production of n-Propyl Propionate. It was also demonstrated that the swarm optimization may be a powerful tool which can simultaneously provide deep information about the TMBR operating regions.

Resumo

O objetivo geral desta tese é o estudo da dinâmica das unidades de Leito Móvel Real (TMB), Leito Móvel Simulado (SMB) e Reator de Leito Móvel Real (TMBR), abordando simultaneamente os problemas inerentes a estas unidades, devidos aos seus complexos comportamentos dinâmicos, e a aplicação de uma unidade TMBR para a síntese de n-Propil Propionato. Os dois primeiros processos citados são caracterizados por possibilitar a separação de misturas complexas em contínuo, como por exemplo a separação de compostos quirais. A última unidade, sendo desenvolvida a partir das duas primeiras, é caracterizada por promover reação e separação em simultâneo e em contínuo.

Devido à dinâmica complexa destas unidades, são encontrados neste campo uma série de problemas, como por exemplo o controlo do processo, a inferência das principais propriedades, o projeto e a otimização da unidade. Desta forma, na presente tese, primeiro foi proposto um método baseado na ortogonalização de Gram-Schmidt para analisar o impacto das variáveis operacionais na resposta dinâmica de uma unidade TMB, e ao mesmo tempo foi feita uma caracterização do comportamento dinâmico deste sistema. Os resultados demostraram que o caudal de reciclagem é a variável operacional com maior impacto num TMB usado para separar os enantiómeros do bi-naftol. Através de uma análise de resposta a perturbações foi possível demonstrar a consistência do método proposto e que algumas das variáveis do processo levam a uma resposta inversa nas recuperações da unidade.

Assim, o método da ortogonalização foi aplicado para a análise de duas unidades SMB, uma com oito e outra com quatro colunas, tendo sido feita também uma análise do comportamento transiente das unidades. Os resultados foram comparados com os obtidos para o caso do TMB. Foi possível observar que a equivalência TMB/SMB é válida apenas em condições em que as regiões de separação/regeneração não são violadas. Além disso, em casos específicos, o comportamento transiente do SMB com quatro colunas pode assemelhar-se mais com o do TMB.

Desta forma, estudou-se o problema do controlo das unidades TMB, propondo-se uma nova estratégia para identificar funções de transferência e aplicá-las numa estratégia de controlo preditivo baseado em modelos (MPC). Além disto, propõe-se uma modificação na forma de predição do MPC, a qual consiste num sistema de seleção em que a função de transferência mais adequada é empregada na predição do controlador de modo a superar os problemas relacionadas com a dinâmica do processo. Os resultados demonstraram que o uso desta metodologia possibilita a fácil identificação das funções de transferência que representam o processo no seu ponto ótimo de operação, e que o MPC consegue controlar com eficiência o processo em regimes servo e regulatório. Foi também demonstrado que a estratégia de identificação das funções de transferência pode ser aplicada no controlo de unidades SMB de quatro colunas dentro das suas condições ótimas.

Estudou-se o problema da inferência através da proposta de um sistema composto por duas redes neuronais artificiais trabalhando concomitantemente com medições laboratoriais, nomeado como Analisador Quasi-Virtual (Q-VOA). Apresenta-se o desenvolvimento do Q-VOA e o sistema proposto foi simulado de modo a verificar a sua eficiência. Os resultados

demonstraram que o Q-VOA é capaz de reduzir os erros de predição e manter a previsão próxima das respostas reais do processo, apresentando melhor desempenho que os analisadores virtuais, os quais são baseados apenas em predições. Além disto, os resultados demonstraram a eficiência do Sistema mesmo perante perturbações não medidas.

Para o projeto e otimização de unidades TMB, propõe-se um novo algoritmo de Otimização por Enxames de Partículas, Hierárquico e Auto-Organizado, com Coeficientes de Aceleração Variáveis e Regiões de Busca Mutáveis (HPSO-TVAC-MSR), juntamente com uma adaptação de um método estatístico para definição de regiões de confiança. Esta metodologia apresentou melhores resultados que o método tradicionalmente usado na literatura, a Teoria do Triângulo. A principal vantagem desta proposta é a possibilidade de rastrear os possíveis regimes de operação da unidade que satisfazem um determinado requisito.

O passo seguinte da presente tese teve o foco na produção do n-Propil Propionato numa unidade TMBR. Desta forma, foi feita uma série de estudos experimentais sobre a separação dos compostos do sistema de reação de síntese do n-Propil Propionato numa coluna cromatográfica de leito fixo empacotada com a resina Amberlyst-46. Determinaram-se as isotérmicas de equilíbrio de adsorção e os correspondentes parâmetros do modelo de Langmuir. Desenvolveu-se um modelo fenomenológico para representar o processo, que foi validado com dados experimentais. Foi também aplicado um método para avaliação das incertezas de todos os passos, e sua propagação, para as previsões do modelo. Os resultados demonstraram que o modelo consegue prever com precisão as experiências de curvas de quebra. Além disto, a

avaliação das incertezas possibilitou a estimativa dos parâmetros e a validação do modelo através de um número reduzido de experiências.

De seguida, a síntese do n-Propil Propionato foi estudada experimentalmente num reator de leito fixo. Foi também desenvolvido um modelo fenomenológico para representar este sistema. Os resultados demonstraram que o modelo apresentado foi capaz de prever com precisão os resultados experimentais, abrindo caminho para o desenvolvimento de uma unidade TMBR para a produção do n-Propil Propionato.

Finalmente, investigou-se a produção do n-Propil Propionato usando uma unidade TMBR empacotada com resina Amberlyst 46. O HPSO-TVAC-MSR, desenvolvido anteriormente neste trabalho, foi aplicado para o projeto e otimização da unidade TMBR. Os resultados demonstraram que a unidade TMBR é capaz de produzir n-Propil Propionato com elevadas pureza e conversão, acima de 99%. Além disto, a produtividade obtida, associada com o baixo consumo de eluente e com a operação a baixas temperaturas, são evidências de que o SMBR pode ser um processo eficiente e competitivo para a produção do n-Propil Propionato. Demonstrou-se também que o HPSO-TVAC-MSR é uma ferramenta poderosa para o desenho do processo, podendo providenciar simultaneamente informação relativa às regiões de operação.

Acknowledgments

Dear Reader, regardless of the reason that brought you here, I would like to thank you; otherwise, without someone to read it, this work would not have a purpose to exist. I hope that you will find something interesting for you here.

Before you start reading this work, I would like to tell you some small and personal words. You may find in the cover of this thesis my name as author; however, I do not know of any work done exclusively by one hand, and in the specific case of this one, many hands contributed. Hands, that gave me opportunities, guidance, freedom of choice, support, correcting my mistakes and showing where I can improve. If you, dear Reader, find some value in this work, it is due to them. About me, I can say that I made my best to correspond to their trust and effort and therefore, if this work does not present the best that it could be, or if you find some mistake here, I can say to you that only my hands are responsible for that.

Thus, I would like to make it clear and recognize the work of everyone who directly or indirectly contributed to this thesis. However, my words are limited, in order not to make this section exhaustive. Then, I must cite here Professor José Miguel Loureiro, who is the author of the idea here developed, and without whom this work would not exist. I have to thank him for being always available as a friend and advisor; Dra. Ana Mafalda Ribeiro the basis of everything that was done here; from the simplest equation to the most complex result there is her tireless effort to make this thesis better; as a mother, she stood there until the end helping me; and Professor Alírio Rodrigues, who followed this work since the beginning, giving his opinion and friendly

advices. It was not a lonely walk, since there were many people who gave their own contribution. Finally, many things that were done here have as basis my previous master dissertation. Thus, I would like to thank Professor Karen Valverde Pontes, Professor Márcio Martins and my colleagues from the Industrial Engineering Graduate Program - Federal University of Bahia who taught me much of the knowledge that you will find here.

Many institutions contributed for the development of this thesis; I should express my gratitude to the Laboratory of Separation and Reaction Engineering in which all the steps here presented were taken, as well as for the Department of Chemical Engineering and Faculty of Engineering of the University of Porto. Part of this work received also the support of the department of Automation and Hydraulics of the Tampere University of Technology represented by Professor Hannu Koivisto, for which I would like also to leave my personal acknowledgment.

If previously I mentioned the intellectual and physical support of this work, I cannot forget to say that this work was financially supported by the Brazilian society represented by the National Council for Scientific and Technological Development (CNPq) under the grant nº 200667/2014-9 of the program Science without Borders. To the Brazilian society, I own part of my graduation and to it I hope that my career will contribute. This work was also financially supported by: Project POCI-01-0145-FEDER-006984 – Associate Laboratory LSRE-LCM funded by FEDER through COMPETE2020 - Programa Operacional Competitividade e Internacionalização (POCI) – and by national funds through FCT - Fundação para a Ciência e a Tecnologia; Finnish Foundation for Technology Promotion (Tekniikan Edistämissäätiö), EDUFI Fellowships programme.

I cannot finish this section without telling you that without the support of my family and my friends it would have not been possible for me to start or finish this work. To my friends, thank you very much, in special Maria João Regufe, Micael Morais and Lasalete Piedade, they were always there when I needed. To my family, I am thankful for all the support they gave me until now, I had the privilege of having three mothers in my life, Ildeci, Ivana and Iracy and even though very far from them, here I am reflecting their dedication to me. I should thank also two little persons who gave me strength to keep on, Isabel, my goddaughter, and Ismael, my brother. And finally, Ellinoora, my wife, who was patient and supporting throughout all the troubles associated with the last steps of a PhD. I cannot go further in this section, even though I would have enough material for another 300 pages, but if you are here until the end of this personal divagation, I have to thank you again, thank you very much.

Contents

Introduction.. 1

Part 1 – TMB and SMB systems analysis and methods development 11

P1-1. Introduction 13

P1-1.1. Processes Dynamics 13

P1-1.2. Processes Control 18

P1-1.3. Online Measurement 23

P1-1.4. TMB design and optimization 27

P1-2. Methods 31

P1-2.1. TMB and SMB models 31

P1-2.2. Study of the units dynamics 37

P1-2.2.1. The orthogonalization method 41

P1-2.3. Control system development and linear functions identification 46

P1-2.3.1. Control Strategy 50

P1-2.4. Virtual analyser development 54

P1-2.4.1. Predictor equations 54

P1-2.4.2. Multistep Predictor 57

P1-2.4.3. Quasi-Virtual Analyser structure 61

P1-2.4.4. Artificial neural network modelling 64

P1-2.5. Process design and optimization – Particle Swarm technique 68

P1-2.5.1. Definition of the objective function 74

P1-2.5.2. Operating variables confidence region evaluation 76

P1-3. Results 83

P1-3.1. TMB dynamics characterization 83

P1-3.1.1. Gram-Schmidt Orthogonalization analysis 83

P1-3.1.2. Step perturbation analysis 85

P1-3.2. SMB dynamics characterization and TMB/SMB comparison 103

P1-3.2.1. Gram-Schmidt Orthogonalization analysis 103

P1-3.2.2. Models comparison: from initial conditions to cyclic steady state 108

P1-3.2.3. Models comparison: dynamic regime 110

P1-3.2.4. Effect of the perturbation size and frequency 120

P1-3.3. TMB linear advanced model predictive control 128

P1-3.3.1. Manipulated variables selection 128

P1-3.3.2. Transfer functions identification 129

P1-3.3.3. Control systems tests 134

P1-3.4. Quasi-Virtual Analyser development 142

P1-3.4.1. Virtual analyser structure definition 144

P1-3.4.2. Quasi-Virtual analyser structure definition 149

P1-3.4.2.1. Virtual analyser parameters tuning 151

P1-3.4.3. Measurement system test 159

P1-3.5. TMB design, optimization and determination of operational confidence regions through HPSO-TVAC-MSR 167

P1-3.5.1. HPSO-TVAC-MSR method validation: Benchmark functions tests 167

P1-3.5.2. TMB optimal design 175

P1-3.5.2.1. First scenario – Process design for minimum purities and recoveries of 95% 176

P1-3.5.2.2. Second scenario – Process design for 95%, 97% and 99% of purities and recoveries 181

P1-3.5.2.3. Third scenario – Process design for a minimum of 95% in the purities and recoveries with pumps limitations 185

P1-4. Conclusions 189

Part 2 – N-Propyl Propionate experimental studies and process modelling 197

P2-1. Introduction 199

P2-1.1. N-Propyl Propionate 199

P2-1.2. Chromatographic separation 201

P2-1.3. Uncertainties Evaluation in Chromatography 202

P2-1.4. True Moving Bed Reactor 204

P2-2. Methods 207

P2-2.1. Reaction system 207

P2-2.1.1. Reaction kinetics 207

P2-2.1.2. Catalyst/Adsorbent 209

P2-2.1.3. Thermodynamic model 212

P2-2.2. Experimental setup and analytical method 214

P2-2.3. Fixed bed hydrodynamics 216

P2-2.4. Langmuir competitive adsorption parameters estimation 216

P2-2.5. Parameters confidence region evaluation 219

P2-2.6. Uncertainties evaluation 226

P2-2.6.1. Uncertainty associated with calibration 228

P2-2.6.2. Combined and expanded uncertainty for chromatographic analysis 230

P2-2.7. Fixed-bed chromatographic separation model 230

P2-2.8. Batch Reactor Model 234

P2-2.9. Fixed bed chromatographic reactor model 235

P2-2.10. True Moving Bed Reactor model 237

P2-2.11. TMBR design and optimization 240

P2-2.12. Confidence region evaluation 241

P2-3. Results 243

P2-3.1. Fixed bed adsorptive unit hydrodynamics 243

P2-3.2. Adsorption equilibrium isotherms 245

P2-3.3. Reaction rate model validation: Batch Reactor 254

P2-3.4. Fixed-bed reactor model validation 256

P2-3.5. True Moving Bed Reactor design and optimization 260

P2-3.5.1. Triangle Theory 261

P2-3.5.1.1. Influence of the switching time 264

P2-3.5.1.2. Influence of the feed concentration 267

P2-3.5.2. HPSO-TVAC-MSR 271

P2-3.5.2.1. Optimal design for 95% of purities requirement 271

P2-3.5.2.2. Optimal design for 99% of purities requirement 273

P2-3.5.2.3. Confidence region evaluation 275

P2-3.6. Comparison between the Chromatographic Reactor and Distillation Reactor 280

P2-4. Conclusions 283

General conclusions 287

Future Works 291

Bibliography……. 293

List of Figures

Figure 1 - Schematic representation of the work developed in this Thesis. 7

Figure 2 – Scheme of a TMB unit. 15

Figure 3 – Scheme of a SMB unit with three columns in each section. 16

Figure 4 - Gram-Schmidt Orthogonalization Method. (Adapted from: Kravaris et al., 2013). 42

Figure 5 - Flowsheet of the proposed process analysis. 45

Figure 6 - Responses of the purity in the extract stream to step perturbations in the recycling flow rate. Comparison between the responses in the optimal and non-optimal conditions. 48

Figure 7 - Schematic representation of the switching system proposed. 49

Figure 8 - General representation of the artificial neural network. 60

Figure 9 - Schematic representation of the proposed virtual analyser. 61

Figure 10 - Schematic representation of the Q-VOA internal structure. 63

Figure 11 - MISO structure of the neural models in the virtual analyser. 64

Figure 12 - Flowsheet of the cross-validation method; example for a total number of 50 neurons and a total number of 50 training trials. 67

Figure 13 - Schematic representation of the possible search spaces ($R1, R2$ and $R3$) of a given function with $L1, L2, L3, L4$ and $L5$ as local minima. 71

Figure 14 - Simplified representation of the model predictions through the global minimum, best minimum found and a given minimum found in the performance variables space, adapted from Benyahia et al. (2013). 77

Figure 15 - Process response after a step perturbation in the recycling flow rate: a.I - extract response to a 10% perturbation; a.II - extract response to a 2% perturbation; b.I raffinate response to a 10% perturbation; b.II - raffinate response to a 2% perturbation; c - separation and regeneration regions..... 91
Figure 16 - Process response after a step perturbation in the solid flow rate: a.I - extract response to a 10% perturbation; a.II - extract response to a 2% perturbation; b.I raffinate response to a 10% perturbation; b.II - raffinate response to a 2% perturbation; c - separation and regeneration regions..... 94
Figure 17 - Process response after a step perturbation in the eluent flow rate: a.I - extract response to a 10% perturbation; a.II - extract response to a 2% perturbation; b.I raffinate response to a 10% perturbation; b.II - raffinate response to a 2% perturbation; c - separation and regeneration regions..... 96
Figure 18 - Process response after a step perturbation in the extract flow rate: a.I - extract response to a 10% perturbation; a.II - extract response to a 2% perturbation; b.I raffinate response to a 10% perturbation; b.II - raffinate response to a 2% perturbation; c - separation and regeneration regions..... 98
Figure 19 - Process response over a step perturbation in the feed concentration of the compound A: a.I - extract response to a 10% perturbation; a.II - extract response to a 2% perturbation; b.I raffinate response to a 10% perturbation; b.II - raffinate response to a 2% perturbation. 100
Figure 20 - Process response over a 10% step perturbation in the feed flow rate: a - extract response, b - raffinate response. 101

Figure 21 - Internal concentration profiles after a 10% perturbation in recycling flow rate: a - internal concentration profile in transient state for the less retained compound; b - internal concentration profile in transient state for the stronger retained compound; c - internal concentration profile in steady state for both compounds, before and after the perturbation. 102

Figure 22 – Concentrations history for: a – most adsorbed component in the extract stream; b - less retained component in the raffinate stream. 109

Figure 23 - TMB, SMB-4 and SMB-8 responses to step perturbations in the recycling flow rate: a – responses of the recovery in extract; b. responses of the recovery in raffinate; c – responses of the purity in extract; d – responses of the purity in raffinate. 112

Figure 24 - TMB, SMB-4 and SMB-8 responses to step perturbations in the solid flow rate (TMB unit) and switching time (SMB units): a – responses of the recovery in extract; b. responses of the recovery in raffinate; c – responses of the purity in extract; d – responses of the purity in raffinate. 113

Figure 25 - TMB, SMB-4 and SMB-8 responses to step perturbations in the eluent flow rate: a – responses of the recovery in extract; b. responses of the recovery in raffinate ; c – responses of the purity in extract; d – responses of the purity in raffinate. 115

Figure 26 - TMB, SMB-4 and SMB-8 responses to step perturbations in the extract flow rate: a – responses of the recovery in extract; b. responses of the recovery in raffinate ; c – responses of the purity in extract; d – responses of the purity in raffinate 116

Figure 27 - TMB, SMB-4 and SMB-8 responses to step perturbations in the feed flow rate: a – responses of the recovery in extract; b. responses of the recovery in raffinate; c – responses of the purity in extract; d – responses of the purity in raffinate. 118
Figure 28 - TMB, SMB-4 and SMB-8 responses to step perturbations in the feed concentration of the more adsorbed component: a – responses of the recovery in extract; b. responses of the recovery in raffinate; c – responses of the purity in extract; d – responses of the purity in raffinate. 120
Figure 29 - TMB, SMB-4 and SMB-8 responses to a sequence of step perturbations: a – Recovery in extract response to a sequence of perturbations in the recycling flow rate; b – Purity in extract response to a sequence of perturbations in the solid flow rate; c – Recovery in raffinate response to a sequence of perturbations in the extract flow rate; d – Response of the recovery in extract to a sequence of perturbations in the extract flow rate. 122
Figure 30 - TMB, SMB-4 and SMB-8 recovery in raffinate responses to step perturbations in the recycling flow rate: a – 10% step; b - 5% step; c – 10% step linear isotherm; d – 2% step..... 124
Figure 31 - TMB, SMB-4 and SMB-8 purity in raffinate responses to step perturbations in the recycling flow rate: a – 10% step; b 5% step; c – 10% step linear isotherm; d – 2% step..... 125
Figure 32 - Units internal concentration profiles. Effect of a +10% perturbation in the recycling flow rate. 128
Figure 33 - Local Transfer Function Identification for the responses in recovery and purity to step perturbations in recycling and extract flow rates respectively. 133

Figure 34 - Process control at the non-optimal condition: (a) Controlled variables; (b) Manipulated variables. 136

Figure 35 - Process control at the optimal condition: (a) Controlled variables; (b) Manipulated variables. 138

Figure 36 - Process control at the optimal condition and open loop responses: (a) Solid and recycling perturbations responses (b) Solid perturbation responses. 139

Figure 37 - Control system simulation with a four columns SMB as plant and the previously identified transfer for the TMB. 141

Figure 38 - Process control under feed concentration fluctuations, setpoint (Red line), controller (Black line) and open loop (Blue line) responses. 141

Figure 39 – Raffinate purity ANN model identification: (a) selection of the optimal number of neurons in the hidden layer; (b) final model validation. The neural model prediction, red dashed lines, cover the process data, black line, during all the represented time. 147

Figure 40 – Extract purity ANN model identification: (a) selection of the optimal number of neurons in the hidden layer; (b) final model validation. The neural model prediction, red dashed lines, cover the process data, black line, during all the represented time. 148

Figure 41 - Virtual analyser actualization tuning in the prediction of the purity in the raffinate stream: (a) Last measurement used as most recent value; (b) Last measurement used as older value. 152

Figure 42 - Virtual analyzer actualization tuning in the prediction of the purity in the extract stream: (a) Last measurement used as most recent value; (b) Last measurement used as older value. 154

Figure 43 - Virtual analyser tuning in the prediction of the purity in the raffinate stream: (a) using a value of $\boldsymbol{wm}$ larger than the optimum found; (b) using the optimum values of $\boldsymbol{wm}$ and $\boldsymbol{wd}$; (c) using a value of $\boldsymbol{wd}$ larger than the optimum found. 157

Figure 44 - Virtual analyser tuning in the prediction of the purity in the extract stream: (a) using a value of $\boldsymbol{wm}$ larger than the optimum; (b) using the optimum values of $\boldsymbol{wm}$ and $\boldsymbol{wd}$; (c) using a value of $\boldsymbol{wd}$ larger than the optimum. 159

Figure 45 - Extract stream purity for the measurement system simulation: Q-VOA simulation (a); Simple VOA simulation (b). 162

Figure 46- Raffinate stream purity for the measurement system simulation: Q-VOA simulation (a); Simple VOA simulation (b). 163

Figure 47 - Relative deviation of the purity in extract between the system prediction and the process response over the simulation time: Q-VOA (a); simple VOA (b). 165

Figure 48- Relative deviation of the purity in raffinate between the system prediction and the process response over the simulation time: Q-VOA (a); simple VOA case (b). 166

Figure 49 - Confidence region and objective function surface for Equation (82). 169

Figure 50 - Confidence region and objective function surface for Equation (83). 170

Figure 51 - Confidence region and objective function surface for Equation (84). 173

Figure 52 - Confidence region and objective function surface for Equation (85). 174

Figure 53 - Scenario 1: Likelihood confidence regions, elliptical confidence region (dashed lines) and objective function map for the operating variables QS/Qe and QS/Qf 179

Figure 54 - Scenario 1: Likelihood confidence regions, elliptical confidence region (dashed lines) and objective function map for the operating variables QS/QX and QS/QIV. 180

Figure 55 – Scenario 2: Likelihood confidence regions, elliptical confidence region (dashed lines) and objective function map for the operating variables QS/Qe and QS/Qf 184

Figure 56 - Scenario 2: Likelihood confidence regions, elliptical confidence region (dashed lines) and objective function map for the operating variables QS/QX and QS/QIV. 185

Figure 57 – Scenario 3: Likelihood confidence regions, elliptical confidence region (dashed lines) and objective function map for the operating variables QS/Qe and QS/Qf 188

Figure 58 - Scenario 3: Likelihood confidence regions, elliptical confidence region (dashed lines) and objective function map for the operating variables QS/QX and QS/QIV. 188

Figure 59 - True Moving Bed Reactor unit representation..... 205

Figure 60 - Reaction routes for the formation of the n-Propyl Propionate (Adapted from: (Duarte 2006)). 210

Figure 61 - Experimental setup. 215

Figure 62 - Simplified representation of the experimental measurements and the model predictions in the parameters space, adapted from Benyahia et al. (2013). 221

Figure 63 - Tracer residence time distribution curves, for the experiments presented in Table 28. 245

Figure 64 - Parameters confidence regions, elliptical confidence region (dashed line) and optimal point (cross), with Q in($mol\ Lads^{-1}$) and K in ($L\ mol^{-1}$). 248
Figure 65 - Langmuir competitive adsorption isotherm for the binary 1-Propanol (a) – n-Propyl Propionate (b) over Amberlyst-46 at 313 K. The lines represent the theoretical adsorption isotherm considering the parameters presented in Table 30. 250
Figure 66 - Langmuir competitive adsorption isotherm for the binary Propionic Acid (a) – n-Propyl Propionate (b) over Amberlyst-46 at 313 K. The lines represent the theoretical adsorption isotherm considering the parameters presented in Table 30. 250
Figure 67 - Langmuir competitive adsorption isotherm for the binary Propionic Acid (a) – Water (b) over Amberlyst-46 at 313 K. The lines represent the theoretical adsorption isotherm considering the parameters presented in Table 30..... 251
Figure 68 - Experimental and predicted breakthrough curves for the binary 1-Propanol– n-Propyl Propionate and the respective uncertainties at 313 K and a flowrate of 7.88 mL/min^{-1}. The lines represent the breakthrough curves predicted by the model while the dots represent the experimental data. 252
Figure 69 - Experimental and predicted breakthrough curves for the binary Acid Propanoic – Water and the respective uncertainties at 313 K and a flowrate of 7.88 mL/min^{-1}. The lines represent the breakthrough curves predicted by the model while the dots represent the experimental data. 252
Figure 70 - Experimental and predicted breakthrough curves for the binary Acid Propanoic – n-Propyl Propionate and the respective uncertainties at 313 K and a flowrate of approximately 7.88

mL/min^{-1}. The lines represent the breakthrough curves predicted by the model while the dots represent the experimental data. 253

Figure 71 - Experimental and simulation results for the production of ProPro in a batch reactor, (a) Experiment 1; (b) Experiment 2 of Table 5. 255

Figure 72 - Synthesis of ProPro in a fixed bed adsorptive reactor at 313 K under the conditions presented in Table 33. 258

Figure 73 - Synthesis of ProPro in a fixed bed adsorptive reactor at 313 K under the conditions presented in Table 33. 259

Figure 74 - Reactive separation regions with $\boldsymbol{t} *= \mathbf{60}$ min and $\boldsymbol{SF} = \mathbf{1.7}$ for purities of 80%, 90% and 95%. 263

Figure 75 - Influence of the switching time on the performance parameters and internal concentration profiles of the TMBR unit. 265

Figure 76 - TMBR internal concentration profiles as function of the switching time, 3D and heat map graphics. 267

Figure 77 - Influence of the molar fraction of AcidPro in the feed stream on the performance parameters and internal concentration profiles. 268

Figure 78 - TMBR internal concentration profiles as function of the molar fraction of AcidPro on the feed stream, 3D and heat map graphics. 270

Figure 79 - Internal concentration profiles for a TMBR unit designed through the equilibrium theory, left side and a TMBR unit designed through the HHPSO-TVAC-MSR, right. 273

Figure 80 - Internal concentration profiles for TMBR optimal design through the HPSO-MMSR with 99% vs 95% of purities requirements. 275

Figure 81 – Confidence regions for the interstitial velocities ratios and objective function vs the values of interstitial velocities ratios in sections II and III. 277

Figure 82 – Optimal points, elliptical confidence regions and confidence regions for the operating variables. 279

List of Tables

Table 1 - Specific objectives of the work developed. 8

Table 2 - An overview of the publications with the focus in the SMB process control. 20

Table 3 - Proposed methodology for the improved HPSO-TVAC. 72

Table 4 - Magnitude of each operating variable of the TMB at each iteration of the dynamic analysis. 84

Table 5 - Data used in the model simulation (Pais et. al 2000). 86

Table 6 - Processes operating conditions. 104

Table 7 - Magnitude of each operating variable at each iteration of the orthogonalization analysis for the SMB-8, SMB-4 and TMB. 106

Table 8 - Data used in the model simulation, suboptimal and optimal conditions used to validate the identification approach. 130

Table 9 - Transfer functions at the optimal point. 131

Table 10 - Transfer functions for the Reaction curve, and proposed method at the non-optimal point. 132

Table 11 - Neural network parameters 145

Table 12 - Step perturbations performed for the Q-VOA tuning. 150

Table 13 - Step perturbations performed on the Q-VOA simulation. 160

Table 14 - Parameter estimation data for Equation (82). 168

Table 15 - Parameter estimation data for equation (83). 169

Table 16 - Comparison between the results obtained with the method here presented and by Schwaab et al. (2008). 171

Table 17 - Parameter estimation data for Equation (84). 172

Table 18 - Parameter estimation data for Equation (85). 173

Table 19 - Optimal unit design comparison, between the present work and the Triangle theory approach by Pais et al. (1998). 177

Table 20 - Optimal unit performance parameters, comparison between the present work and Triangle theory approach by Pais et al. (1998). 178

Table 21 - Optimal unit design for different requirements of purities and recoveries. 182

Table 22 - Optimal unit performance parameters for different requirements of purities and recoveries. 182

Table 23 - Optimal unit design for the different operating regions. 186

Table 24 - Optimal unit performance parameters for the different operating regions. 187

Table 25 - Catalyst characterization, Amberlyst 46 physical properties (Duarte 2006; The Dow Chemical Company 2014). 211

Table 26 - Reaction equilibrium and kinetic constants (Duarte 2006). 212

Table 27 - NRTL binary parameters (Samarov et al. 2016). 214

Table 28 - Tracer experiments results. 244

Table 29 - Calculated values of relative standard uncertainties, combined standard uncertainties and expanded uncertainties for the determination of the experimental concentrations. 246

Table 30- Langmuir competitive adsorption parameters over Amberlyst-46 and their uncertainties, calculated from the parameters confidence regions and HPSO-TVAC-MSR, with Q in ($mol\ Lads^{-1}$) and K in ($L\ mol^{-1}$)). 247

Table 31 - Langmuir adsorption competitive parameters over Amberlyst 46 estimated by the Generalized Reduced Gradient algorithm. 249

Table 32 - Experimental and batch model simulation conditions of Duarte (2006). 254

Table 33 - Fixed bed reactor experimental conditions. 256

Table 34 – Conditions considered in the simulations of the TMBR unit. 260

Table 35 - Operating conditions and performance parameters obtained through the triangle theory. 262

Table 36 - Operating conditions and performance parameters obtained through the HHPSO-TVAC-MSR and triangle theory. 272

Table 37 - Operating conditions and performance parameters obtained through HHPSO-TVAC-MSR for 99% of purities. 274

Table 38 - Performance variables limits for the previously presented operating confidence regions 280

Nomenclature

$\vec{a}$	Generic vector
a	Activity
A	Concentration of active sites
B	Coefficients of the partial fractions
c	Fluid phase concentration/acceleration coefficients
$Conv$	Conversion
C_T	Total molar concentration in the fluid phase
d_p	Particle diameter
D	Diffusivity coefficient
D_L/D_{ax}	Axial dispersion coefficient
EC	Eluent consumption
E	Activation energy/residence time distribution
e	Difference between optimal point and global minimum
F	Diagonal matrix with components corresponding to the stable poles/Fisher–Snedecor criteria
f	Function
g	Energy parameter
H	Enthalpy

h	Difference between the parameters for the optimal set of operating conditions and for a given set
I	Identity matrix
J	Objective function
K	Langmuir adsorption constant
K_{eq}	Equilibrium constant
K_∞/k_0	Pre-exponential factors
k	Mass transfer coefficient/time instant/iteration/constant rate
L	Length
m	Mass
M	Magnitude
n	Number of correspondent subscript
N_t	Number of moles
Pe	Peclet number
Pur	Purity
Pr	Productivity
p	Number of particles
q	Adsorbed phase concentration
q^*	Adsorbed phase concentration in equilibrium with c
POH	1-Propanol
$ProPro$	n-Propyl Propionate

$ProAc$	Propanoic Acid
Q	Flow rate/Equilibrium adsorption capacity
R	Residual matrix /search region/Recovery uncertainty
R_p	Particle radius
Re	Reynolds number
Rec	Recovery
r	Reaction rate
S	Sensitivity matrix
S^O	Orthogonal matrix
S_{max}	Column of the previous matrix with greater magnitude
Sc	Schmidt number
Sh	Sherwood number
s	Partial derivative
s'	Coefficients of the Sensitivity matrix
w	Weight
T	Temperature
t	Time
t^*	Switching time
u	Velocity/input variable/uncertainty
U	Combined uncertainty
V	Volume/Variance

x	Dimensionless axial position in the bed/stable states/particle position/signal value
y	Given response/molar fraction
$\hat{y}$	Prediction of a given response
y_i	Molar fraction in the fluid phase
z	Axial position in the bed/output prediction
0	Null matrix

Subscripts and Superscripts:

A	Component in the feed stream
a	Past values of responses
B	Component in the feed stream
b	Past values of process variables
c	Column/Number of components
d	Delay
E	Eluent
e	Number of experiments
F	Feed
i	Number of moles
I	Section 1

II	Section 2
III	Section 3
IV	Section 4
i	Number of performance indicators/ Component
j	Section
M	Molar
n	Number of time instants
p	Number of operating conditions/particle
R	Raffinate
S	Solid
t	Number of time instants
v	Number of elements of the vector
X	Extract
y	Number of process responses

Greek symbols:

α	Number of mass transfer units/non-randomness in the systems
ε	Bed porosity/error
δ	Penalty/coverage factor
γ	Ratio between fluid and solid interstitial velocities/activity coefficients

θ Performance indicator/Parameter

η Fluid viscosity

v Fluid interstitial velocities/white noise

ϑ Stoichiometric coefficient (Negative for the reactants and positive for the products)

ρ Fluid density

τ Dimensionless time variable

φ Model input vector

χ Chi square distribution

Introduction

Relevance and motivation

The adaptation of the human activities in order to preserve the environment and avoid environmental degradation has become one of the main topics of interest in the last decades. Among those activities, the chemical industry can be highlighted as one of the most harmful to the environment. Thus, several studies have been developed in order to promote improvements and changes in the chemical processes that attend to the new environmental and social standards. Those changes were done in all the industrial structure, ranging from the development of new process units, to the replacement of chemical compounds considered as environmental harmful by ones that are considered more environmentally friendly. In this scenario, process intensification plays an important role, proposing new alternatives which are more suitable for nowadays standards, from which the use of multifunctional units are a relevant example (Duarte 2006; Pereira et al. 2008; Graça et al. 2012; Xu et al. 2014).

Multifunctional units are capable of integrating reaction and separation in the same unit, replacing the traditional way of production, in which it is usual to employ one specific unit for each step of the production route. Through these technologies, it is possible to improve the selectivity towards a given product, while potentially reducing the capital investment and the energy consumption. Therefore, multifunctional units usually lead to lower energy, operating

and investment costs. Furthermore, those processes are normally presented as safer and less harmful to the environment.

Among multifunctional units, the Simulated Moving Bed Reactor (SMBR) can be highlighted. Several works have been published showing that Chromatographic Reactors can be efficiently applied to equilibrium limited reactions. Those units allow overtaking the equilibrium conversion by continuously removing at least one of the products from the reaction medium (Constantino et al. 2015a). Several studies were published in the last five years, reporting the work done with different types of esterification reactions in Chromatographic Reactors (Son et al. 2011; Constantino et al. 2015a; Regufe et al. 2016), but none with the focus on the n-Propyl Propionate system.

In the field of industrial solvents, n-Propyl Propionate is among the chemicals considered as a better environmental option. This compound is readily biodegradable, non-toxic, and considered as a non-hazardous air pollutant by the U.S. Environmental Protection Agency. The n-Propyl Propionate may be used in several industrial applications, such as in drugs, coatings and inks production, in polymerization reactions, and as additive for foods and perfumes. It presents as main properties its high volatility, high electrical resistance, a good scent and non-toxicity (The Dow Chemical Company 2002; Duarte 2006).

The aforementioned benefits of this compound and its complex synthesis reaction system led to several studies being presented in the literature about the ProPro production through an

alternative route which uses a multifunctional unit, the Reactive Distillation (RD) (Duarte 2006; Altman et al. 2010; Cruz-Díaz et al. 2012; Xu et al. 2014).

The previous referred works have shown that the RD production route for n-Propyl Propionate presents a significant improvement to the traditional route (Duarte 2006; Altman et al. 2010; Cruz-Díaz et al. 2012; Xu et al. 2014). However, as in the traditional production route, the outlet steams of the unit are composed by a mixture of the main product and the non-converted reactants. Klöker et al., (2003) studied the impact of the operating variables of a Reactive Distillation unit, including the downstream purification by a conventional liquid-liquid separator. In the referred work, it was demonstrated that the downstream purification plays an important role in the process efficiency. In Altman et al. (2010), the problems related to the downstream purification are also addressed highlighting the fact that this is still a problematic point in the field.

In this way, alternative improvements for n-Propyl Propionate production could be the employment of chromatographic separation in the downstream purification step of the Reactive Distillation production or in the traditional production route. A further improvement in this process could be performing the reaction and separation simultaneously in a continuous chromatographic unit like a Simulated Moving Bed Reactor. However, there isn´t any work in the literature with the focus on the behaviour of this system in a chromatographic unit.

In this way, one of the focus of this work is to study the production of n-Propyl Propionate in chromatographic reactor units, presenting this route as one novel alternative to its synthesis.

However, the modelling, optimization and control of Simulated Moving Bed Reactor (SMBR) and Simulated Moving Bed (SMB) units are crucial steps to accomplish the implementation of this type of processes in industry, and deeper studies are still required. Therefore, another major focus of this work is the development of new methodologies for the modelling, optimization and control of these processes. Bibliographic reviews (Rajendran et al. 2009; Sá Gomes and Rodrigues 2012; Aniceto and Silva 2015) show the increasing importance of SMB/SMBR processes revealing a high number of publications and patents on this topic. This shows the increasing interest in the development of the topic with special attention to industrial applications. This field of study is still in development in this area and many aspects need to be further investigated and deepened.

Normally, True Moving Bed (TMB) and SMB units are employed in processes where the final product presents a high value and strict quality specifications, such as fine chemicals, pharmaceutical compounds and petrochemicals. Those factors associated with robust phenomenological models and complex process dynamics lead to challenging problems in the SMB/TMB units optimal design, inference, optimization and control. Thus, the first part of the present work addresses those problems considering as case study a well-known system, an enantiomers separation unit previously studied in the Laboratory of Separation and Reaction Engineering (LSRE). In this way, the methods here proposed could be applied and verified with a simpler and known case. First, a detailed simulation study of the dynamic behaviour of the TMB/SMB units for enantiomers separation is done, followed by the development of a new control strategy for these processes. Then, an alternative to the measuring problems found in the field is proposed and finally a methodology for process design and optimization by Particle

Swarm Optimization (PSO) is developed. Once the methodology is verified, it can be consistently applied to SMBR units.

The present work is divided in two lines that are complementary to each other. One with the focus on the mathematical aspects and methodologies development and another focused on the experimental determinations for the n-Propyl Propionate system. The structure of the thesis, concomitantly with specific objectives are presented in the next section.

Outline and Objectives

As aforementioned, this work contemplates two different and complementary lines, each one with different objectives.

The first part of this work (Part 1) is dedicated to the development of a deeper comprehension of the dynamics of the chromatographic systems True Moving Bed (TMB) and Simulating Moving Bed (SMB). To accomplish this, the bi-naphthol enantiomers separation using 3,5-dinitrobenzoyl phenylglycine bonded to silica gel as adsorbent and heptane-isopropanol as eluent is studied by simulation. The model parameters were estimated and previously validated experimentally by Pais et al. (2000) in a SMB pilot plant located at LSRE. Hence, the main objective of this part of

the present work is to study the dynamics, control, inference, design and optimization problem of TMB and SMB units.

Part 1 is divided in four chapters that sequentially present: an introduction to the topics covered in P1-1; the developed methodologies - TMB and SMB models, study of the units dynamics, orthogonalization method, control system development and linear transfer functions identification, quasi-virtual analyzer development and process design and optimization by Particle Swarm technique – in P1-2; the results obtained for each point presented in the methodology in P1-3; and the conclusions of this part in P1-4.

The second part of this work (Part 2) is dedicated to the experimental studies about the production of n-Propyl Propionate. The main objective of this part is to study, through a series of experiments, the behaviour of the compounds that compose the reaction system of n-Propyl Propionate. In this step, a characterization of the system adsorption equilibrium, fixed bed separation and fixed bed reaction is done, concomitantly with the development and validation. Similarly to Part 1, Part 2 is divided in four chapters that sequentially present an introduction to the topics covered (P2-1); the applied methodologies: Fixed bed unit models, uncertainties

evaluation, confidence regions identification and TMBR model (P2-2); the results obtained (P2-3); and the conclusions of this part (P2-4).

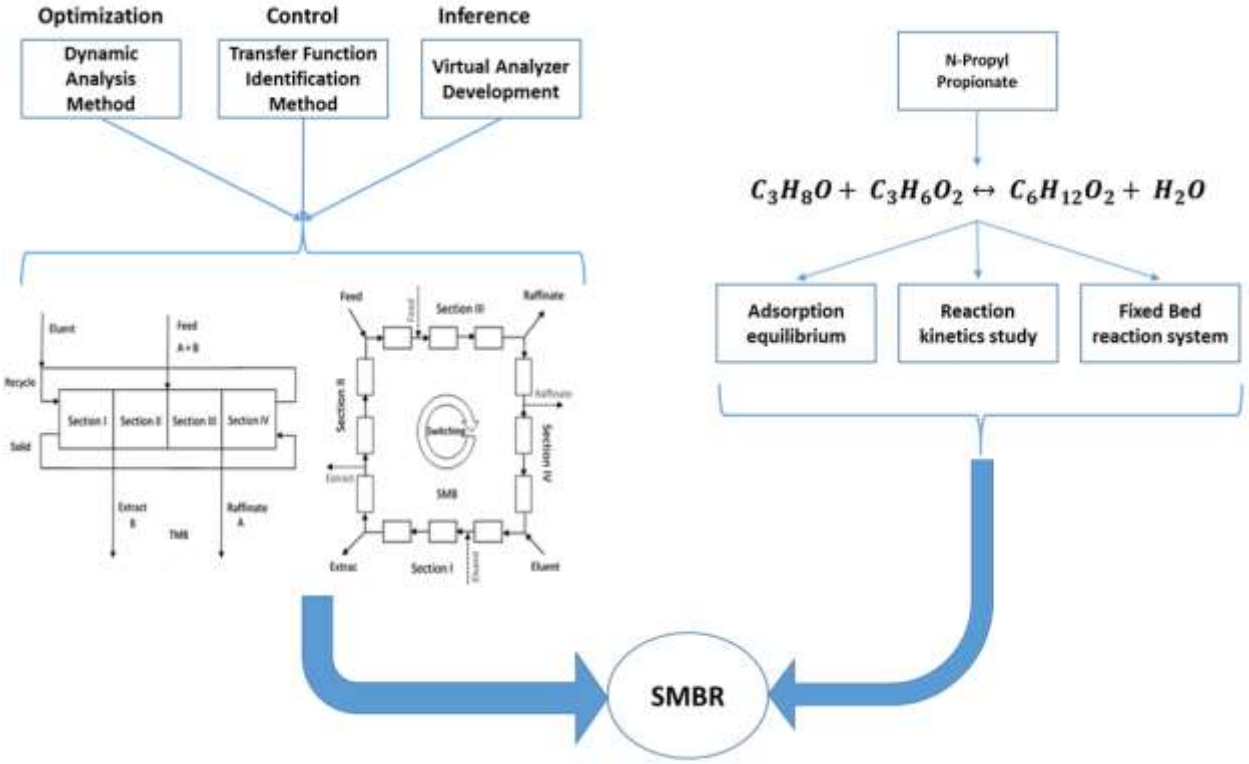

Figure 1 - Schematic representation of the work developed in this Thesis.

Table 1 presents a list of specific objectives of the work developed in this thesis with reference to the corresponding sub-chapters.

Table 1 - Specific objectives of the work developed.

Sub-chapters	Objective
P1-2.2.1	Development of a method to analyse the impact of the operating variables in a TMB unit response and characterization of the dynamic behaviour of the system.
P1-2.3.	Propose a method to identify the TMB unit transfer functions, development of several control strategies in order to control the unit purities and recoveries.
P1-2.4.	Development of a neural system capable of providing online and real-time information about the process purity of both raffinate and extract streams in a TMB unit.
P1-2.5.	Optimization of the operating conditions of a TMB unit through the particle swarm optimization method.

P1-3.1. **P1-3.2.**	Application of the method previously developed to analyse the impact of the operating variables in a TMB/SMB unit response, characterization of the dynamic behaviour of the system and comparison with the results obtained for the TMB unit case.
P1-3.3.	Application of the method previously developed to identify the SMB unit transfer functions, development of several control strategies in order to control the unit purities and recoveries and comparison of the control strategies applied in the TMB and SMB units.
P1-3.4.	Development of a neural system capable of providing online and real-time information about the process purity of both raffinate and extract streams in a SMB unit.
P1-3.5.	Optimization of the operating conditions of a SMB unit through the particle swarm optimization method and comparison with the optimization of the TMB unit.

P2-2.4 **P2-2.7** **P2-3.2**	Determine the adsorption equilibrium isotherms of the compounds of the n-Propyl Propionate reaction system, develop a model for the n-Propyl Propionate system separation in a fixed bed reactor and validate the model through laboratory experiments.
P2-2.1 **P2-2.9** **P2-3.4**	Develop a model for the n-Propyl Propionate reaction in a fixed bed reactor and validate the model through laboratory experiments.
P2-2.10	Develop a model for the n-Propyl Propionate production in a TMBR unit.
P2-2.11 **P2-2.12** **P2-3.5**	Design and optimization of the operating conditions of the TMBR unit through traditional methods and the particle swarm optimization method. Comparison of the design and optimization methods.

Part 1 – TMB and SMB systems analysis and methods development

P1-1. Introduction

This part of the work is dedicated to the study of the dynamics of True Moving Bed (TMB) and Simulated Moving Bed (SMB) units. In this chapter the motivations that led to the developments of this part of the work are presented together with a brief bibliographic revision of the topics covered.

P1-1.1. Processes Dynamics

Separation processes based on simulated moving bed (SMB) units have acquired great importance. These processes are able to efficiently promote difficult separations of different mixtures. Several studies were published proving the application of these processes in complex systems such as propane/propylene separation (Martins et al. 2015); fructose-glucose separation (Azevedo and Rodrigues 2001); xylene isomers separation (Minceva et al. 2008) and enantiomers separation (Pais et al. 2000; Rajendran et al. 2009; Grossmann et al. 2010; Ribeiro et al. 2011a; Sá Gomes and Rodrigues 2012). Further developments in these processes allowed reaction and separation to be conducted simultaneously in the same unit, giving rise to the Simulated Moving Bed Reactor (SMBR). This type of reactors presents the advantage of producing separated products in conditions of lower temperature and pressure, when compared with the traditional units. Several works were published with the focus on the production of some compounds by SMBR showing the efficiency of these units when compared with the traditional routes of production (Kawase et al. 1999; Toumi and Engell 2004; Minceva et al. 2008; Pereira et al. 2008,

2009b). The high number of patents and publications about SMB and SMBR processes show the relevance that these processes have acquired over the years (Lehoucq et al. 2000; Lode et al. 2001; Minceva and Rodrigues 2005; Zhang et al. 2007; Pereira et al. 2009b; Ribeiro et al. 2011b; Pereira and Rodrigues 2013; Suvarov et al. 2014a; Constantino et al. 2015b; Choi et al. 2017).

Recent publications on the topic focus on the optimization and control of such units (Toumi and Engell 2004; Amanullah et al. 2007; Paredes and Mazzotti 2007; Toumi et al. 2007; Ribeiro et al. 2011b; Bentley et al. 2013; Li et al. 2014; Aniceto et al. 2016; Vignesh et al. 2016). This is a newer field of study in this area and still many aspects need to be further developed and deepened.

The modelling and design of moving bed processes can follow two approaches, the true moving bed (TMB) and the simulated moving bed (SMB). The concept of TMB is based on actual movement of the solid phase (the adsorbent) countercurrently to the movement of the fluid phase (eluent). A scheme of a TMB unit is shown in Figure 2. The unit is fed with a mixture (A+B), of which one of the compounds has higher affinity towards the adsorbent and is obtained in the extract stream (B). The less adsorbed component is obtained in the raffinate stream (A). The TMB unit is divided in four sections that have specific roles in the process. Sections II and III are responsible for promotion of the separation between the more and the less adsorbed components, while sections I and IV are responsible for the regeneration of the adsorbent and of the eluent, respectively.

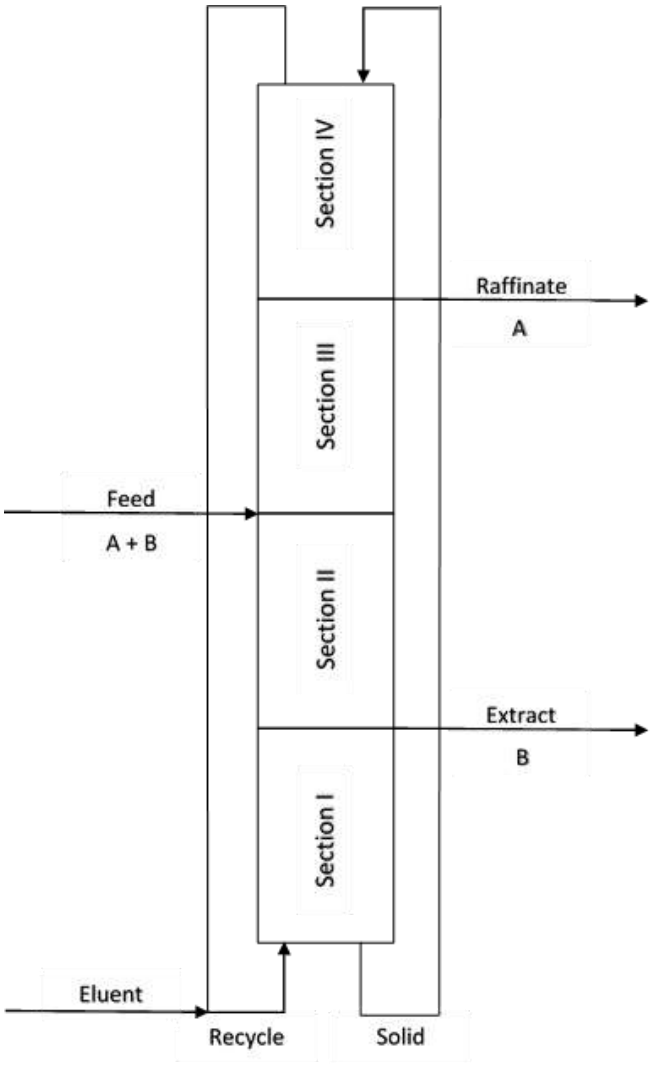

Figure 2 – Scheme of a TMB unit.

In practice, it is not trivial to promote the movement of the solid phase. Thus, the concept of TMB is applied through simulated moving bed units. The SMB operating principle is based on the concept of the true moving bed where the solid movement is simulated by the synchronized changing of the positions of the inlet and outlet streams (ports) at predefined times. In its conventional configuration, the SMB unit has two inlet streams, feed and eluent, and two outlet streams, extract and raffinate. Figure 3 shows a schematic representation of a SMB unit with

three columns in each section, where the switching of the ports in the direction of the fluid flow is shown by the dashed arrows.

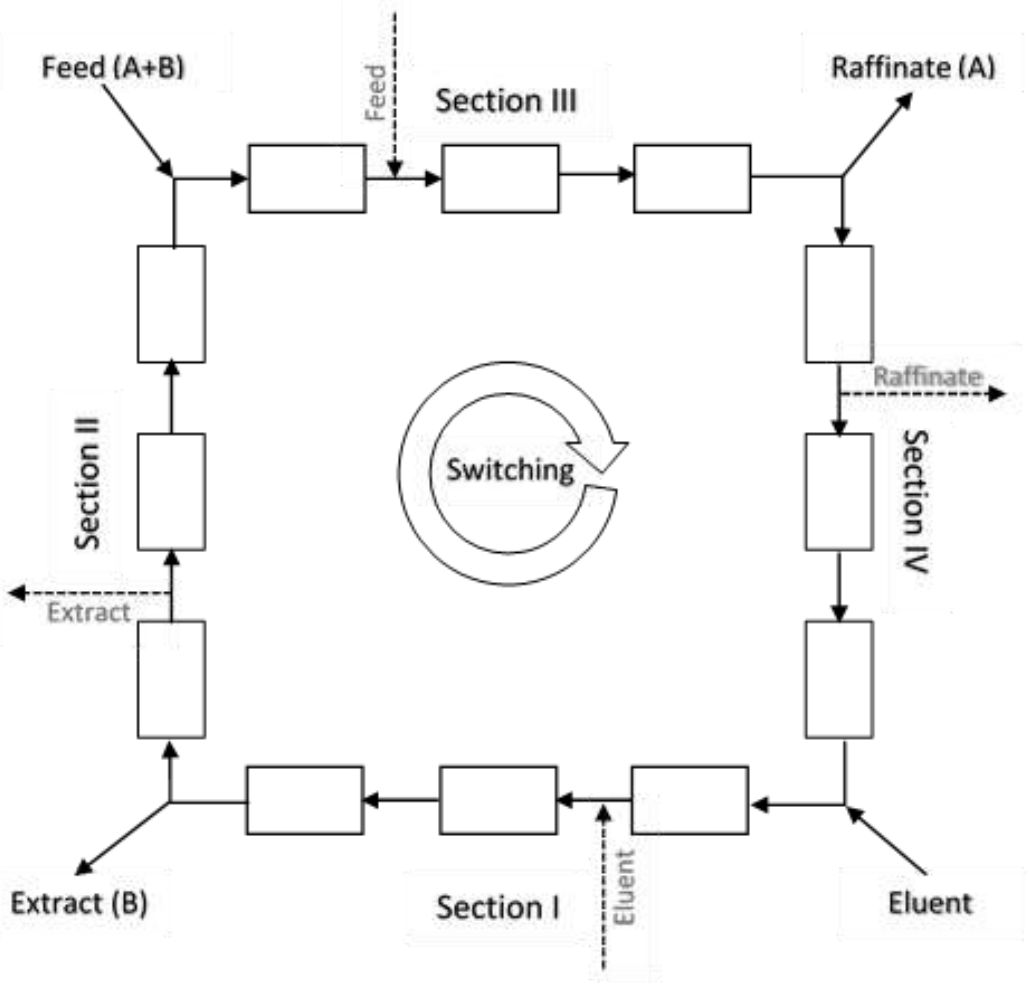

Figure 3 – Scheme of a SMB unit with three columns in each section.

Usually, the design and simulation of the SMB unit is done using the TMB approach (Chu and Hashim 1995; Storti et al. 1995; Pais et al. 2000; Kaspereit et al. 2007; Minceva et al. 2008; Sá Gomes et al. 2009; Ribeiro et al. 2011a). The equivalence between the two units is demonstrated by comparing the results obtained for the steady state of the TMB with the average of the results obtained over a cycle in the cyclic steady state (CSS) of the SMB. Following this approach, it was

shown (Pais et al. 1998) that the results for the SMB unit approach the ones of the TMB as the number of columns in the SMB increases.

However, in terms of dynamic behaviour, the two processes may follow quite distinct paths before reaching the respective steady (or cyclic steady) state. The study and evaluation of the dynamic behaviour is very important for the optimization and control of these units, as in industrial operation the units may be subject to external perturbations that can momentarily or definitively change the process state. Furthermore, it is important to know how the system behaves in the transition between different operating conditions. In spite of its importance, studies on the dynamic behaviour of these systems are still scarce in the literature.

The SMB unit, as presented in Figure 3, is characterized by the synchronous movement in the position of its inlet and outlet streams in the direction of the fluid flow, at fixed time intervals. This leads to a complex dynamic behaviour where no steady state exists, and a cyclic steady state is reached instead. Furthermore, the dynamics of the system is highly sensitive to the process parameters, such as the adsorption isotherms, the column packing, etc. The process also presents a high sensitivity to changes in its operating conditions, such as perturbations in the process flow rates. These points make the SMB process optimization and control a difficult task that still requires further studies.

Finally, the operation of these units is often designed with safety margins for purity and recovery to deal with uncertainties and disturbances which is a simpler way to overcome the aforementioned problems and is usually applied in the industry. This is done in order to make

the process less sensitive to the possible variations. On the other hand, the suboptimal operation leads to a more expensive production, far from the economical optimum. Hence, further developments in SMB optimization and control are required in order to improve the industrial operating performance of these units. Therefore, this is the focus of the first part of this work, to investigate the details of the dynamics of these processes in order to propose more efficient control and optimization strategies for those units while overcoming the system limitations.

P1-1.2. Processes Control

The control of SMB units was first introduced by Kloppenburg and Gilles (1999) where the authors proposed the process purity control through the manipulation of the extract and raffinate flow rates. In their work, the authors proposed a nonlinear model-based automatic controller based on a state estimator in order to predict the process purities. The referred work showed that SMB control could be a promising solution for operating these separation units in optimal conditions.

In Klatt et al. (2002), a two layer controller system was proposed to control an SMB unit for fructose/glucose separation. The first layer of the proposed system was computed by an offline optimization of the operating trajectory. The optimization was based on the process phenomenological model. An indirect control of the process purities was proposed by the authors. To do this, the deviations from the optimal column internal concentration profile in four different points of the column, Δp, were used as controlled variables. β factors, which depend on the process adsorption isotherms and process flowrates, were used as manipulated variables.

The process control through the manipulation of variables that depend on process parameters, such as the β factors, may not be the best option in terms of operational implementation, since these variables do not depend only on process operating flow rates, but also on process adsorption equilibria. This means that the changes made by the control system do not imply necessarily a direct change in the process variables, and therefore an indirect effect can be masked by other factors. Furthermore, the process control through the adsorption and desorption fronts could require several concentration measurements. Moreover, the real-time measurement of concentrations is still a problem in this type of processes, mainly in the enantiomers separation. Usually, the assembled elution profile (AEP) is used in order to reduce the number of measurements to obtain the internal concentration profile. Even in this case, a complex measurement system may be required. Finally, in the development of a control system, it is always better to have a strategy that requires minimal information about the phenomenological system.

The repetitive model predictive control (RMPC) concept was well explored in the literature for controlling SMB units (Erdem et al. 2004; Abel et al. 2005; Grossmann et al. 2008). This control concept was first introduced by Lee et al. (2001) where the RMPC was developed from the idea of the repetitive control (RC) and the model predictive control (MPC). In Erdem et al. (2004) the RMPC is applied in the control of the concentration of the extract and raffinate streams of an SMB unit through the manipulation of the column internal flow rates. In the referred work, the model for the control system was identified from the phenomenological model through a model reduction method. One of the limitations of the RMPC control system is the assumption that the

switching time of the process is constant which limits the control system, since the switching time could be used as a manipulated variable of the controller.

Table 2 - An overview of the publications with the focus in the SMB process control.

Authors	Year	Control Strategy	Process Variables	Manipulated Variables
Kloppenburg and Gilles	1999	FBC	Pr ,Px	QX,QR
Klatt et al.	2002	IMC	Δp	βIV, βI, βII, βIII
Erdem et al.	2004	RMPC	Cr ,Cx	QIV,QI,QII,QIII
Toumi and Engell	2004	NMPC	Px	βIV, βI, βII, βIII
Abel et al.	2005	RMPC	Pr ,Px	mI,mII,mIII,mIV
Song et al.	2006	MPC	Pr ,Px	mII,mIII
Grossmann et al.	2008	RMPC	Pr ,Px	mI,mII,mIII,mIV
Suvarov et al.	2012	NMPC	Pr ,Px	QIV,QE,QR,QF
Suvarov et al.	2014	AC	Pr ,Px	mI,mII,mIII,mIV
Neto et al.	2016	NMPC	Pr, Px	QX,QE,QR,QF

AC – Adaptive Control
βIV, βI, βII, βIII – Internal factor
FBC – Feedback Control
IMC – Internal Model Control
MPC –Model Predictive Control
NMPC – Non-linear Model Predictive Control
RMPC – Repetitive Model Predictive Control
mI,mII,mIII,mIV – Internal flow rate ratios
Cr – Raffinate concentration
Cx – Extract concentration
Δp - the deviations from the optimal column internal concentration profile
Pr – Raffinate Purity
Px – Extract Purity
QE – Eluent Flow rate
QF – Feed Flow Rate
QR – Raffinate Flow Rate
QX – Extract Flow Rate
QIV,QI,QII,QIII – Internal flow rate

In Andrade Neto et al. (2016), a non-linear MPC (NMPC) system applied in the control of an SMB unit for a chiral separation is presented. The authors propose a control system with optimization and parameters reestimation which showed a good performance in different scenarios (Andrade Neto et al. 2016). Table 2 presents an overview of publications with focus on the control of SMB units.

It is possible to note in Table 2 that the majority of the reviewed works used the purities as controlled variables. Only two works from these make direct use of process operating variables as direct manipulated variables. Furthermore, only a few number of works were found where the simultaneous control of the purity and recovery is done. Finally, it was not found in the literature works that identify the transfer functions of the processes in study.

The employment of advanced control techniques instead of the traditional ones is justified in industrial processes with complex dynamic behaviour, strong interactions between variables and with process and economic restrictions (Martins et al. 2014). Consequently, advanced control techniques are indicated to solve the SMB control problem. In the last two decades, significant advances on the control theory have been made, from the development of new control strategies as the infinite horizon model predictive control (Pannocchia et al. 2003; Rodrigues and Odloak 2003) and the robust model predictive control (Badgwell 1997; Odloak 2004), to the studies about the control system stability (Rawlings and Muske 1993a; Mayne et al. 2000; Löfberg 2001; Lee 2007; Huang et al. 2011). In general, the application of NMPC technique for complex systems is common in the literature (Toumi and Engell 2004; Ali et al. 2007; Suvarov et al. 2012; Fontes et al. 2014; Andrade Neto et al. 2016). However, the available NMPC solutions seem still far from

the practical application stage, mainly due to problems related with systematic methods to tune the controller parameters, guarantee of stability, and convergence of the NMPC coupled to the state estimator. On the other side, a linear MPC controller may overcome some of those problems, and some schemes may even guarantee stability. An MPC controller with guaranteed stability means that it will always find an optimal solution regardless of its tuning parameters. There is a vast number of strategies to ensure the robustness and nominal closed-loop stability of a predictive control system, which usually aim to reformulate the controller cost function in order to force it to play the role of a Lyapunov-like function (Rawlings and Muske 1993b; Mayne et al. 2000; Diehl et al. 2011).

A great number of these techniques, that are available in the literature and have their robust stability proved, are based on linear models decomposed in the state-space form which has stability assured. In order to make use of such type of control systems in the SMB process, the first step is to define a way of identifying the linear models of the process and apply them in the control system.

The transfer functions are linear models that can not only be identified through the process reaction curve (Seborg et al., 2003), but can also be directly and easily identified through experiments or industrial data, and therefore they are a different approach when compared to others proposed in the literature for SMB control, such as the state-space models. Additionally, the parameters of the transfer functions models can be easily re-estimated online, an advantage that can be used in an adaptive controller. In this way, the possibility of developing an advanced process control for a SMB unit through a simple identification procedure, without the need of a

process phenomenological model or more complex linearization methods, is an important contribution to the field, mainly for the industrial application of these units.

In the present work, the development of a novel strategy to identify transfer functions of TMB/SMB units is also proposed, which allows the application of classical linear model predictive controllers based on transfer functions to control these processes. The identification of transfer functions is proposed since it is an easier way to identify the process linear model. The idea of using multiple linearized models within a control scheme for SMB control is employed in Erdem et al. (2004) where multiple state-space models are employed in a RMPC system.

P1-1.3. Online Measurement

A usual problem found in several engineering fields is the measurement of unmeasurable quantities. To overcome those problems the concept of soft sensors, or virtual analysers, was proposed, which is based on measurable variables and nonlinear function that correlate those first variables with the variable to be measured. Thus, the soft sensor is based on the mathematical representation of nonlinear systems, the predictors, which are developed to correlate measurable variables to unmeasurable ones. The soft sensor concept has been successfully applied in different fields, such as chemical processes (Sharmin et al. 2006; Jalee and Aparna 2016), mechanical systems (Capriglione et al. 2017), industrial applications (Roy et al. 1999), and environmental field (Huang et al. 2015; Sánchez et al. 2018)

However, the development of those predictors is still an open problem in the literature. On one hand, the predictors can be developed through the Nonlinear Auto Regressive Moving Average with Exogenous inputs (NARX) approach, which is the most common in the literature (P. Menezes Jr. and Barreto 2006; Menezes and Barreto 2008; Ghosh and Maka 2011; Jalee and Aparna 2016). However, when the application is intended for performing long-term predictions or simulations, the NARX approach presents a degradation of its efficiency with time (Nelles 2001). On the other hand, the most suitable approach for long-term predictions or simulations is the Nonlinear Output Error (NOE). However, the development of a NOE model becomes much more complex than the training of a NARX model, since the partial derivative of its predictions in order to time depends on the partial derivative of its parameters, which are being estimated (Nelles 2001). In this way, the present work proposes the development of a NARX based artificial neural network (ANN) model concomitantly with a correcting error system, through the experimental measurements available, to perform long-term predictions in order to solve the concentration measurement problem, usually found in the cyclic adsorption processes field.

The real-time measurement problem is in general associated with a low frequency of measurements of some property such as the concentration. The low frequency of measurements is a well-known problem in the chemical industry. This problem is usually associated with profit losses by production of out of specification products. For example, in polymerization processes the real time measurement of the polymers main properties, such as the melt flow index, density and molecular weight distribution, is an important subject of study (Gonzaga et al. 2009; Zhao et al. 2009; Nogueira et al. 2017). In other fields, these problems appear when the product main

property is associated with measurements of concentrations, since the online measurement of concentrations is not a trivial task.

An important point in the enantiomers separation is the measurement of the concentration of each chiral compound. This is a problem that impairs further developments in the field, for example the application of an online controller. This has not been possible yet because an appropriate online monitoring system is not available. In the work of Amanullah et al. (2007), the authors present a system composed by a UV detector, that measures the enantiomers global composition and a polarimeter, that measures the composition of each enantiomer. The authors point as limitations of their technique the lack of information during the first switching period and the incomplete information during the last switching period of a cycle. Furthermore, these techniques involved a substantial effort to circumvent inherent limitations of the optical detectors as pointed by Grossmann et al. (2010).

The empirical modelling based on artificial neural networks (ANN) to solve engineering problems acquired a significant importance nowadays (Behbahani et al. 2009; Yap and Karri 2013; Mirsoleimani-azizi et al. 2015; Yu et al. 2015; Torrecilla et al. 2016; Wang et al. 2016; Sorrosal et al. 2017). Wang et al. (2003) propose the prediction of the internal axial concentration profile of an SMB unit with a neural model. In the referred work, the ANN model was pointed as an efficient alternative to the use of the phenomenological model, since the complexity of the latter leads to a large computational effort (Wang et al. 2003). The authors conclude their work validating the ANN model and suggesting its implementation in a predictive control system based on the ANN model.

Other works in the chiral separations with SMB units employ an offline monitoring of the system outlet composition using HPLC measurements. This method can lead to a considerable measurement dead time, which compromises the process control and/or optimization. For example, in Ribeiro et al. (2011a), the authors measure flurbiprofen concentration by collecting samples at the end of a cycle (equivalent to 13.55 min) and later on they measure the samples in an HPLC. In Ribeiro et al. (2011b), the authors use the same procedure to measure the chiral concentration; in this case, their measurement dead time can reach 37.5 minutes. In Langel et al. (2009), an HPLC system is proposed in order to reduce the measurement dead time. However, the HPLC system still presents a low frequency of measurement, which in this case is equal to a cycle time.

Therefore, on one hand, the ANN predictions might degrade over time due to its NARX structure, and on the other hand, offline measurements carry long dead times. In this way, this work proposes a quasi-virtual on-line analyser (Q-VOA) which combines the ANN and offline measurements to do online and real-time monitoring of the purity of a TMB unit. The combination of both techniques results in a pseudo-measurement soft-sensor that can provide reliable real-time estimations of the process purity. The measurement actualization is proposed to improve the ANN model prediction. However, this actualization cannot be done at every time instant since it would then incorporate the measurement time delay, as is explained in detail in Section P1-2.4.

P1-1.4. TMB design and optimization

The design of a TMB consists in the definition of the unit internal flow rates that will meet the required conditions of quality and productivity. The unit internal flow rates are directly correlated to the external flow rates, or the operating variables of the process. One of the first design and optimization method in this field was proposed in 1993 based on a robust design concept, the triangle theory (Storti et al. 1993). Since then, this technique became the traditional way to design those processes. However, this technique is based on the equilibrium theory, and presents limitations when applied for systems in which the mass transfer is a significant factor. In those cases, the optimal point provided by the triangle theory does not guarantee the complete separation (Aniceto et al. 2016). Further development of the triangle theory was proposed by Azevedo and Rodrigues (1999), where the authors evaluate the effect of the mass transfer coefficient in the separation regions of the triangle theory. Furthermore, in the referred work, the authors propose an extension of the first theory into the separation volumes. Since then, the design of those type of units has been done mainly through the triangle theory or separation volumes technique.

Those methods are well-known, and represent a simple and practical way to design TMB/SMB units; however they are computationally expensive and also present some limitations. Such as the mass transfer question aforementioned and the difficulty to evaluate all possible operating conditions simultaneously. This last one is due to the fact that the method presupposes to fix a low value of the unit feed flow rate and evaluate the remaining operating conditions in order to

draw the separation region limits. The procedure is then repeated, to evaluate different feed flow rates of increasing value through this method until a feed flow rate is reached for which no conditions that allow separation are found. This becomes a massive work because it is necessary to repeat the method for each feed flow rate value that is wished to be evaluated. This also leads to another problem, that is, the discrete nature of this method for the optimization of the system. In order to overcome those problems, Aniceto et al., (2016) proposed a robust design technique based on design of experiments and response surface to optimize SMB processes. In the referred work, the authors demonstrate that alternative techniques for TMB design and optimization can present superior results when compared with the traditional ones, triangle theory and separation volumes.

The evaluation of new alternatives for the design and optimization of those type of processes is still an important contribution to the field. Furthermore, those type of processes deal with high value products and, in terms of its operation, it is important to have available tools capable of providing a range of possible operating points for which the process can reach its maximum potential. Concomitantly, after the process design and optimization, during the operation, the process is constantly under conditions where unexpected deviations from its optimal condition may occur. The system uncertainty, that cannot be predicted or accounted for in the design and optimization step, can led the process to a different behaviour than the previously analysed. In this way, besides the operating range, the evaluation of the confidence regions of the operating point is also an important tool to improve the process performance and avoid losses in the process due the unknown system uncertainty and deviations.

The traditional process design and optimization procedures normally provide a point where the process will meet the desirable requirements. However, it is important for continuous quality improvement to determine how accurate are these optimal operating conditions, in other terms, to determine the region within the operating range of the process for which these conditions are still satisfied. This can be done by considering interval estimation for a single variable or by joint confidence regions for multiple variables (Park 2013). A method based on bootstrap technique for the determination of the confidence region of optimal operating conditions in robust process design is proposed by Park (2013) where the author presents the importance of the evaluation of the accuracy of the optimal point in the process design. Schwaab et al. (2008) present a simple and efficient method to evaluate confidence regions of model parameters. In the referred work, the authors show that the determination of the confidence regions can be easily done through the results of an optimization using a method based on populations, such as the Particle Swarm Optimization (PSO).

Particle Swarm Optimization is a method developed in 1995 by Kennedy and Eberhart (1995) where the authors propose a concept for the optimization of nonlinear functions based on social behaviour of living organism communities such as birds flocks or fish schools. Since then, the method has been applied to solve several optimization problems in different fields, such as parameters estimation (Koduru et al. 2007; Schwaab et al. 2008), control system (Nery et al. 2014; Al-Dunainawi et al. 2017; Soufi et al. 2017) and to solve optimization problems in general (Hu and Eberhart 2002; Parsopoulos and Vrahatis 2002; Jiang et al. 2007; Engelbrecht 2012). For

the last two decades, studies have been published with developments and improvements in the PSO technique (Ratnaweera et al. 2004; Jiang et al. 2007; Engelbrecht 2012).

The PSO algorithm is presented as an efficient way to optimize complex problems with a simple implementation. Furthermore, the population generated by the algorithm can be considered as a cloud of points that can be employed to plot the confidence region of the optimized variables. However, there are still some open questions in the literature about this technique, such as the initialization velocity, which is addressed by Engelbrecht (2012); the acceleration coefficients addressed in Ratnaweera et al., (2004); the application of PSO in multi-objective problems addressed by Hu and Eberhart (2002).

This topic of the work has as main objective to design and optimize a TMB unit and draw the confidence regions of its operating variables with an improved Self-Organizing Hierarchical Particle Swarm Optimizer with Time-Varying Acceleration Coefficients with mutable searching region technique. The main contribution of this work is to propose a technique capable of providing the set of best designs of a TMB unit, where all possible operating conditions that obey to the process design constraints are determined. It is an important tool for the operation of those type of processes and is presented as an alternative to the classical approach, where it is necessary to re-design the unit each time a new operating condition is desirable. Another contribution of the present work is to adapt the past developments in PSO algorithms and confidence regions evaluation which were employed in the field of parameters estimation, to process robust design and optimization. Furthermore, the PSO approach here proposed presents new contributions to the swarm optimization field.

P1-2. Methods

This chapter is dedicated to the description of the methods and developments proposed in this work. The methodologies here described will be applied for each process in study (TMB and SMB). The results obtained for the TMB and SMB studies will be presented at the end of this part in the results chapter. All steps of the work were conducted in a computer with an Intel core i5 processor and 8 GB of RAM memory.

P1-2.1. TMB and SMB models

Two phenomenological models were developed in order to describe the TMB and SMB processes presented in Section P1-1.1. In the True Moving Bed system model, a set of two partial differential equations (PDEs) describes the conservation (mass balance) of each component in the fluid and solid phases of a volume element of the bed. The model assumes multicomponent adsorption equilibrium, axial dispersed plug flow of the fluid phase and the linear driving force approximation to describe the intraparticle mass transfer. The TMB unit is composed by four sections ($j = I, II, III, IV$) and the system in study is a binary separation. In a volume element of the TMB column with a section length, L_j, where the solid phase moves with given velocity, u_s, and for a given component i, these PDEs can be expressed as:

Mass balance to the fluid phase in a volume element of the section:

$$\frac{\partial c_{ij}}{\partial \tau} = \gamma_j \left\{ \frac{1}{Pe_j} \frac{\partial}{\partial x} \left(C_T \cdot \frac{\partial y_{ij}}{\partial x} \right) - v_j \frac{\partial c_{ij}}{\partial x} \right\} - \frac{(1-\varepsilon)}{\varepsilon} \alpha (q_{ij}^* - q_{ij}) \quad (1)$$

where $\tau = \frac{t}{(L_j/u_s)}$, $x = \frac{z}{L_j}$ are the dimensionless time and axial coordinates, C_T is the total concentration and y_{ij} is the molar fraction in the fluid phase, c_{ij} and q_{ij} are the fluid phase and average adsorbed phase solute concentrations, and q_{ij}^* is the adsorbed phase concentration in equilibrium with c_{ij}; v_j is the interstitial fluid velocity, $Pe = v_j L_j \, / D_{Lj}$ is the Peclet number, $\alpha = k \, L_j / u_s$ is the number of mass transfer units, ε is the bed porosity and $\gamma_j = v_j / u_s$ is the ratio between fluid and solid interstitial velocities; t is time, z is distance from the section inlet, *k* is the mass transfer coefficient, and D_{Lj} is the axial dispersion coefficient in section j of the column.

Mass balance to the solid phase:

$$\frac{\partial q_{ij}}{\partial \tau} = \frac{\partial q_{ij}}{\partial x} - \alpha_j (q_{ij}^* - q_{ij}) \quad (2)$$

Similarly to the TMB, the SMB unit has four sections. Each section may have a different number of columns and each column may be considered as an independent fixed-bed unit connected to other columns. For a SMB unit with a given switching time t^*, and a given number of columns, each with a length L_c, the mass balance to each component i in the fluid phase in a given column c is expressed by:

$$\frac{\partial c_{ic}}{\partial \tau} = v_c \left\{ \frac{1}{Pe_c} \frac{\partial}{\partial x} \left(C_T \cdot \frac{\partial y_{ic}}{\partial x} \right) - \frac{\partial c_{ic}}{\partial x} \right\} - \frac{(1-\varepsilon)}{\varepsilon} \alpha (q_{ic}^* - q_{ic}) \quad (3)$$

where $\tau = \frac{t}{t^*}$ is the dimensionless time obtained by the ratio between the actual operation/simulation time and the switching time; and $x = \frac{z}{L_c}$ is the dimensionless axial coordinate; v_c is the interstitial fluid velocity, $Pe_c = \frac{v_c^* L_c}{D_{Lc}}$ is the Peclet number.

The mass balance to the solid phase for each component, i, in each bed, c, is given by:

$$\frac{\partial q_{ic}}{\partial \tau} = \alpha(q_{ic}^* - q_{ic}) \tag{4}$$

The case study adopted in this work was the bi-naphthol enantiomers separation using 3,5-dinitrobenzoyl phenylglycine bonded to silica gel as adsorbent and heptane-isopropanol as eluent. The adsorbed quantities in equilibrium for this system can be evaluated by dual site Langmuir isotherms. The parameters of the isotherm were estimated by Pais et al. (2000) through tests performed in an adsorption column with the chemical components of the system. The bi-Langmuir isotherms of this system are represented as:

$$q_A^* = \frac{2.69 c_A}{1 + 0.0336 c_A + 0.0466 c_B} + \frac{0.10 c_A}{1 + c_A + 3 c_B} \tag{5}$$

$$q_B^* = \frac{3.73 c_B}{1 + 0.0336 c_A + 0.0466 c_B} + \frac{0.30 c_B}{1 + c_A + 3 c_B} \tag{6}$$

One SMB cycle consists of the number of switches necessary for the system to come back to its initial positions. In this way, each column, along one cycle, will be part of the different sections. This is considered in the mathematical model by the change of the boundary conditions used for

each section at different times. The initial and boundary conditions presented below are valid for the TMB and SMB and therefore the indexes j and c are omitted, those conditions being valid for each columns/sections of the units. Hence, the boundary and initial conditions for each section or column of the TMB and SMB units can be expressed as:

$$\tau = 0; t = 0: \; c_i = q_i = 0 \tag{7}$$

The index 0 represents the inlet of a column (c) or a section (j). For example, $c_{i,0}$, is the inlet concentration of the component i.

$$x = 0; \; z = 0: \; c_i - \frac{D_L}{v_j}\frac{\partial c_i}{\partial z} = c_{i,0} \tag{8}$$

$x = 1; \; z = L$:

$$q_{iIV} = q_{iI,0}, \qquad q_{iI} = q_{iII,0}, \qquad q_{iII} = q_{iIII,0}, \qquad q_{iIII} = q_{iIV,0}, \tag{9}$$

For all columns in a node without an inlet stream (in the SMB process) including for the Extract and Raffinate nodes:

$$c_{i(j\ or\ c)-1} = c_{i(j\ or\ c),0} \tag{10}$$

For the Eluent node:

$$c_{i,IV} = \frac{Q_I}{Q_{IV}} c_{i,I,0} \tag{11}$$

For the Feed node:

$$c_{iII} = \frac{Q_{III}}{Q_{II}} c_{iIII,0} - \frac{Q_F}{Q_{II}} c_i{}^f \quad (12)$$

The node global balances can be expressed as:

$$Q_I = Q_{IV} + Q_E \quad (13)$$

$$Q_{II} = Q_I - Q_X \quad (14)$$

$$Q_{III} = Q_{II} + Q_F \quad (15)$$

$$Q_{IV} = Q_{III} - Q_R \quad (16)$$

And the unit global balance is given by:

$$Q_F + Q_E = Q_R + Q_X \quad (17)$$

where Q_E is the eluent flow rate, Q_X the extract flow rate, Q_F the feed flow rate, Q_R the raffinate flow rate.

The processes performance indicators are:

$$Pur_X = \frac{c_{X,i}}{\sum_{i=1}^{n_i} c_{X,i}} \quad (18)$$

$$Pur_R = \frac{c_{R,i}}{\sum_{i=1}^{n_i} c_{R,i}} \quad (19)$$

$$Rec_X = \frac{Q_X c_{X,B}}{Q_F c_{F,B}} \quad (20)$$

$$Rec_R = \frac{Q_R c_{R,A}}{Q_F c_{F,A}} \quad (21)$$

$$EC = \frac{Q_{E+}Q_F}{Q_F \sum_{i=1}^{n_i} C_{F,i}} \quad (22)$$

$$Pr = \frac{Q_F(c_{F,A} + c_{F,B})}{V_T} \quad (23)$$

where Pur_X, is the extract purity, Pur_R, is the raffinate purity, Rec_X, is the extract recovery, Rec_R, is the raffinate recovery, $C_{X,i}$, is the concentration of the component i in the extract stream, $C_{R,i}$, is the concentration of the component i in the raffinate stream and $C_{F,i}$, is the concentration of the component i in the feed stream, V_T, is the volume of the unit, *EC,* is the eluent consumption and Pr is the unit productivity. As a chiral separation is being considered as case study, the eluent is also present in the feed and therefore the eluent consumption is usually calculated as defined by Equation (22) (Rodrigues et al. 2015).

This model was validated by Pais et al. (2000) in a pilot plant located in the Laboratory of Separation and Reaction Engineering (LSRE). Three models here presented were implemented in the gPROMS modelling builder (Process Systems Enterprise 2015), as this is a suitable software for modelling complex processes. One model corresponds to the true moving bed system and

the other two models to simulated moving bed processes, one with four columns and another with eight columns. Each zone of the TMB and column of the SMBs are defined by 4 partial differential equations (PDEs), while the node balances and the Langmuir isotherms are algebraic equations (AEs). Therefore, the TMB and SMB-4 systems are described by a set of 16 PDEs and 9 AEs while the SMB-8 is described by a set of 32 PDEs and 9 AEs. The numerical method used to solve the PDE systems was orthogonal colocation in finite elements with 50 intervals and 2nd order polynomials.

P1-2.2. Study of the units dynamics

It is well known that each process variable has a different effect on the process response. In process control and optimization, it is very important to know the behaviour of the process before any variation in the operating conditions. These effects depend on the importance of each variable in the system, where some process variables may be correlated with others. The dependence between the different variables can lead to a masked effect if they are observed individually. During real operation of the unit, one or more process operating variables can vary simultaneously. The effect of a simultaneous variation is generally more intense than the effect of the variation of only one variable at a time. However, even in this case, it is expected that the intensity of the effect be dominated by the response observed for the variable that has greater impact in the process.

In terms of design, optimization and process control, it is important to know the isolated effect of each variable in the process performance parameters. Furthermore, a method to evaluate the

effect of each operating condition that takes in consideration the correlations between the other variables can be an important tool in this field. Once this is known the prediction of simultaneous variations can be done. Therefore, it is very important that all variables of the process be analysed simultaneously considering their correlations. It is well known that the effect of the variables in the response of a given system through time can be represented in a Jacobian or sensitivity matrix as Equation (24).

$$S = \begin{bmatrix} s'_{1,1}\big|_{t_1} & \cdots & s'_{1,n_p}\big|_{t_1} \\ \vdots & \ddots & \vdots \\ s'_{1,1}\big|_{n_t} & \cdots & s'_{1,n_p}\big|_{t_n} \\ \vdots & \vdots & \vdots \\ s'_{n_y,1}\big|_{t_1} & \cdots & s'_{n_y,n_p}\big|_{t_1} \\ \vdots & \ddots & \vdots \\ s'_{n_y,1}\big|_{n_t} & \cdots & s'_{n_y,n_p}\big|_{n_t} \end{bmatrix}_{(n_y \times n_t) \times n_p} \tag{24}$$

Defining s as the partial derivative of a given response y_i over a given operating condition, θ_p, in a given time, t, calculated by:

$$s_{i,p} = \left.\frac{\partial y_i}{\partial \theta_p}\right|_{t=t_n}, \quad p = 1,2,3,\dots,n_p;\ i = 1,2,3,\dots,n_y;\ \ t_n = \mathrm{t}_1,\dots,n_t; \tag{25}$$

where n_y is the number of process responses, n_p, the number of operating variables and n_t the total instants of time taken into consideration. Each column of the sensitivity matrix (which corresponds to a specific process indicator) is evaluated at different time instants from t_1 to n_t.

As each variable has different dimensions and order of magnitude, it is recommended the scaling of the partial derivatives. Yao et al. (2003) suggested that the scaling is done by the following Equation:

$$s'_{i,p} = \frac{\theta_p}{y_i}\frac{\partial y_i}{\partial \theta_p}\bigg|_{t=t_n} \tag{26}$$

where the $s'_{i,p}$ are the coefficients of the sensitivity matrix given in Equation (24). In this equation, the indicators and response values are calculated by the mathematical model at each time instant. By scaling the coefficients ($s'_{i,p}$), they have the same order of magnitude allowing an efficient comparison between the effect of the variables. It should be noted that the scaling is essential for the analysis and that other authors also recommend that the scaling is done by Equation (26) (Lin et al. 2010; Benyahia et al. 2013).

Since the objective of this analysis is to evaluate the effect of the operating conditions in the process, the scaled partial derivative presented in Equation (27) can be calculated through its numerical definition:

$$\frac{\theta_p}{y_i}\frac{\partial y_i}{\partial \theta_p}\bigg|_{t=t_n} = \frac{\theta_p}{\mathbf{y_i}}\frac{\mathbf{y_i}(t_n, \theta_p + \Delta\theta_p) - \mathbf{y_i}(t_n, \theta_p)}{\Delta\theta_p} \tag{27}$$

Each column of the matrix represents the influence of a given operating variable and each line represents the response of the model in a given instant. The final dimension of this matrix is the number of responses evaluated, n_y, times the number of instants considered, n_t, per number of process variables, n_p. It should be noted that this matrix takes into consideration the dynamics

of the system. Finally, the dynamic Jacobian matrix contains the influence of all operating variables on all responses in a given operating period. This is an important information about the influence of the operating conditions on the process behaviour. However, a tool that can extract this information from the matrix is still necessary.

Considering each column of the Jacobian matrix as a vector, each vector can be correlated with the others, and one can use a statistic tool or an algebraic tool to analyse the behaviour of these vectors in the system. Many tools are available in literature, such as, the Principal Component Analysis, Height Values and Height Vector Analysis, and Gram-Schmidt Orthogonalization Method. Those methods are well known in the field of parameters estimation and model reduction analysis, used as tools of the process called “Identifiability or Estimability analysis” (Lund and Foss 2008; Quaiser and Mönnigmann 2009; Wu et al. 2012; Kravaris et al. 2013).

Among the tools available, the orthogonalization method can be highlighted. It is an algebraic concept that takes into consideration the correlation between vectors. The method is simple to implement in an algorithm and has shown good results in the field of parameters estimation (Quaiser and Mönnigmann 2009; Zhao and Stadtherr 2011; Kravaris et al. 2013). With these considerations, the present work adopts this tool as the basis for the processes analyses here described.

P1-2.2.1. The orthogonalization method

The orthogonalization method was first proposed by Yao et al. (2003). The method shows efficient results solving problems in the field of parameters estimation in complex models of systems with a large number of parameters. The methodology proposed in this work is based on the orthogonalization method introduced by Yao et al. (2003) for estimation analysis, adapted here for the assessment of the influence of operating conditions on the performance indicators. A method capable of investigating the influence of the operating variables along time in a cyclic adsorption process based on a True Moving Bed model is therefore developed.

To use the orthogonalization method, first an indicator of the importance of each matrix column in the vector space is necessary. Considering each column of the Jacobian Matrix as a vector, its importance can be measured by the vector length calculated as:

$$\|\vec{a}\| = \sqrt{a_1^2 + a_2^2 + \cdots + a_{n_v}^2} \tag{28}$$

where $\vec{a}$ is a generic vector and n_v represents the number of elements of the vector. To make the evaluation simpler a new variable can be defined, the magnitude (M) that is equal to:

$$M = \|\vec{a}\|^2 = \sum_{i=1}^{n_v} a_{\mathrm{i}}^2 \tag{29}$$

The magnitude provides the information about the length of the vector and consequently the total influence of each process variable in its response. The larger the magnitude value, the more important is that variable in the process.

For example, in a system with four main variables the influence of each variable in the process response over time can be represented as shown in Figure 4. The Jacobian matrix of the system is the vector space formed by the four vectors represented in the figure by: $S^{(1)}_1$, $S^{(1)}_2$, $S^{(1)}_3$ e $S^{(1)}_4$.

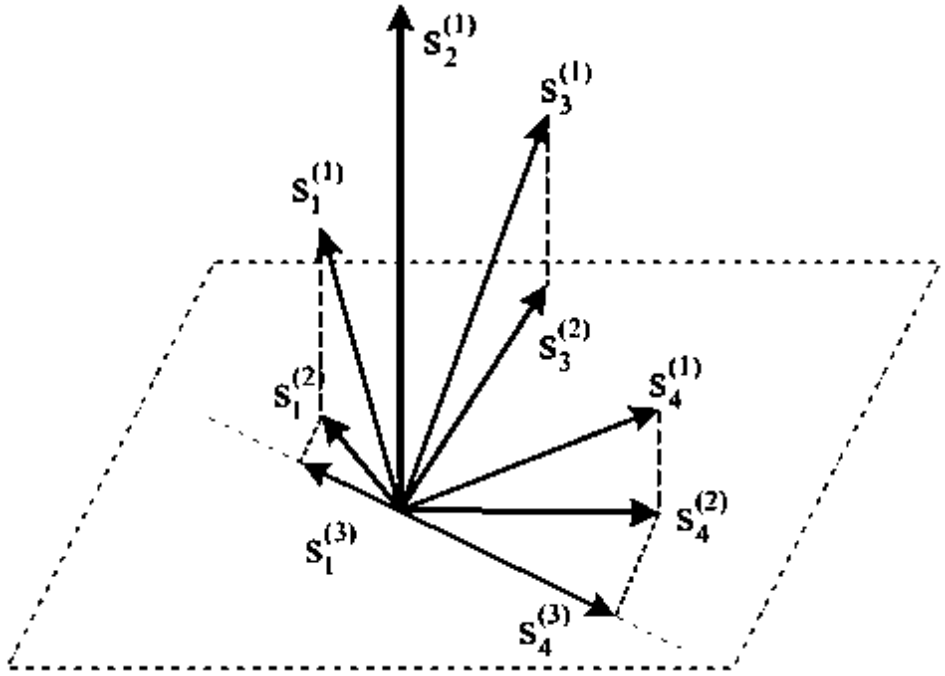

Figure 4 - Gram-Schmidt Orthogonalization Method. (Adapted from: Kravaris et al., 2013).

The magnitude of each vector can be evaluated and the variable with the highest impact in the process determined. In Figure 4, this variable corresponds to the vector S_2. After selecting the main operating variable in the process, the importance of the remaining vectors is evaluated. At

this point the Gram-Schmidt Orthogonalization Method is applied in order to eliminate the possible correlations between the remaining process variables and the previously selected one. In the figure, it can be noted that the three remaining vectors are correlated with S_2 since they are linearly dependent. The orthogonalization projects the remaining vectors in a plane perpendicular to the selected vector. Therefore, the remaining vectors have no influence from the previous ones and the analysis can continue with the projected vectors $S^{(2)}$. The orthogonalization can be done as:

$$S^O = S_{max}\left({S_{max}}^T S_{max}\right)^{-1} {S_{max}}^T S \tag{30}$$

where S^O is a new matrix formed by the projected vectors in the new orthogonal vector space, S_{max} is the vector over which the system was orthogonally projected. Through Equation (30) one notes that the matrix S^O has only one column that does not change in comparison with the Jacobian matrix. That column corresponds to the vector S_{max}. A new matrix that does not contain any information about the vector previously selected can then be used, the residual matrix (R). This matrix can be calculated by:

$$R = S - S^o \tag{31}$$

With the residual matrix, the magnitude of its columns can be calculated again and the next operating condition with the second largest effect in the process selected. The analysis follows the same procedure as described above until all vectors are analysed or until when the magnitude of the vectors reaches a minimum value that can be defined as a criterion to finish the analysis.

All these steps are generically represented in Figure 4, where the superscript in the vectors indicates the current step. In Figure 5, the analysis is detailed in a logical flowsheet. The main difference between the method here presented and the one proposed by Yao et al. (2003) can be observed in the second column of the flowsheet in Figure 5. In the previously proposed method, after the column of the residual matrix with greater magnitude is selected, the orthogonalization is done over the first Jacobian matrix S. Here, it is proposed to do the orthogonalization over the residual matrix R. Using this approach, the calculation of the residual matrix eliminates the columns of the previous selected vectors, and the successive orthogonalization of the produced residual matrix ensures that the method, at each step, takes into consideration only the vectors not yet selected. This cannot be guaranteed if the orthogonalization is continuously done over the S matrix. As the main objective of the method here presented is to analyse the influence of the operating variables in the process response, the previous consideration is important.

The limitation of this method is its dependence on the values of the process variables. That limitation can be suppressed by using information from the literature, by previous expertise on the process or by performing a previous steady state study of the process. The proposed method was first employed in the analysis of a chiral separation adsorption process represented by a true moving bed model in order to test the method consistence. After this, the method was used to analyse the other models studied in this work.

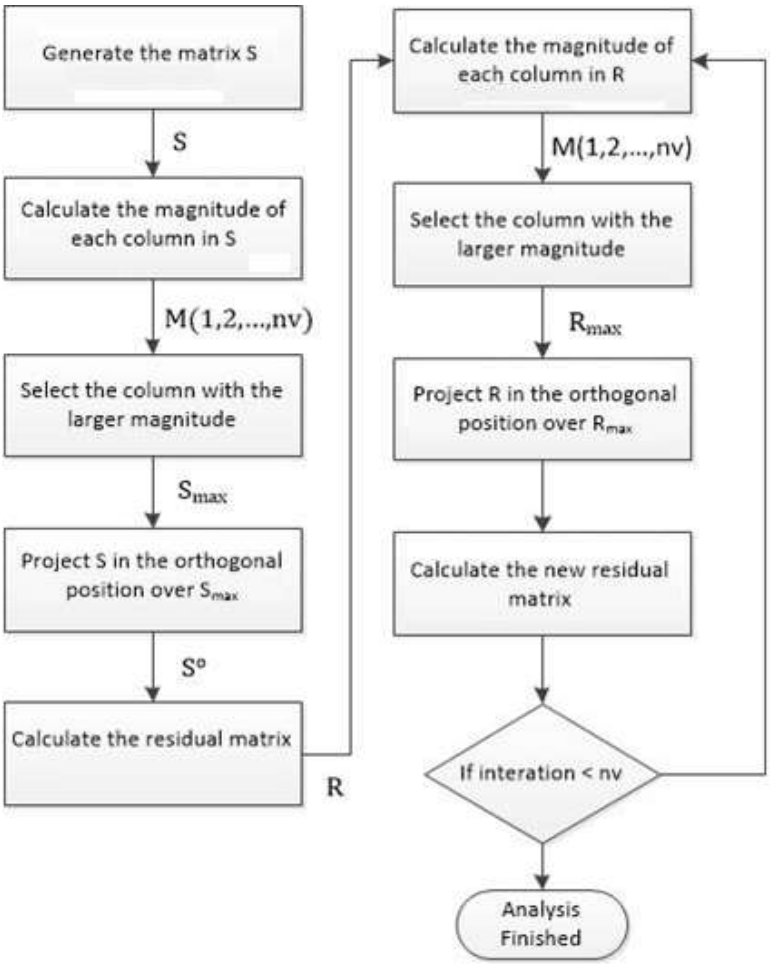

Figure 5 - Flowsheet of the proposed process analysis.

The above presented method is the basis for the analysis of the influence of the operating parameters on the dynamics of the systems. Through the orthogonalization method, it is possible to verify the influence of the operating variables in the processes responses during the transient and steady states. The method will also serve as a basis for the identification of the manipulated variables in the processes control and in the empirical modelling.

The Gram-Schmidt Orthogonalization analysis here presented was implemented in the MatLab software. To run the analysis, a communication between gPROMS, where the process models

were written, and MatLab, was used through the go:MATLAB extension (Process Systems Enterprise 2015). It was possible for MatLab to run externally the model and collect the responses of the process simulation.

P1-2.3. Control system development and linear functions identification

A plot of the output response of a process to a step change in input is sometimes referred to as the process reaction curve. If the process can be approximated by a linear model, the model parameters can be obtained by inspection of the process reaction curve (Seborg et al. 2003). The traditional way to identify transfer functions of complex processes consists in performing a step perturbation in an operating (inlet) variable and, through the process reaction (outlet) curve, adjust the parameters of a given transfer function.

The dynamics of an SMB/TMB system becomes more complex as it gets closer to the optimal point, at which purity and recovery constraints are both satisfied. This can be seen in Figure 6, which presents responses of the purity in the extract stream of a TMB unit to step perturbations in the recycling flow rate, of a process operating in optimal conditions and of a process operating in non-optimal conditions. Four step perturbations were performed, two of 10% above the initial value of the recycling flow rate (before the instant 2500 min, the first between the instants 10 – 800 min and the second between the instants 1400 – 2000 min), and two others of 10% below the initial value of the recycling flow rate (after the instant 2500 min, the first between the

instants 2500 – 3100 min and the second between the instants 3500 – 4100 min). In Figure 6, the line closer to 1 is the response of the system in its optimal point while the response line closer to the 0.7 value corresponds to the one in non-optimal conditions. It is possible to note that, at the non-optimal point, positive and negative steps correspond respectively to purity increase and decrease. On the other hand, the responses at optimal conditions show a decrease in purity for both types of steps. It is in this sense that the process is referred as having a more complex dynamic. Consequently, the usual way to identify the process transfer function, through the process reaction curve, cannot be directly applied in this case. This occurs because any perturbation at the optimal condition may lead the process to a point outside of the zone of complete separation and adsorbent/eluent regeneration. In this way, in the industry these units are usually operated in suboptimal conditions to avoid these problems in the process. However, the process control at its optimal conditions would reduce the process loss due to a suboptimal operation. In order to allow the identification of linear models through the process reaction curve at the optimal point, it is proposed the employment of a transfer function switching system, Figure 7.

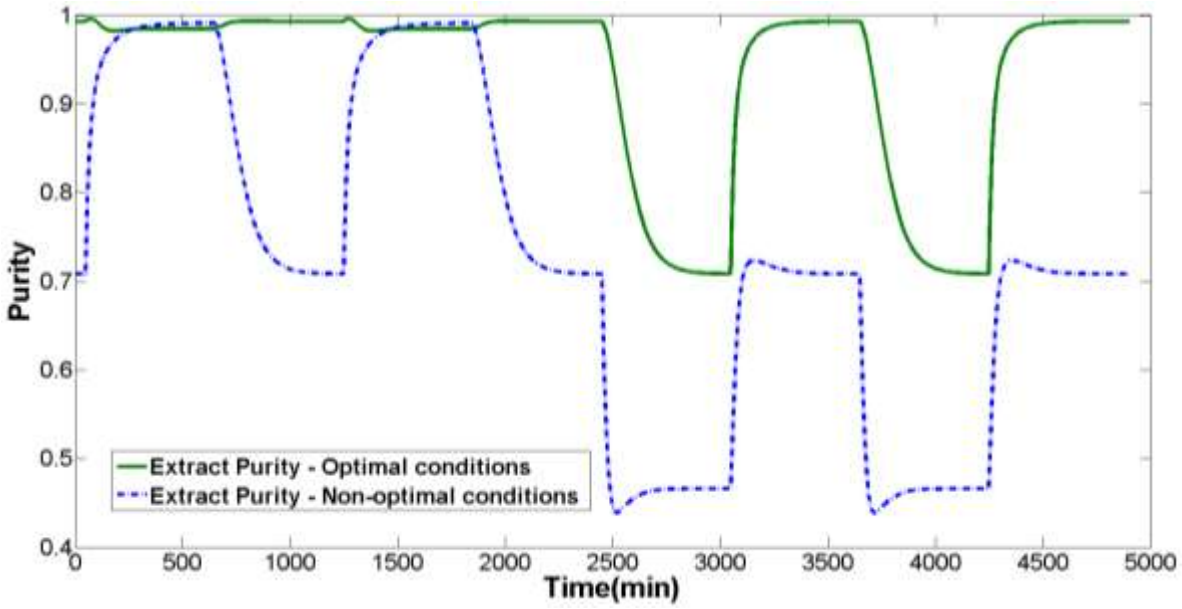

Figure 6 - Responses of the purity in the extract stream to step perturbations in the recycling flow rate. Comparison between the responses in the optimal and non-optimal conditions.

In the present work, it is proposed the identification of two local transfer functions in order to overcome the aforementioned problems. One transfer function to a step perturbation corresponding to an increase in the process flow rates and another transfer function (TF) to a step perturbation corresponding to a decrease in the flow rates. Once the two local TFs are identified, they are employed in the controller through a switching system, Figure 7, where the most adequate TF is used to predict the process future behaviour. The system consists in an on/off switch, where the response of one of the transfer functions is selected in accordance to the variation in the flow rates, as presented in Figure 7. In this way, it is expected to improve the performance of the predictive control in comparison with the traditional employment of this technique. A model predictive controller is based on an optimizer, where the future inputs are computed through the solution of the system objective function, and a predictive model, where

the predicted outputs are computed using the future inputs. In the present work, a switching system is proposed, which consists in the selection of the transfer function to perform the predictions in accordance with the variation of a given manipulated variable, Q_{MV}; this means that, depending on whether the difference between the future value of Q_{MV} and its past value is positive or negative, ΔQ<0 or ΔQ>0, a different transfer function is chosen to perform the prediction.

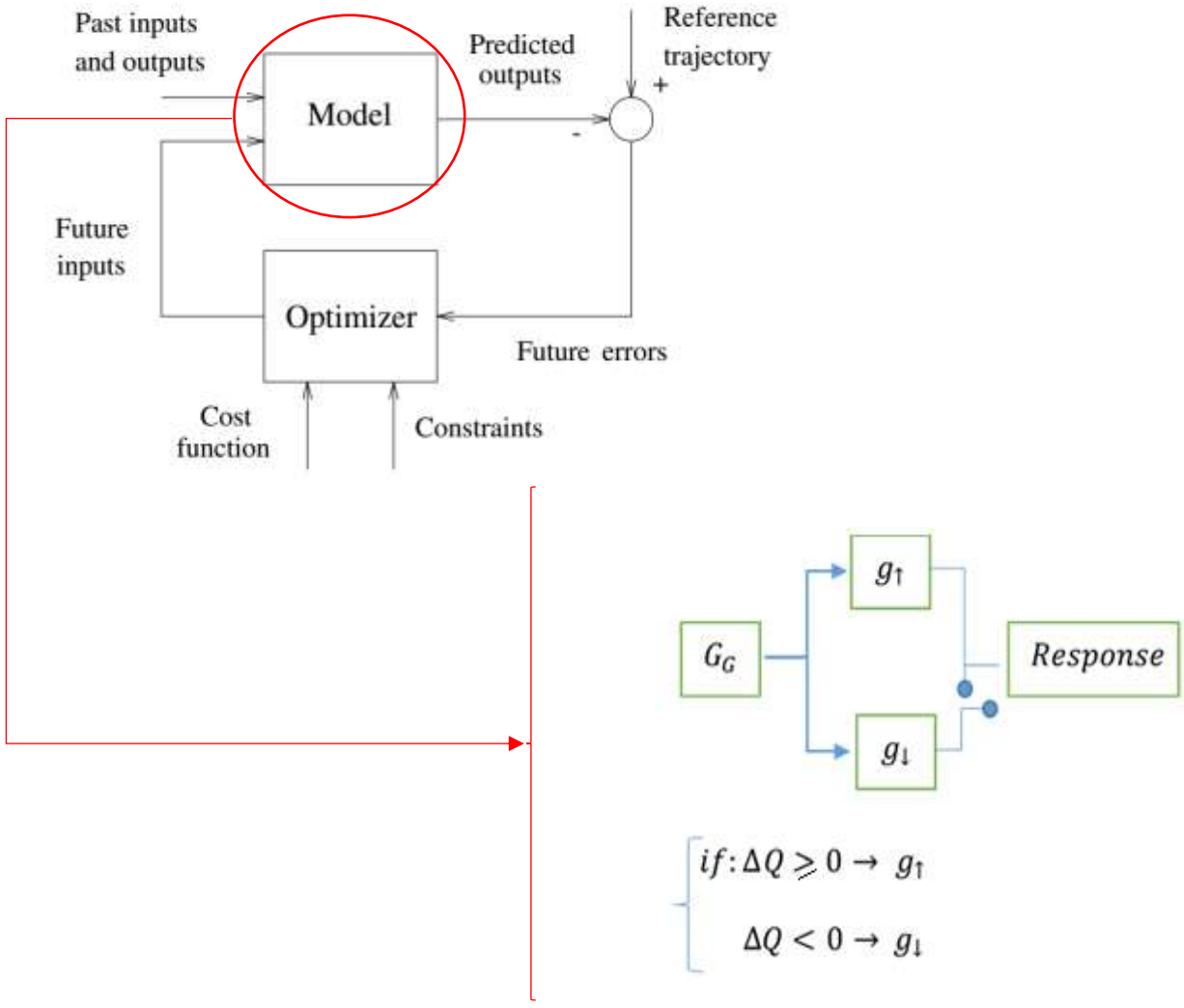

Figure 7 - Schematic representation of the switching system proposed.

As mentioned above, it was possible to note in Figure 6 that, as the operating point moves away from the optimal point, the process dynamic behaviour becomes simpler. Then, using a point far from the optimal, it becomes possible to identify a transfer function through the traditional procedure (process reaction curve – G_{RC}). In order to test the transfer function identification methodology here proposed, two matrices of transfer functions were generated from the operation of the process at non-optimal conditions (as shown in Figure 6) for the traditional identification method (G_{RC}) and two matrices of transfer functions for the proposed method ($G_{G\ non\text{-}opt}$). The matrices G_{RC} and $G_{G\ non\text{-}opt}$ were applied in an MPC control system and the control performance was compared. It is expected to obtain equally efficient control systems with both transfer functions if the proposed methodology can represent the process with precision. Additionally, another set of TFs was identified with the methodology here proposed, but starting with the system operating at optimal conditions ($G_{G\ opt}$).

P1-2.3.1. Control Strategy

The model predictive control is based on the future predictions of process output variables over a determined prediction horizon, p. The process outputs are predicted with respect to their past values, $y(k+1|k)$, and the present inputs, u, the manipulated variables.

The control system is related with an optimization problem that minimizes the difference between the future values of the process output and the set point through smooth movements

in the input variables. The optimization problem is evaluated under the process restrictions, such as the limits of the manipulated variables. At each time instant, k, the controller sends to the process the optimal values of the manipulated variables in order to keep the process in the desirable operating point (Lee 2007).

The general formulation of an MPC optimization problem can be expressed as:

$$\min_{\Delta u} V(k) = \sum_{j=1}^{p} \left\| y(k+j|k) - y_{sp} \right\|_Q^2 + \sum_{j=0}^{m-1} \left\| \Delta u(k+j|k) \right\|_R^2 \tag{32}$$

Subject to:

$\Delta u(k+j) \in \mathbb{U}$,

$$\mathbb{U} = \begin{cases} -\Delta u_{max} \leq \Delta u(k+j) \leq \Delta u_{max} \\ \Delta u(k+j|k) = 0, \forall_j \geq m \\ -u_{min} \leq u(k-1) + \sum_{i=1}^{j} u(k+j|k) \leq u_{max} \end{cases} \tag{33}$$

where Q and R are the diagonal matrices that represent the weights of each term of the objective function. The controller objective function is given by:

$$\begin{aligned} \min_{\Delta u} V(k) = \sum_{j=1}^{p} (& \left\| P_X(k+j|k) - y_{sp,P_X} \right\|_{Q_1}^2 + \left\| P_R(k+j|k) - y_{sp,P_R} \right\|_{Q_2}^2 \\ & + \left\| R_X(k+j|k) - y_{sp,R_X} \right\|_{Q_3}^2 + (\left\| R_R(k+j|k) - y_{sp,R_R} \right\|_{Q_4}^2) \\ & + \sum_{j=0}^{m-1} (\left\| \Delta Q_{Iv}(k+j|k) \right\|_{R_1}^2 + (\left\| \Delta Q_X(k+j|k) \right\|_{R_2}^2 + (\left\| \Delta Q_S(k+j|k) \right\|_{R_3}^2 \\ & + (\left\| \Delta Q_E(k+j|k) \right\|_{R_4}^2 \end{aligned} \tag{34}$$

The control strategy is formulated here from an offset-free control law in a one-step optimization problem. This formulation is based on Alvarez and Odloak (2012), where the detailed rules to obtain the matrices can be found. Based on a state space representation, it considers the integral action through the incremental form of its inputs to predict the process future behaviour. In the present case, the state space approach is deduced from the transfer function matrices of the process obtained through the methodology here proposed:

$$\begin{bmatrix} x^s(k+1) \\ x^d(k+1) \\ z_1(k+1) \\ z_2(k+1) \\ \mathsf{M} \\ z_p(k+1) \end{bmatrix} = \begin{bmatrix} I_{ny} & 0 & B_1^s & B_2^s & \ldots & B_{p-1}^s & B_p^s \\ 0 & F & B_1^d & B_2^d & \ldots & B_{p-1}^d & B_p^d \\ 0 & 0 & 0 & 0 & \ldots & 0 & 0 \\ 0 & 0 & I_{nu} & 0 & \ldots & 0 & 0 \\ \mathsf{M} & \mathsf{M} & \mathsf{M} & \mathsf{O} & \ldots & \mathsf{M} & \mathsf{M} \\ 0 & 0 & 0 & 0 & \ldots & I_{nu} & 0 \end{bmatrix} \begin{bmatrix} x^s(k) \\ x^d(k) \\ z_1(k) \\ z_2(k) \\ \mathsf{M} \\ z_p(k) \end{bmatrix} + \begin{bmatrix} B_0^s \\ B_0^d \\ I_{nu} \\ 0 \\ \mathsf{M} \\ 0 \end{bmatrix} \Delta u(k) \tag{35}$$

$$y(k) = \begin{bmatrix} I_{ny} & \Psi & 0 & 0 & \ldots & 0 \end{bmatrix} \begin{bmatrix} x^s(k) \\ x^d(k) \\ z_1(k) \\ z_2(k) \\ \mathsf{M} \\ z_p(k) \end{bmatrix} \tag{36}$$

Where:

$$\Psi = \begin{bmatrix} \Phi & & 0 \\ & O & \\ 0 & & \Phi \end{bmatrix} \in \mathsf{R}^{ny \times nd}$$, $\Phi = \begin{bmatrix} 1 & \mathsf{L} & 1 \end{bmatrix} \in \mathsf{R}^{nu.na}$, $x^s(k) \in \mathsf{R}^{ny}$, $p = \max_{i,j} \gamma_{i,j}$, $x^d(k) \in \mathsf{R}^{nd=ny.nu.\max(na)}$

, $z_1(k), \mathsf{K}, z_p(k) \in \mathsf{R}^{nu}$, $x(k) \in \mathsf{C}^{nx}$, and $nx = ny + nd + p.nu.$

Considering that a process system is composed of ny outputs and nu inputs, and each pair (y_i, u_j) comprises na distinct stable poles and its corresponding time delay is designated as $\gamma_{i,j}$, the matrices $B^s_{l=0,K,p}$ and $B^d_{l=0,K,p}$ are expressions of the coefficients of the partial fractions expansion of the step response, F is a diagonal matrix with components corresponding to the stable poles, and I_{ny} and 0_{ny} are the identity and null matrices of dimension ny, respectively. Furthermore, in the system representation described by Equations (35) and Equation (36), the vector x^s represents the integrating states produced by the incremental form of the inputs, which is associated with the predicted output steady-state, and x^d corresponds to the stable states of the system.

In this system, it is not possible to measure all state variables. This is why it was necessary to employ a state estimator to predict future states from actual output measurements. For that purpose, a Kalman filter is used inside the controller in order to update the process present state at each instant. The details about the development of this filter can be found in the literature (Welch and Bishop 2006).

The transfer functions and control strategy here presented were implemented in the MatLab software. To run the FTs identification and simulation, a communication between gPROMS, where the models were written, and MatLab, was used through the go:MATLAB extension

(Process Systems Enterprise 2015). It was possible for the control systems in MatLab to run externally the model and collect the responses of the process simulation.

P1-2.4. Virtual analyser development

The most common structure of an artificial neural network (ANN) model is the feedforward, in which there are no feedback communications between neural layers. This structure can solve efficiently complex problems, such as pattern recognition. However, in dynamic systems, in which the present output depends on the past inputs and outputs, these models need to be modified to be applied. To do that, a feedback system is built in which the outlet layer of the neural model is connected to the inputs layer. The backpropagation of the past outputs to make the future prediction is done in order to compute the process dynamics, i.e., in order for the virtual analyser to compute the influence of the past system state in the present response. The development of the predictor equations of the ANN model used in this work is presented in the next sub-section.

P1-2.4.1. Predictor equations

The Nonlinear Auto Regressive Moving Average with Exogenous inputs (NARX) and Nonlinear Output Error (NOE) are the most important representations of nonlinear systems (Koivisto 1995). The NARX model can be expressed by Equation (37) considering a given dynamic system with

white noise $v(t)$, its actual output y, which depends on the past behaviour and of the present inputs, u.

$$\boldsymbol{y}(t) = \boldsymbol{F}[\boldsymbol{y}(t-1), \dots, \boldsymbol{y}(t-1-n_a), \boldsymbol{u}(t-d), \dots, \boldsymbol{u}(t-d-n_b+1)] + \boldsymbol{v}(t) \quad (37)$$

Where, y are the output values, u are the process input values, n_a, n_b the number of past values and d is the delay.

In the case of the Nonlinear Output Error model it can be described as below:

$$\begin{aligned} \boldsymbol{z}(t) &= \boldsymbol{F}[\boldsymbol{z}(t-1), \dots, \boldsymbol{z}(t-1-n_a), \boldsymbol{u}(t-d), \dots, \boldsymbol{u}(t-d-n_b+1)] \\ \boldsymbol{y}(t) &= \boldsymbol{z}(t) + \boldsymbol{v}(t) \end{aligned} \quad (38)$$

where $\boldsymbol{z}$ is the output prediction. These models are identified as normal one-step-ahead predictors but can be used for multistep purposes. A minimum variance one-step-ahead NARX predictor is:

$$\hat{\boldsymbol{y}}(t) = \boldsymbol{f}[\boldsymbol{y}(t-1), \dots, \boldsymbol{y}(t-1-n_a), \boldsymbol{u}(t-d), \dots, \boldsymbol{u}(t-d-n_b+1), \boldsymbol{\theta}] \quad (39)$$

where, $\boldsymbol{f}(\varphi, \boldsymbol{\theta})$, is some parameterized function. The same representation can be applied to the NOE case, as:

$$\begin{aligned} \hat{\boldsymbol{z}}(t) &= \boldsymbol{f}[\hat{\boldsymbol{z}}(t-1), \dots, \hat{\boldsymbol{z}}(t-1-n_a), \boldsymbol{u}(t-d), \dots, \boldsymbol{u}(t-d-n_b+1), \theta] \\ \hat{\boldsymbol{y}}(t) &= \hat{\boldsymbol{z}}(t) \end{aligned} \quad (40)$$

As can be noted in Equation (40), the NOE model depends on its past predictions in order to evaluate the present output value. In the NARX, Equation (39), the prediction of the present

output relies only on independent variables, past values of inputs and outputs. Thus, the training of a NOE model becomes much more complicated than the training of a NARX model, since the partial derivative of its predictions in order to time depends on the partial derivative of its parameters, which are being estimated.

The correct training of the NOE demands the use of gradient descent techniques with dynamic gradient calculation, because of its recurrent nature (Roy et al. 1999). Therefore, the normal approach in the literature is to employ a NARX model in the development of an ANN model. However, when the application is to perform long-term prediction or simulation, the NOE approach is more indicated.

The present work proposes the development of a NARX based ANN model to perform long-term predictions. As previously stated, this approach is easier to train, but not the most adequate for the application. To overcome this problem, it is proposed to use a correcting error system, through the experimental measurements available, in an integrated system of predictions and measurement here called Quasi-Virtual Analyser (Q-VOA).

The implementation of the NARX representation in a neural model is usually done in the literature to model dynamic systems (Su and McAvoy 1993; Wang et al. 2003; Costa et al. 2008; Noor et al. 2010). However, the NARX model, Equation (38) and Equation (39), is defined in the form of one-step-ahead prediction for the outputs. Therefore, this is not a recommended approach for systems with high dead time measurement, since for those systems it is necessary to perform multi-step-ahead predictions during the time for which there are no measurements.

In this sense, the multi-step-ahead prediction is similar to model predictive control systems, where it is necessary to perform multiple step predictions during the control.

The NARX and NOE models here presented include a static nonlinear function approximation (function $\boldsymbol{f}$) and time delay lines. Those approaches were proposed in a way that any efficient function approximator can be applied. Several different approximations have been used in literature, like Artificial Neural Network models (Gonzaga et al. 2009; Delnavaz et al. 2010; Li et al. 2016; Sánchez et al. 2018), Fuzzy models (Frank et al.; Lima et al. 2009), adaptive network-based fuzzy inference system (ANFIS) (Jalee and Aparna 2016; Al-Dunainawi et al. 2017) models and support vector machine (SVM) models (Liu et al. 2010, 2016). Among those approaches the ANN models with Multilayer Perceptron (MLP) structure have been pointed out as easy to adapt to process time series and can solve complex problems efficiently (Narendra and Parthasarathy 1990; P. Menezes Jr. and Barreto 2006; Menezes and Barreto 2008; Schaul et al. 2015). In this way, the present work applies ANN based on MLPs as function approximator, since it has been presented in the literature as suitable to solve complex problems and presents the required flexibility in its architecture, which is necessary to implement the Q-VOA system.

P1-2.4.2. Multistep Predictor

The main task is to formulate the predictive equations in the presence of Integrated (I) or Integrated Moving Average (IMA) noise.

For convenience purposes, the time t here represents k future step. The most recent measurement, $y(t)$, is known and the corrective prediction error, $\epsilon(t|t)$, can be computed: the task is to compute recursively future k-step ahead predictions $\hat{y}(t+i|t), i = 1, \dots, k$ which take into account recent prediction errors. The final prediction $\hat{y}(t+k|t)$ is used as Virtual Sensor output.

The design task is now analogous to a normal MPC predictor design, except that, the future inputs $\mathrm{u}(t+i-1), i = 1, \dots, k$ are known. It is possible to adopt any additive noise model and use the existing literature for the multistep predictor design. Here, the development presented in Koivisto (1995) and Tian et al. (2014) is followed.

A typical noise model for multistep prediction is additive integrated white noise. The NARX-I process is assumed:

$$\boldsymbol{y}(t) = \boldsymbol{F}[\boldsymbol{y}(t-1), \dots, \boldsymbol{y}(t-1-n_a), \boldsymbol{u}(t-d), \dots, \boldsymbol{u}(t-d-n_b+1)] + \frac{\boldsymbol{v}(t)}{\Delta} \tag{41}$$

here $\boldsymbol{v}(t)$ is white noise and $\Delta = 1 - q^{-1}$ is included to allow the representation of integrated noise / trend like disturbances. The corresponding NOE-I is:

$$\begin{aligned} \boldsymbol{z}(t) &= \boldsymbol{F}[\boldsymbol{z}(t-1), \dots, \boldsymbol{z}(t-1-n_a), \boldsymbol{u}(t-d), \dots, \boldsymbol{u}(t-d-n_b+1)] \\ \boldsymbol{y}(t) &= \boldsymbol{z}(t) + \frac{\boldsymbol{v}(t)}{\Delta} \end{aligned} \tag{42}$$

Therefore, for the NOE case, the correction is computed at every time step when the delayed measurement is available (assuming $d = 1$ now to keep the notation simple):

$$\boldsymbol{\epsilon}(t|t) = \boldsymbol{y}(t) - \hat{\boldsymbol{z}}(t) = \boldsymbol{y}(t) - \boldsymbol{f}(\boldsymbol{\varphi}(t), \boldsymbol{\theta}) \;\; with$$
$$\boldsymbol{\varphi}(t) = [\hat{\boldsymbol{z}}(t-1), \dots, \hat{\boldsymbol{z}}(t-1-n_a), \boldsymbol{u}(t-1), \dots, \boldsymbol{u}(t-n_b)] \tag{43}$$

After that, the multistep predictors can be computed for $i = 1, \dots, k$ as:

$$\hat{\boldsymbol{z}}(t+i) = \boldsymbol{f}(\boldsymbol{\varphi}(t+i), \boldsymbol{\theta}) \;\; with$$
$$\boldsymbol{\varphi}(t+1) = [\hat{\boldsymbol{z}}(t+i-1), \dots, \hat{\boldsymbol{z}}(t+i-1-n_a), \boldsymbol{u}(t+i-1), \dots, \boldsymbol{u}(t+i-n_b)] \tag{44}$$
$$\hat{\boldsymbol{y}}(t+i) = \hat{\boldsymbol{z}}(t+i) + \epsilon(t|t)$$

Most of the internal predictor values $\hat{\boldsymbol{z}}(t+i)$ are already computed. Only the newest should be computed and the recent correction $\epsilon(t|t)$ is added to all of them. The final prediction value $\hat{\boldsymbol{y}}(t\ +\ k)$ is used as the soft sensor output.

For the NARX-I case this is more complex. To perform multistep-ahead predictions, the past process output samples in the model input vector $\boldsymbol{\varphi}$ are gradually replaced by their predicted values. For this, an auxiliary measurement state vector, $\boldsymbol{y_m}(t)$, is defined. At every time step:

$$\boldsymbol{y_m}(t-j) = \boldsymbol{y}(t-j), \qquad \forall_j = 1, \dots, n_a - 1 \tag{45}$$

When a new measurement is available, the corrector is computed as:

$$\boldsymbol{y_m}(t) = \boldsymbol{y}(t)$$
$$\boldsymbol{\epsilon}(t|t) = \boldsymbol{y_m}(t) - \boldsymbol{f}(\boldsymbol{\varphi}(t), \boldsymbol{\theta}) \;\; with \tag{46}$$
$$\boldsymbol{\varphi}(t) = [\boldsymbol{y_m}(t-1), \dots, \boldsymbol{y_m}(t-n_a), \boldsymbol{u}(t-1), \dots, \boldsymbol{u}(t-n_b)]$$

After that, the multistep predictors can be computed for $i = 1, \dots, k$ as:

$$\boldsymbol{y_m}(t+i) = \boldsymbol{f}(\boldsymbol{\varphi}(t+i), \boldsymbol{\theta}) + \epsilon(t|t) \;\; with$$
$$\boldsymbol{\varphi}(t+1) = [\boldsymbol{y_m}(t+i-1), \dots, \boldsymbol{y_m}(t+i-1-n_a), \boldsymbol{u}(t+i-1), \dots, \boldsymbol{u}(t+i-n_b)] \quad (47)$$
$$\hat{\boldsymbol{y}}(t+i) = \boldsymbol{y_m}(t+i)$$

Plant model mismatch is continuously compensated in the multistep recursive model prediction propagation, which improves the accuracy of multistep prediction. This requires the whole sequence to be recomputed at every time step. The final prediction value $\hat{\boldsymbol{y}}(t+i)$ is used as the soft sensor output. Finally, the neural model that composes the virtual analyser can be expressed as presented in Figure 8.

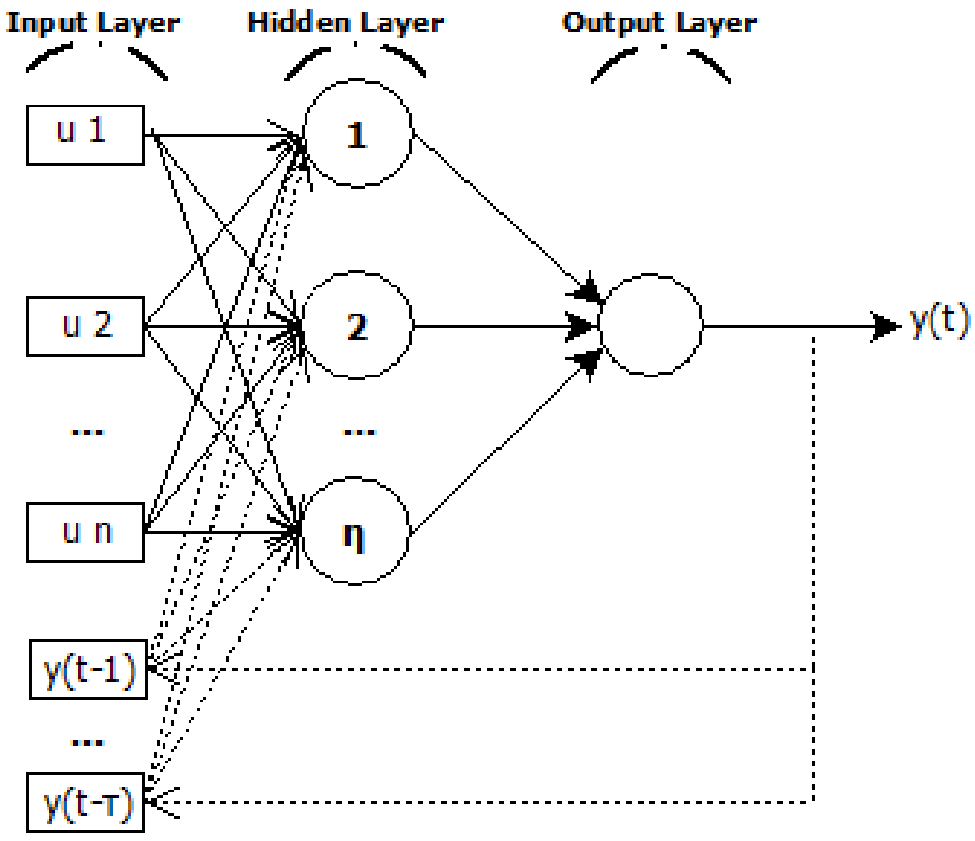

Figure 8 - General representation of the artificial neural network.

P1-2.4.3. Quasi-Virtual Analyser structure

In this work, a measurement system based on a virtual analyser and an offline measurer are proposed to make the online monitoring of the purity of a SMB unit. To do this, the analyser must be linked to the process and receive the information of the process inputs in real time. Figure 9 shows the schematic representation of the proposed system.

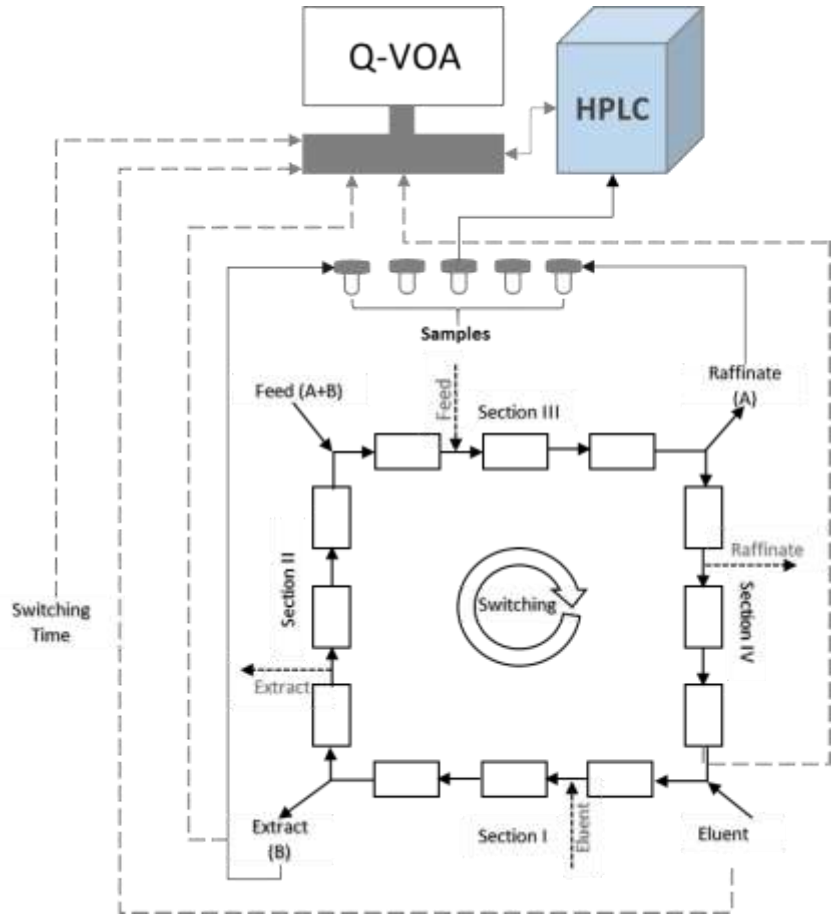

Figure 9 - Schematic representation of the proposed virtual analyser.

The system consists in a virtual analyser based on a neural model, which makes real time predictions using the process inputs and the past predictions, and is actualized by laboratory

measurements, when available, and if the measurements are in accordance with the process behaviour, as explained later on.

From the previous deduction, presented in Section P1-2.4.2, it is possible to note that the Q-VOA takes in consideration the current measurement and the past predictions. However, due to the large delay, a past measurement can refer to a process behaviour different from the present one and it may impair the virtual analyser prediction. This is so because any prediction will be about 10 minutes in advance of the measurement. In this case, the measurement can bring back the predictions to a past point that may be far from the present state.

In order to avoid the previously mentioned problem, the virtual analyser should verify its own derivative and the variation between its prediction and the previous measurements. If the difference between the prediction and the measurement is large this can lead to two different conclusions, either the system is on a transient regime or the VOA presents an offset in its prediction. The derivative test provides a way to evaluate in which scenario the process is. If the derivative of the analyser predictions is large, it means that the process is in a transient regime. In this case, the analyser should not use that measurement to make its actualization. In other words, the virtual analyser has to assess the error between its prediction and the measurements, and its own derivative, and then make a balance. Two weights are introduced, one for each criterion, w_d, the derivative weigth, and w_m, the measurement/prediction error. The adjustment of these weights will lead to the tuning of the virtual analyser, as is presented in the Results chapter. The Q-VOA internal structure is schematically represented in Figure 10, where the

subscript n, refers to the total number of process inputs evaluated and T refers to the total number of past outputs used as inputs.

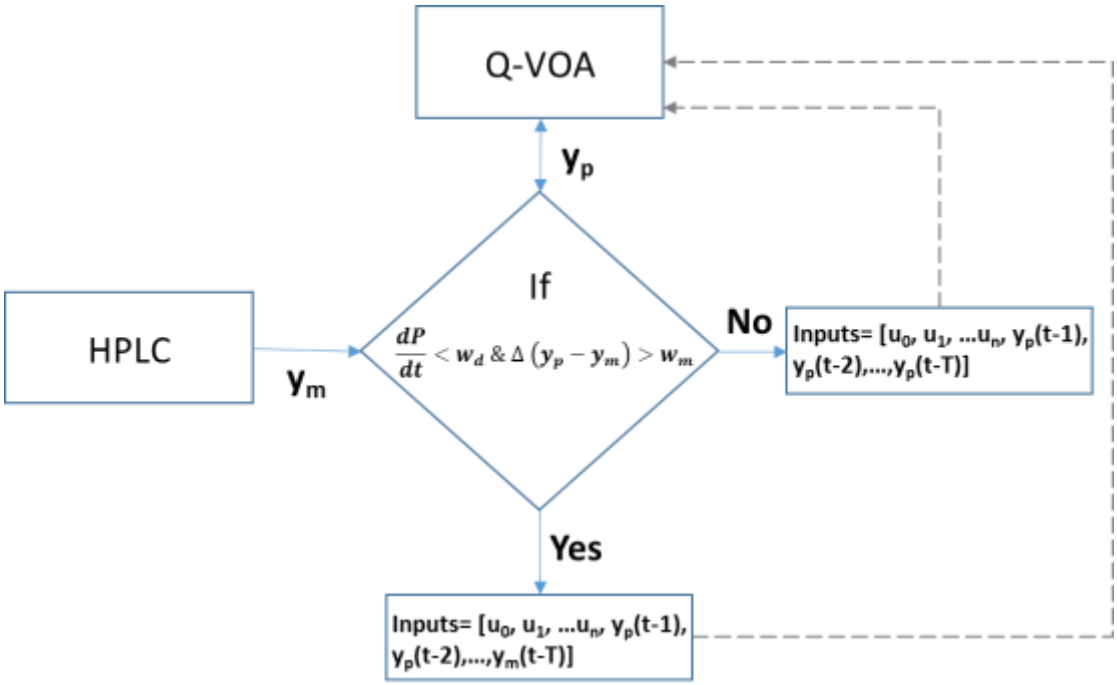

Figure 10 - Schematic representation of the Q-VOA internal structure.

The derivative of the system prediction, $\hat{y}$, through time, t, is calculated at each instant by its numerical definition:

$$\left.\frac{\partial \hat{y}}{\partial t}\right|_{t=t_s} = \frac{\mathbf{P}(t+\Delta t) - \mathbf{y}(t)}{\Delta t} \tag{48}$$

The Q-VOA system is composed by two output variables, the purities of the extract and raffinate streams; consequently, it becomes a multiple-input and multiple-output system (MIMO). In order to simplify the modelling step, the system was reduced to a multiple-input and single-output

system (MISO) (Wang et al. 2003; Costa et al. 2008). In this way, two neural models, one for each process output, compose the virtual analyser. Finally, the Q-VOA model assumes the general representation shown in Figure 11.

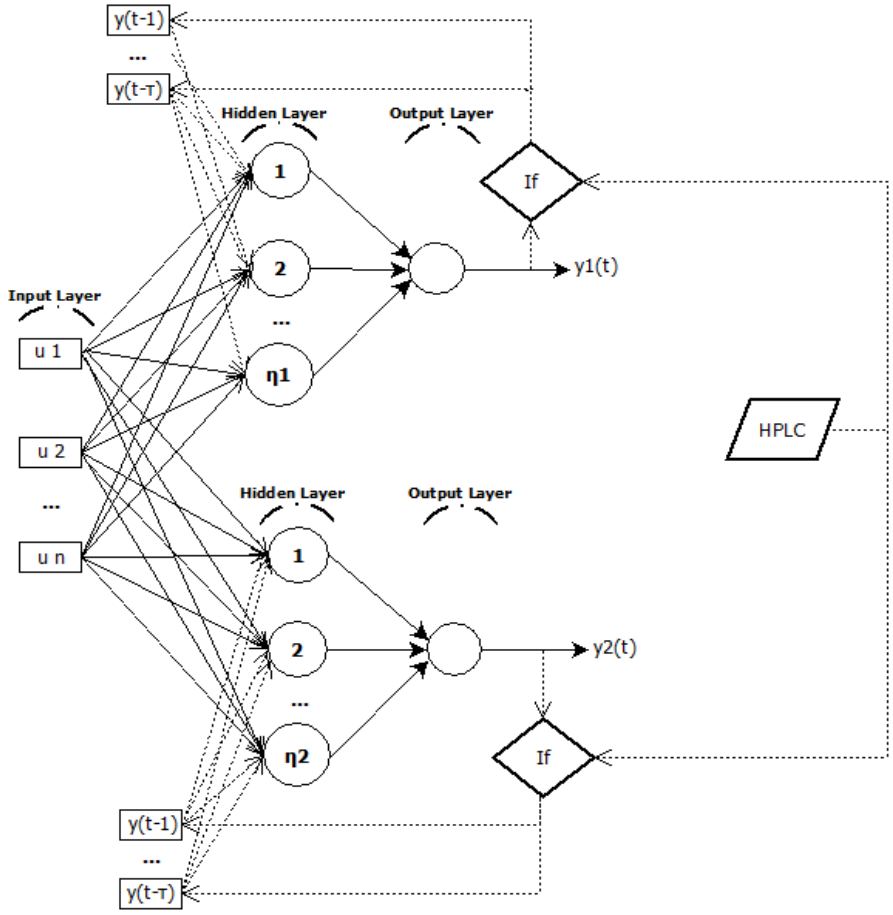

Figure 11 - MISO structure of the neural models in the virtual analyser.

P1-2.4.4. Artificial neural network modelling

In Figure 8, the generic structure of the neural model is presented. Generally, an artificial neural network has one input layer, one output layer and a given number of hidden layers and its

artificial neurons. In the input layer is located a number, n, of inputs that will be analysed by the model. In this layer, the retro-propagation of the past outputs is done through the NARX shown in Equation (37). In the hidden layer, the process inputs will be pondered by the weights and bias of this layer. The total number of weights is equal to the number of inputs evaluated, n, times the number of neurons, η, in this layer. The output layer has a number of neurons equal to the number of outputs evaluated. In addition, this layer has a given number of weights and bias that is equal to the number of neurons in the previous layer. The total number of weights and bias of an ANN forms the set of parameters of the empirical model that must be estimated in the learning/training phase.

The modelling through an ANN structure can be divided in three phases: selection of the number of hidden layers, selection of the optimal number of neurons in the hidden layers and estimation of the model parameters, which is usually referred as the learning or training step. Hunt et al. (1992) showed that one hidden layer is enough to develop an ANN model (Hunt et al. 1992).

To select the optimal number of neurons in the hidden layer, the cross-validation method was proposed by Schenker and Agarwal (1996), in order to guarantee that the recurrent neural networks can deal with dynamics of partial differential equations. It is important to note that the validation method here presented is different from what is usually applied in the literature. The cross-validation is normally referred in the literature as the simple division of the data set in three different groups and parameter estimation of the neural model from these groups (Ramaiah et al. 2010; Ventouras et al. 2011). However, the method proposed by Schenker and Agarwal (1996) consists in the use of two data sets to develop two different models and validate each model

with the training group that was used in the development of the other. For example, for a given number of neurons in the hidden layer, Nn, a set of data is used to train a network MA, and another set is used to train a network MB. The models are trained a given number of trials, Nt, and the model with the best training performance is selected. After the training step, the network MA is validated with the data from the network MB and the reverse, i.e, MA is used to validate MB. The validation error is held in a vector and the process is repeated for another number of neurons in the hidden layer. When Schenker and Agarwal (1996) proposed the cross-validation, they used a system with few data available. Previous work from Nogueira et al. (2017), though, showed that the cross-validation presents efficient results when applied to a larger database. The method to select the optimal number of neurons in the hidden layer is described in Figure 12. In this work, this method was applied but with a larger data set than the one used in the original work.

Both virtual and quasi-virtual analysis, as well as the neural network identifications here proposed were implemented in the MatLab software. The go:MATLAB extension (Process Systems Enterprise 2015) was used in order to establish a communication between gPROMS, where the process models were written, and MatLab. Hence, it was possible for the virtual and quasi-virtual analysers in MatLab to run externally the model and collect the responses of the process simulation.

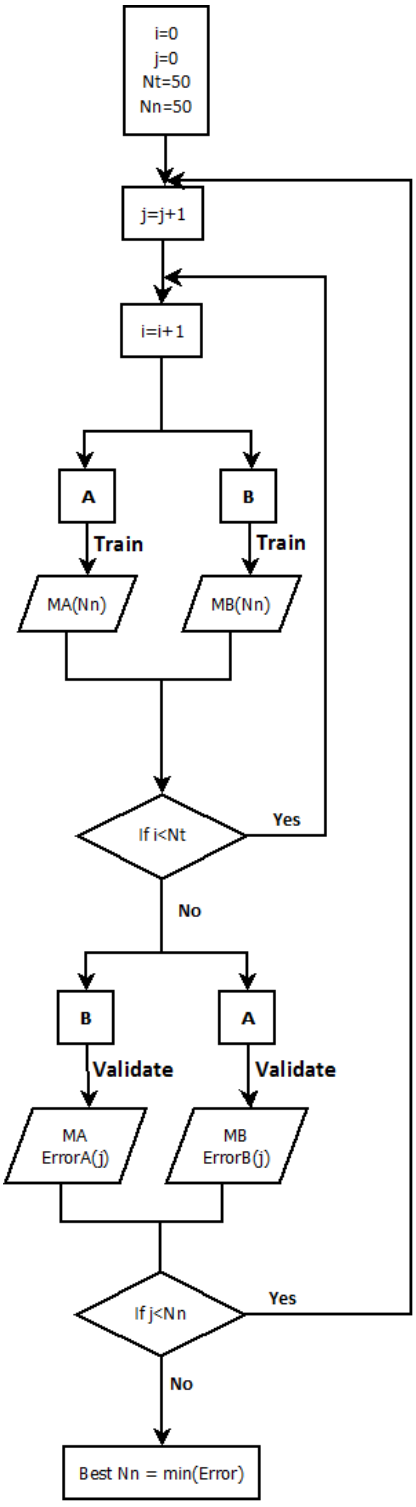

Figure 12 - Flowsheet of the cross-validation method; example for a total number of 50 neurons and a total number of 50 training trials.

P1-2.5. Process design and optimization – Particle Swarm technique

The PSO technique is based on the concept that a group composed by a given number of particles, p, will fly over a defined search region searching for the optimal point. Each member of the swarm presents its specific position, x_p, in the search space and a specific velocity, v_p, which are memorized and shared among all the particles after each iteration, k, of the method. It can be represented as:

$$v_p^{k+1} = v_{p,d}^k + c_1 r_1 (x_p^{per} - x_p^k) + c_2 r_2 (x_p^{glo} - x_p^k) \tag{49}$$

$$x_p^{k+1} = x_p^k + v_p^{k+1} \tag{50}$$

where c_1 and c_2 are the search parameters known as the acceleration coefficients and r_1 and r_2 are uniform distributions randomly generated in a range between 0 and 1. In general, those two equations represent the computation of the new velocity of each particle after each iteration, which depends on the best position of all the particles in all iterations, x_p^{glo}, and the particle personal best position in the previous iterations, x_p^{per}.

Kennedy and Eberhart (1995) also proposed an alternative version of PSO where the term of the previous velocity is eliminated from the calculus of the next velocity term. The authors concluded that, though simplified, that version, was ineffective to find the global optimum. However, in Ratnaweera et al. (2004), the authors investigated this problem and proposed a Self-Organizing

Hierarchical Particle Swarm Optimizer With Time-Varying Acceleration Coefficients (HPSO-TVAC), where a PSO without the previous velocity term is proposed, introducing a necessary momentum for the particles, which overcame the problems pointed out previously and resulted in finding more rapidly the global optimum solution even in the absence of the previous velocity term. The authors showed that, for most part of the benchmark functions, the HPSO presented a better solution than the other PSO types evaluated, and for the other cases, it presented similar results with a faster convergence.

As the design and optimization of TMB units is a heavy task, simple and fast methods are better suited in order to reduce the computational effort and optimization time. In this way, in the present work the HPSO-TVAC was chosen as the basis for the PSO here proposed, which can be represented as:

$$v_p^{k+1} = c_1 r_1 (x_p^{per} - x_p^k) + c_2 r_2 (x_p^{glo} - x_p^k) \tag{51}$$

$$x_p^{k+1} = x_p^k + v_p^{k+1} \tag{52}$$

with the acceleration coefficients computed as:

$$c_1 = (c_{1f} - c_{1i}) \frac{k}{k_{total}} + c_{1i} \tag{53}$$

$$c_2 = (c_{2f} - c_{2i}) \frac{k}{k_{total}} + c_{2i} \tag{54}$$

where the c_{1f}, c_{1i}, c_{2f} and c_{2i} are constants and k_{total} is the total number of iterations. The acceleration coefficient c_1 will decrease through the simulation while the acceleration coefficient

c_2 will increase. In Ratnaweera et al. (2004), the best solution was found employing a c_1 varying from 2.5 to 0.5 and a c_2 varying from 0.5 to 2.5.

Another important point in the PSO application is the initialization velocity. In Engelbrecht (2012), the author evaluates the effect of the initialization velocity and concludes that the particles tend to leave the boundaries of the search space when the velocities are initiated randomly. The author demonstrated that the final result is directly dependent on the method of initialization of the particles velocity. Furthermore, the author shows that random initialization increases the number of roaming particles, and that this has a negative impact on the convergence time. Finally, it was also shown in the referred work, that using an initialization velocity equal to zero or random value around zero, presents the best solution, saving efforts and avoiding the significant number of roaming particles problem. In this way, the PSO-TVAC was here employed with initialization velocity equal to zero which differs from what was proposed originally by Ratnaweera et al. (2004).

Another problem in the application of PSO to solve optimization problems is dealing with dynamic multi-modal landscapes. In this type of problems, where the peaks can vary in height as well as location, the ordinary PSO strategy cannot be successfully applied because small changes in the function peak height might lead to a large change in the position of the global optimum (Poli et al. 2007). In this way, the PSO tends to get stuck in one local minimum, depending on its searching region. The multi-population PSO is normally proposed to overcome this type of problems (Koduru et al. 2007). However, this strategy is more complex, more difficult to implement and requires more computational effort.

To avoid this problem, it is proposed here an approach in which the particles change their flying landscape during the simulation, here called as searching region mutation. This mutation is based on the social learning of the particles through the simulation. To illustrate better this problem, Figure 13 presents a given function that presents a total of five local minima when evaluated with a search region R_3. In this case, an ordinary PSO algorithm will tend to one of those minima, depending on its parameters and its search region, and might not identify the whole topography of the region, which is a problem in the drawing of the operating confidence regions, since it is intended to evaluate all possible operating conditions that satisfy the process design conditions.

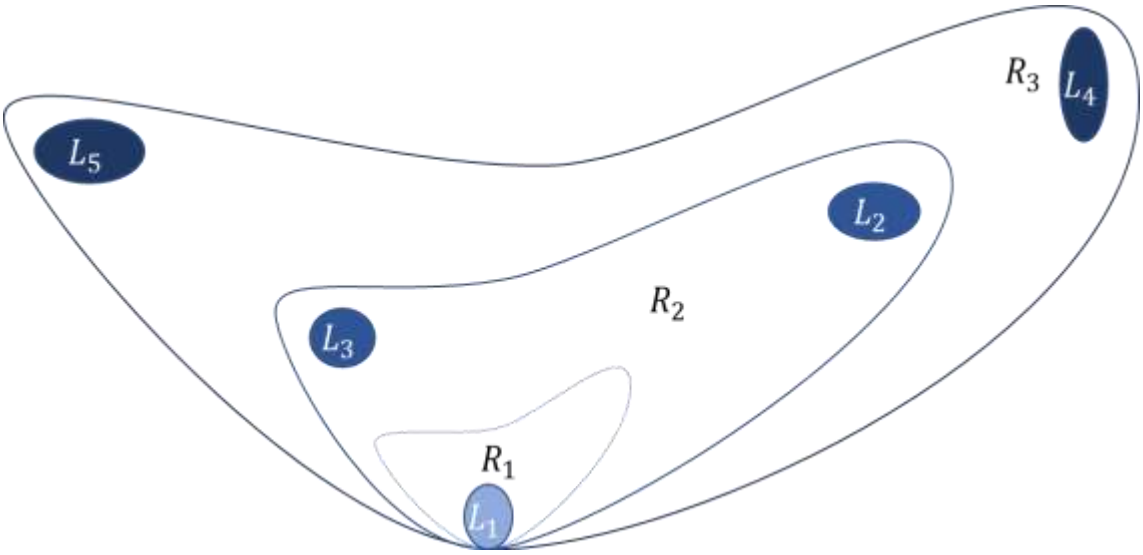

Figure 13 - Schematic representation of the possible search spaces (R_1, R_2 and R_3) of a given function with L_1, L_2, L_3, L_4 and L_5 as local minima.

The concept of varying the size of the search region was presented in Koduru et al. (2007), where a dynamic multi-modal landscapes problem was solved through a hybridized PSO algorithm based on multi-population, mutation and crossover on particles cloud, the contour particle

swarm optimization C-PSO, and the results were compared with the uniform covering by probabilistic rejection (UCPR) technique. In the present work, a similar approach is proposed; however, instead of using a multi-population algorithm where each swarm searches a specific region, here only one particle swarm that changes its flying region during the simulation is applied.

Given a function with a search space described by Figure 13, the methodology here proposed consists in the gradual expansion of the search region of the HPSO-TVAC from R_1 to R_3. Before each expansion of the searching region, the particles will memorize the previous information about the minimum point found and avoid flying over that region, which pushes the particles to move to different minimum points. This is done through the creation of a restriction inside the search space. The restrictions are created after a determined number of iterations for which the particles remain in a fixed optimal point. Following the space restriction, the search space is expanded and the process is repeated. In this way, the algorithm here proposed can be described as given in Table 3.

Table 3 - Proposed methodology for the improved HPSO-TVAC.

1	Set HPSO-TVAC parameters, c_{1f}, c_{1i}, c_{2f} and c_{2i}, number of iterations, k, number of particles that compose the swarm, p, initial search region limits, R_1,and set the maximum number of iterations as criterion to change the region.
2	Initialize randomly the particles position within the current search space: $x_p^1 = R_{i,min} + rnd(R_{i,max} - R_{i,min})$

where, $R_{i,min}$ is the inferior limit of the initial search region, $R_{i,max}$ is the superior limit and rnd is a random value between 0 and 1.

3 Initialize the velocities to zero.

4 Calculate the maximum velocity:

$$v_{max,i} = (R_{i,max} - R_{i,min})/2$$

5 Evaluate the objective function for each particle position $fob(x_p^1)$

6 Calculate the acceleration coefficients through Equation (53) and Equation (54).

7 Evaluate the new velocity v_p^{k+1} through Equation (51).

8 If the velocity v_p^{k+1} is higher than v_{max}, compute a new velocity value as proposed in Schwaab et al. (2008):

$$v_p^{k+1} = v_{max} sign(v_p^{k+1})$$

9 Calculate the new positions, x_p^{k+1}, through Equation (52).

10 If the particle position x_p^{k+1} is not inside the searching limits or if it is inside of one of the internal restrictions, x_{restri}^i, then: $x_p^{k+1} = R_{i,max}$

11 If the minimum position, x_p^{glo}, is repeated for the number of times set in the maximum criterion, then create a space restriction and go to step 12:

$$x_{restri}^i = P x_p^{glo}$$

where P is a constant between 1 and 2, that defines the size of restricted space around x_p^{glo}. If this criterion is not met return to step 5.

12 Initialize a new iteration.

13	Expand the search region, return to step 2 and continue until the maximum number of regions is reached.

The PSO is a simple algorithm and its implementation is easy. As Schwaab et al. (2008) stated, the computational time required for PSO calculations is very small when compared to the time required for computation of model predictions and evaluation of objective function values for all particles. Consequently, the total time required for optimization is basically the time required for model evaluations (Schwaab et al. 2008). The present work takes advantage of this to propose an alternative to solve the design and optimization of TMB and SMB processes.

P1-2.5.1. Definition of the objective function

The definition of the optimization objective function is an essential step in an optimization problem. In the present case, the main goal is to define the set of operating flow rates (Q_F, Q_E, Q_{IV} and Q_X) that will maximize the unit productivity while the eluent consumption is minimized, since these variables are the ones that mostly affect the process costs. However, while searching for economic goals, sometimes it is necessary to keep the process in its minimum quality requirement, in other cases it is also desirable to maximize its quality parameters, increasing the final product value. In order to comply with the quality requirement, the present work proposes the application of an objective function with penalties. This is a well-known optimization technique applied in the field of constrained optimization. The simplest approach to solve optimization problems with penalties is to apply a constant penalty to the solutions

which violate the defined constraints, the so-called static penalty functions. Given the following constrained optimization problem:

$$\min_{\theta} J(\boldsymbol{y}) \tag{55}$$

subject to:

$$Pur_j \geq Pur_{min} \tag{56.R1}$$

$$Pux_j \geq Pux_{min} \tag{57.R2}$$

where $\boldsymbol{y}$ is the vector of process performance parameters and θ is the set of process variables to be optimized. The constraints presented in Equation (56.R1) and Equation (57.R2) are set in order to satisfy a minimum quality specification of the production. However, it can be desirable to obtain a high as possible purity while the other criteria are satisfied. Thus, the differences between the purities and one were added in the objective function in order to maximize the purities over the minimum requirement. Therefore, for the present case the objective function can be defined as:

$$\mathrm{J} = \sum_{k}^{n_k} \Big((1 - Pur_k)^2 + (1 - Pux_k)^2 + (1 - Recr_k)^2 + (1 - Recx_k)^2 + \frac{1}{Pr_k} + Ec_k \Big) + \sum_{c=1}^{n_c} C_c \delta_c \tag{58}$$

subject to:

$$\delta_1 = 1, if\ Constraint\ (56.\mathrm{R1})\ is\ violated \quad (59.R1)$$

$$\delta_1 = 0, if\ Constraint\ (56.\mathrm{R1})\ \ is\ satisfied \quad (60.R1)$$

$$\delta_2 = 1, if\ Constraint\ (57.\mathrm{R2})\ \ is\ violated \quad (61.R1)$$

$$\delta_2 = 0, if\ Constraint\ (57.\mathrm{R2})\ is\ satisfied \quad (62.R1)$$

where C is the penalty constant imposed in case of violation of the constraint c of the process variables to be optimized, n_k is the total number of instants of evaluation of the performance parameters, Pux, is the extract purity, Pur, is the raffinate purity, $Recx$, is the extract recovery, $Recr$, is the raffinate recovery; as presented by the model equations in Section P1-2.1, these parameters are dependent on the concentration of component i in the extract stream, $C_{X,i}$, concentration of the component i in the raffinate stream, $C_{R,i}$, and concentration of the component i in the feed stream, $C_{F,i}$; *EC,* is the eluent consumption and Pr is the TMB productivity.

P1-2.5.2. Operating variables confidence region evaluation

In the present work, it is proposed the evaluation of the confidence region of the process variables. This provides important information in the process operation, since, instead of a fixed point, it is provided a region where the process can be operated meeting the optimal conditions,

giving more flexibility to the process. The confidence region evaluation based on PSO optimization for parameters estimation is presented in Schwaab et al. (2008). In Benyahia et al. (2013), a similar approach is used to determine the confidence regions of polymerization model parameters. In the present work, the methodology was adapted in order to evaluate the confidence regions of the process operating variables, after the optimization. The steps here presented were based on Benyahia et al. (2013) and Schwaab et al. (2008) works, where further information about the development and assumptions, for the parameters estimation case, can be found.

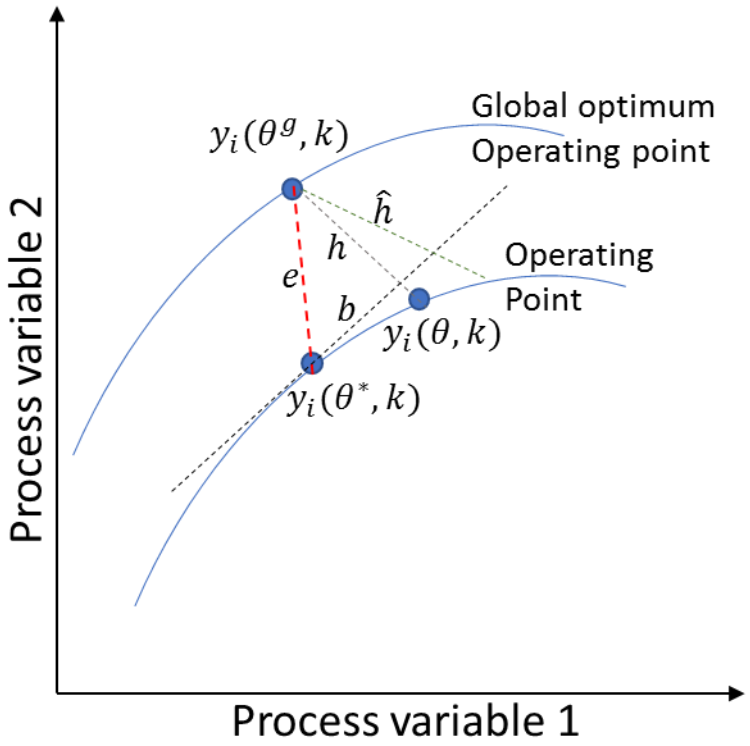

Figure 14 - Simplified representation of the model predictions through the global minimum, best minimum found and a given minimum found in the performance variables space, adapted from Benyahia et al. (2013).

Considering the optimization problem presented, the optimization space for two given process variables is presented in Figure 14. In this Figure, e corresponds to the difference between the values (y) of a given process performance parameter, i, in a given optimization instant, k, evaluated at $\boldsymbol{\theta}^*$ and $\boldsymbol{\theta^g}$**,** and given by: $y_i(\boldsymbol{\theta}^*, k)$ and $y_i(\boldsymbol{\theta^g}, k)$; where $\boldsymbol{\theta}^*$ is the vector of the best operating conditions values determined in the optimization (in the present case it means that $\boldsymbol{\theta}^*$ corresponds to the best position found by the particles) and $\boldsymbol{\theta^g}$ is the vector of operating conditions values of the global minimum of the objective function, which is a theoretical concept. By its turn, h corresponds to the difference between the value of the process performance parameters $y_i(\boldsymbol{\theta}, k)$ and $y_i(\boldsymbol{\theta^g}, k)$, where $\boldsymbol{\theta}$ is the vector of best operating conditions values evaluated in a given iteration of the optimization. Thus, in a given instant, k, for a given process performance parameter, i, the squared error between the process optimal point and the global minimum is given by:

$$e^2{}_{ik} = (y_i(\boldsymbol{\theta}^*, k) - y_i(\boldsymbol{\theta^g}, k))^2 \tag{63}$$

This error can be normalized with respect to the variance as:

$$e^2{}_{ik} = \frac{(y_i(\boldsymbol{\theta}^*, k) - y_i(\boldsymbol{\theta^g}, k))^2}{V_i} \tag{64}$$

From Equation (64) and following an approach similar to the one presented by Benyahia et al. (2013), the error can be generalized to all instants, n_k, considered in the optimization.

$$e^2 = \sum_{i=1}^{n_y}\sum_{k=1}^{n_k} e_{ik}^2 = \sum_{i=1}^{n_y}\sum_{k=1}^{n_k} \frac{(y_{i,k}(\boldsymbol{\theta}^*, k) - y_{i,k}(\boldsymbol{\theta^g}, k))^2\ )}{V_i} \quad (65)$$

Where n_y is the total number of process performance parameters considered in the optimization. Considering the variance of a given performance parameter with respect to the vector of the best position found for the process operating variables ($V_i(\boldsymbol{\theta}^*)$) as:

$$V_i(\theta^*) = \frac{1}{n_k}\sum_{k=1}^{n_k}(y_{i,k}(\boldsymbol{\theta}^*, k) - y_{i,k}(\boldsymbol{\theta^g}, k))^2 \quad (66)$$

Thus, from Equation (65) and Equation (66) the error can be presented as:

$$e^2 = \sum_{i=1}^{n_y}\sum_{k=1}^{n_k} \frac{n_k V_i(\boldsymbol{\theta}^*)}{V_i} \quad (67)$$

Considering the assumption that the error e is Gaussian distributed with zero mean, the e^2 has a chi square distribution with $n_k - (ny - 1)$ degrees of freedom, χ^2, where:

$$e^2 \ \rightarrow\ \chi^2(n_k - ny + 1) \quad (68)$$

In the same way, the difference between the process performance parameters for the optimal set of operating conditions and for a given set of parameters can be represented as:

$$h^2{}_i = (y_i(\boldsymbol{\theta}, k) - y_i(\boldsymbol{\theta^g}, k))^2 \quad (69)$$

$$h^2 = \sum_{i=1}^{n_y}\sum_{k=1}^{n_k} \frac{n_k V_i(\boldsymbol{\theta})}{V_i} \quad (70)$$

The same development and assumptions presented for e can be applied to h, which in this way also has a chi square distribution with $n_k - (n_\theta + n_y - 1)$ degrees of freedom. We finally obtain the approximation:

$$h^2 \rightarrow \chi^2(n_k - n_\theta - n_y + 1) \tag{71}$$

where n_θ is the number of optimized operating variables. Thus:

$$e^2 - h^2 \rightarrow \chi^2(n_\theta) \tag{72}$$

The approximation, proposed in Benyahia et al. (2013), can be also applied here as:

$$\frac{b^2}{\hat{h}^2} = \frac{e^2 - h^2}{\hat{h}^2} \cong \frac{e^2 - h^2}{h^2} \tag{73}$$

As Equation (73) presents the ratio between two chi square distributions, $e^2 - h^2$ with n_θ degrees of freedom and h^2 with $n_k - n_\theta - n_y + 1$ degrees of freedom, and knowing that those distributions are independent, this can be represented as a Fisher-Snedecor distribution, as:

$$\frac{\frac{e^2 - h^2}{n_\theta}}{\frac{h^2}{n_k - n_\theta - n_y + 1}} \rightarrow F_\alpha(n_\theta, n_k - n_\theta - n_y + 1) \tag{74}$$

Furthermore, from Equations (67), (69) and (74):

$$\sum_{i=1}^{n_y}\sum_{k=1}^{n_k}\frac{n_k V_i(\boldsymbol{\theta}^*)}{V_i}-\sum_{i=1}^{n_y}\sum_{k=1}^{n_k}\frac{n_k V_i(\boldsymbol{\theta})}{V_i}$$
$$\rightarrow\sum_{i=1}^{n_y}\sum_{k=1}^{n_k}\frac{n_k V_i(\boldsymbol{\theta})}{V_i}\frac{n_\theta}{n_k-n_\theta-n_y+1}F_\alpha(n_\theta,n_k-n_\theta-n_y+1) \quad (75)$$

where α is the confidence level considered. The objective function $J(\theta)$ can be expanded in a second-order Taylor expansion around the minimum point found in the optimization, θ^*, Schwaab et al. (2008), as:

$$J(\theta)=J(\theta^*)+(\theta-\theta^*)\nabla J_{\theta^*}+\frac{1}{2}(\theta-\theta^*)^T\boldsymbol{H}_{\theta^*}(\theta-\theta^*) \quad (76)$$

where ∇J_{θ^*} is the gradient vector and $\boldsymbol{H}_{\theta^*}$ the Hessian matrix of the objective function. This matrix is related to the covariance matrix of the process operating variables as (Bard 1974; Schwaab et al. 2008):

$$\boldsymbol{H}_{\theta^*}=2V_\theta^{-1} \quad (77)$$

From Equation (77), Equation (76) can be rewritten as:

$$J(\theta^*)-J(\theta)=(\theta^*-\theta)^T V_\theta^{-1}(\theta^*-\theta)\equiv\ \chi^2(n_\theta) \quad (78)$$

Equation (75) can be rewritten through Equation (78) as:

$$J(\theta)-J(\theta^*)\rightarrow\sum_{i}^{n_y}\frac{n_k V_i(\theta)}{V_i}\frac{n_\theta}{n_k-n_\theta-n_y+1}F_\alpha(n_\theta,n_k-n_\theta-n_y+1) \quad (79)$$

And finally, considering that V_i provides a good approximation of $V_i(\theta)$, the process operating conditions confidence region can be evaluated through:

$$J(\theta) \leq J(\theta^*) + \frac{n_k n_\theta}{n_k - n_\theta - n_y + 1} F_\alpha(n_\theta, n_k - n_\theta - n_y + 1) \quad (80)$$

The above criterion is the Fisher–Snedecor test which is applied here to draw the confidence regions and also to verify the existence of local minima.

The PSO-MSR, objective function and Fisher–Snedecor test here presented were implemented in the MatLab software. To run the optimization, a communication between gPROMS, where the process models were written, and MatLab was used through the go:MATLAB extension (Process Systems Enterprise 2015). It was possible for MatLab to run externally the model and collect the responses of the process simulation.

P1-3. Results

In this chapter are presented all the results obtained from the application of the methodologies described in chapter P1-2. The presentation of the results follows the order of presentation of the methods described in the previous chapter.

P1-3.1. TMB dynamics characterization

P1-3.1.1. Gram-Schmidt Orthogonalization analysis

The assessment of the performance of cyclic adsorption systems is usually addressed in literature in terms of steady state. To reach further developments in this field, the characterization of the dynamic behaviour of the processes becomes necessary. This step of the present work has the focus on the application of a method based on Gram-Schmidt Orthogonalization, presented in section P1-2.2.1, to analyse the impact of the operating variables in the dynamic response of a TMB unit where the chiral separation of a bi-naphthol enantiomers mixture using a 5-dinitrobenzoyl phenylglycine bonded to silica gel is processed. Another objective is to characterize the dynamic system behaviour through a step perturbation analysis and compare it with the orthogonalization method results.

A time horizon of 400 minutes and a sampling time of 0.001 minutes was considered to perform the analysis. The raffinate flow rate value was not defined in order to keep the degree of freedom

of the model. The method results first indicated the recycling flow rate as the most important operating variable of the TMB. The remaining variables were classified in the following sequence, from the one with the largest to the lowest influence: solid flow rate (Q_s), eluent flow rate (Q_E), extract flow rate (Q_x), feed flow rate (Q_F) and feed concentration. In Table 4 are presented the magnitude values obtained for all the operating variables in each iteration of the dynamic analysis. The selected variable in each iteration is highlighted. It is important to note that the value of each variable tends to zero in the next iteration after being selected by the analysis. It can also be noted that the zero value remains until the end of the analysis. This was expected since the method was modified with this objective. It ensures that, once selected, the variable is not taken in consideration in the next steps of the analysis.

Table 4 - Magnitude of each operating variable of the TMB at each iteration of the dynamic analysis.

	Operating Variables						
Iteration	$M_{C_{f,A}}$	$M_{C_{f,B}}$	M_{Q_s}	$M_{Q_{IV}}$	M_{Q_E}	M_{Q_F}	M_{Q_X}
1	1.13×10^{3}	2.94×10^{3}	3.26×10^{6}	9.84×10^{8}	7.75×10^{5}	1.32×10^{4}	2.18×10^{5}
2	1.12×10^{3}	2.69×10^{3}	2.78×10^{6}	1.60×10^{-22}	7.73×10^{5}	1.30×10^{4}	1.95×10^{5}
3	9.36×10^{2}	2.34×10^{3}	2.63×10^{-25}	1.17×10^{-22}	5.91×10^{5}	1.19×10^{4}	4.62×10^{4}
4	8.94×10^{2}	2.33×10^{3}	2.43×10^{-25}	1.16×10^{-22}	1.81×10^{-25}	6.97×10^{3}	3.38×10^{4}
5	8.75×10^{2}	2.25×10^{3}	2.32×10^{-25}	1.16×10^{-22}	1.38×10^{-25}	6.95×10^{3}	4.12×10^{-27}
6	7.32×10^{2}	1.01×10^{3}	2.30×10^{-25}	1.13×10^{-22}	1.04×10^{-25}	1.46×10^{-27}	3.54×10^{-27}
7	5.63×10^{2}	1.37×10^{-28}	2.26×10^{-25}	1.13×10^{-22}	9.90×10^{-26}	1.02×10^{-27}	3.14×10^{-27}
8	2.52×10^{-27}	1.37×10^{-28}	2.26×10^{-25}	1.13×10^{-22}	9.90×10^{-26}	1.02×10^{-27}	3.14×10^{-27}

It should be noted that the order of importance of the operating variables obtained in this analysis is characteristic of the case study considered and that it may change if another system is considered or if other constraints are imposed in the mathematical model (for example, if

pressure drop constraints are introduced). Nevertheless, the developed methodology, once validated in this case study, can still be applied to quantify the relative importance of the operating variables on the system behaviour.

P1-3.1.2. Step perturbation analysis

After this analysis, a step perturbation in each operating variable was done. The objective was to check and compare the results obtained with the ones of the previous analysis. As the system has only a few number of variables (7), the graphical analysis can be done easily. From simple observation of the graphical results, it is possible to assess visually the magnitude of the influence of the perturbations on the performance indicators and confirm the order of importance of the different operating parameters obtained in P1-3.1.1. Therefore, this analysis can be used as a tool to check the consistence of the method proposed. Furthermore, the step response analysis can provide important information about the dynamic behaviour of this process. Usually, in the literature, the results of the effect of the operating parameters on the performance indicators of the cyclic adsorption systems are only reported for cyclic steady state or steady state, even when transient models are developed (Pais et al. 1997, 1998, 2000; Minceva et al. 2003; Erdem et al. 2004; Leão and Rodrigues 2004; Toumi and Engell 2004; Kaspereit et al. 2007; Sá Gomes and Rodrigues 2012). However, the dynamic characterization of the system is also an important aspect.

A step perturbation of 10% and 2% in the absolute value was done to each variable. The step perturbation was done over a given steady-state of the process which was obtained using the parameters given in Table 5, corresponding to the ones defined by Pais et. al (2000).

Table 5 - Data used in the model simulation (Pais et. al 2000).

Process Variables		**Model Parameters**	
$c_{A/B}{}^{f}$	2.9 g.l^{-1}	k	0.1 s^{-1}
Q_E	21.45 ml.min^{-1}	D_L	0.025 cm^2.s^{-1}
Q_X	17.98 ml.min^{-1}	ε	0.4
Q_F	3.64 ml.min^{-1}	L_j	21.0 cm
Q_S	11.15 ml.min-1	Column diameter	2.6 cm
Q_{IV}	27.95 ml.min^{-1}		

The mass transfer coefficient was chosen following the work of Pais et al. (1997) where its effect in these processes (TMB, SMB-4, SMB-8) steady state was studied. The value used in the simulation corresponds to a zone where the mass transfer effect in the process is not very significant although it cannot be neglected. This situation is closer to what is usually found in a TMB/SMB system. Even though k is a lumped parameter that accounts for the film mass transfer resistance (which depends on the fluid velocity) and intraparticle mass transfer resistance, the latter is normally the controlling mechanism in this type of processes, and therefore the effect of fluid velocity is very small. Therefore, the same value of k was used in all sections of the process. In this way, a variation in any flow rate was compensated by the value of the raffinate flow rate in the global mass balance.

The results from the step perturbations are presented in the following figures. All graphics are represented in terms of deviation variables (purity and recovery values from 0 to 1). The perturbations on the operating flow rates change the internal flow rates as can be seen from the global mass balances in Section P1-2.1, Equation (13) to Equation (16)(3). On the other hand, variations on the internal flow rates affect the fluid concentrations, which changes the unit concentration profiles and may consequently affect the process recovery and purity. The system separation and regeneration regions were also obtained in order to verify the system behavior in terms of its steady state performance. In the construction of the separation and regeneration regions a purity of 95% in the outlet streams was considered as process restriction. So, these regions represent the operating values that satisfy the purity restriction. The regions are represented in terms of the ratio between fluid and solid interstitial velocities, $\gamma_j = v_j/u_s$. A given separation region is obtained for fixed flow rates in sections I and IV. But if the flow rates of sections I and IV are varied, and if mass transfer effects are being considered, separation volumes are obtained (Azevedo and Rodrigues 2001) from which other separation regions for given pairs of flow rates of sections I and IV are obtained. As explained above, the perturbations in the operating flow rates change the internal flow rates. When these changes affect the flow rate of section I and/or section IV, new separation regions must be calculated. This is the case, for example, for the perturbation on the recycling flow rate that increases the flow rate of all sections. However, perturbations in the extract flow rate (which, as explained above, are compensated by changes in the raffinate flow rate as given by the global balance) do not affect

the flow rates in sections I and IV and therefore it is not necessary to calculate a new separation region.

The dynamic analysis together with the separation and regeneration regions can provide important information about the system behavior and enable the comparison between the steady and dynamic approaches. The results obtained are shown in the following figures, one for each operating variable, ordered by their magnitude of influence in the process (from the one with the largest to the one with the lowest influence as indicated by the analysis reported above).

Figure 15 represents the step perturbation in the recycling flow rate and its effect on the separation and regeneration regions. It can be noted that a 10% perturbation in the recycling flow rate has a significant effect on the purity and recovery of both extract and raffinate streams. It can be also noted that this 10% perturbation gives rise to a significant decrease in the separation region and that the new operating point violates the separation and regeneration conditions. These effects were expected, since a variation in the recycling flow rate affect all separation zones in the TMB unit. In Figure 15 it can also be seen the dynamic behavior of the system after a variation in Q_{IV}. The extract recovery presents a strong inverse response, while the raffinate recovery presents a smooth inverse response.

Analyzing the 2% perturbation in Figure 15 it is possible to conclude that the new operating point generated by this perturbation remains inside the separation and regeneration regions and high purity products are still obtained. The 2% perturbation has almost no effect in the system if only the steady state and separation regions are taken in consideration. But the same dynamic behavior as seen in the 10% perturbation was observed for this case. Taking in consideration the

dynamic behavior, in a period of time the system shows a strong inverse response which leads momentarily the process to a lower recovery. These variations can have great impacts on the process profit and/or quality control. In this way, the dynamic characterization of the process is an important information that must be taken in consideration in the field of process control and optimization.

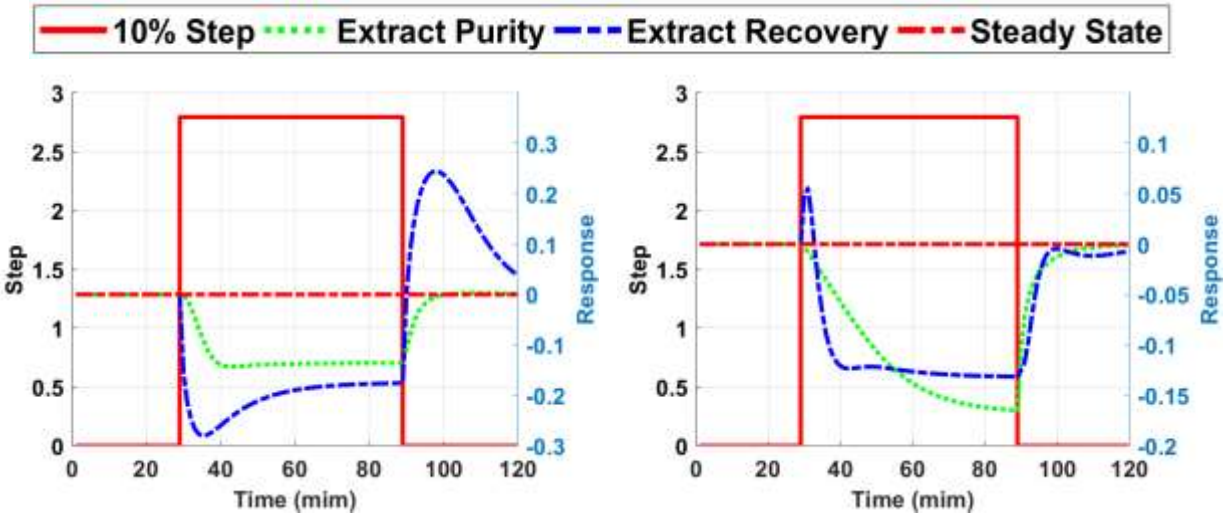
10% Step
Extract Purity
Extract Recovery
Steady State
Step
Response
Time (mim)

a.I b.I

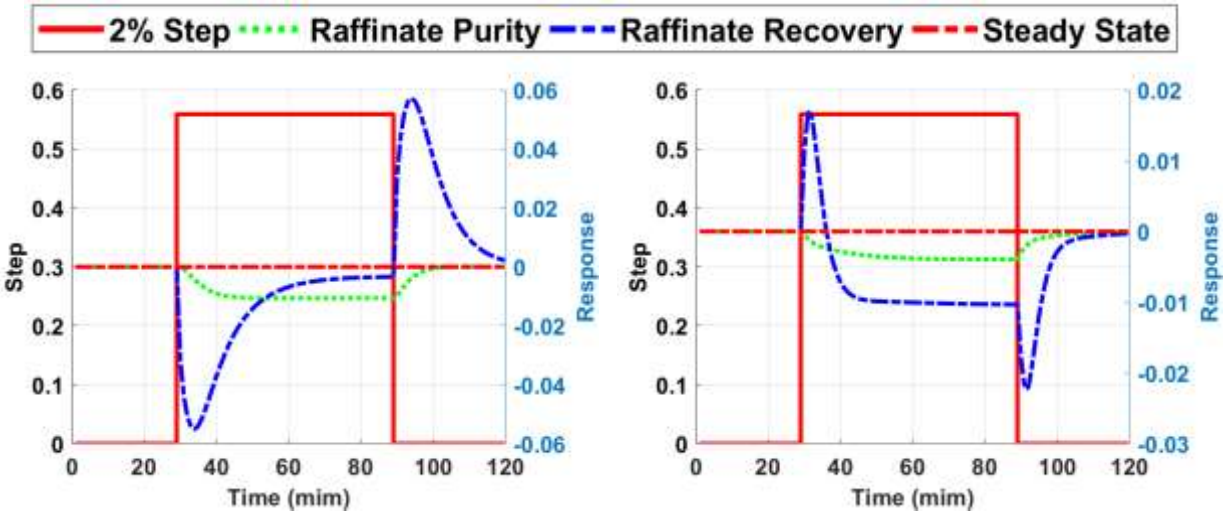
2% Step
Raffinate Purity
Raffinate Recovery
Steady State
Step
Response
Time (mim)

a.II b.II

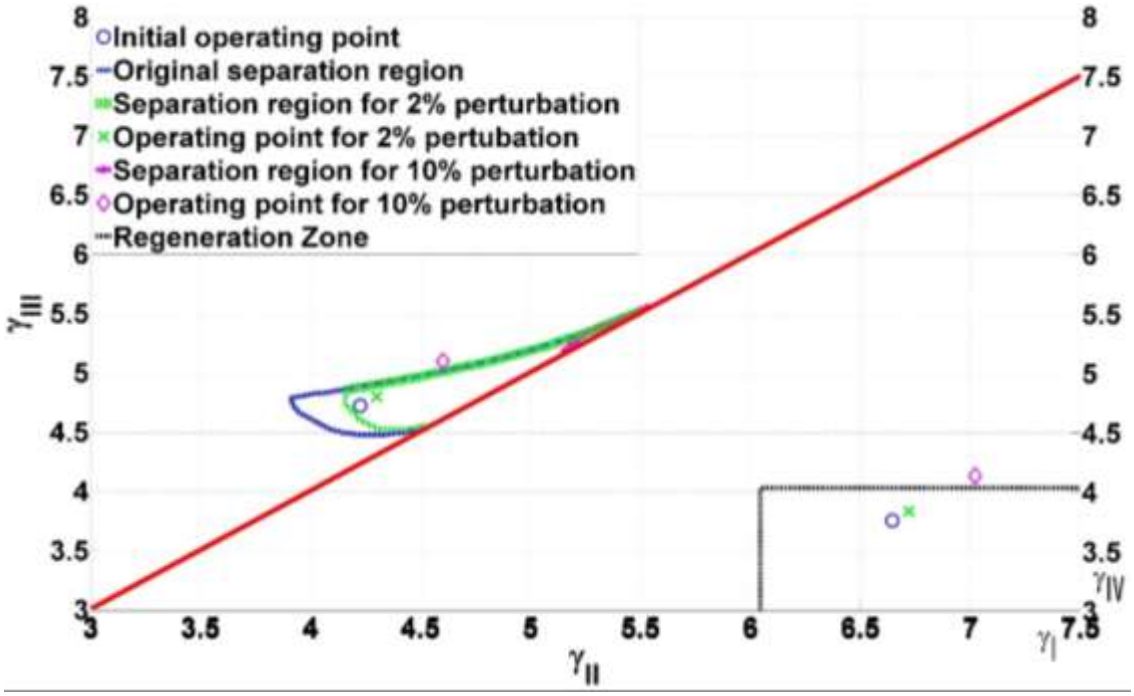

c

Figure 15 - Process response after a step perturbation in the recycling flow rate: a.I - extract response to a 10% perturbation; a.II - extract response to a 2% perturbation; b.I raffinate response to a 10% perturbation; b.II - raffinate response to a 2% perturbation; c - separation and regeneration regions.

Following Q_{IV}, the next variable presented is the solid flow rate, Figure 16. This variable presents a considerable effect on the extract purity and raffinate recovery, but not as strong as the Q_{IV} effect, which is consistent with the orthogonalization analysis. In Figure 16, it can be noted that perturbations in the solid flow rate move the separation region to the left side of the graphic. For the 10% perturbation, the operating points move out of the separation and regeneration regions, resulting in lower product purity. Also, here the process recovery presents an inverse response after the perturbation and the 2% perturbation presents the same dynamic behavior as observed in the 10% perturbation.

Comparing the solid flow rate and the eluent flow rate effects, Figure 17, it can be observed that both variables have similar effects in terms of magnitude. Both variables originate a strong inverse response in the system recovery. With a smoother effect in the Q_E response when compared with the Q_S response. It is important to point out that only with a graphical analysis it is hard to evaluate which is the most influent variable, Q_S or Q_E. But the orthogonalization analysis indicates that Q_S has a stronger effect in the system when compared with Q_E. The perturbation on the eluent flow rate affects mainly the extract recovery and the raffinate purity. In terms of separation regions, for this particular case, the Q_E has no impact in the final zone. This may occur because, for the operating conditions considered, the size of the separation region within the separation volume is not affected by the value of γ_I (Azevedo and Rodrigues 2001).

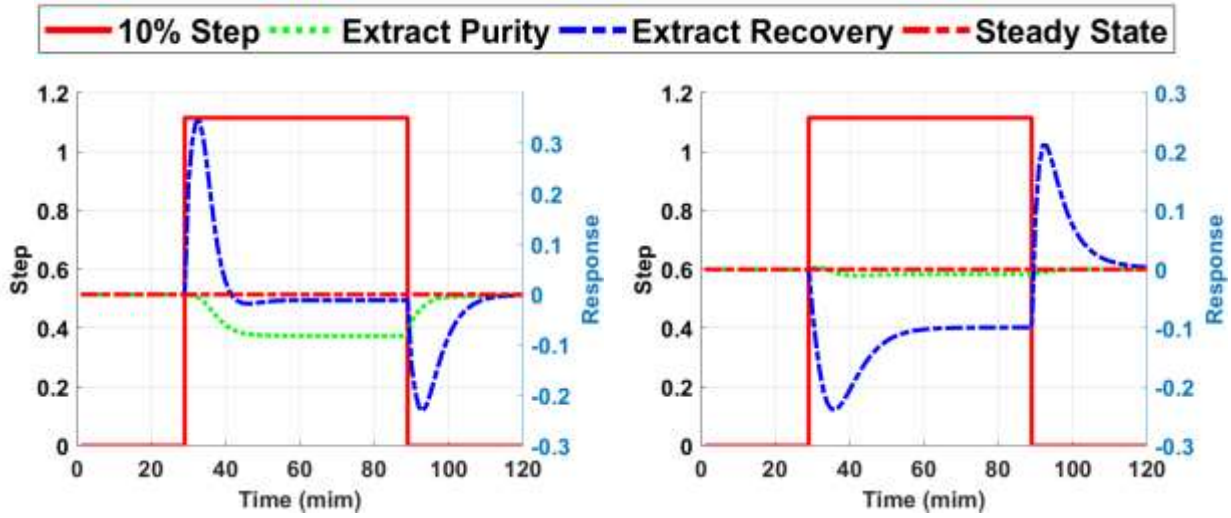
10% Step
Extract Purity
Extract Recovery
Steady State
Step
Response
Time (mim)

a.I b.I

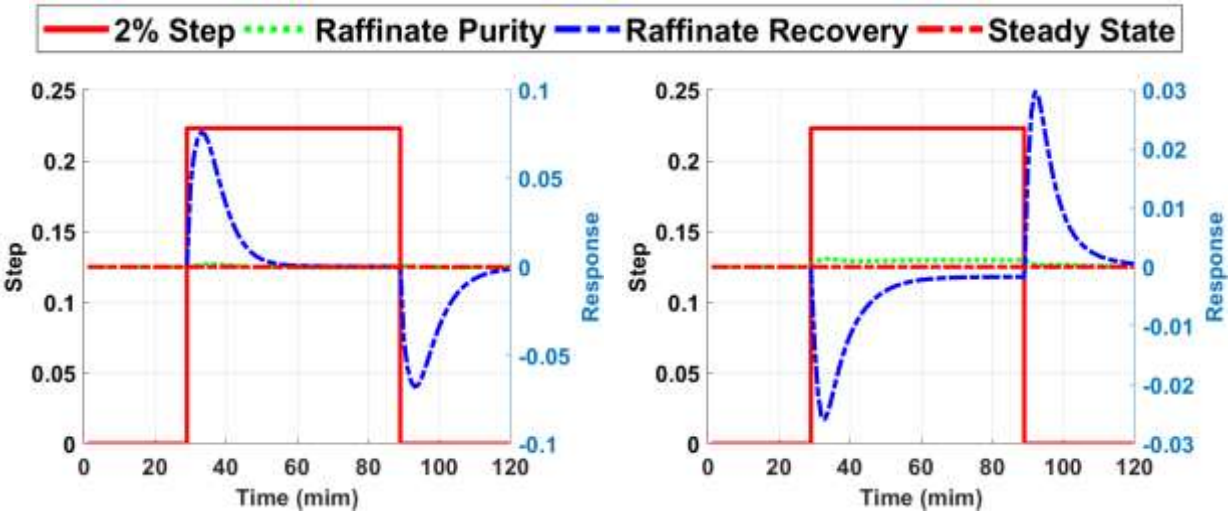
2% Step
Raffinate Purity
Raffinate Recovery
Steady State
Step
Response
Time (mim)

a.II b.II

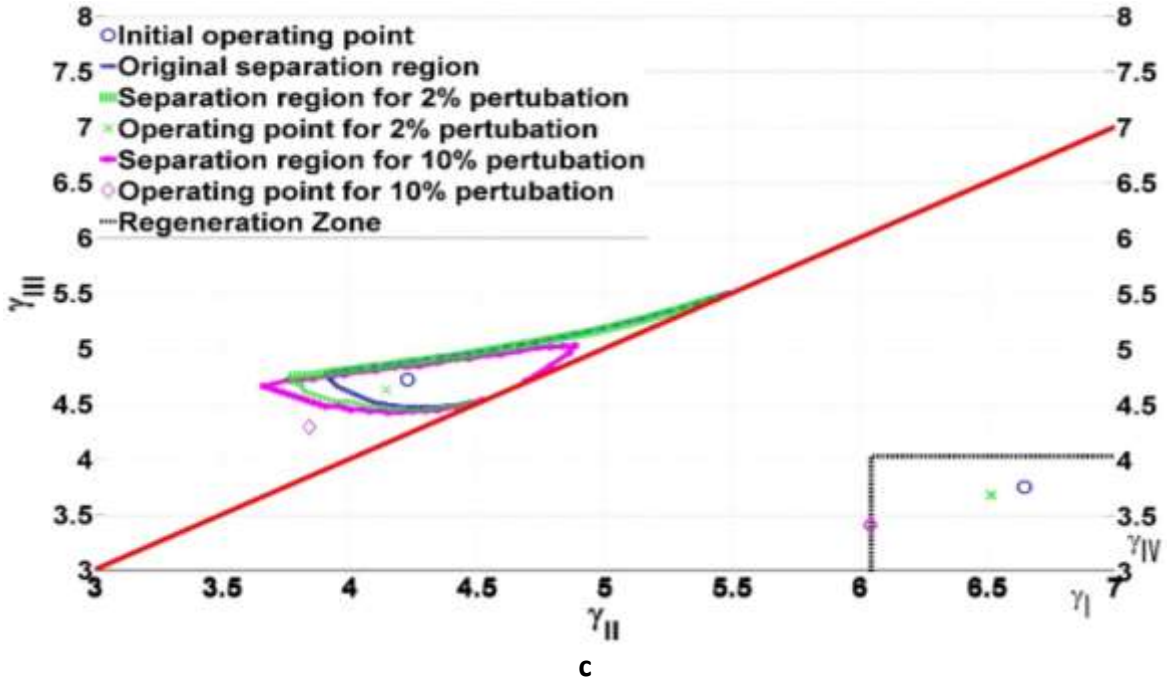

c

Figure 16 - Process response after a step perturbation in the solid flow rate: a.I - extract response to a 10% perturbation; a.II - extract response to a 2% perturbation; b.I raffinate response to a 10% perturbation; b.II - raffinate response to a 2% perturbation; c - separation and regeneration regions.

As can be observed in Figure 17 the perturbations only move the operating point towards the right side of the graphic. In the case of the operating point, in the regeneration region, it can be noted that the movement is done over a horizontal line, as the raffinate flow rate compensates the eluent increase and therefore the flow rate in zone IV is kept constant. That means that the changes in eluent flow rate only affect the regeneration in zone I of the TMB column. The 10% perturbation operating point in the separation region is located in the limit of the region. This means that with the new steady state, generated by the perturbation, 95% purity is still obtained. This is an important information since, in this case, no changes in the separation regions are observed, but strong changes in the recovery happen momentarily. These changes are a

consequence of the system dynamics and can be as high as 30%, which can be significant in terms of process profit.

Finally, the extract flow rate, Figure 18, has a smooth effect in the system response, with an inverse response for the recovery performance indicator. This operating variable presents no effect in the separation region, since the variation in the extract flow rate is compensated by the raffinate flow rate in order to keep the mass balance of the system. In the same way, the operating point in the regeneration zone is constant. While the operating point in separation zone moves outside the separation region after the 10% perturbation.

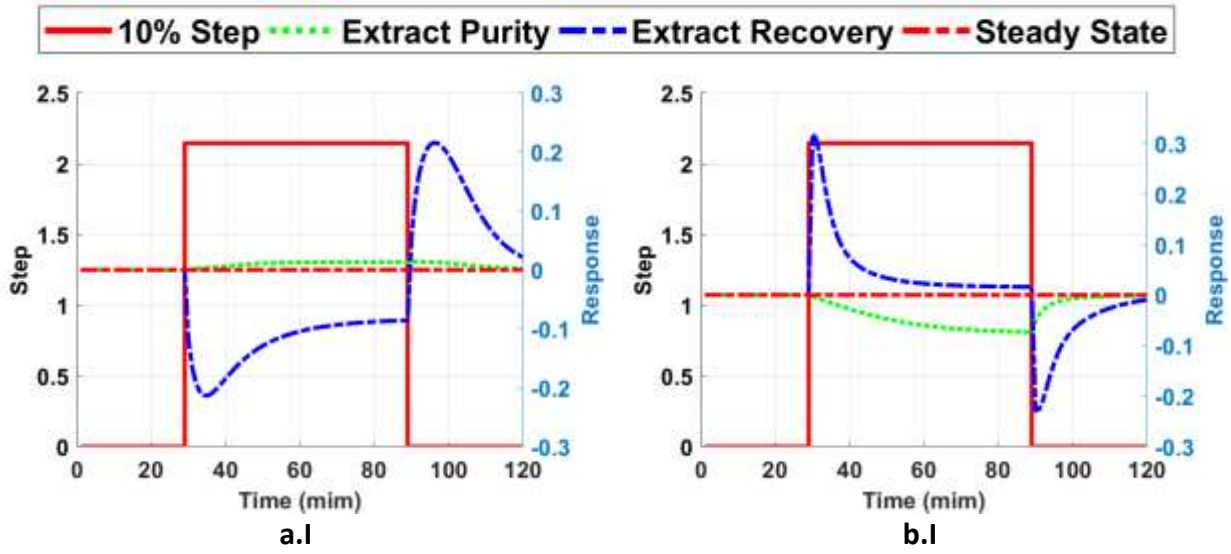

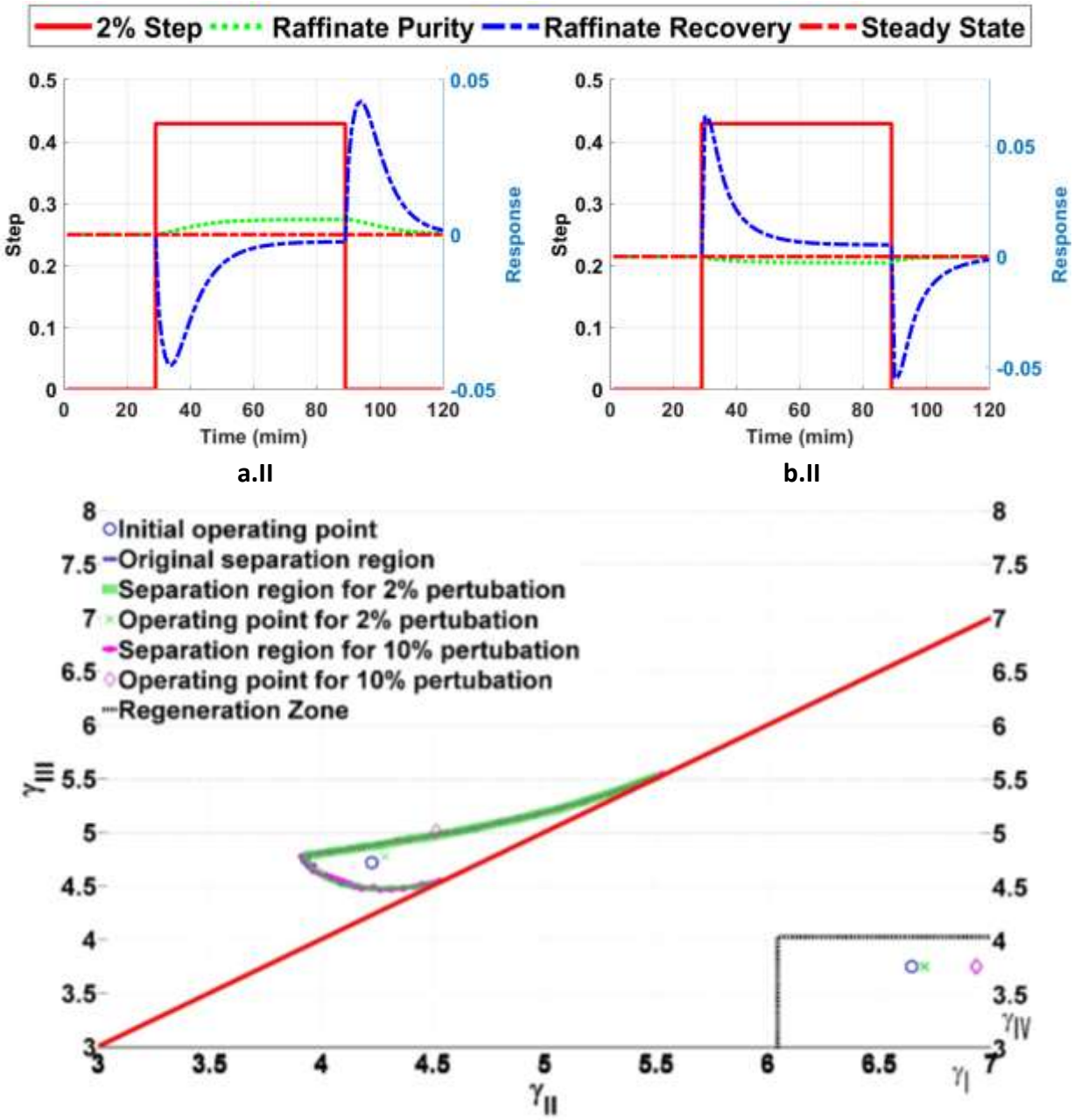

Figure 17 - Process response after a step perturbation in the eluent flow rate: a.I - extract response to a 10% perturbation; a.II - extract response to a 2% perturbation; b.I raffinate response to a 10% perturbation; b.II - raffinate response to a 2% perturbation; c - separation and regeneration regions.

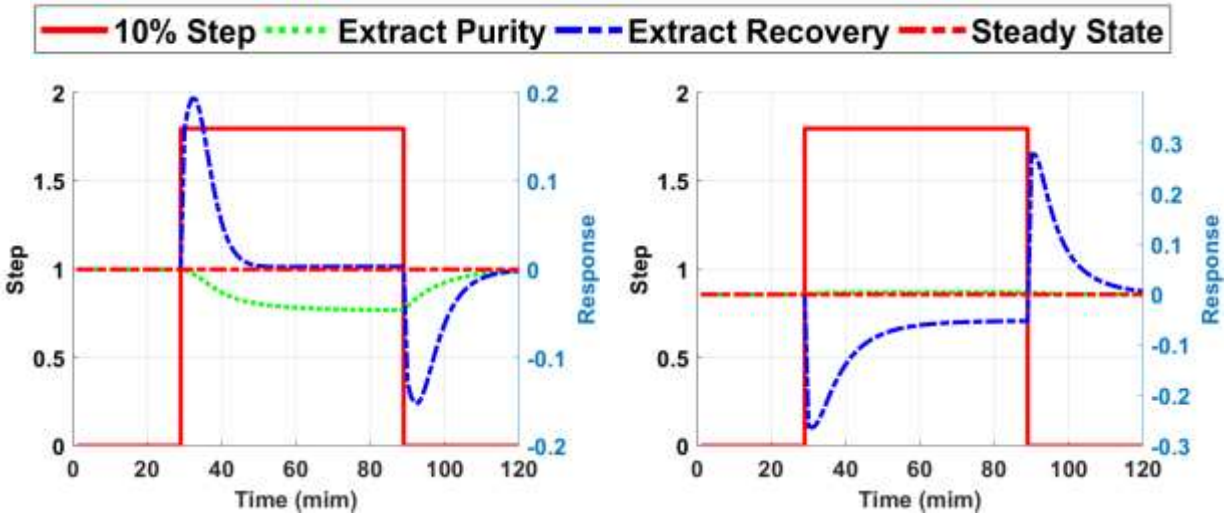
10% Step
Extract Purity
Extract Recovery
Steady State
Step
Response
Time (mim)

a.I b.I

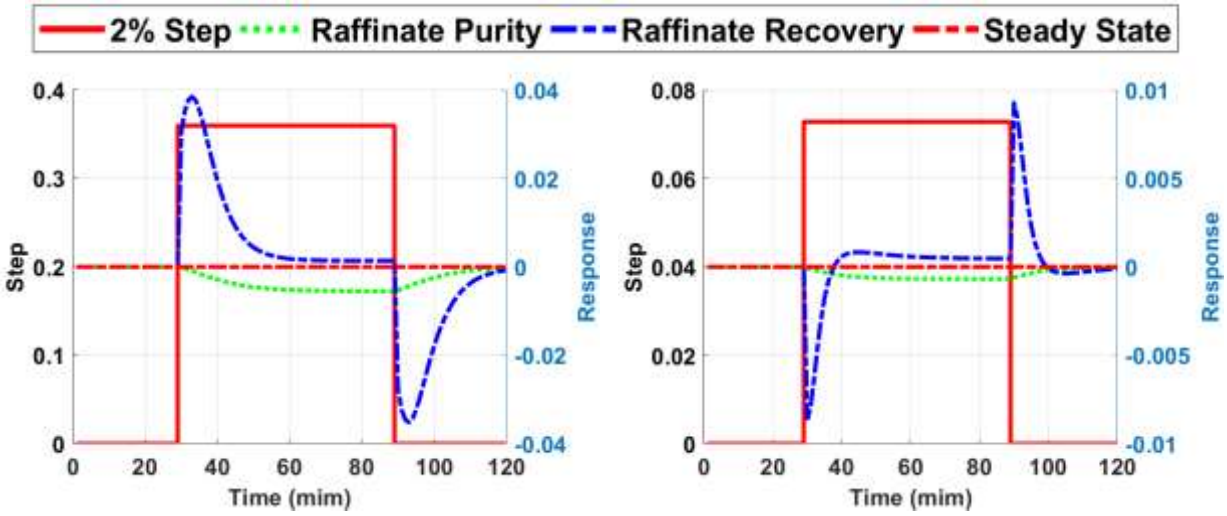
2% Step
Raffinate Purity
Raffinate Recovery
Steady State
Step
Response
Time (mim)

a.II b.II

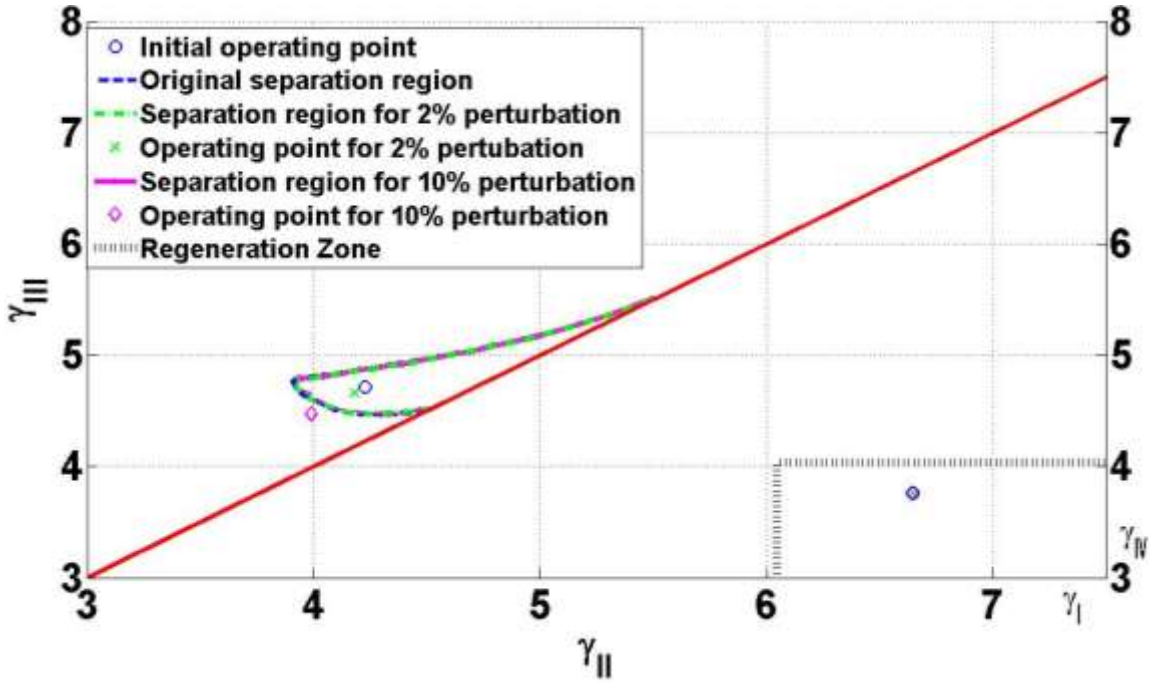

Figure 18 - Process response after a step perturbation in the extract flow rate: a.I - extract response to a 10% perturbation; a.II - extract response to a 2% perturbation; b.I raffinate response to a 10% perturbation; b.II - raffinate response to a 2% perturbation; c - separation and regeneration regions.

For the operating conditions considered, the feed concentration and flow rate have almost no effect in the system response. However, the feed concentration usually tends to undergo a larger deviation than the flow rates in real industrial operations. This is because the feed concentration can vary within a relatively large interval according to the feed source or feed-preparation upstream conditions. Therefore, even though the feed concentration presents a weak effect in the process, it is important to know what happens to the process in the presence of perturbations of greater magnitude in it. To analyze this, Figure 19 presents the results for 2% and 10% perturbations on the feed concentration of compound A. The results for compound B present a similar behavior, and therefore are not presented. From this Figure, it can be seen that even in the presence of the 10%

perturbation in the feed concentration, the effect on the purity is not significant. On the other hand, the recovery performance indicator in the raffinate stream presents a major inverse response that momentarily assumes values 15% lager/lower than the steady state. The results for the perturbations on the feed flow are shown in Figure 20 where it can be seen that the perturbations have a very small effect on the purity and recovery.

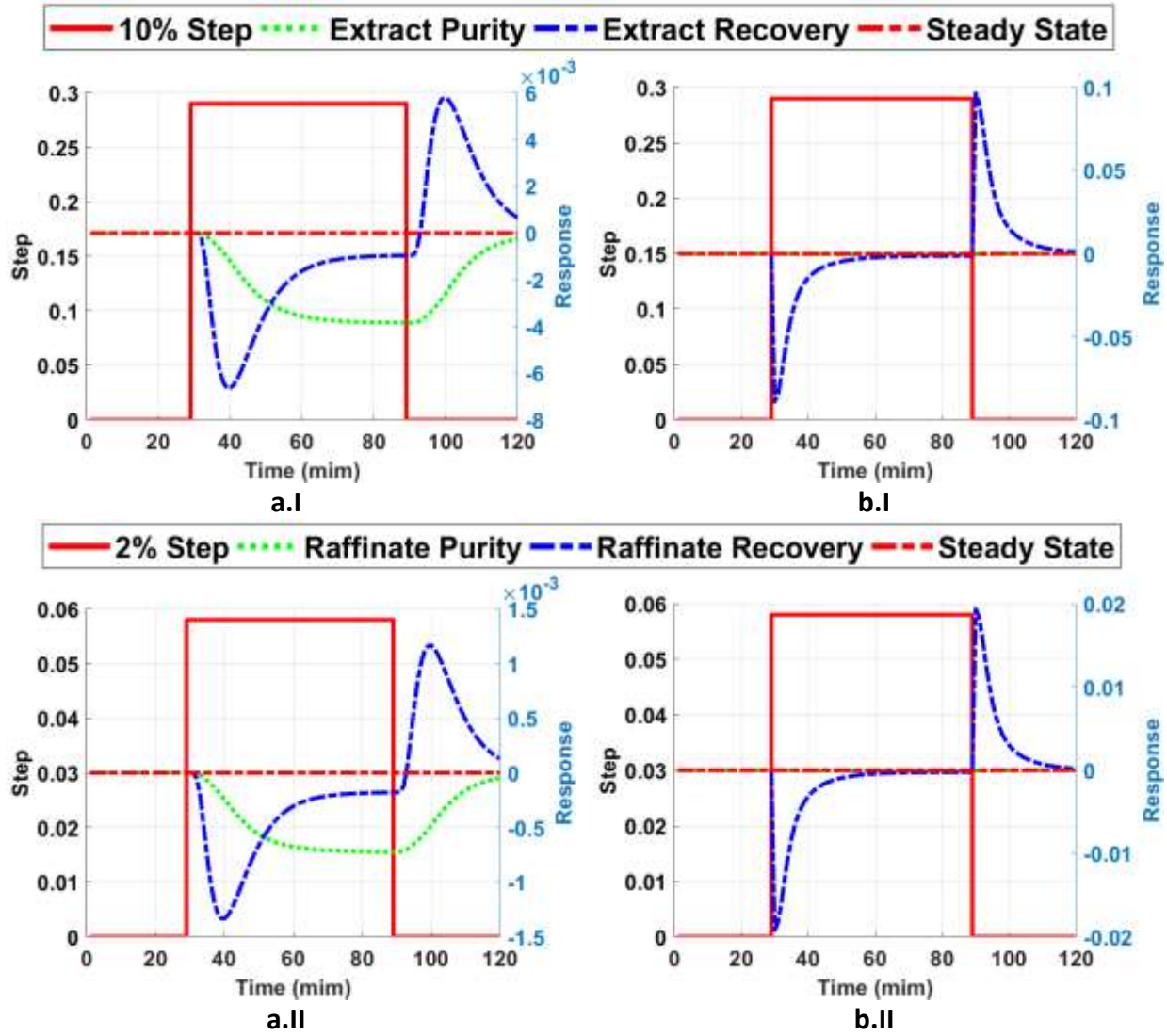

Figure 19 - Process response over a step perturbation in the feed concentration of the compound A: a.I - extract response to a 10% perturbation; a.II - extract response to a 2% perturbation; b.I raffinate response to a 10% perturbation; b.II - raffinate response to a 2% perturbation.

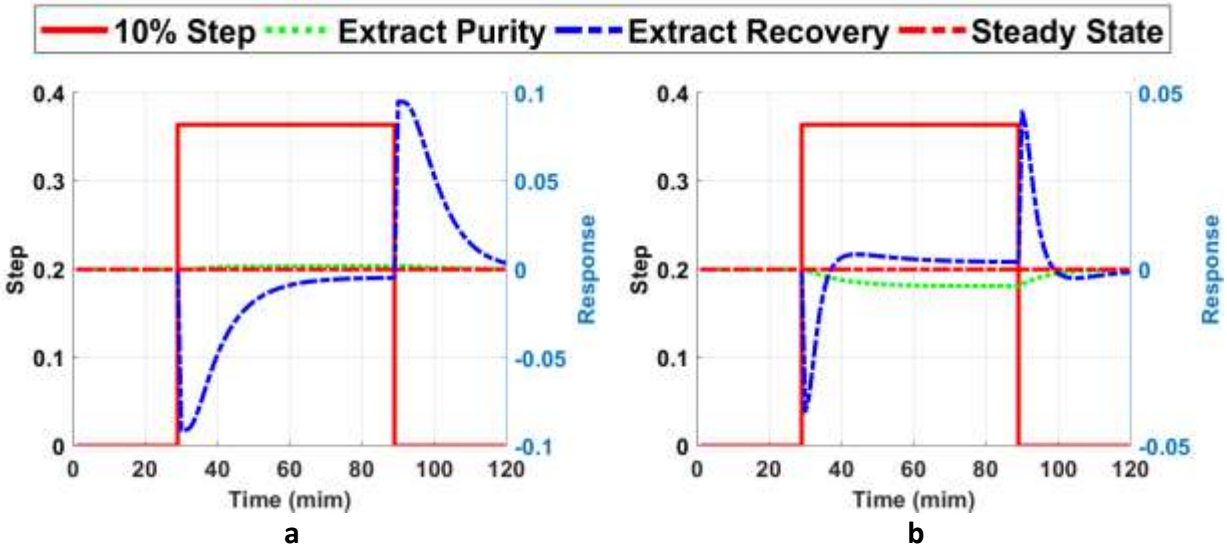

Figure 20 - Process response over a 10% step perturbation in the feed flow rate: a - extract response, b - raffinate response.

In order to analyze the influence of a step perturbation in the separation process, the internal concentration profiles before and after a step perturbation in the recycling flow rate are shown in Figure 21, together with the dynamic change in the internal profiles. The recycling flow rate was the operating condition selected because it is the variable with the greater impact in the process.

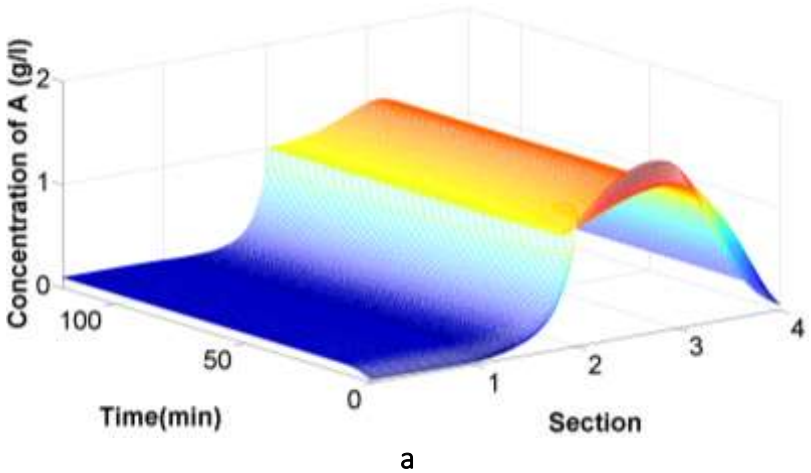

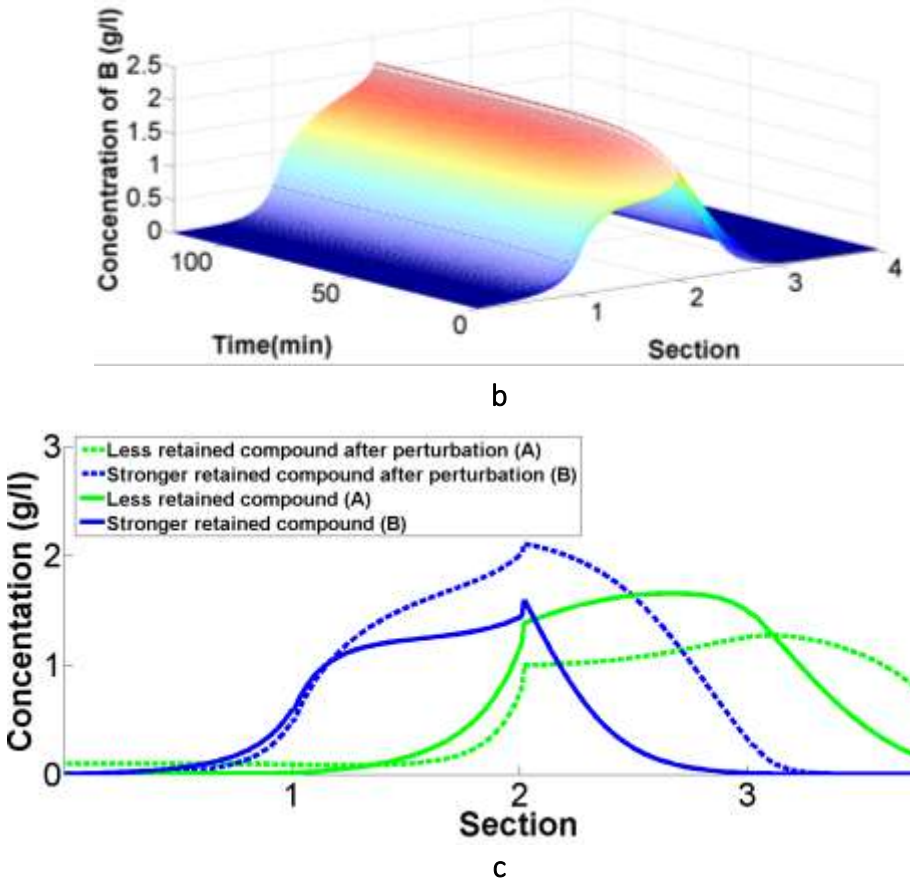

Figure 21 - Internal concentration profiles after a 10% perturbation in recycling flow rate: a - internal concentration profile in transient state for the less retained compound; b - internal concentration profile in transient state for the stronger retained compound; c - internal concentration profile in steady state for both compounds, before and after the perturbation.

This perturbation leads to an increase in the internal velocities of all TMB sections. As a consequence, the internal profiles of the two compounds move forward in the bed. The more retained compound reaches the raffinate port and contaminates this product. Also, the fluid is not efficiently cleaned in section IV, and the less retained compound is recycled to section I together with the eluent and therefore the extract stream is contaminated.

The methodology presented in this work was applied to a TMB model which is an approximation of the SMB operation. The results presented in this section validated the orthogonalization method and showed its consistency; the methodology was then applied to study the behavior of SMB processes as shown in the next section.

P1-3.2. SMB dynamics characterization and TMB/SMB comparison

P1-3.2.1. Gram-Schmidt Orthogonalization analysis

In order to compare the dynamic behaviour of a TMB unit and SMB units, two configurations for the SMB were considered, the SMB-4 and the SMB-8. The SMB-4, corresponding to the unit with four columns, has one column per section, while the SMB-8 unit with eight columns has two columns per section. The processes operating conditions and parameters used for each process are presented in Table 6. The parameters and conditions used keep the equivalence between the TMB unit and the SMB units.

Table 6 - Processes operating conditions.

Process Variables					**Models Parameters**		
TMB		**SMB**				**SMB-4/TMB**	**SMB-8**
$c_{A/B}{}^{f}$	2.9 g.l^{-1}	$c_{A/B}{}^{f}$	2.9 g.l^{-1}		Pe	2000	1000
Q_{IV}	27.95 ml.min^{-1}	Q_{IV}	35.38 ml.min^{-1}		ε	0.4	0.4
Q_E	21.45 ml.min^{-1}	Q_E	21.45 ml.min^{-1}		L_c	21.0 cm	10.5 cm
Q_X	17.98 ml.min^{-1}	Q_X	17.98 ml.min^{-1}		L_j	21.0 cm	21.0 cm
Q_F	3.64 ml.min^{-1}	Q_F	3.64 ml.min^{-1}		α	36.0	18.0
Q_s	11.15 ml.min^{-1}	t^*	**SMB-4**	**SMB-8**	Column diameter	2.6 cm	2.6 cm
			6 min	3 min			

Again, in order to keep the degree of freedom of the model, the raffinate flow rate value was not defined. This means that a variation in any inlet or outlet flow rate was compensated by the value of the raffinate flow rate in mass balance as expressed by Equation (1) to Equation (16).

An analysis of the impact of the operating variables (feed concentrations, extract, recycle, eluent and feed flow rates) of the different processes on their performance parameters (purity, recovery and eluent consumption) was carried out first. In this analysis, it was considered a time horizon of 400 minutes and a sampling time of 0.1 minutes. Since the main goal of the present work is to analyse the process in its dynamic regime, the smallest sampling time for which any decrease in this variable has no effect on the resulting ranking was used (which leads to a total time instants of $n_t = 4000$). This provides detailed information about the process dynamics.

The results from these analyses for the SMB units and the TMB unit are shown in Table 7. The processes variables with the largest magnitude in each iteration are highlighted in this table. These values represent the operating variable with the greatest influence in the process at the corresponding iteration. As described in section P1-2.2.1, at the end of an iteration, the remaining variables are projected in a space orthogonal to the selected variable. Thus, the new space will be free from the influence of this variable. This can be seen in the following table, where the magnitude of a variable that has been selected has a value of approximately zero on the remaining iterations after its selection. The magnitude values presented in Table 7 for the TMB are different from the ones presented in Table 4 because a different sampling time was employed. However, the same order of importance was obtained and therefore the conclusions are the same.

Table 7 - Magnitude of each operating variable at each iteration of the orthogonalization analysis for the SMB-8, SMB-4 and TMB.

		Operating Variables						
	Iteration	$C_{f,A}$	$C_{f,B}$	Q_{IV}	Q_X	Q_F	Q_e	t^* or Q_s
SMB-8	**1**	9.48X10^5	3.11X10^6	4.89X10^9	7.31X10^8	6.11X10^6	4.29X10^7	7.68X10^7
SMB-4	**1**	2.97X10^6	3.75X10^6	1.39X10^9	1.37X10^8	9.00X10^6	1.30X10^8	4.51X10^8
TMB	**1**	5.15X10^2	1.59X10^2	1.25X10^7	4.21X10^6	5.14X10^3	5.97X10^6	5.16X10^6
SMB-8	**2**	9.95X10^4	2.98X10^6	3.59x10^{-21}	6.04X10^7	6.07X10^6	4.22X10^7	7.65X10^7
SMB-4	**2**	2.71X10^6	3.61X10^6	3.58x10^{-22}	1.23X10^8	8.55X10^6	1.17X108	4.12X10^8
TMB	**2**	4.79X10^2	1.22X10^2	2.73x10^{-24}	3.13X10^5	1.91X10^3	3.79X10^5	3.86X10^5
SMB-8	**3**	9.80X104	2.96X10^6	1.92x10^{-22}	6.03X10^7	6.05X10^6	4.14X10^7	1.48x10^{-23}
SMB-4	**3**	1.80X10^6	2.69X10^6	8.31x10^{-23}	9.89X10^7	6.15X10^6	1.01X10^8	5.79x10^{-23}
TMB	**3**	4.79X102	1.22X102	2.67x10^{-24}	1.15X10^5	1.69X10^3	3.04X10^5	8.19E-26
SMB-8	**4**	7.81X104	1.65X10^6	1.68x10^{-22}	6.69x10^{-23}	4.42X10^6	1.60X10^7	2.47E-24
SMB-4	**4**	1.58X10^6	2.04X10^6	8.27x10^{-23}	7.78X10^7	5.84X10^6	1.07x10^{-23}	2.39x10^{-23}
TMB	**4**	4.75X10^2	1.14X10^2	2.66x10^{-24}	6.44X10^3	1.02X10^3	6.41x10^{-26}	6.91x10^{-26}

The first iteration of the method indicates that the recycle flow rate, Q_{IV}, is the operating variable with the greatest influence in the process performance parameters for all processes.

In the second iteration, the method indicates the switching time/solid flow rate as the variable with the second largest influence on the processes. After the orthogonalization around the recycle flow rate, it is possible to observe for the SMB-8 and TMB, a significant reduction (an order of magnitude) in the value of the magnitude of the extract flow rate, Q_X. This indicates the existence of correlations between Q_X and Q_{IV}. Such correlations can be identified through the node balances (equations presented in chapter P1-2.1). Besides being correlated with Q_{IV}, Q_X is also correlated with other variables and some of the main performance parameters of the process, as can be observed in the model equations. Consequently, and as expected from the phenomenological knowledge about the processes, the orthogonalization indicates this variable as one of the most important variables in the process.

After the orthogonalization of the system around the switching time/solid flow rate (t^*/Q_S) the extract flow rate showed a higher reduction in its magnitude for the SMB-4 and TMB when compared with the SMB-8. This is an indication that the higher the t^*, the greater is its impact on the other variables of the process. Since t^* will decrease with the increase in number of columns, the SMB-4 is the limit case for the switching time value (larger value).

For the SMB-8, after selecting the switching time in the second iteration, t^*, the method indicated the following order: extract flow rate (third iteration), effluent flow rate (fourth iteration), feed flow rate (fifth iteration) and feed concentrations (sixth and seventh iterations).

In the case of SMB-4 and TMB the order was: eluent flow rate (third iteration), extract flow rate (fourth iteration), feed flow rate (fifth iteration) and feed concentrations (sixth and seventh

iteration). The feed flow rate and concentrations present a very small effect in the processes responses and their iteration is not presented in Table 7. In terms of rank it is possible to observe that the SMB-4 unit is more similar to the TMB unit. This conclusion is opposite to what is commonly reported in the literature for the comparison between the SMB cyclic steady state and TMB steady state conditions, that is, as the number of columns in the SMB increases, the process approaches the TMB behaviour.

P1-3.2.2. Models comparison: from initial conditions to cyclic steady state

In order to analyse the evolution of the different processes, simulations of the three units from the start-up conditions to (cyclic) steady state were performed. The evolution over time of the concentration of the more retained component in the extract stream and of the less retained component in the raffinate stream are represented in Figure 22.a and Figure 22.b, respectively. Each graphic represents the values obtained for the TMB unit, for the SMB-8 unit and for the SMB-4 unit, as well as the average concentrations obtained for the SMB units. In order to maintain the equivalence between the models, the switching time for the SMB unit with eight columns was set equal to 3 min, while the switching time for the unit with four columns was set equal to 6 min. Such graphical representation is commonly presented in the literature when the comparison between the different models is made.

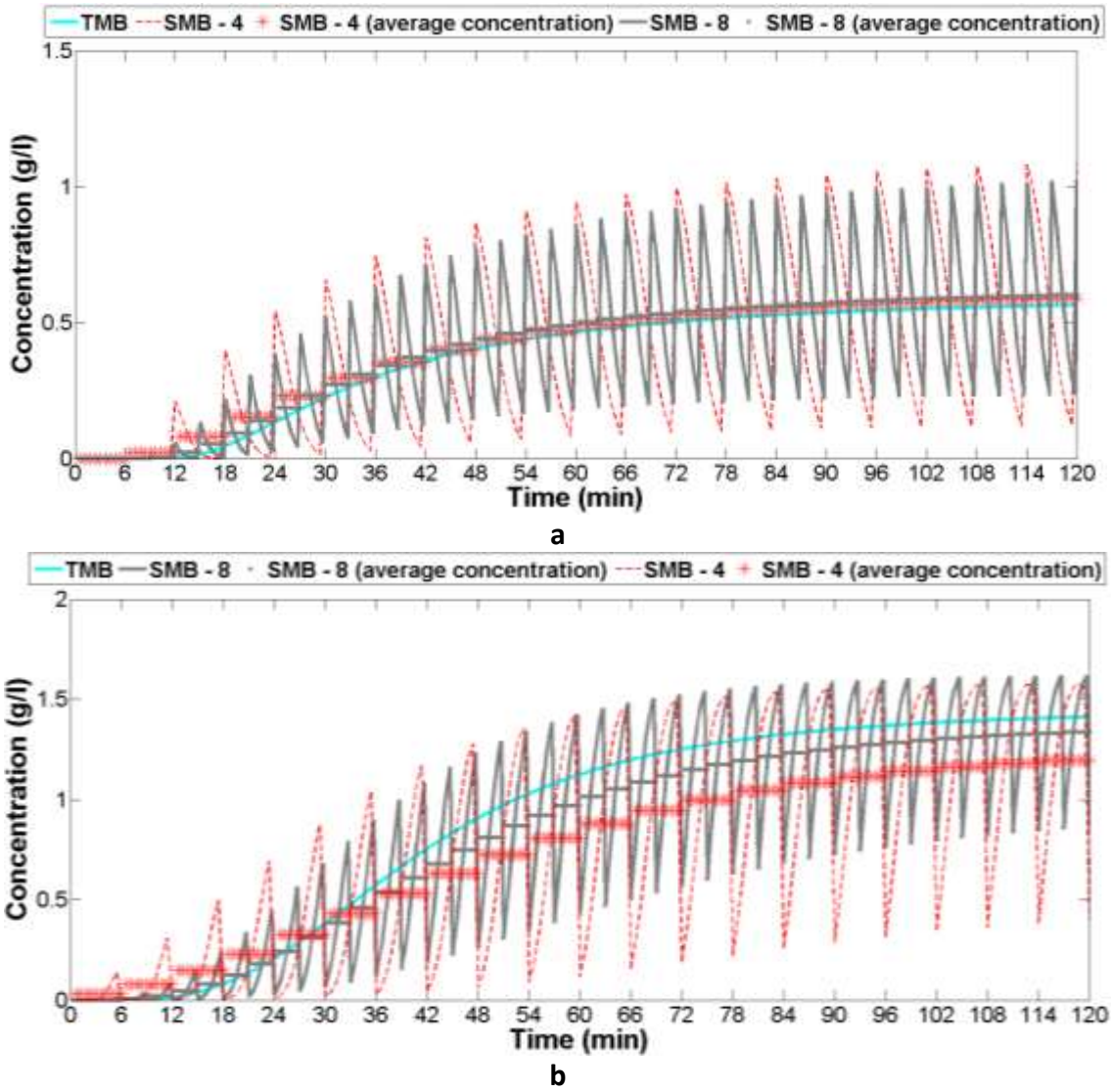

Figure 22 – Concentrations history for: a – most adsorbed component in the extract stream; b - less retained component in the raffinate stream.

It is observed that the trend of the average concentrations of the more retained component in the extract stream of the SMB units, Figure 22.a, is equivalent to the evolution over time in the TMB unit, although the SMB with eight columns resembles more the behaviour of the TMB. In the case of the raffinate stream, Figure 22.b, comparing with the TMB unit, there is a greater difference in the evolution of the average concentrations of the less retained component.

However, the results obtained for the SMB-8 are closer to the results of the TMB when compared to those of the SMB-4. These results are in accordance with the literature. This indicates that the history until the steady state of the average concentrations of the SMB will approximate the TMB as the number of columns of the SMB increases. However, the analysis based on the orthogonalization method, which resulted in a different conclusion, considers the instantaneous concentrations and is based on the sensitivity matrix of the process response over time relative to the operating variables.

In order to assess the dynamic behaviour of the different processes, the effect of step changes in operating variables on the responses of the performance parameters (purity and recovery) will be presented in the next section.

P1-3.2.3. Models comparison: dynamic regime

The initial conditions of the simulations presented in this section correspond to the (cyclic) steady state of each process as presented in Figure 22. Two individual step perturbations were performed to each of the operating variables, corresponding respectively to more and less 10% of their values for feed concentrations, and eluent, extract and feed flow rates. In the case of perturbations to the recycling flow rate and switching time, in order to keep the equivalence between the processes, the perturbations were done as follows. A 10% perturbation on the value of the solid flow rate was considered and equivalent perturbations on the switching times of the SMB-4 and SMB-8 were set from the equation $u_s = {}^{L_c}/_{t^*}$. For the recycling flow rate a

perturbation of 10% for the TMB case was performed and the equivalence to the SMB was considered by $Q_{IV} = Q_{IV}^{SMB} - \frac{\varepsilon}{1-\varepsilon} Q_s$. The results are presented in deviation values, relative to the corresponding steady state, which facilitates the analysis of the results. In the following figures, the processes (TMB, SMB-4 and SMB-8) responses in terms of average and instantaneous purity and recovery values are given.

The responses to the steps perturbations in the recycling flow rate are shown in Figure 23. From Figure 23.a and Figure 23.c it is possible to observe that after the first perturbation (increase of 10%), all processes reach a new steady state, in which the values for the SMB-4 unit are higher than that of the SMB-8 and closer to the TMB results.

In terms of dynamic behaviour, all units present an inverse response to the perturbation. It is also possible to observe that in all cases the instantaneous values obtained for the SMB-4 unit present larger amplitude when compared to the SMB-8.

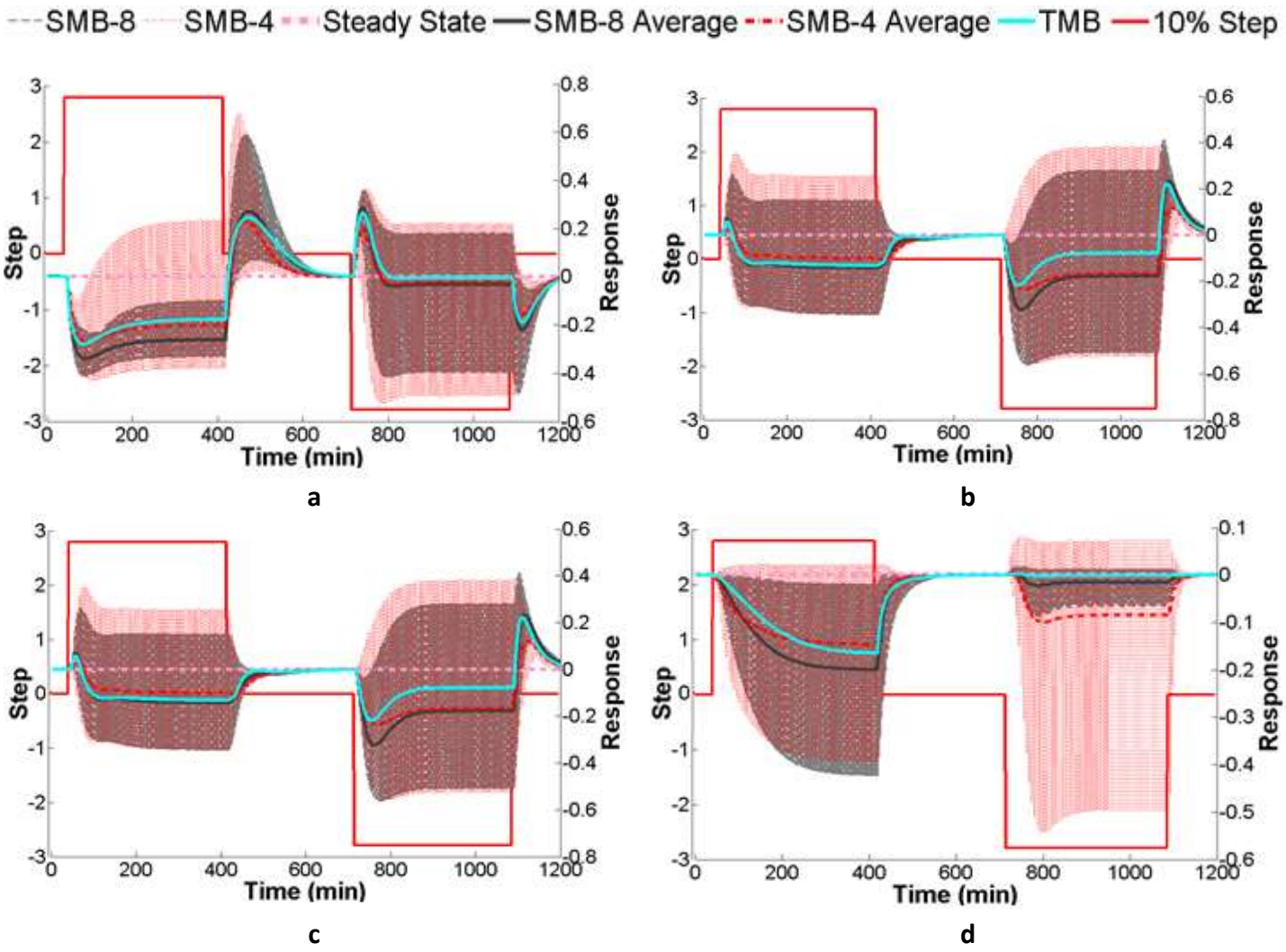

Figure 23 - TMB, SMB-4 and SMB-8 responses to step perturbations in the recycling flow rate: a – responses of the recovery in extract; b. responses of the recovery in raffinate; c – responses of the purity in extract; d – responses of the purity in raffinate.

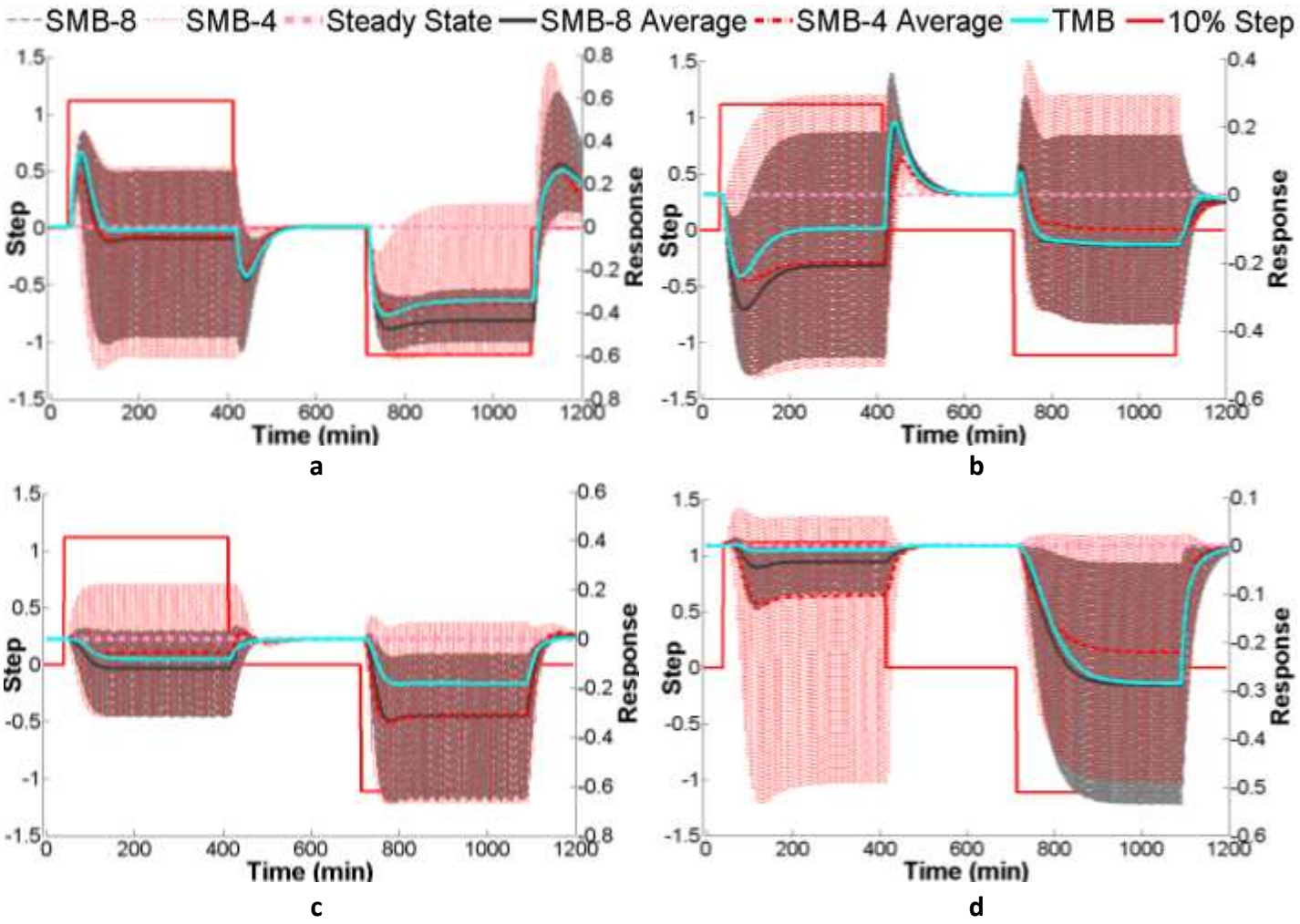

Figure 24 - TMB, SMB-4 and SMB-8 responses to step perturbations in the solid flow rate (TMB unit) and switching time (SMB units): a – responses of the recovery in extract; b. responses of the recovery in raffinate; c – responses of the purity in extract; d – responses of the purity in raffinate.

In Figure 24, the responses to the step perturbations in the solid flow rate u_s (in the case of the TMB unit) or to the switching time (in the case of the SMB units) are given. It is possible to observe that the processes responses to perturbations in the recycling flow rate and solid flow rate/switching time are almost mirror images. Just by simple graphical analyses, it is practically

impossible to detect which of these two operating parameters has the greatest influence on the processes. In this point, the orthogonalization method is a complementary method to the graphical analysis and essential for this distinction.

In this case, the results of the SMB-4 are also closer to the TMB, Figure 24.a and Figure 24.c, but with a significant deviation between the TMB and the SMB units, Figure 24.c, Figure 24.b and Figure 24.d. This occurs because the perturbations lead the process to an operating condition outside the separation region, as previously shown in Section P1-3.1.2; perturbations of this kind can easily occur in industrial operation and, if not taken into account, can lead to low productivity and to the production of products out of specification.

Figure 25 presents the processes responses to the steps perturbations on the eluent flow rate. In this case, all processes tend to similar states and exhibit similar dynamics. However, in Figure 25.a and Figure 25.b, in the early stages after the first perturbation, the SMB units have different dynamic behaviours when compared to the TMB unit. Although it does not influence the final state, this fact is important in the optimization and control of these processes and can lead to conflicts in the resolution of optimization problems if not considered. For example, in the case of the processes control, when a TMB model is considered to control a SMB unit, this can be a complex task due to the measurement problems characteristic of these units (Zenoni et al. 2000; Langel et al. 2009) and the huge effort that requires to run non-linear models over large prediction horizons, which is required due the significant differences found in the dynamics of both systems.

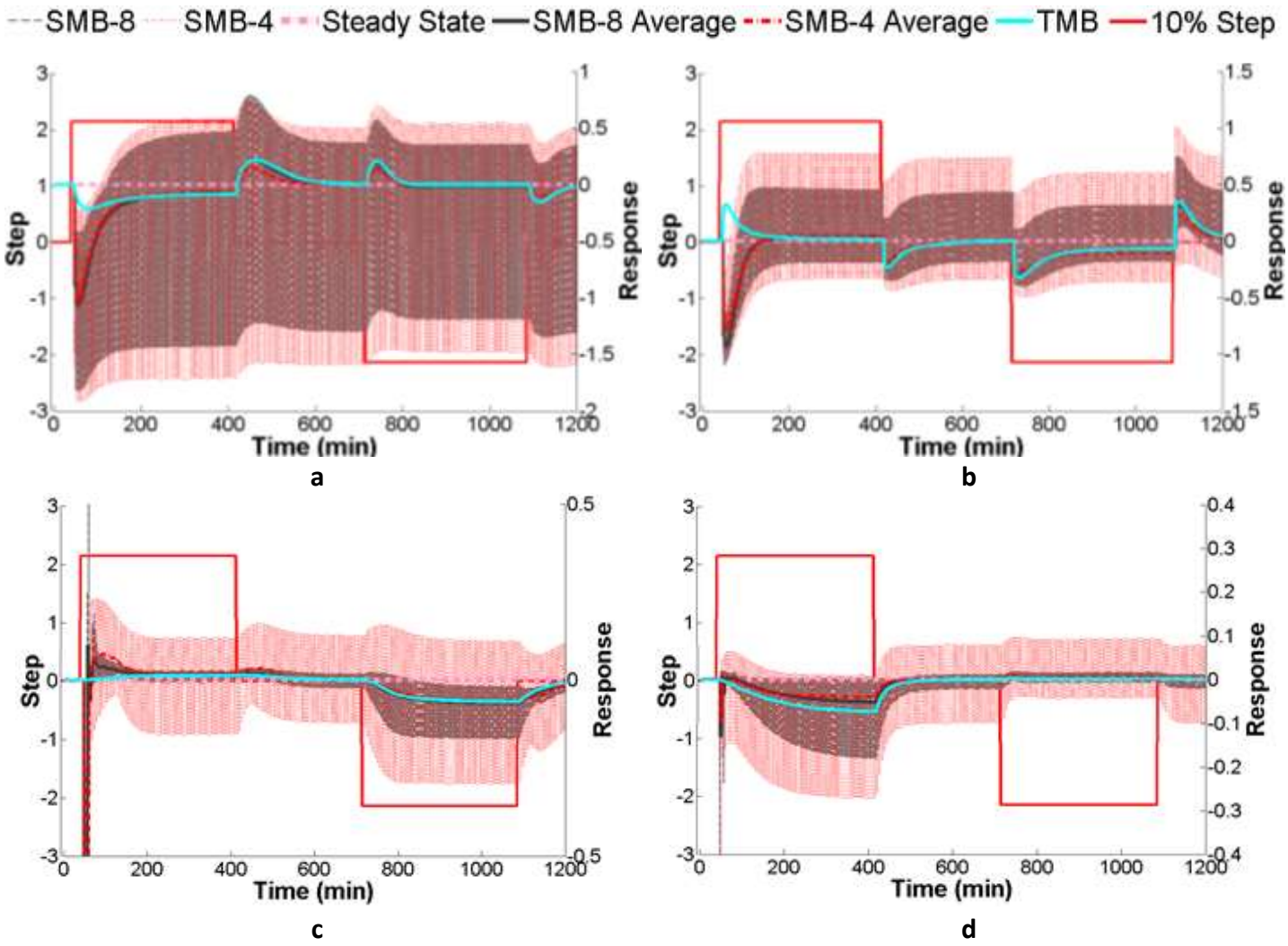

Figure 25 - TMB, SMB-4 and SMB-8 responses to step perturbations in the eluent flow rate: a – responses of the recovery in extract; b. responses of the recovery in raffinate ; c – responses of the purity in extract; d – responses of the purity in raffinate.

The processes response to step perturbations in the extract flow rate are shown in Figure 26. A similar behaviour to that observed for variations in the eluent flow rate can be seen, but reversed. This occurs because an increase in the eluent flow rate will cause an increase in the flow rate of

section II while an increase in the extract flow rate will cause a reduction in flow rate of section II. So the two variables have opposite effects in the separation zone of the units.

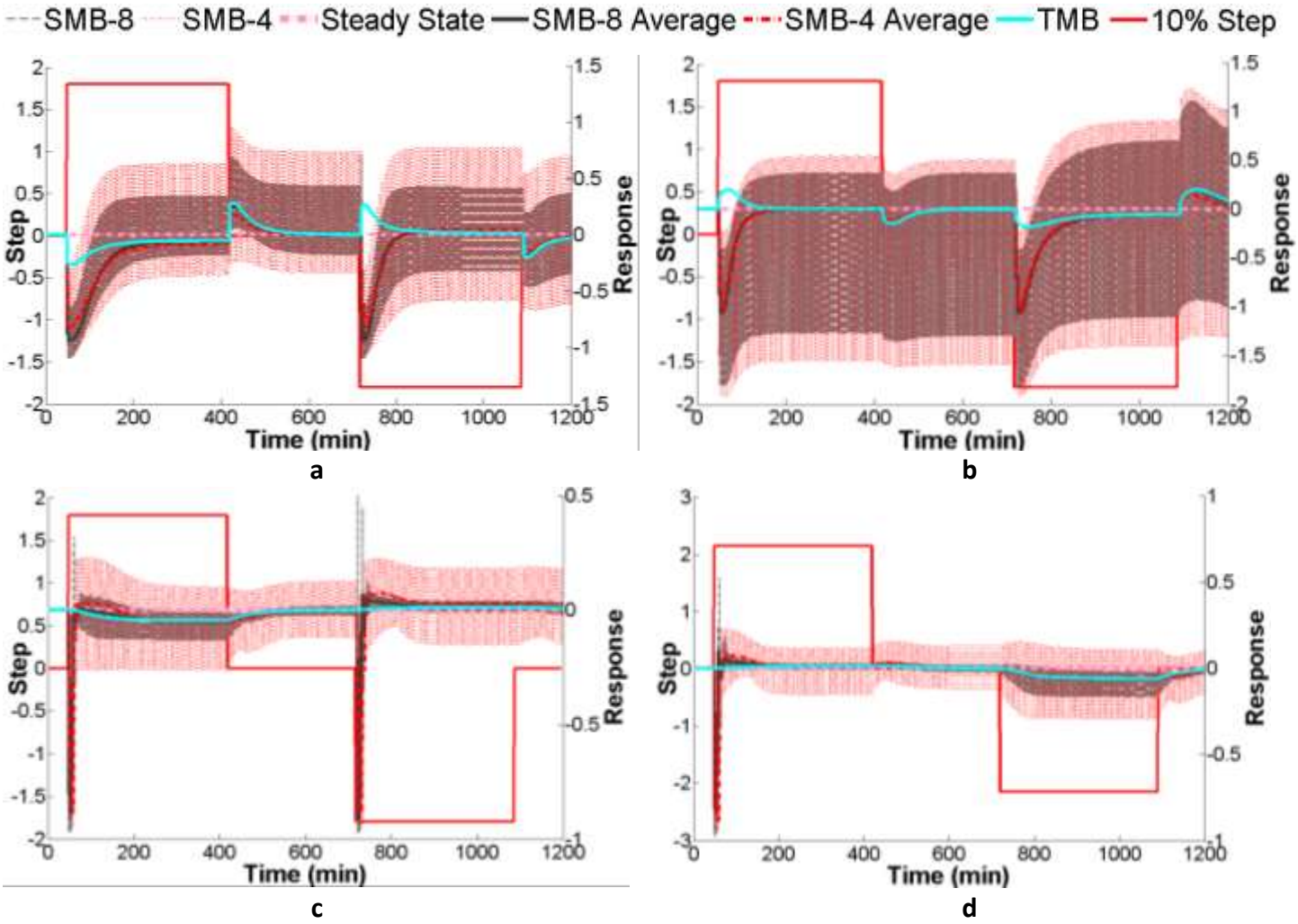

Figure 26 - TMB, SMB-4 and SMB-8 responses to step perturbations in the extract flow rate: a – responses of the recovery in extract; b. responses of the recovery in raffinate ; c – responses of the purity in extract; d – responses of the purity in raffinate .

As noted in Figure 25 and Figure 26, the perturbations in these variables cause a small change in the steady state condition. Section P1-3.1.2 also presented the effect of these variations in the regeneration zone of the TMB unit, showing that after these variations the operating conditions

were still inside both separation and regeneration zones. Furthermore, the results obtained from the orthogonalization method also showed that these variables have less influence in the process when compared with the recycling flow rate and the solid flow rate/switching time.

Figure 27 shows the response of the different processes to perturbations in the feed flow rate. It can be seen that the processes have a lower sensitivity to variations in this variable. However, the decrease disturbance has higher impact in the instantaneous purities and recoveries in opposition to what is observed for the increase disturbance. In Figure 27.a and Figure 27.b, in the early stages after the second perturbation, an opposite response of the SMB processes relative to the TMB is observed.

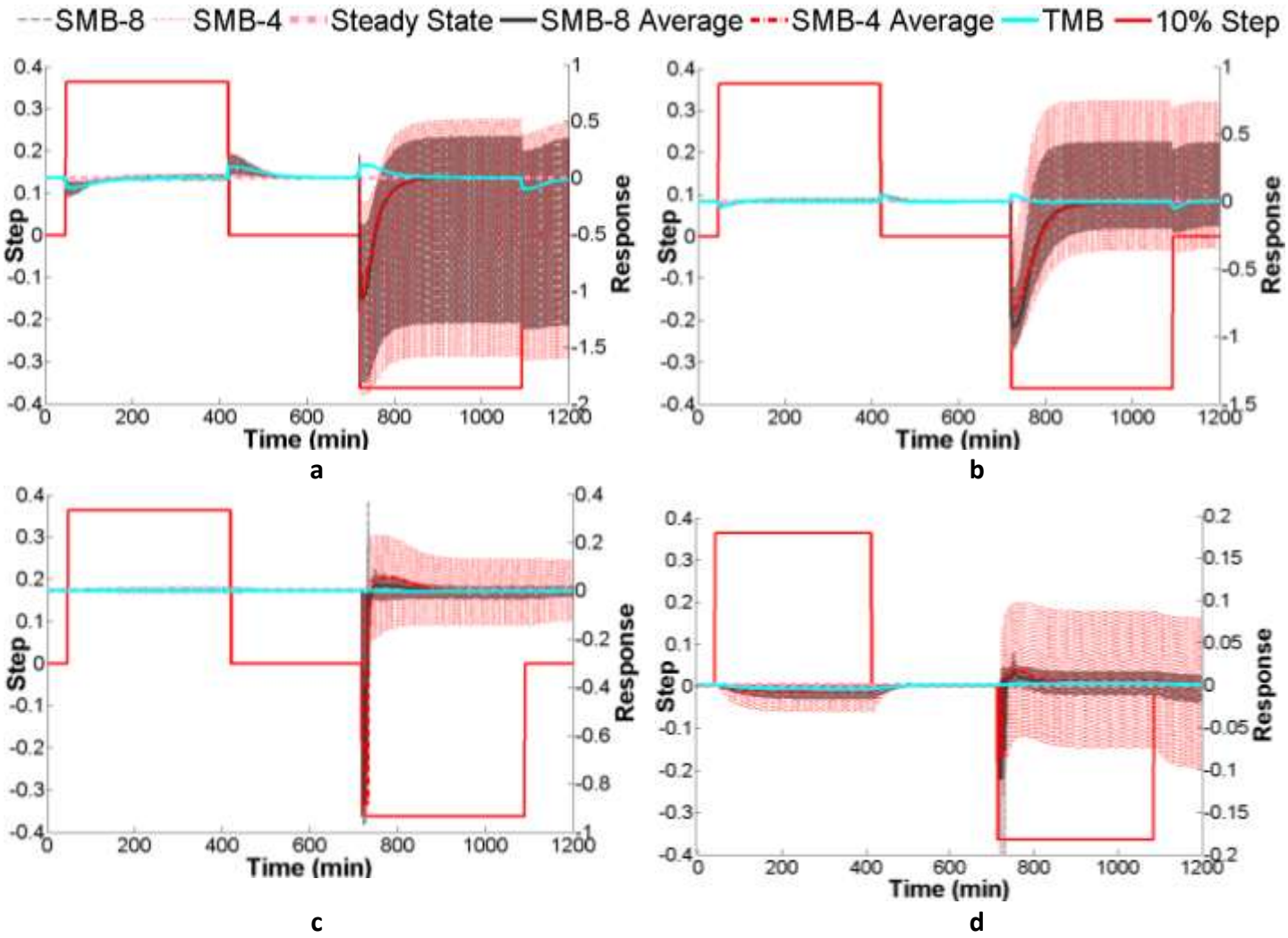

Figure 27 - TMB, SMB-4 and SMB-8 responses to step perturbations in the feed flow rate: a – responses of the recovery in extract; b. responses of the recovery in raffinate; c – responses of the purity in extract; d – responses of the purity in raffinate.

A series of step perturbations was performed in the feed concentration in order to ascertain the effect of changing the feed composition in the systems. The responses to perturbations in the feed concentration of the more adsorbed component are given in Figure 28, where once again it can be seen that the processes have little sensitivity to this variable. However, in this case, the SMB-8 results are closer to those of the TMB when compared to the SMB-4 results, which

presents a significant deviation. Comparing Figure 28.c with Figure 28.d it is possible to note a mirror effect on the process purities. The variation of the feed concentration will lead the system to two different situations, where more or less compound B will be fed to the column. This way, when the concentration of B is increased, the purity of the raffinate stream decreases and the purity of the extract stream increases, while in the reverse situation, the reverse effect is observed. Consequently, a mirror effect is observed on the graphics.

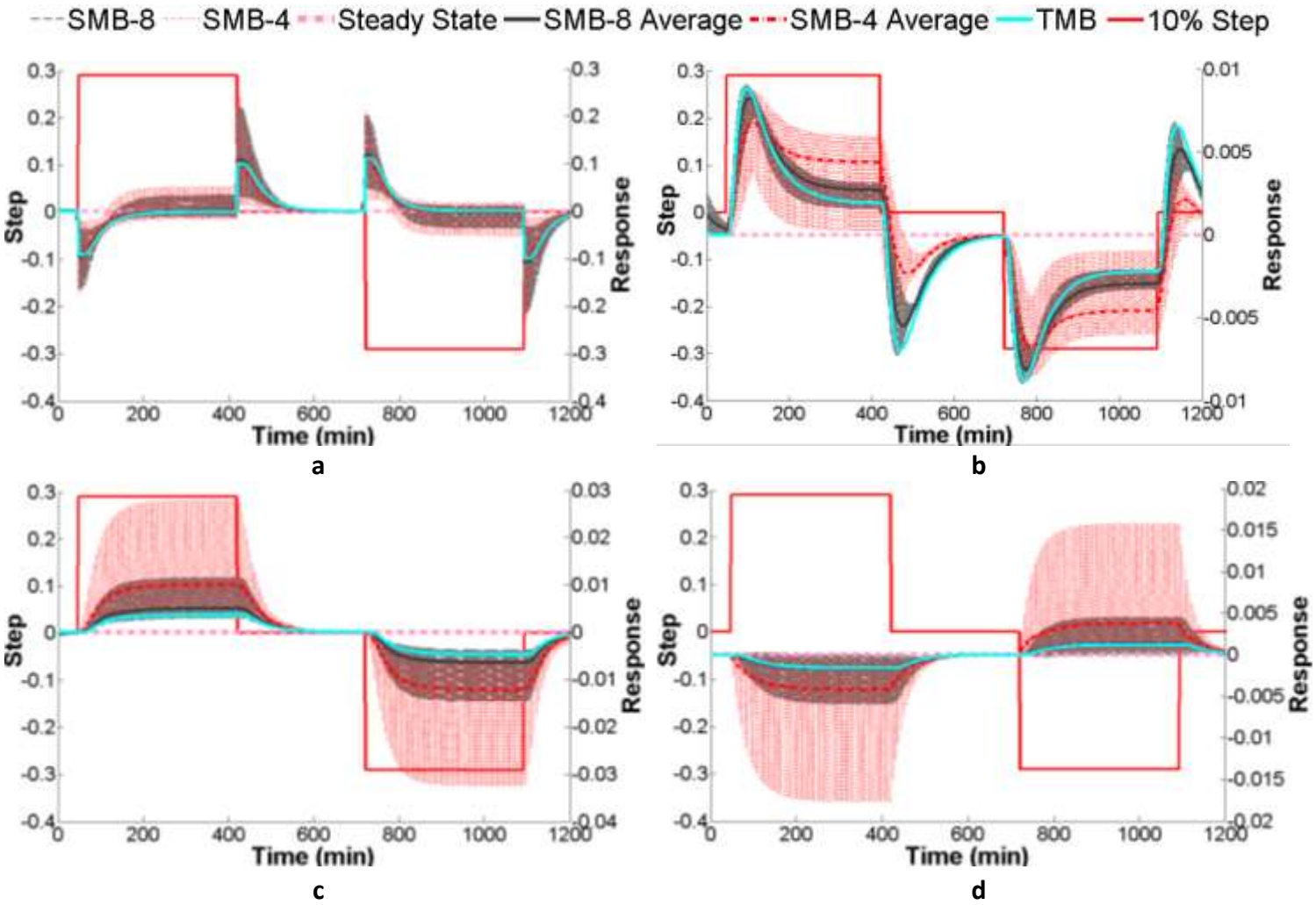

Figure 28 - TMB, SMB-4 and SMB-8 responses to step perturbations in the feed concentration of the more adsorbed component: a – responses of the recovery in extract; b. responses of the recovery in raffinate; c – responses of the purity in extract; d – responses of the purity in raffinate.

P1-3.2.4. Effect of the perturbation size and frequency

A sequence of step perturbations with different sizes and time lengths was performed in the processes in order to do a deeper analysis in the systems dynamic response. Figure 29 presents a sequence of four steps with a short time length equal to one cycle. This was done in order to

avoid the process to reach the cyclic steady state, contrarily to what was done in the previous analysis. The objective in this new situation is to analyse the process behaviour in the presence of an intermittent perturbation. From Figure 29.a and Figure 29.b it is possible to note an interesting behaviour in the response of the recovery in the extract to the sequence of perturbations in recycling flow rate and the response of the purity in the extract to a sequence of perturbations in solid flow rate. The response of these two variables after the short step shows that the SMB-4 gets closer to the TMB while the SMB-8 becomes more distant. After the perturbation ends, this order is reversed and the SMB-8 gets again closer of the TMB. This behaviour repeats at every step perturbation done in the system. From Figure 29.c and Figure 29.d a different behaviour can be noted in the responses of the recovery in the raffinate and of the recovery in extract to the sequence of perturbations in extract flow rate. In this case, both responses of the SMB4 and SMB8 units are far from the response of the TMB but a long time after the second step perturbation, the processes get closer.

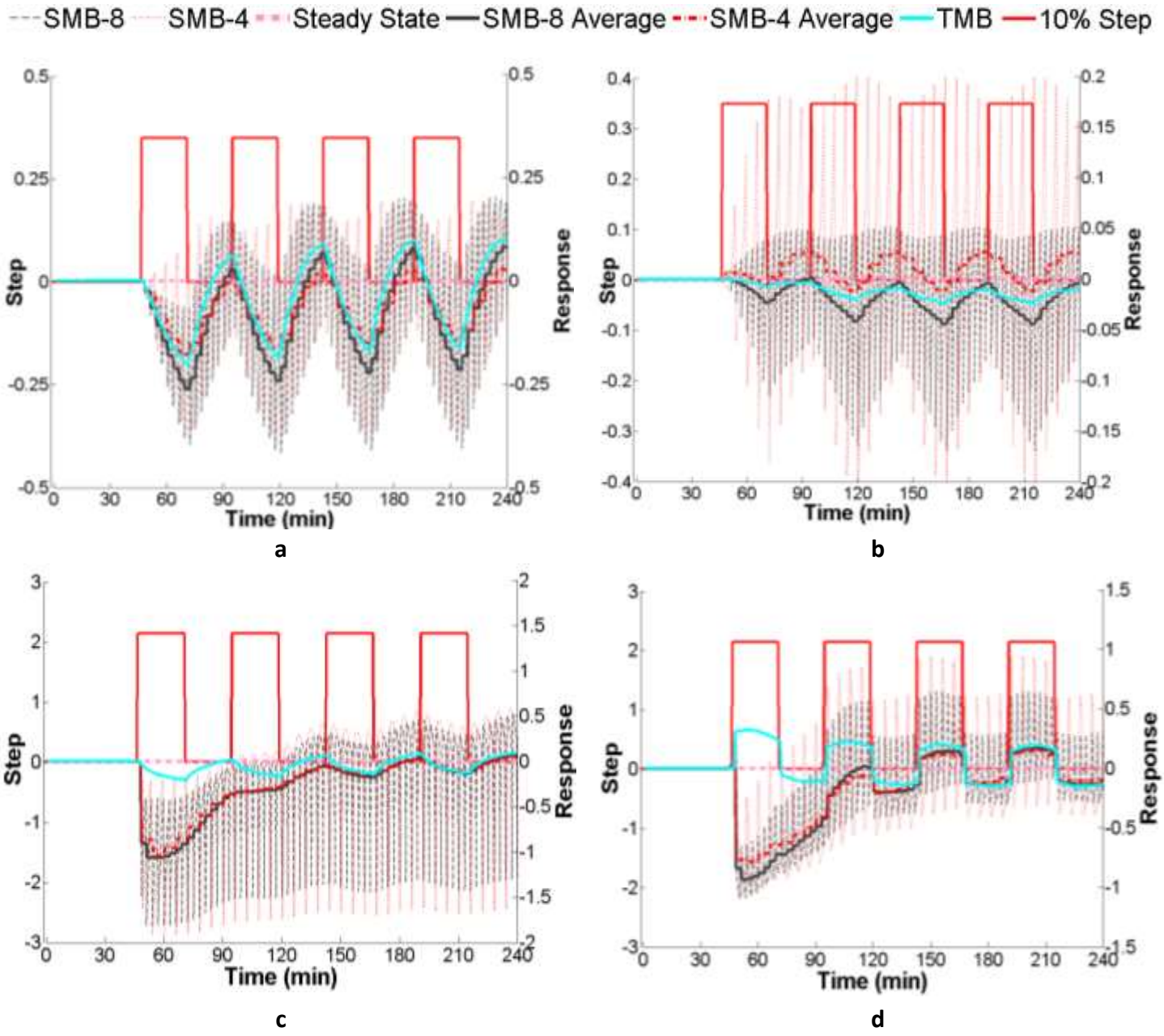

Figure 29 - TMB, SMB-4 and SMB-8 responses to a sequence of step perturbations: a – Recovery in extract response to a sequence of perturbations in the recycling flow rate; b – Purity in extract response to a sequence of perturbations in the solid flow rate; c – Recovery in raffinate response to a sequence of perturbations in the extract flow rate; d – Response of the recovery in extract to a sequence of perturbations in the extract flow rate.

In Figure 30 and Figure 31 are presented the responses of the recovery and purity in raffinate to two (sequential up and down) step perturbations of different intensities, 10%, 5% and 2%. In the two figures it is also presented the step response of systems with linear isotherm to a 10% step perturbation. From the two figures it is possible to note that, when the intensity of the perturbations decreases, the processes dynamic behaviour gets closer to each other. This happens because there is a minimum perturbation strength after which the system operating point leaves the respective separation region. In this way, it is possible to conclude that, when the process is operated in a zone outside of the separation region, the dynamic behaviour of the process is clearly different of what was expected from the steady state analysis previously done in the literature. This conclusion is very important in the process control where the process takes the risk of suffering perturbations of any intensity. This dynamic behaviour must be taken into consideration in the formulation of a control problem to this system. The same conclusions can be drawn from the analyses of the step perturbations in the other process operating variables.

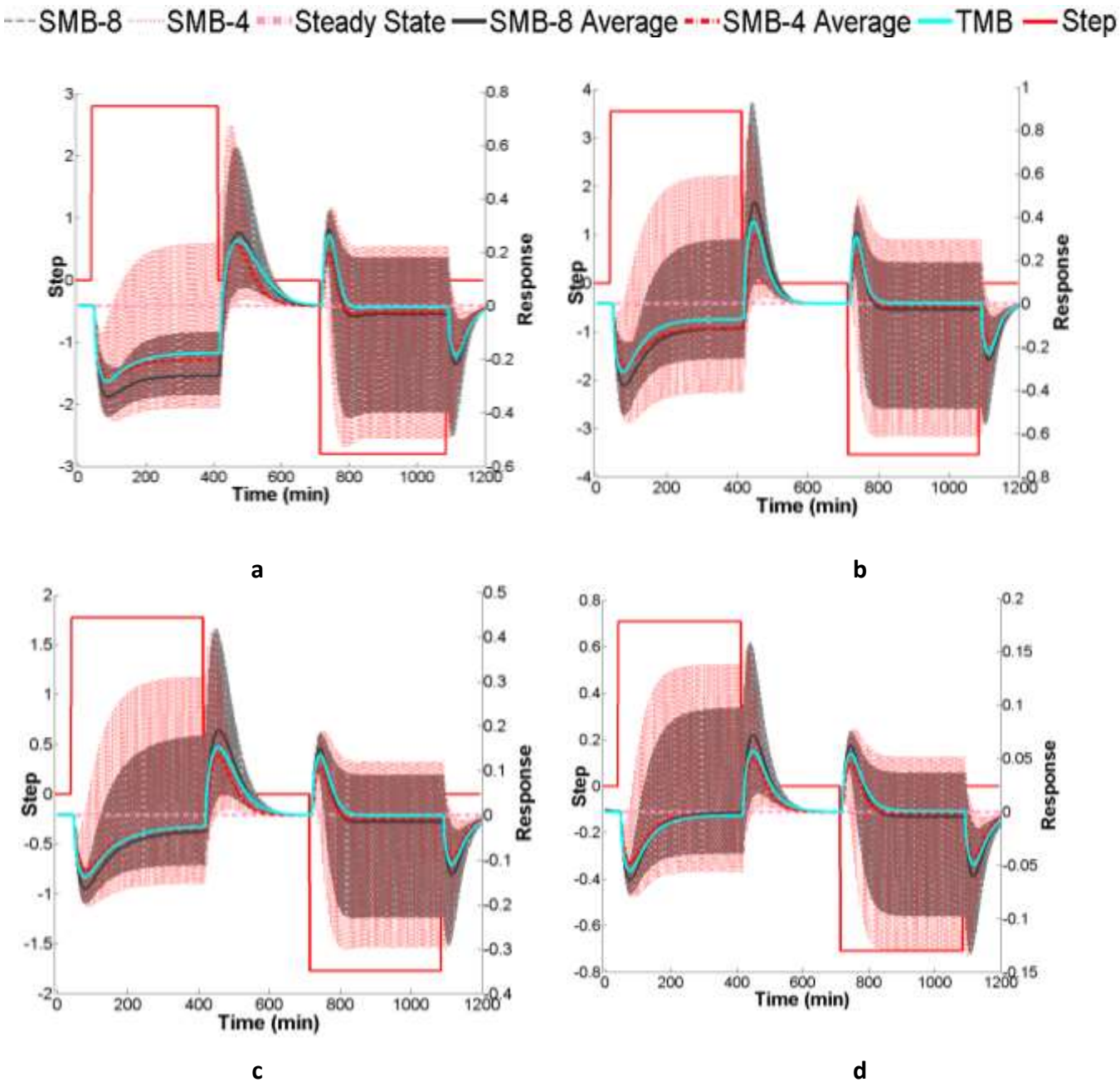

Figure 30 - TMB, SMB-4 and SMB-8 recovery in raffinate responses to step perturbations in the recycling flow rate: a – 10% step; b - 5% step; c – 10% step linear isotherm; d – 2% step.

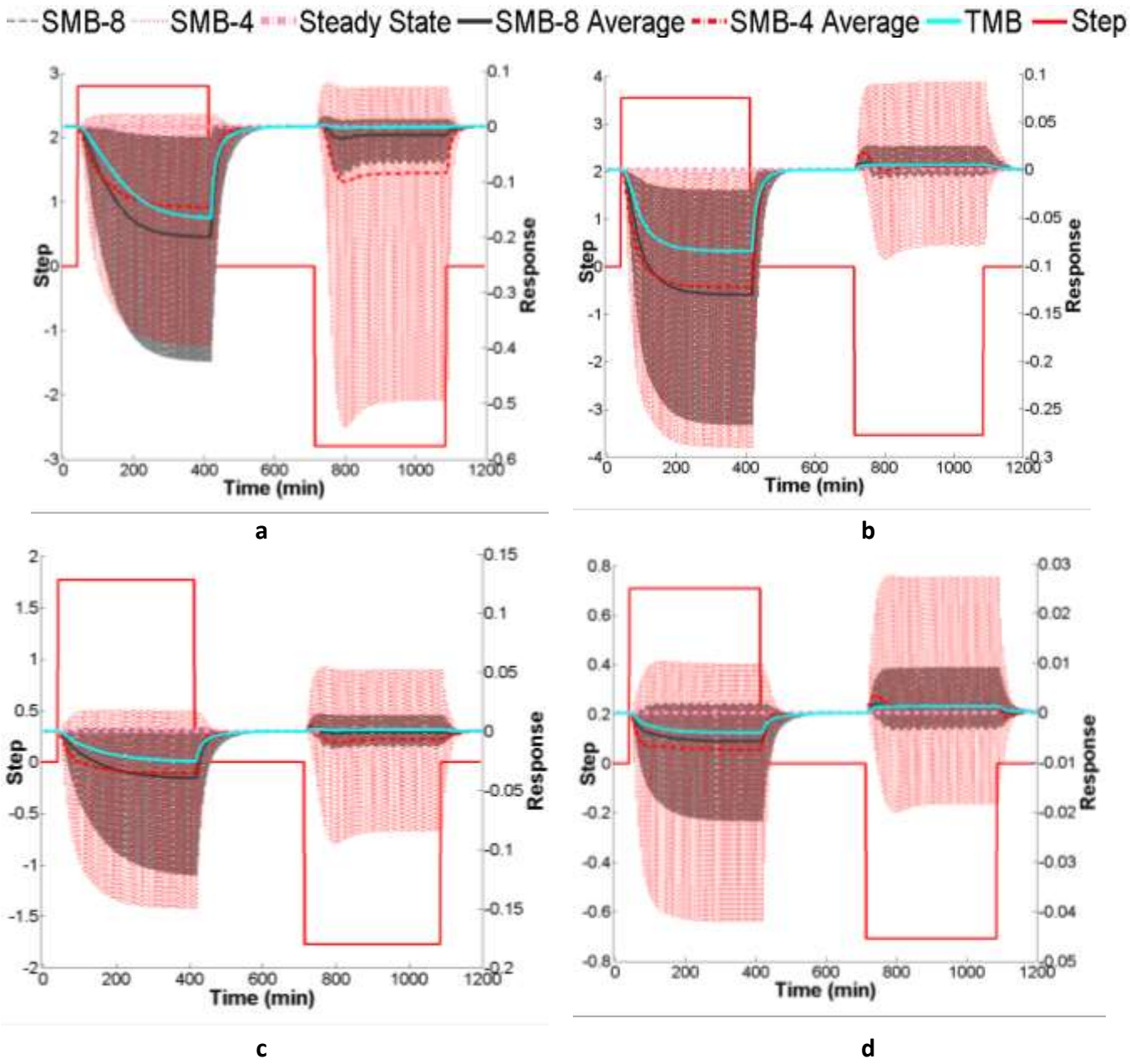

Figure 31 - TMB, SMB-4 and SMB-8 purity in raffinate responses to step perturbations in the recycling flow rate: a – 10% step; b 5% step; c – 10% step linear isotherm; d – 2% step.

Figure 32 presents the internal concentration profile after a +10% perturbation in the recycling flow rate is imposed, as showed in Figure 23. It can be seen that the new steady state moves the processes towards a region of less purity in both outlet streams. For this case, the extract stream

of the SMB units, Figure 23.c, presents a lower purity when compared with the TMB, and a similar value when compared to each other. However, in the raffinate stream, Figure 23.c, the SMB-4 unit presents the highest purity and closer to the TMB when compared with the SMB-8. This difference can be observed in terms of internal profile concentrations, Figure 32, where in the raffinate stream, after reaching the new steady state, the SMB-8 presents a concentration of the stronger retained compound 77% higher than the concentration of the same compound in the SMB-4. Figure 32.d and Figure 32.e present the evolution of the internal concentration profiles of the stronger and less retained compounds along time and column length. It is possible to note that although the evolution of the SMB-8 profile seems closer to the TMB profile after the perturbation, the SMB-4 unit presents a better separation than both the other units. As a matter of fact, the perturbations lead the processes to regions outside the equilibrium triangle inducing an unexpected behaviour in the units.

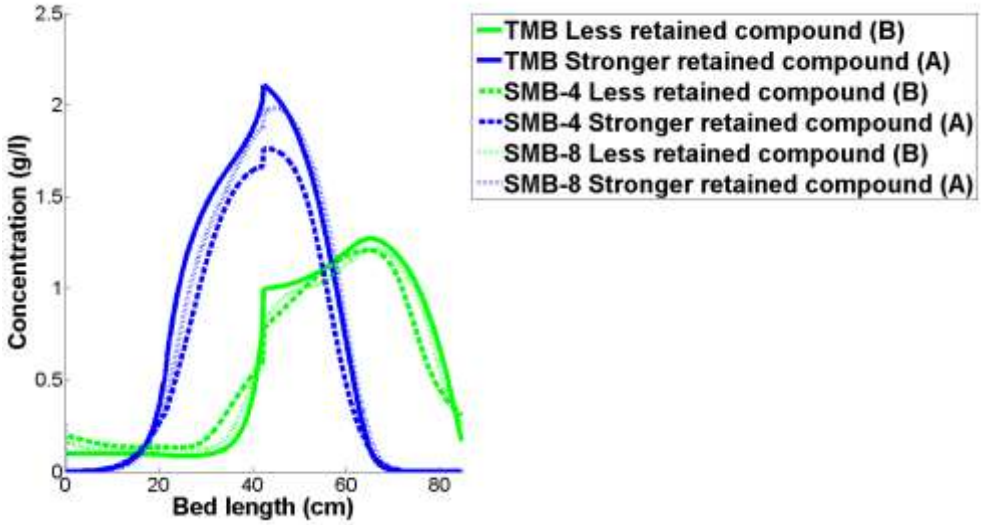
TMB Less retained compound (B)
TMB Stronger retained compound (A)
SMB-4 Less retained compound (B)
SMB-4 Stronger retained compound (A)
SMB-8 Less retained compound (B)
SMB-8 Stronger retained compound (A)
Concentration (g/l)
Bed length (cm)

a.

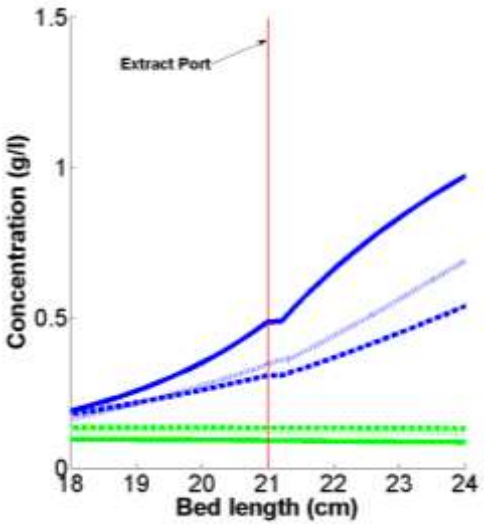
Extract Port
Concentration (g/l)
Bed length (cm)

b.

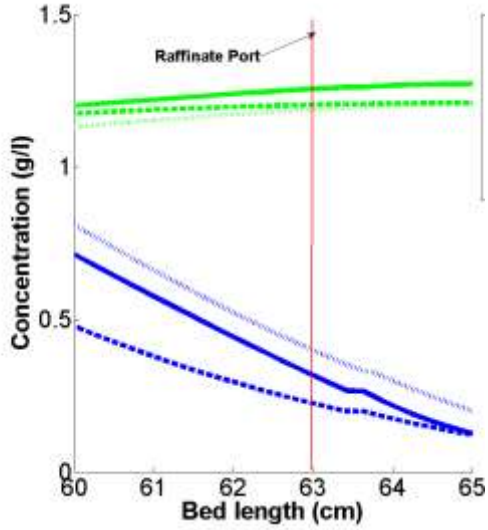
Raffinate Port
Concentration (g/l)
Bed length (cm)

c.

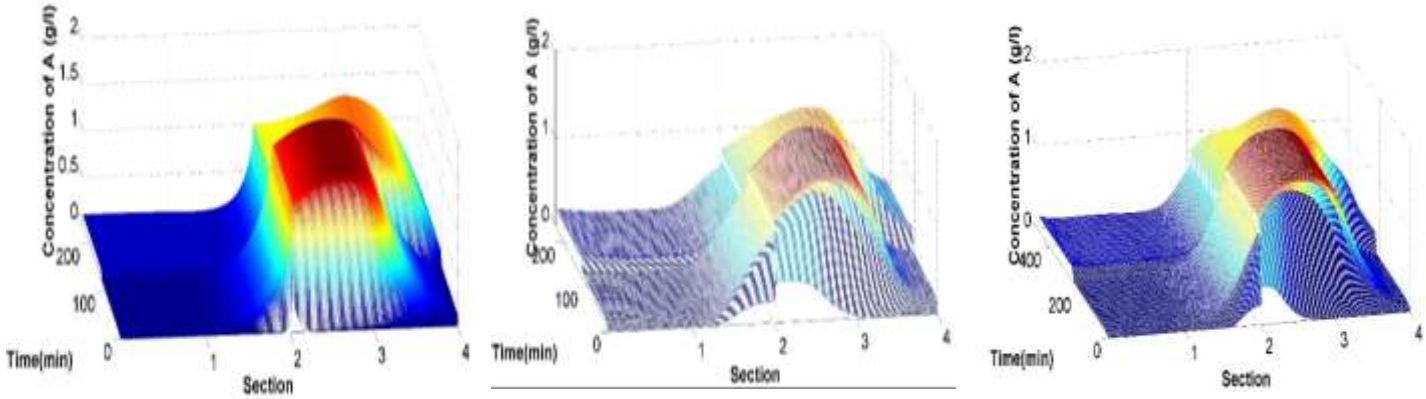
Concentration of A (g/l)
Time(min)
Section

d.I.TMB – Stronger retained compound.

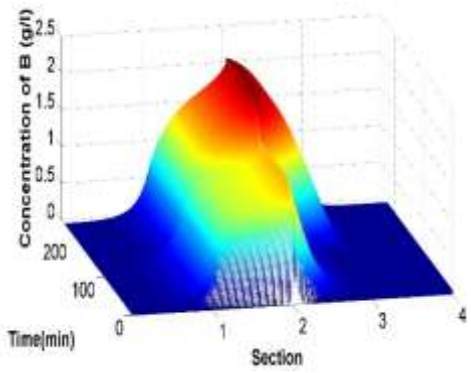

d.II.SMB-4 – Stronger retained compound.

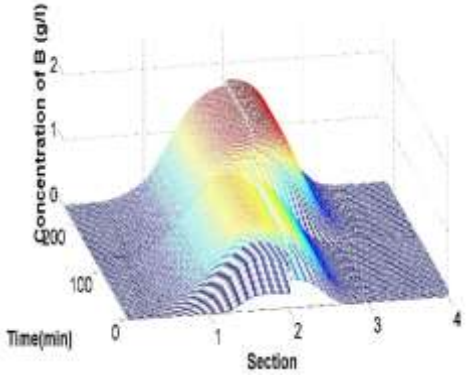

d.III.SMB-8 – Stronger retained compound.

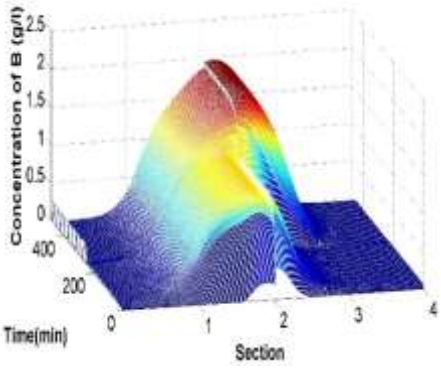

e.I.TMB – Less retained compound

e.II.SMB-4 – Less retained compound

e.III.SMB-8 – Less retained compound

Figure 32 - Units internal concentration profiles. Effect of a +10% perturbation in the recycling flow rate.

P1-3.3. TMB linear advanced model predictive control

P1-3.3.1. Manipulated variables selection

The main objective of this work is to control the purities and recoveries of an SMB unit. The first step to do this is to carefully choose the set of process variables to be used in the system control as manipulated variables (MV). In order to identify the set of MVs, the mathematical method based on the orthogonal projection described in P1-2.2.1 was applied.

As presented in P1-3 the recycling flow rate, Q_{IV}, presents a major effect in this process response. Following the Q_{IV}, the extract flow rate, Q_X, the eluent flow rate, Q_E, and the solid flow rate, Q_S, present the major effects in this sequence. The feed flow rate and feed concentrations have a

minor impact, as can be noted by their magnitude values. As a consequence, the recycling, solid, eluent and extract flow rates were used as manipulated variables. This leads to a 4x4 system with four manipulated variables and four controlled variables. Following the proposed method in Section P1-2.3 for the definition of G_G, 32 transfer functions must be identified, 16 TFs for each local linear model.

The SMB optimal operating conditions and the model parameters used were based on Pais et al. (2000). The process was moved from its optimal conditions in order to identify the transfer functions as previously described. This was done through a perturbation of -15% in the solid flow rate. The data used in the simulations at the optimal condition are given in Table 8.

P1-3.3.2. Transfer functions identification

As explained in Section P1-2.3, the strategy suggested in this work requires the determination of transfer functions at optimal operating conditions and at non-optimal operating conditions. For the simulations at the optimal conditions, the operating conditions determined in Pais et al. (2000) were employed. For the simulations at non-optimal conditions a perturbation of -15% in the solid flow rate was considered. The corresponding operating parameters are given in Table 8.

Table 8 - Data used in the model simulation, suboptimal and optimal conditions used to validate the identification approach.

Process Variables			Model Parameters	
	Suboptimal Conditions	**Optimal Conditions**	k	0.1 s^{-1}
$c_{A/B}{}^{f}$	2.9 $g.l^{-1}$	2.9 $g.l^{-1}$	D_L	0.025 $cm^2.s^{-1}$
Q_E	21.45 $ml.min^{-1}$	21.45 $ml.min^{-1}$	ε	0.4
Q_X	17.98 $ml.min^{-1}$	17.98 $ml.min^{-1}$	L_j	21.0 cm
Q_F	3.64 $ml.min^{-1}$	3.64 $ml.min^{-1}$	Column diameter	2.6 cm
Q_S	10.03 $ml.min^{-1}$	11.15 $ml.min^{-1}$		

At the non-optimal point, three different matrices of transfer functions, relating the manipulated with the controlled variables, were identified, two using the method here proposed ($G_{G\ non\text{-}opt}$) and another from the full process reaction curve (G_{RC}). This was done in order to make a comparison between the two methods and to assess the method consistency, as shown in the next section. Furthermore, the control strategy proposed in this work was applied to the process operating in optimal conditions and two other matrices of TFs were obtained ($G_{G\ opt}$).

To identify the transfer functions, the unit was simulated under a series of step perturbations in its manipulated variables. For the method here proposed, a total of 9600 points were generated from the process simulation, where 2400 were used for each process condition previously mentioned, optimal (positive and negative perturbations) and non-optimal (positive and negative perturbations). To evaluate the method, more 2400 points were generated in the non-optimal

condition to be applied in the traditional reaction curve identification. Table 9 presents the process transfer functions identified at the optimal point. Table 10 presents the transfer function identified by the Reaction Curve and the here presented method for the non-optimal point.

Table 9 - Transfer functions at the optimal point.

$g_{\downarrow}$	Q_s	Q_{IV}	Q_X	Q_E
Pur_X	$\frac{6.229}{72.98s + 1}$	$\frac{0.0245}{59.29s + 1}$	$\frac{1.22}{88.78s + 1}$	$\frac{-0.03455}{6.671s + 1}$
Pur_R	$\frac{4.367}{40.23s + 1}$	$\frac{1.192}{62.55s + 1}$	$\frac{-0.4388}{185.1s + 1}$	$\frac{1.517}{106.9s + 1}$
Rec_X	$\frac{1.904}{60.55s + 1}$	$\frac{265.2s + 0.7857}{1365\,s^2 + 84.15s + 1}$	$\frac{-349.5s - 0.2683}{55.06s^2 + 74.65s + 1}$	$\frac{390.4s + 1.036}{766.1s^2 + 55.36s + 1}$
Rec_R	$\frac{4.761}{0.001s + 1}$	$\frac{-202.8s + 0.04866}{924.5s^2 + 60.81s + 1}$	$\frac{669s + 0.6388}{2320s^2 + 153.2s + 1}$	$\frac{-216.7s + 0.0142}{993.8s^2 + 63.05s + 1}$
$g_{\uparrow}$	Q_s	Q_{IV}	Q_X	Q_E
Pur_X	$\frac{-0.2139}{55.16s + 1}$	$\frac{-2.625}{88.79s + 1}$	$\frac{0.134}{61.12s + 1}$	$\frac{-1.532}{91.6s + 1}$
Pur_R	$\frac{-1.916}{62.45s + 1}$	$\frac{-2.654}{42.1s + 1}$	$\frac{-1.373}{109s + 1}$	$\frac{0.395}{207s + 1}$
Rec_X	$\frac{-348.1s - 1.294}{1651s^2 + 81.27s + 1}$	$\frac{-1.38}{64.28s + 1}$	$\frac{-377.5s - 0.9327}{744.1s^2 + 54.56s + 1}$	$\frac{242.8s + 0.3477}{471.7s^2 + 43.44s + 1}$
Rec_R	$\frac{308.4\,s - 0.1416}{847.1s^2 + 58.21s + 1}$	$\frac{-2.187}{0.001s + 1}$	$\frac{280.1s + 0.02945}{835.3s^2 + 68.91s + 1}$	$\frac{-1.72}{0.001s + 1}$

Table 10 - Transfer functions for the Reaction curve, and proposed method at the non-optimal point.

G_{RC}	Q_s	Q_{IV}	Q_X	Q_E
Pur_X	$\frac{0.238}{21.62s+1}$	$\frac{0.2389}{21.62s+1}$	$\frac{0.155}{23.13s+1}$	$\frac{0.3972}{28.34s+1}$
Pur_R	$\frac{0.0809}{21.62s+1}$	$\frac{0.1211}{27.16s+1}$	$\frac{0.1347}{28.34s+1}$	$\frac{0.1347}{28.34s+1}$
Rec_X	$\frac{0.1259}{21.62s+1}$	$\frac{0.1882}{27.16s+1}$	$\frac{0.0819}{23.13s+1}$	$\frac{0.2094}{28.34s+1}$
Rec_R	$\frac{0.1577}{27.16s+1}$	$\frac{0.1577}{27.16s+1}$	$\frac{0.0687}{23.13s+1}$	$\frac{0.1755}{28.34s+1}$
$G_{G\ non\text{-}opt}$ $g_{\downarrow}$	Q_s	Q_{IV}	Q_X	Q_E
Pur_X	$\frac{0.1473}{41.87s+1}$	$\frac{0.3935}{24.72s+1}$	$\frac{0.1286}{34.52s+1}$	$\frac{0.3017}{47.58s+1}$
Pur_R	$\frac{0.0499}{41.87s+1}$	$\frac{0.1334}{42.1s+1}$	$\frac{0.0435}{34.52s+1}$	$\frac{0.1023}{47.58s+1}$
Rec_X	$\frac{0.07765}{41.87s+1}$	$\frac{0.2074}{24.72s+1}$	$\frac{0.0677}{34.52s+1}$	$\frac{0.159}{47.58s+1}$
Rec_R	$\frac{0.0650}{41.87s+1}$	$\frac{0.1739}{24.72s+1}$	$\frac{0.0568}{34.52s+1}$	$\frac{0.133}{47.58s+1}$
$G_{G\ non\text{-}opt}$ $g_{\downarrow}$	Q_s	Q_{IV}	Q_X	Q_E
Pur_X	$\frac{0.329}{30.26s+1}$	$\frac{0.3199}{2.471\times10^{7}s+1}$	$\frac{0.1758}{51.47s+1}$	$\frac{0.5008}{36.49s+1}$
Pur_R	$\frac{0.1116}{30.26s+1}$	$\frac{0.00828}{6.685\times10^{4}s+1}$	$\frac{0.05962}{51.45s+1}$	$\frac{0.1697}{0.001s+1}$
Rec_X	$\frac{0.1734}{30.26s+1}$	$\frac{0.2003}{1.710\times10^{5}s+1}$	$\frac{0.09268}{51.48s+1}$	$\frac{0.264}{36.49s+1}$
Rec_R	$\frac{0.1454}{30.26s+1}$	$\frac{0.2394}{1.959\times10^{6}s+1}$	$\frac{0.07769}{51.47s+1}$	$\frac{0.2213}{36.49s+1}$

Figure 33 presents an example of the models identification using process data that were generated through a sequence of two 10% increase and two 10% decrease step changes in all manipulated variables, simulated at the optimal point. As can be noted, the transfer function can adjust the reaction curve with a significant precision. The selection of the transfer functions structure and their parameters estimation was done with the MatLab identification toolbox. Following a parameter estimation procedure, the best fit criterion was used, based on the MSE (mean squared error) between the test data and models prediction, in order to select the best models structure and parameters. The procedure consists in a two-step identification; the first is the definition of the transfer function characteristics followed by the estimation of its parameters. The procedure was repeated until the best MSE is found.

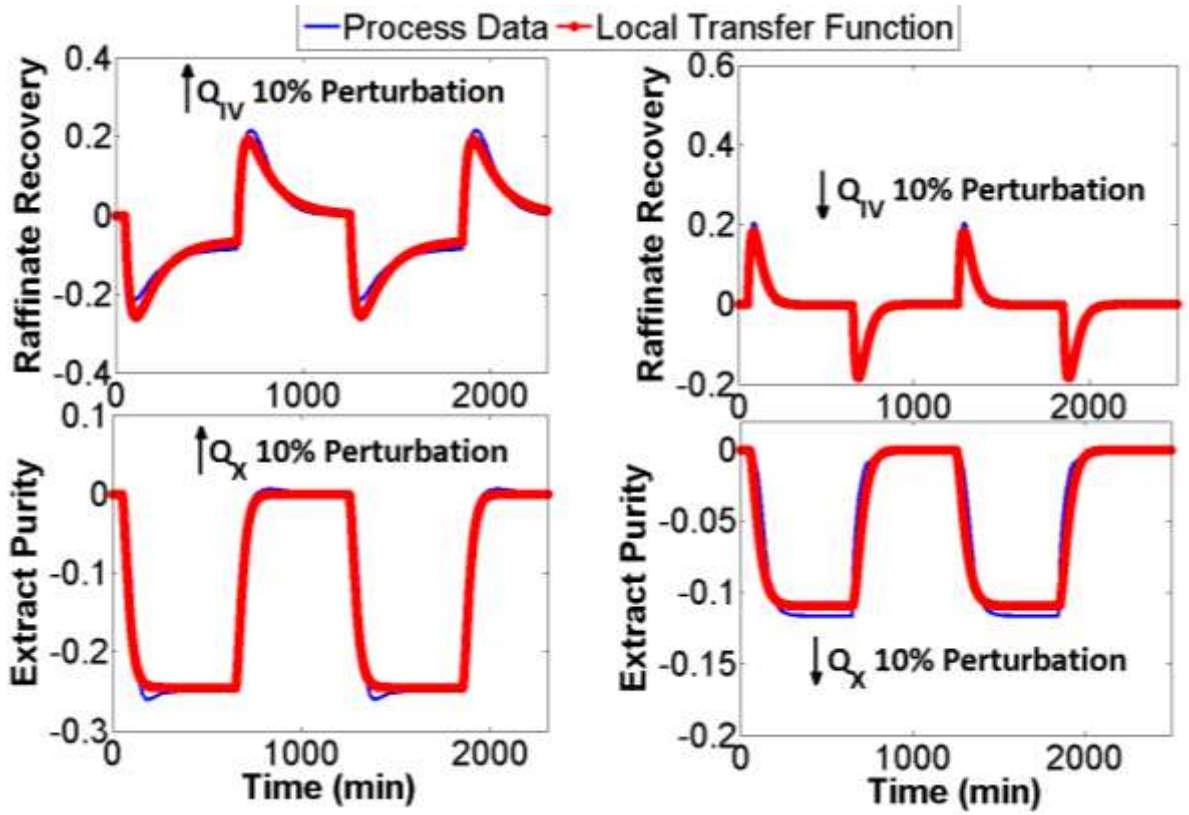

Figure 33 - Local Transfer Function Identification for the responses in recovery and purity to step perturbations in recycling and extract flow rates respectively.

P1-3.3.3. Control systems tests

Several tests were done in order to evaluate the performance of the control systems presented. First, a simulation was conducted at the process non-optimal condition in order to validate the methodology here proposed. After the first test, the methodology was applied in the optimal condition and its performance was evaluated. It is important to highlight that, when applied the traditional MPC or PID controller at the optimal condition, the problem becomes infeasible.

The following scenarios were tested during the control systems simulations for the non-optimal condition:

1. Set point changes, which is usual during the operation. Those were performed in both directions of increase and decrease of process purities and recoveries;
2. A perturbation in the extract flow rate, which can happen due to several reasons, for example a malfunction in the pump.

Figure 34 presents the results of the system control by the MPC using the transfer functions identified in the suboptimal condition; in this case, the process is represented by the phenomenological model. The control system is turned on when the process reaches its steady state. After that, a set point change is simulated by setting purity and recovery in both streams equal to 99%. Using the equivalence between the TMB/SMB, where an equivalent cycle corresponds to 6 minutes, with a controller sample interval of 1 minute, it is possible to note that both MPCs can easily lead the process to its new set point of purity, in a period of approximately 16 cycles or 100 minutes. Analysing the recovery response, it can be noted that the MPCs need more time to lead the process to the new set point, about 30 cycles.

After the set point change, an external perturbation in the extract flow rate was simulated. The MPCs show an efficient result in keeping the process in the set point. Finally, a new set point change was simulated, a reduction to 95% of both purity and recovery. The MPCs again show a significant efficiency leading the process to its new set point in a short period of time. A comparison between the two controllers shows that both present similar behaviour. The major difference is observed in the control of the raffinate recovery, where the MPC that makes use of the transfer function identified through the method here proposed leads the process to a larger variation in the transient state. However, the results show that both MPCs can control the process with success.

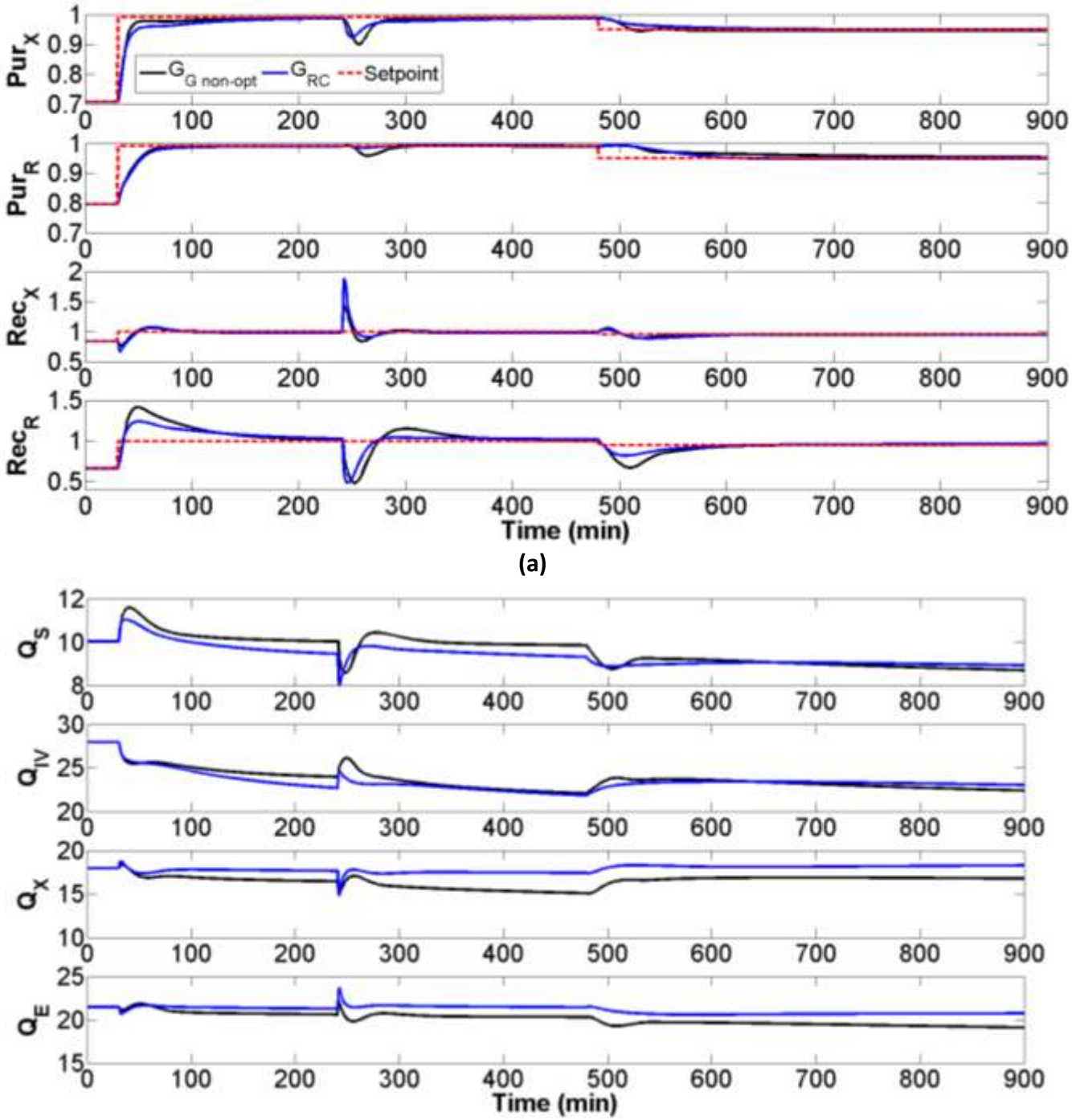

Figure 34 - Process control at the non-optimal condition: (a) Controlled variables; (b) Manipulated variables.

A new simulation was done in order to verify if the process can be efficiently controlled using the transfer functions identified at the optimal point. In this case, it is expected that the proposed

transfer function switching system makes the control problem feasible and leads to an efficient control of the unit. The following scenarios were tested during the control systems simulations for the optimal condition:

1. A perturbation in the extract flow rate;
2. Set point changes;
3. A perturbation in the solid flow rate.
4. Plant model mismatch, through simulation of measurement noise.

Figure 35 shows the results obtained for the process control with the last MPC that makes use of the G_{Gopt} transfer function. Two external perturbations of approximately +10% and -10% were simulated in the extract flow rate and the solid flow rate at the cycles 5 and 80. It was also simulated a set point change from the optimal point to a value of 95% in the process purities and recoveries (in cycle 40). From Figure 35 it is possible to note that the control system can efficiently control the process in all simulated scenarios. It is important to note that, in a period of less than 5 cycles (30 minutes), the MPC can lead the process recovery to the established set point. In the process purities case, the MPC presents a slower response when compared with the recovery but, even in this case, the controller presents efficient results when compared with the usual 30 cycles. The worst case was 25 cycles to conduct the process to the new set point of purity in the raffinate. In the other cases, the process was conducted to its established set point faster than usually. Finally, it is important to note, from Figure 35.b, that the controller could control the process through smooth movements in the manipulated variables.

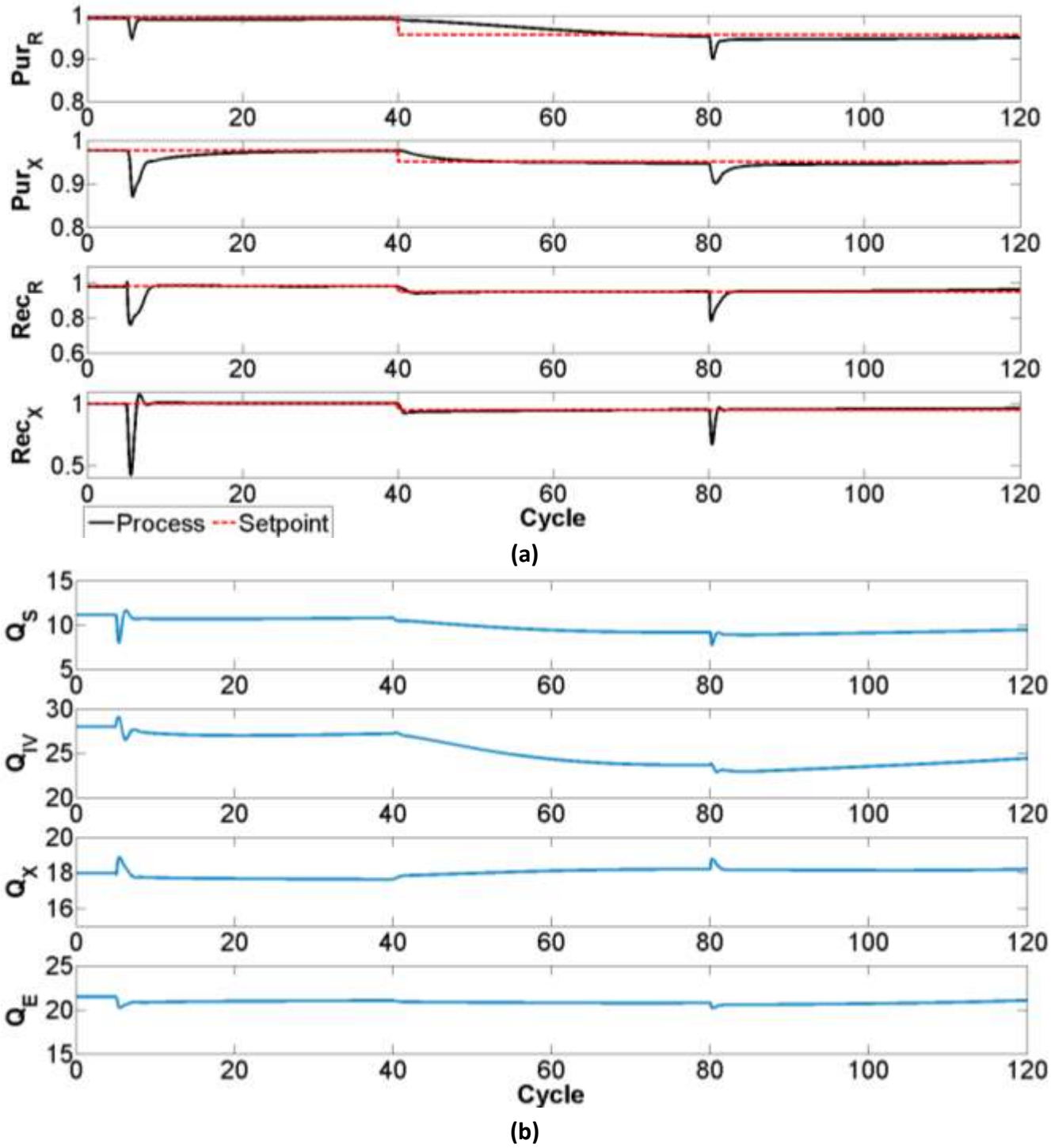

Figure 35 - Process control at the optimal condition: (a) Controlled variables; (b) Manipulated variables.

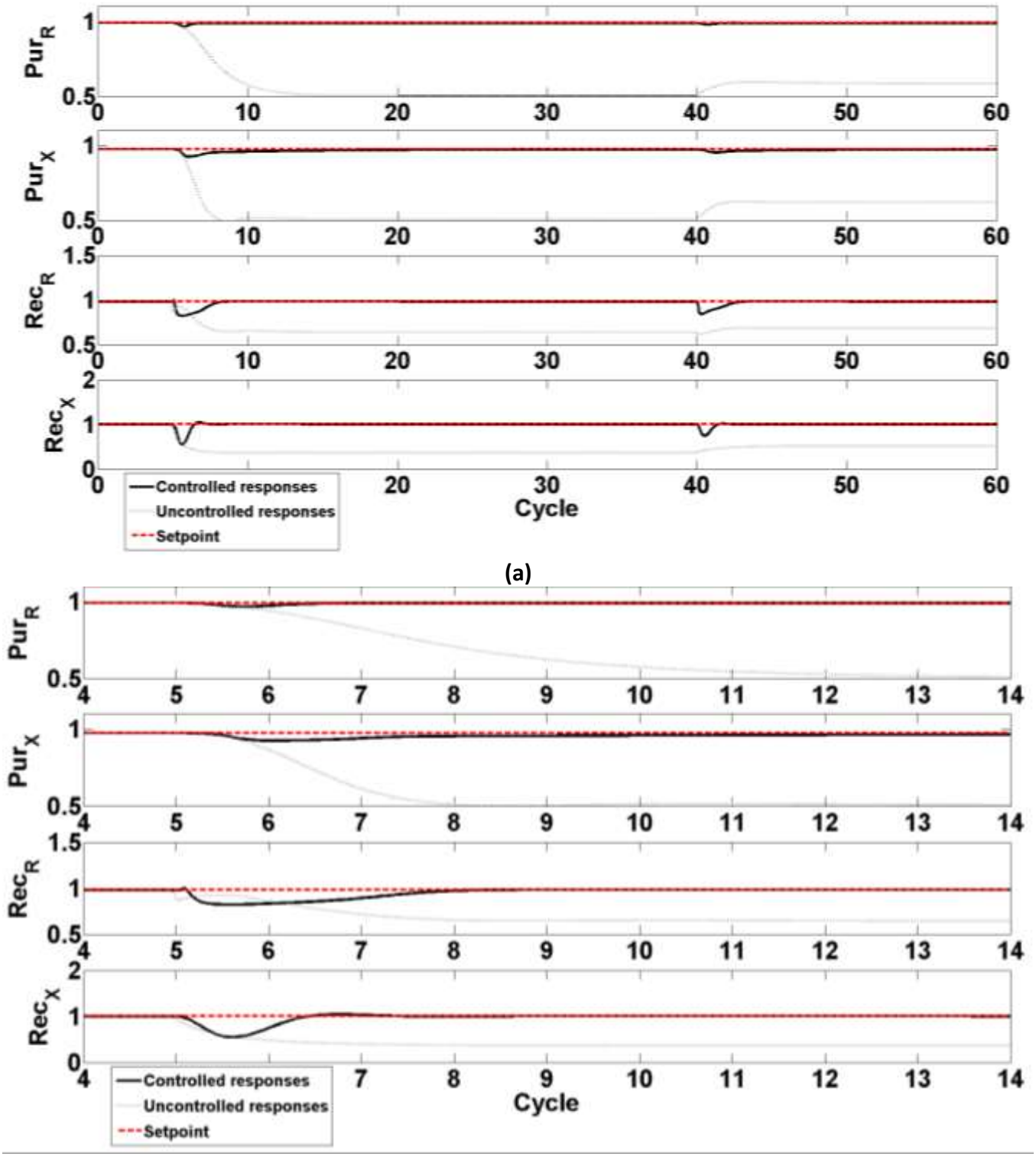

Figure 36 - Process control at the optimal condition and open loop responses: (a) Solid and recycling perturbations responses (b) Solid perturbation responses.

Figure 36 presents the open loop and controlled responses for the TMB unit. In this simulation, the process is kept at its optimal point and two external perturbations are introduced, first in the solid flow rate followed by a perturbation in the recycling flow rate. It is possible to observe that the controller is capable of keeping the process in the optimal condition after each perturbation. Figure 36.b presents a zoom to the instant where the process responds to the solid flow rate perturbation, where it is possible to verify in more detail the open loop behaviour.

Figure 37 presents the control system simulation with a four columns SMB as plant and the previously identified transfer function for the TMB. After the SMB unit reaches its cyclic steady state, the controller is started in order to keep the process in its optimal point. First, one external perturbation in the switching time is simulated (at a time corresponding to 1.45 cycles), followed by a setpoint change (at a time corresponding to 7.5 cycles). As presented in Figure 37, the controller is capable of keeping the process in its setpoint in both situations, taking approximately 4 cycles for the control to stabilize the process after both disturbances.

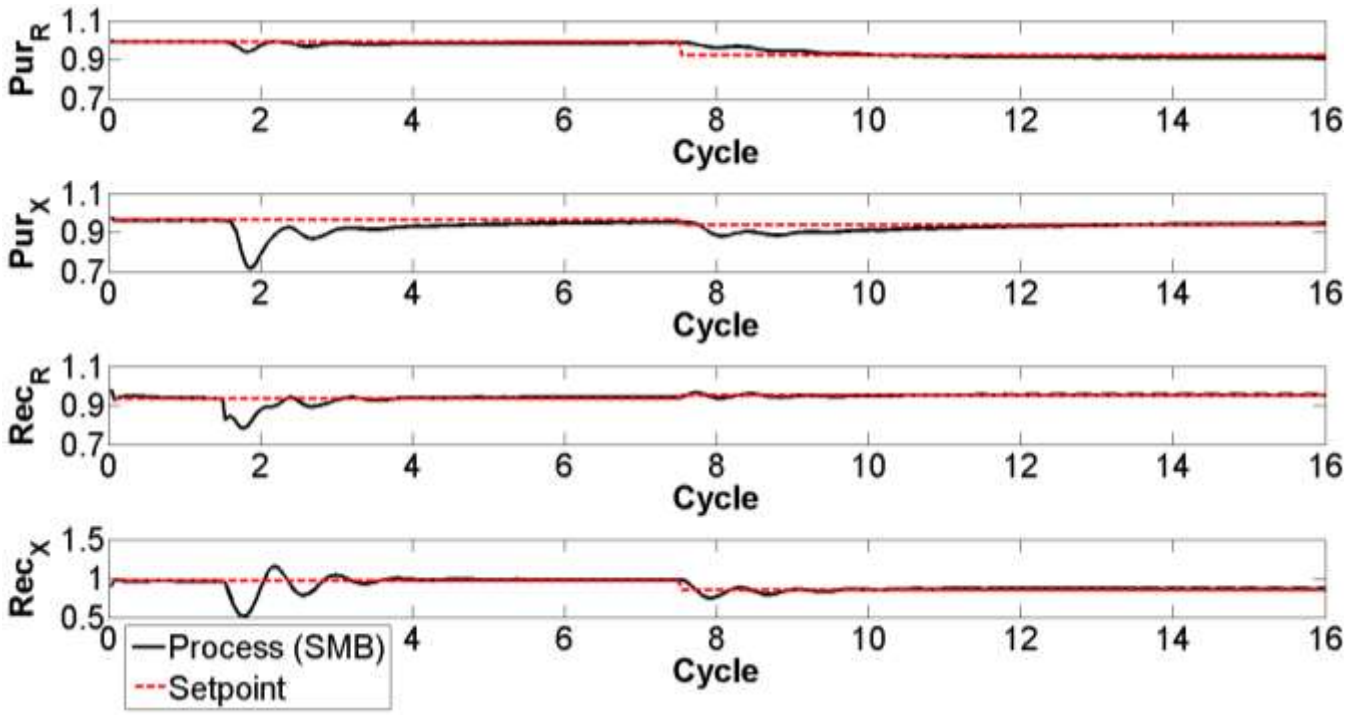

Figure 37 - Control system simulation with a four columns SMB as plant and the previously identified transfer for the TMB.

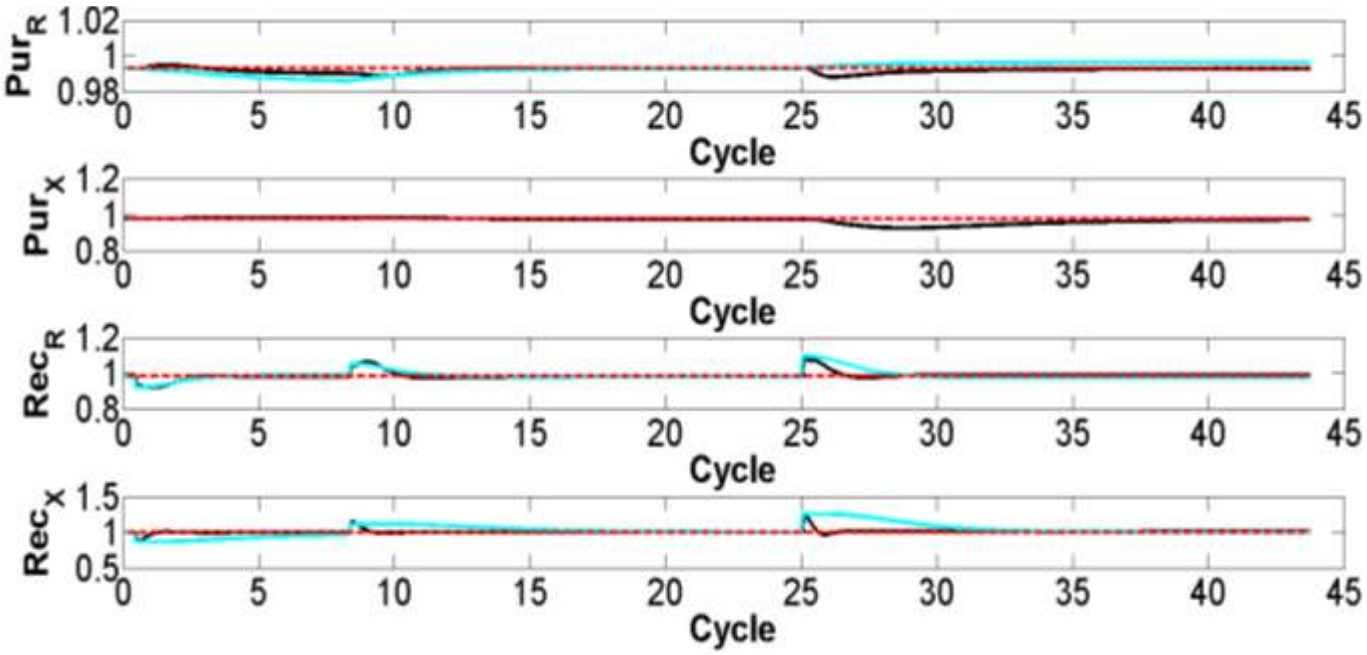

Figure 38 - Process control under feed concentration fluctuations, setpoint (Red line), controller (Black line) and open loop (Blue line) responses.

Finally, as showed by the orthogonalization analysis, the feed concentrations and flow rates have a small effect on the quality parameters (purities and recoveries). However, in order to verify the purities sensitivity to feed concentration, which can sometimes fluctuate in SMB operation, a new simulation with feed concentration fluctuation was performed. In a simulation, two perturbations were done, one of +15% and another of -20%. The following Figure 38 presents the controller (Black line) and open loop (Blue line) responses for the simulation. It is possible to see in the result that the perturbations were not enough to change the process steady state. However, it is also possible to note that, for the recoveries, the controller was able to conduct the process back to its steady state faster than the open loop response.

P1-3.4. Quasi-Virtual Analyser development

The main objective of the quasi-virtual analyser here proposed is to do a real-time monitoring of the purity of the process raffinate and extract streams. To do this, the analyser must receive the information about the process inputs and past outputs. The problem with the past outputs was presented in the P1-2.4 section. In terms of the process inputs, it is necessary to identify the set of process inputs that have the greatest impact on the process. For nonlinear identification problems, the dimension of the model inputs is a crucial factor which greatly affects the computational expense and the performance of the resulting model (Wang et al. 2003). This problem here is addressed applying the orthogonalization method presented in section P1-2.2.1.

Thus, the selection analysis of the input variables was done through the orthogonal analysis. The set of process variables with greater impact only in the process purity was identified and the

operating variables to be used in the development of the Q-VOA were selected. In this way, based on the results of the application of the orthogonalization method to the TMB unit, presented in Section P1-3.1.1, the set of input variables for the virtual analysers was selected. From those results it was concluded that the magnitude of the feed flow rate (Q_F) and feed concentrations ($C_{f,A}\ and\ C_{f,B}$) present the lowest order when compared with the magnitude of the other variables. Furthermore, the step perturbation analysis presented in Section P1-3.1.2 shows that these three variables present a low influence on the process. In order to simplify as much as possible the ANN model, only the recycling (Q_{IV}), eluent (Q_E), solid (Q_s) and extract (Q_X) flow rates were selected as the operating variables to be computed in the Q-VOA system.

Hence, it was possible to build a database of the process responses to variations in these four flow rates ($Q_{IV},\ Q_E, Q_s, Q_X$). The data were acquired through the simulation of the phenomenological model. The data to develop the ANNs models were generated through a sequence of step perturbations in these four process flow rates. The steps had different magnitudes in order to analyse if the process dynamic behaviour, under different conditions, is kept in the ANN model. All step perturbations had a time length enough for the process to reach a new steady state. This was done in order to transmit the process steady states information to the ANN model, which is an important information for the process operation. A total of 39,000 points were acquired corresponding to a period of approximately 40 hours of operation. The data obtained was divided in three groups and the cross-validation method was applied in the development of the neural model (Schenker and Agarwal 1996).

P1-3.4.1. Virtual analyser structure definition

From Section P1-2.4.1 and Figure 8 it can be noted that the number of past outputs, n_a, used to update the ANN model is an adjustable parameter. In the present work, the parameters of the NARX structure were defined as: $n_a = 2, n_b = 1$ and $d = 1$. This numbers showed efficient results when compared with the other predictors configurations.

The training was done using the Levenberg–Marquardt algorithm (Schenker and Agarwal 1996). This step was conducted to avoid the so-called overtraining problem. This problem happens when the network is overflowed with the training data specific information, but with a poor prediction capacity (Schenker and Agarwal 1996; Bowden et al. 2002; Hoque et al. 2011). To avoid this, the early stop method was adopted. This method consists in stopping the training after a given number of iterations in which the validation error grows instead of decreasing, the early stop criterion. If the early stop criterion is not satisfied, the training finishes when the total number of iterations or a minimum gradient of the error derivative is reached. The errors in the training and validation steps were calculated by the mean squared error (MSE) function. In order to analyse the final model prediction, the mean absolute percentage deviation (MAPE) was calculated. The MAPE will give a general idea about the total prediction error in comparison with the simulation, and can be calculated as:

$$MAPE = \frac{1}{n} \cdot \sum_{t=1}^{n} \left| \frac{y - \hat{y}}{\hat{y}} \right| \cdot 100\ (\%) \tag{81}$$

where n is the length of the data set available. The parameters used to develop the neural models and the MAPE of each model are presented in Table 11. It is important to note that the number

of trainings done corresponds to the repetition of the same training to the same number of neurons. This means that, for each neuron, 45 or 40 neural models (for the purity in the extract or purity in the raffinate respectively) were trained, and the one with the minimum MAPE was selected to represent the corresponding neuron number. Furthermore, the number of neurons corresponding to the smallest MAPE and which respect the performance criteria of minimum gradient and early stop was selected as the optimal network structure. The optimal number of neurons in the hidden layer corresponds also to the one which leads to a model that presents the minimum error, as proposed by Schenker and Agarwal (1996) and presented in Figure 39 and Figure 40.

Table 11 - Neural network parameters.

	ANN model for Purity in extract	**ANN model for Purity in raffinate**
Total number of neurons evaluated	45	40
Total number of trainings	45	40
Total iterations in training step	300	300
Minimum gradient	10^{-6}	10^{-6}
Early stop criteria	10	10
Transfer function in the first layer	Hyperbolic tangent sigmoid	Hyperbolic tangent sigmoid
Transfer function in the output layer	Linear function	Linear function
Mean absolute percent deviation	0.060	0.0035

Table 11 presents also the performance criteria used to select the final ANN structure. Those criteria were chosen in accordance with the literature in order to select the most suitable structure to be employed in the problem in study. As it is possible to note, the ANNs models presented a very low mean percentage deviation from the validation data, less than 1%. Finally, following the cross-validation method, Figure 39 and Figure 40 present the simulations of those models employed as a simulator. Figure 39 presents the results of the neural model identification for the purity in the raffinate stream. In Figure 39.a, it can be noted that the five neurons in the hidden layer structure presented the smallest absolute error. In Figure 39.b, the validation of the final neural model is presented. This model is composed by five neurons in its hidden layer and six inputs: four process operating variables and two past predictions. As can be noted in Figure 39.b, the model predicts the data with a good precision, presenting a mean absolute percentage deviation of 0.0035%. The computational time taken in the development of this neural model was approximately 10.5 hours.

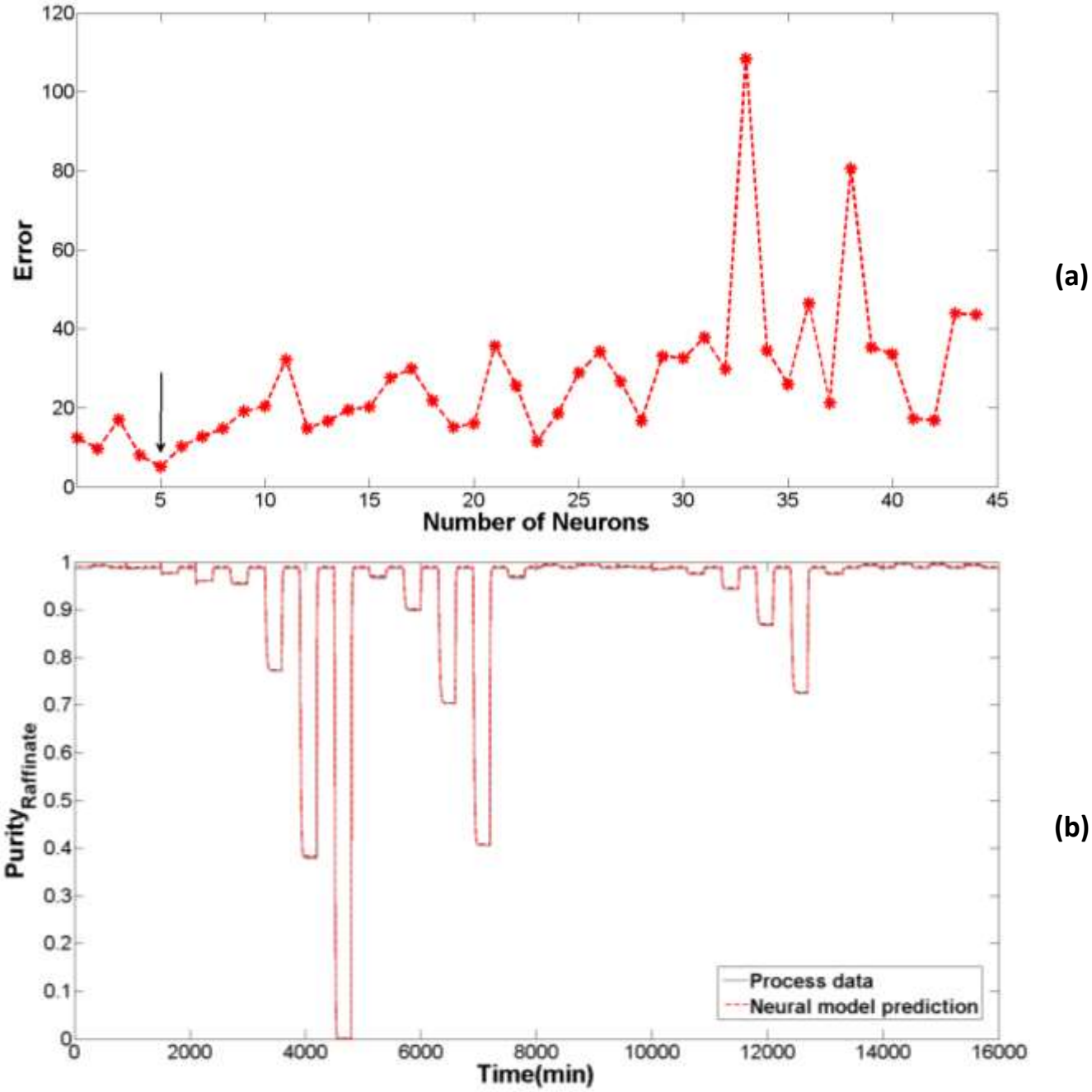

Figure 39 – Raffinate purity ANN model identification: (a) selection of the optimal number of neurons in the hidden layer; (b) final model validation. The neural model prediction, red dashed lines, cover the process data, black line, during all the represented time.

Figure 40 presents the results of the neural model identification for the purity in the extract stream. In Figure 40.a we can note that 17 neurons is the optimal number of neurons in the

hidden layer, presenting the smallest absolute error. In Figure 40.b the validation of the final neural model is presented.

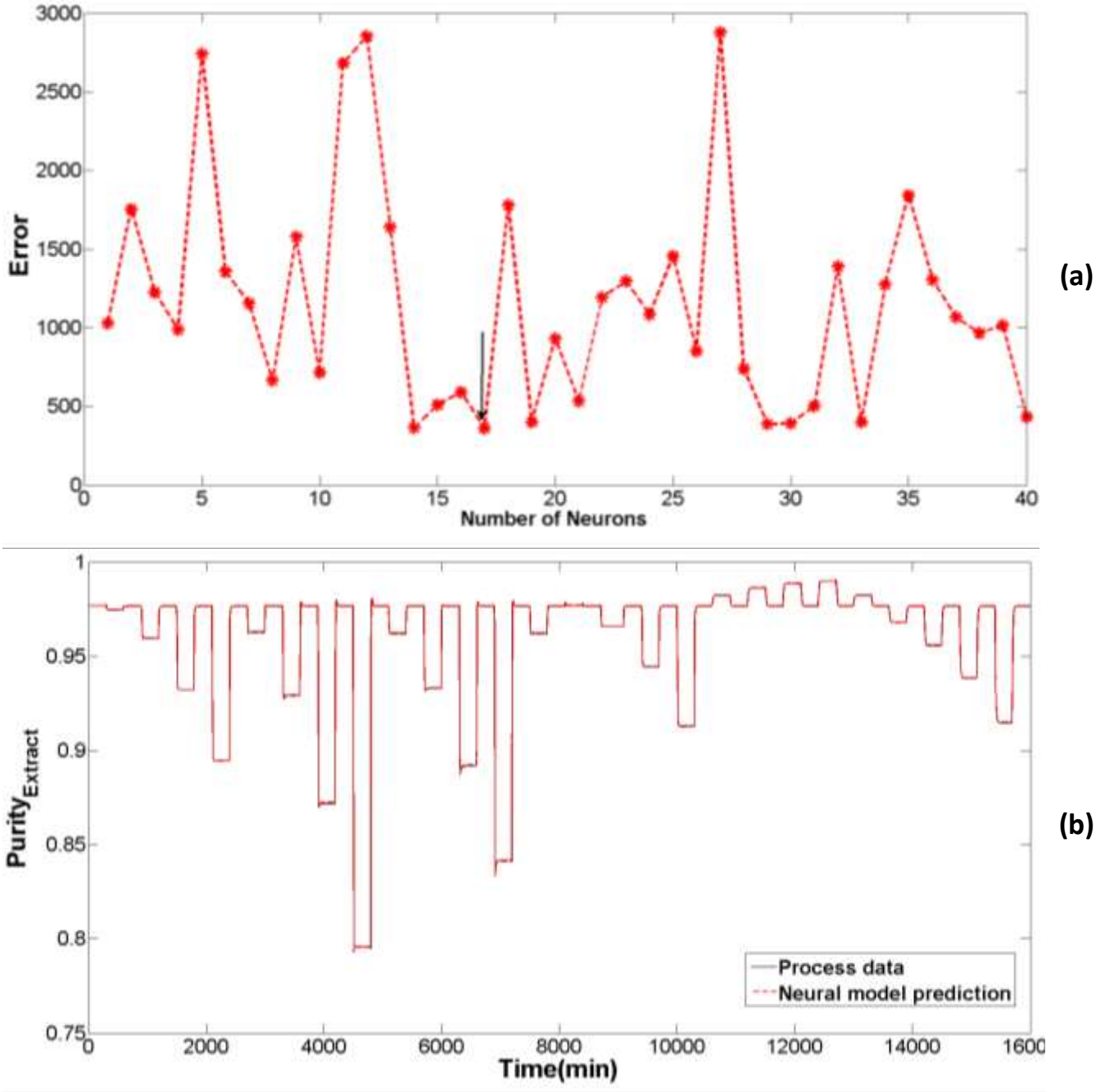

Figure 40 – Extract purity ANN model identification: (a) selection of the optimal number of neurons in the hidden layer; (b) final model validation. The neural model prediction, red dashed lines, cover the process data, black line, during all the represented time.

This model has a similar structure to the previous one, albeit with a different number of neurons in the hidden layer. The computational time taken in the development of this neural model was approximately 38 hours. In order to reduce the computational effort, the number of neurons and training trials was reduced, in this case to 40. With 17 neurons, a structure with the minimum validation error was found. Even with 40 neurons, an error close to the global minimum error showed in Figure 40.a is found and therefore, an evaluation with a larger number of neurons, greater than 20, is not necessary. An excessive number of neurons produces a model with a large number of parameters, which can lead to problems in the estimation step or to an overfitting problem that will degenerate the prediction capability of the final model (Schenker and Agarwal 1996). After selecting the number of neurons, a final model is developed with this number.

P1-3.4.2. Quasi-Virtual analyser structure definition

The system simulation was done with the help of the phenomenological model in order to imitate the case where the Q-VOA is implemented in a laboratory plant to do the online monitoring. It was considered a dead time of 10 minutes for the measurements. In this way, the process model gave the measurements while the Q-VOA made the real-time predictions. At each 10 minutes, the Q-VOA evaluates the system steady state, as explained in Section P1-2.4.3. The phenomenological model responses are used to compare and verify the Q-VOA efficiency. To do this, the process model is kept running in parallel with the Q-VOA system, giving information about the real state of the process and allowing the evaluation of the Q-VOA performance. In order to make the tuning of the Q-VOA parameters and verify its efficiency, addressing the capacity of the proposed system to predict the process dynamic behaviour, a series of

perturbations in the process inputs are made. The responses in the performance parameters of both the process model and the Q-VOA are presented. Perturbations were performed in all variables indicated by the orthogonalization method. Table 12 presents the characteristics of each perturbation made. In Section P1-3.4.3 is presented the Q-VOA prediction, measurements, measurements used in the Q-VOA actualization and phenomenological model response.

Table 12 - Step perturbations performed for the Q-VOA tuning.

Process Variable	Perturbation	Value (%)	Time (min)
Initial Steady State	-	-	0 - 31
Extract flow rate	↓	15%	31 - 261
Initial Steady State	-	-	261 - 391
Recycling flow rate	↓	14%	391 - 521
Initial Steady State	-	-	521 - 651
Recycling flow rate	↑	8%	651 - 881
Initial Steady State	-	-	881 - 911
Feed flow rate	↑	20%	911 - 1141
Initial Steady State	-	-	1141 - 1271
Eluent flow rate	↓	17%	1271 - 1401
Initial Steady State	-	-	1401 - 1500

P1-3.4.2.1. Virtual analyser parameters tuning

The two weights of the virtual analyser must be tuned to ensure the Q-VOA effectiveness. Furthermore, the ANN models use the two most recent past outputs as input, meaning that the Q-VOA can use the measurement, when necessary, in two different positions. As mentioned in Section P1-2.4.1, the present response, y, depends on the number of past responses evaluated, that here is defined as $n_y = 2$. It means that the input vector of the VOA will contain 2 past outputs, one corresponding to the instant $y(t-1)$, the most recent value, and another corresponding to the instant $y(t-2)$, the older value. In this way, there are two possibilities for the VOA to use a measurement to actualize itself, either with the most recent value or with the older value. Therefore, the way which the VOA uses a measurement can improve or not the Q-VOA performance. This can be also considered as a tuning parameter of the Q-VOA system, giving a total number of three parameters to be tuned.

The first step is to choose the position that will be used in the Q-VOA actualization. This can be easily done through the simulation of the system using both cases. In this way, to evaluate the best case, the two options were implemented and the results are presented in Figure 41. In order to select the best option, the MAPE criterion was used. The selected option is the one with the smaller MAPE.

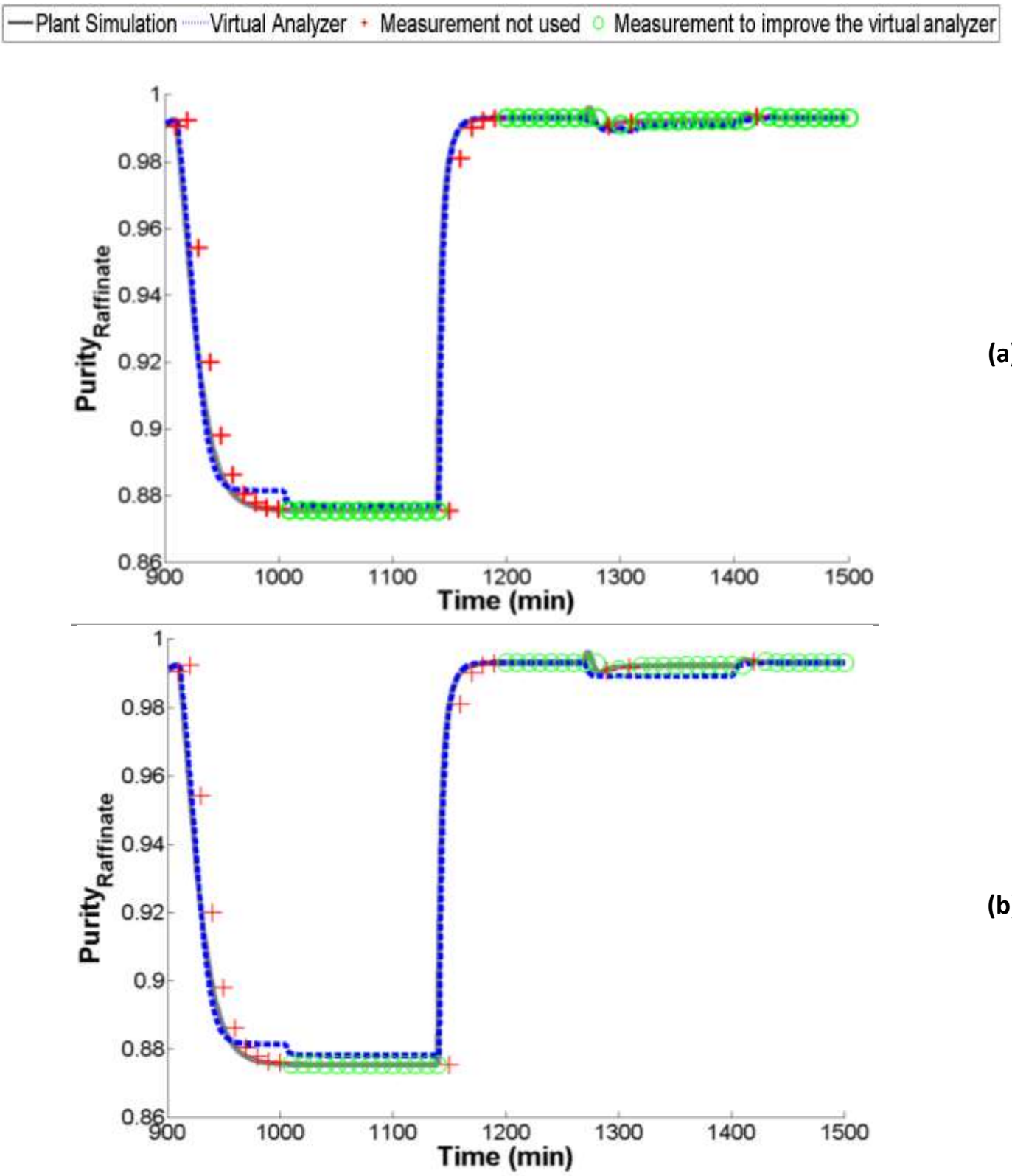

Figure 41 - Virtual analyser actualization tuning in the prediction of the purity in the raffinate stream: (a) Last measurement used as most recent value; (b) Last measurement used as older value.

From Figure 41, we can note that the system responds smoother when the Virtual analyser uses the measurement as the older value. However, in this case the system presents a small offset when the predictions are compared with the phenomenological model results. On the other side, the system responds aggressively with no offset when the VOA uses the measurements as the most recent value. This means that the VOA gives a major importance to the immediately past value than to the older one. As can be noticed from Figure 41, the best option in this case is to use option (a). The disadvantage of this case is that the VOA presents some instability after the last perturbation and a delay after the first perturbation. However, this last case shows a global result better than the one that uses the older value. The MAPE was computed for the two cases; when the measurement is used as the older value, the error was $MPE_1 = 8.66 \times 10^{-4}$ and, in the other case, the error was $MPE_1 = 9.51 \times 10^{-4}$.

The difference between the two cases becomes clearer when comparing the results obtained for the purity in the extract stream, Figure 42. When the measurement is used as the older value, for this system, the actualization is detrimental to the VOA making the analyser lose the process response, Figure 42.b. On the other hand, when the actualization is used as the most recent value, the VOA can predict the purity and follow the process dynamics with a significant precision. Here the MAPE was also computed for the two cases; when the measurement is used as the older value, the error was $MPE_1 = 2.92 \times 10^{1}$ and, in the other case, the error was $MPE_1 = 4.51 \times 10^{-2}$.

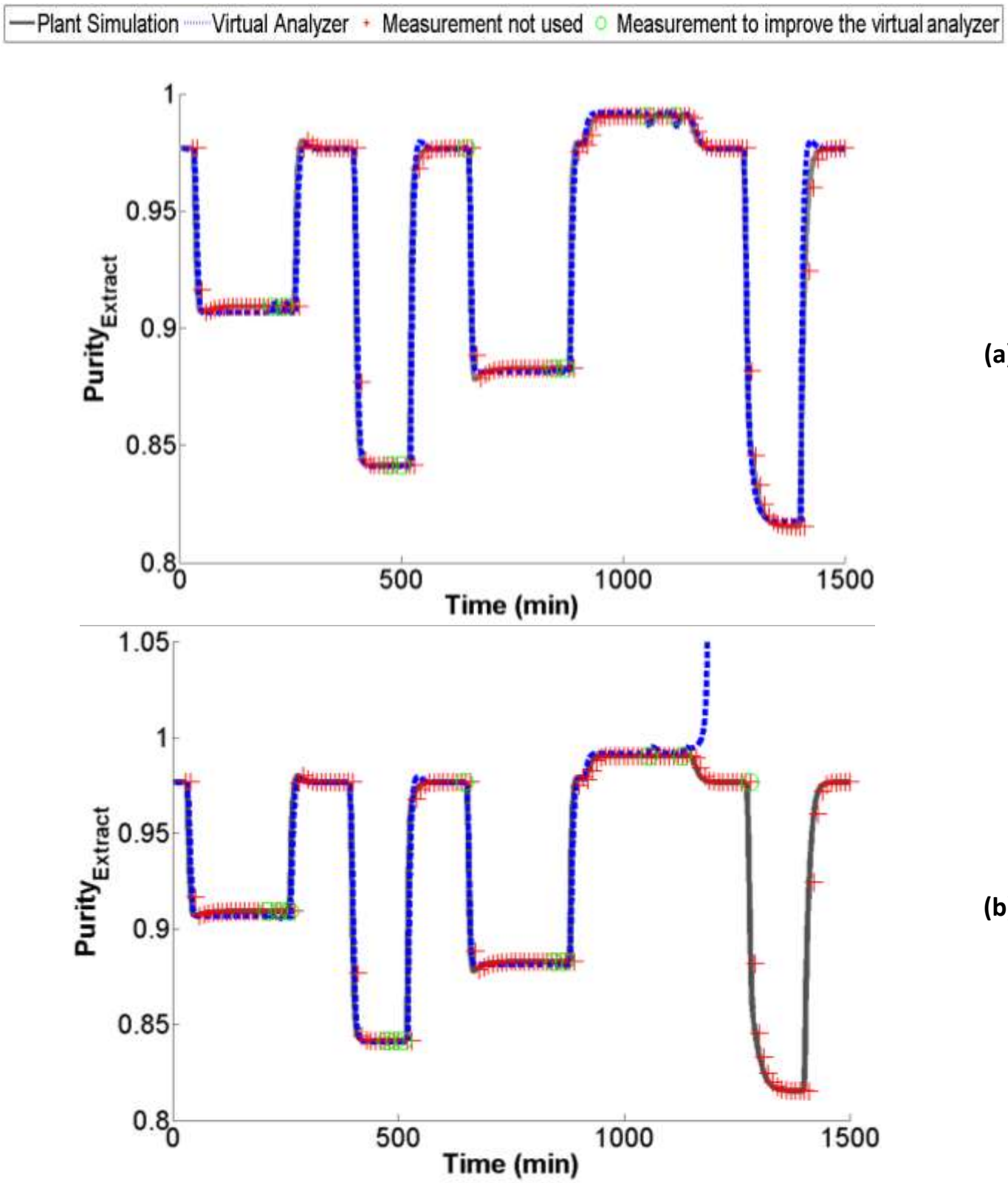

Figure 42 - Virtual analyzer actualization tuning in the prediction of the purity in the extract stream: (a) Last measurement used as most recent value; (b) Last measurement used as older value.

After selecting the method by which the VOA should be actualized with the measurement, the next step is to define the analyser weights. These weights are used in order for the virtual analyser to decide if it is necessary to use the measurement to actualize itself. A bad choice of values for these parameters can introduce instability in the system predictions. For example, a high value for the weight of the measurement implies that all measurements must be used in the VOA actualization. This leads the analyser to a state closer to the measurements than to the real process. Consequently, the VOA predictions will have a dead-time equal to the dead-time of the measurements. On the other hand, if the weight of the virtual analyser derivative is high, the system will give a great importance to the process dynamics, which will introduce an offset in the analyser prediction at some points. An intermediate value must be defined in order to obtain a good performance of the VOA. No work was found in the literature that uses a VOA based on these considerations. Consequently, there is not an established method to tune the parameters of the Q-VOA system considered in this work. A deeper study about this question can be developed in the future. Here, a trial and error method was used to define these parameters. The values of these parameters were varied from 1 to 10^{-10} and the system responses were analysed. In Figure 43, three cases for different values of the parameters (w_m and w_d) are presented. In the first case, Figure 43.a, the results using a value of w_m larger than the optimal weight for the measurement variation are shown; in Figure 43.b, the results using the optimal weights are presented while in Figure 43.c the results with a larger than the optimal weight to the VOA derivative (w_d) are shown. From this figure, it is possible to note that, in the optimal case, the VOA actualization eliminates the offset and the system does not show dead time. The optimal set of weights found corresponds to values of $w_m = 4.2\text{x}10^{-4}$ and $w_d = 2.0\text{x}10^{-4}$.

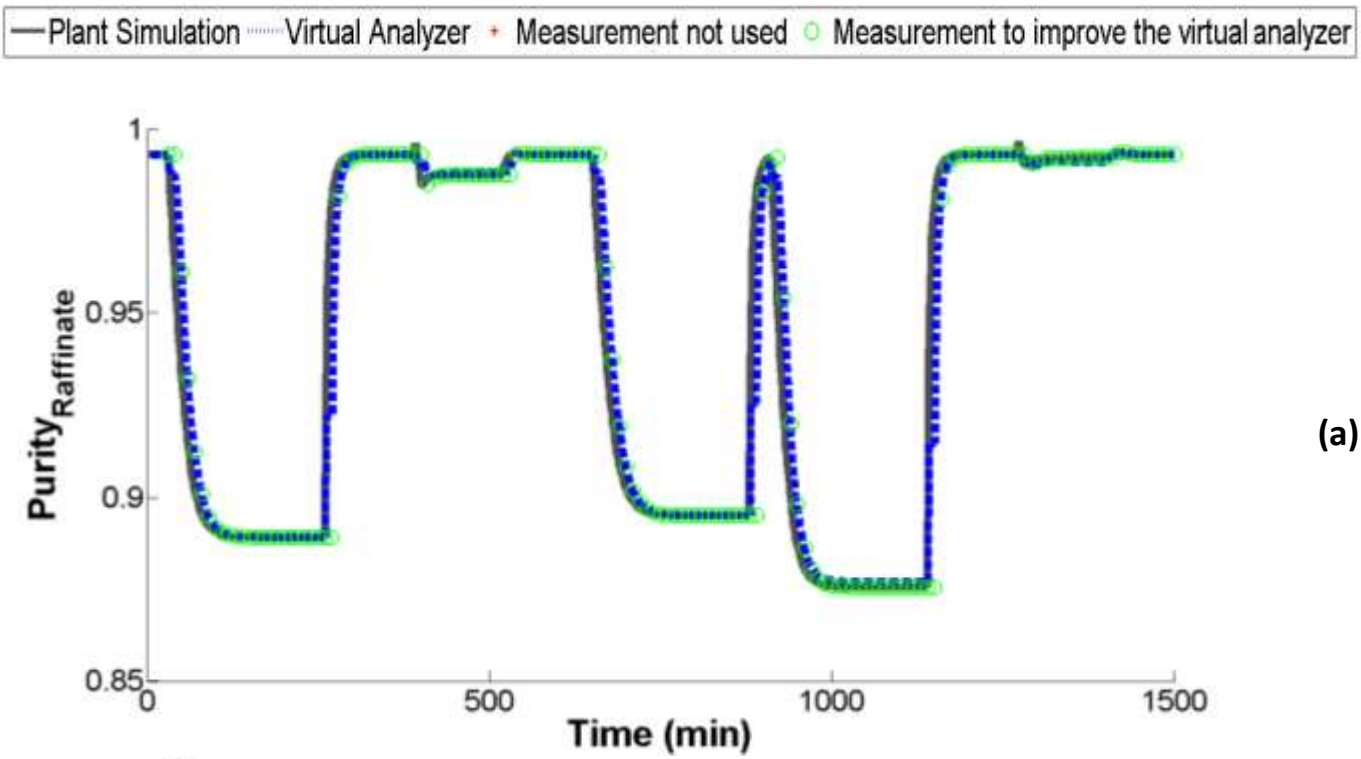
Plant Simulation
Virtual Analyzer
Measurement not used
Measurement to improve the virtual analyzer
Purity Raffinate
Time (min)
1
0.95
0.9
0.85
0
500
1000
1500

(a)

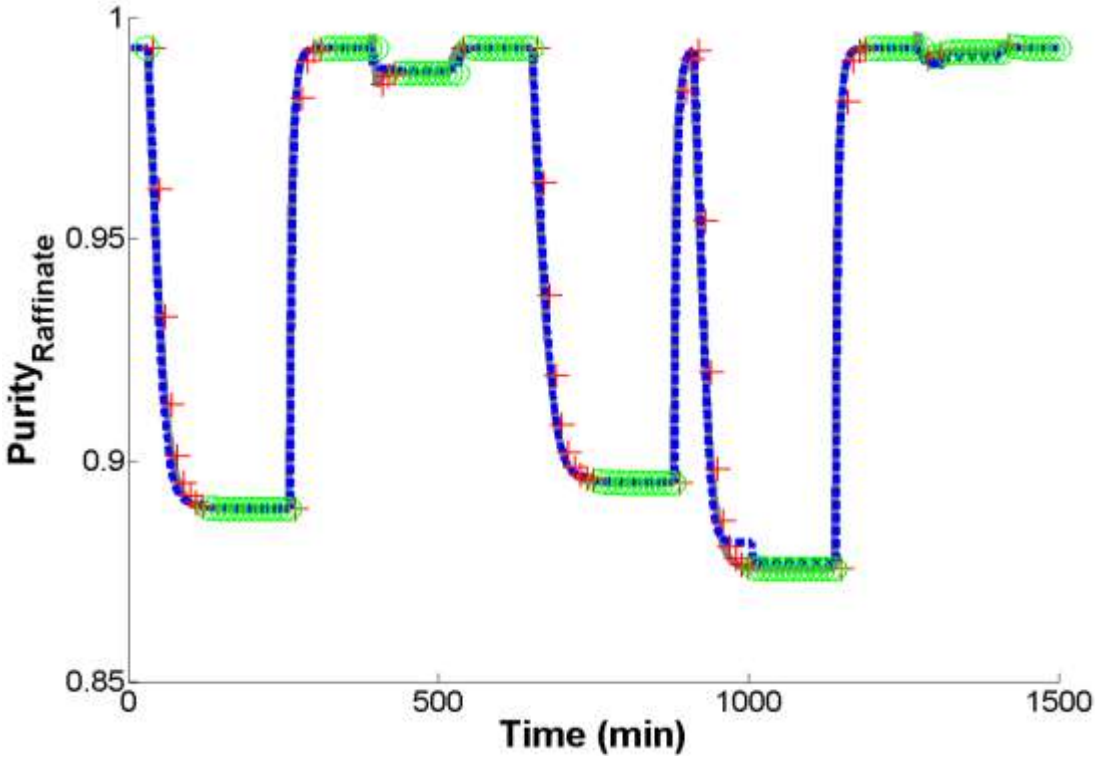
Purity Raffinate
Time (min)
1
0.95
0.9
0.85
0
500
1000
1500

(b)

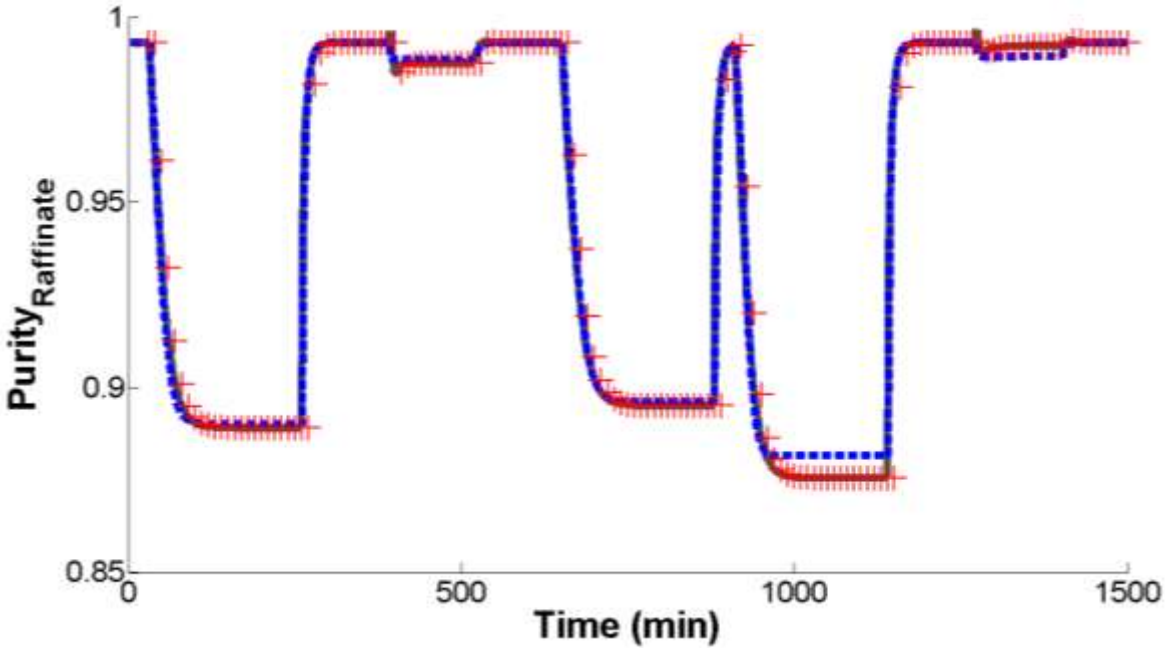

(c)

Figure 43 - Virtual analyser tuning in the prediction of the purity in the raffinate stream: (a) using a value of $\boldsymbol{w_m}$ larger than the optimum found; (b) using the optimum values of $\boldsymbol{w_m}$ and $\boldsymbol{w_d}$; (c) using a value of $\boldsymbol{w_d}$ larger than the optimum found.

For the purity in the extract stream, the VOA system is more sensitive to the tuning parameters. The results of the tuning in this case are presented in Figure 44 where it is possible to observe that a large weight of the derivative term induces the system to an unstable zone. On the other hand, a very small weight introduces a time delay to the system, as seen in the previous case. The optimal set of weights found corresponds to $w_m = 1\text{x}10^{-6}$ and $w_d = 2\text{x}10^{-7}$.

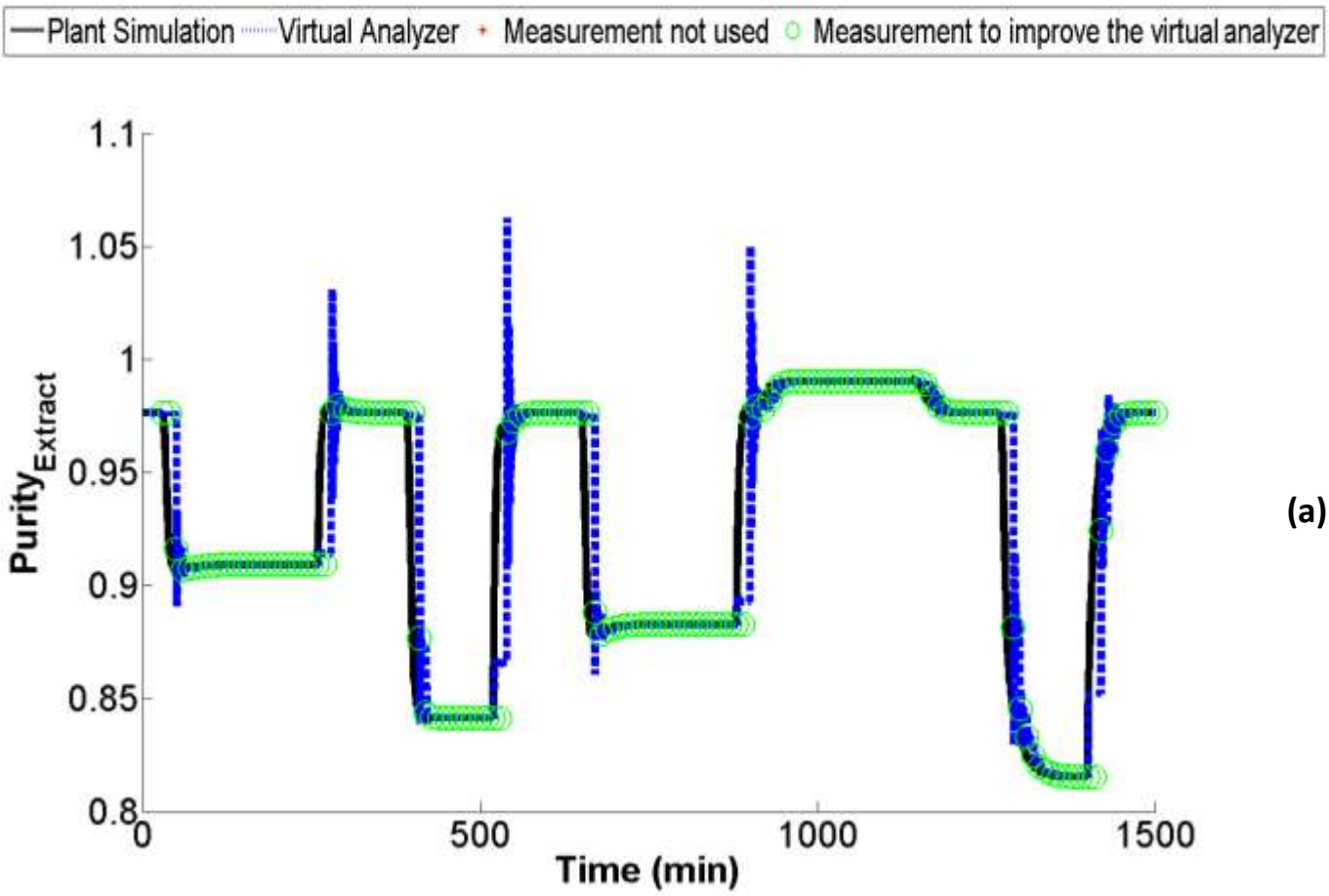
Plant Simulation
Virtual Analyzer
Measurement not used
Measurement to improve the virtual analyzer
Purity Extract
Time (min)
1.1
1.05
1
0.95
0.9
0.85
0.8
0
500
1000
1500

(a)

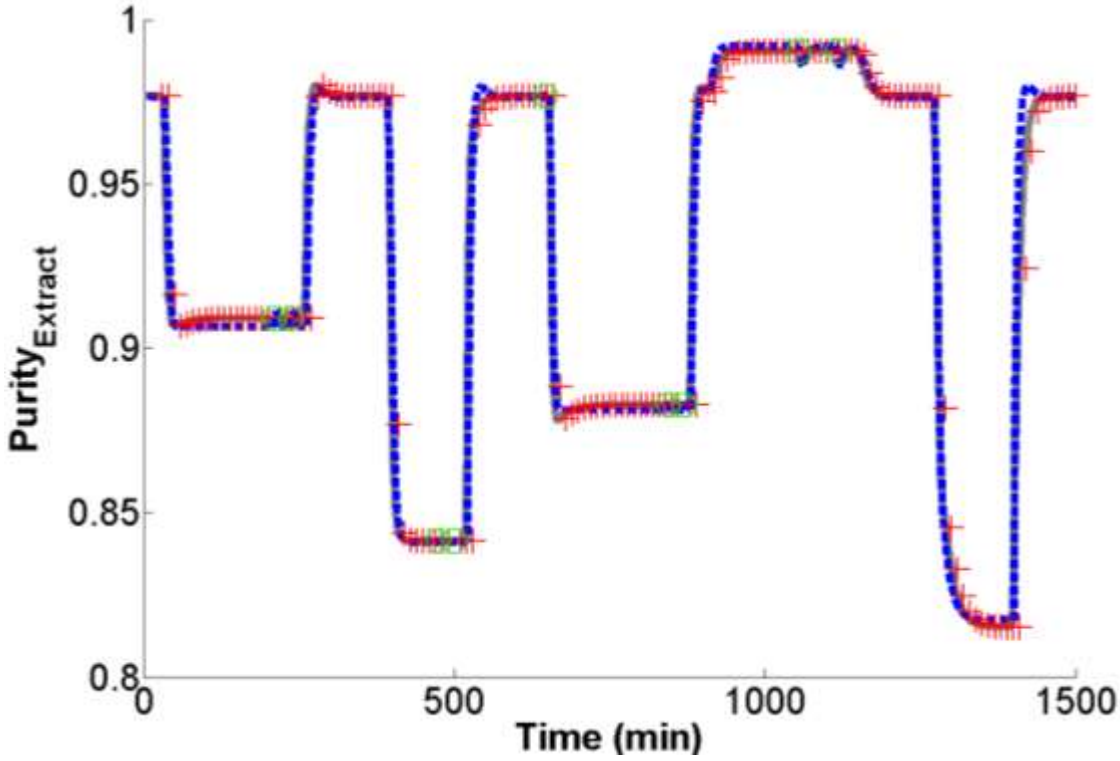
Purity Extract
Time (min)
1
0.95
0.9
0.85
0.8
0
500
1000
1500

(b)

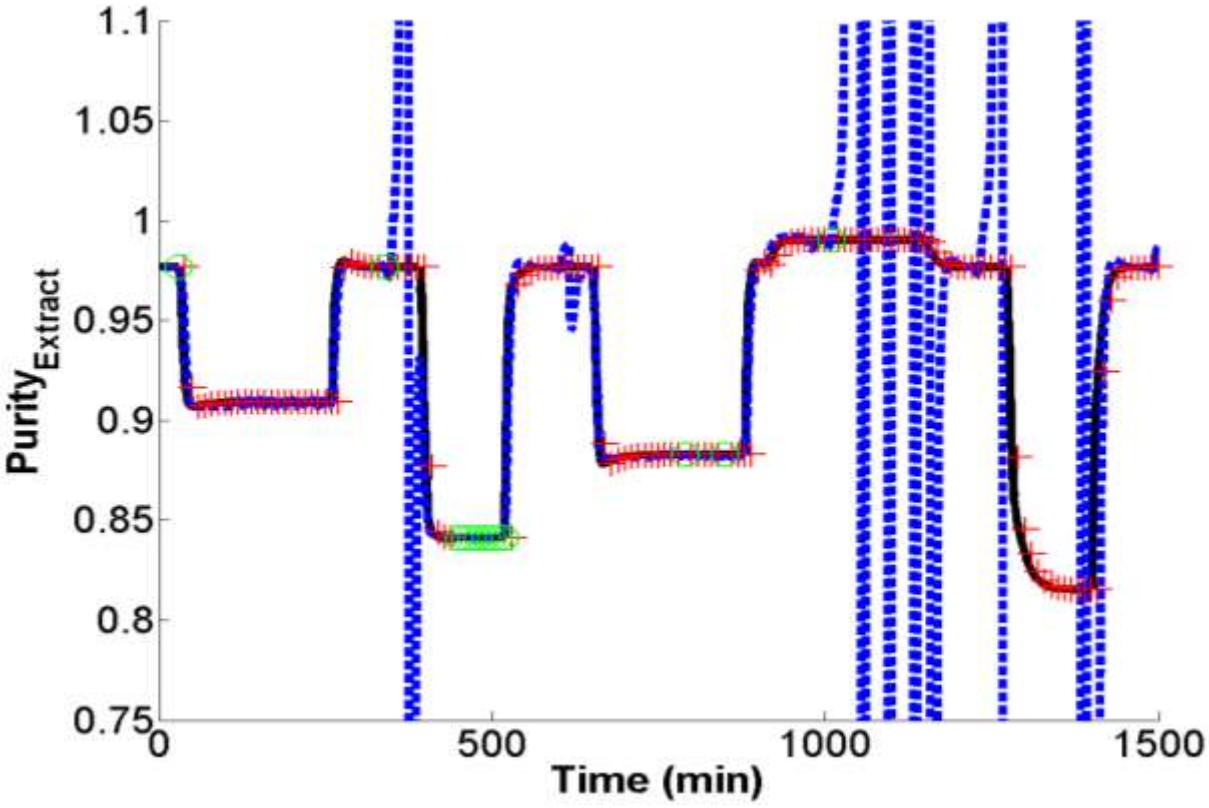

(c)

Figure 44 - Virtual analyser tuning in the prediction of the purity in the extract stream: (a) using a value of $\boldsymbol{w_m}$ larger than the optimum; (b) using the optimum values of $\boldsymbol{w_m}$ and $\boldsymbol{w_d}$; (c) using a value of $\boldsymbol{w_d}$ larger than the optimum.

P1-3.4.3. Measurement system test

Once the Q-VOA system is tuned, the final step was to test the measurement system through a process simulation. This was done in order to compare the Q-VOA performance with the simple VOA. It is expected that the VOA presents a poor performance, since that it is employed as a NOE model. A sequence of step perturbations was performed with different durations in order to evaluate different dynamic behaviours. It should be noted that a step variation was even done to the feed flow rate in order to verify the Q-VOA efficiency under the presence of an external perturbation. Table 13 presents the sequence of perturbations done in the system.

Table 13 - Step perturbations performed on the Q-VOA simulation.

Process Variable	Perturbation	Value (%)	Time (min)
Initial Steady State	-	-	0 - 31
Extract flow rate	↓	15%	31 - 261
Initial Steady State	-	-	261 - 391
Recycling flow rate	↓	4%	391 - 521
Initial Steady State	-	-	521 - 651
Recycling flow rate	↑	9%	651 - 881
Initial Steady State	-	-	881 - 911
Feed flow rate	↑	20%	911 - 1141
Initial Steady State	-	-	1141 - 1271
Eluent flow rate	↓	25%	1271 - 1401
Initial Steady State	-	-	1401 - 1500
Extract flow rate	↓	15%	1500 - 1540
Initial Steady State	-	-	1540 - 1650
Solid flow rate	↓	5%	1650 - 1750
Initial Steady State	-	-	1750 - 1800

In Figure 45 and Figure 46 are presented the simulation results for the TMB unit over the perturbations presented in Table 13. The quasi-virtual online analyser response is presented in Figure 45.a and the virtual analyser is presented in Figure 45.b. Comparing both cases, it is possible to note that, after the actualizations, the Q-VOA is conduced to a state closer to the real state of the plant, while the VOA presents an offset. The most important point is that, under the presence of an external perturbation (an unmeasured perturbation in feed flow rate from the instant 911 to 1141, Table 13), the Q-VOA was capable to identify, with the help of the measurements, the new state even not having the information about this input process variation. This can be performed by the system actualization through the HPLC measurement. Finally, it is possible to note that both the VOA and the Q-VOA represent with precision the process dynamic behaviour.

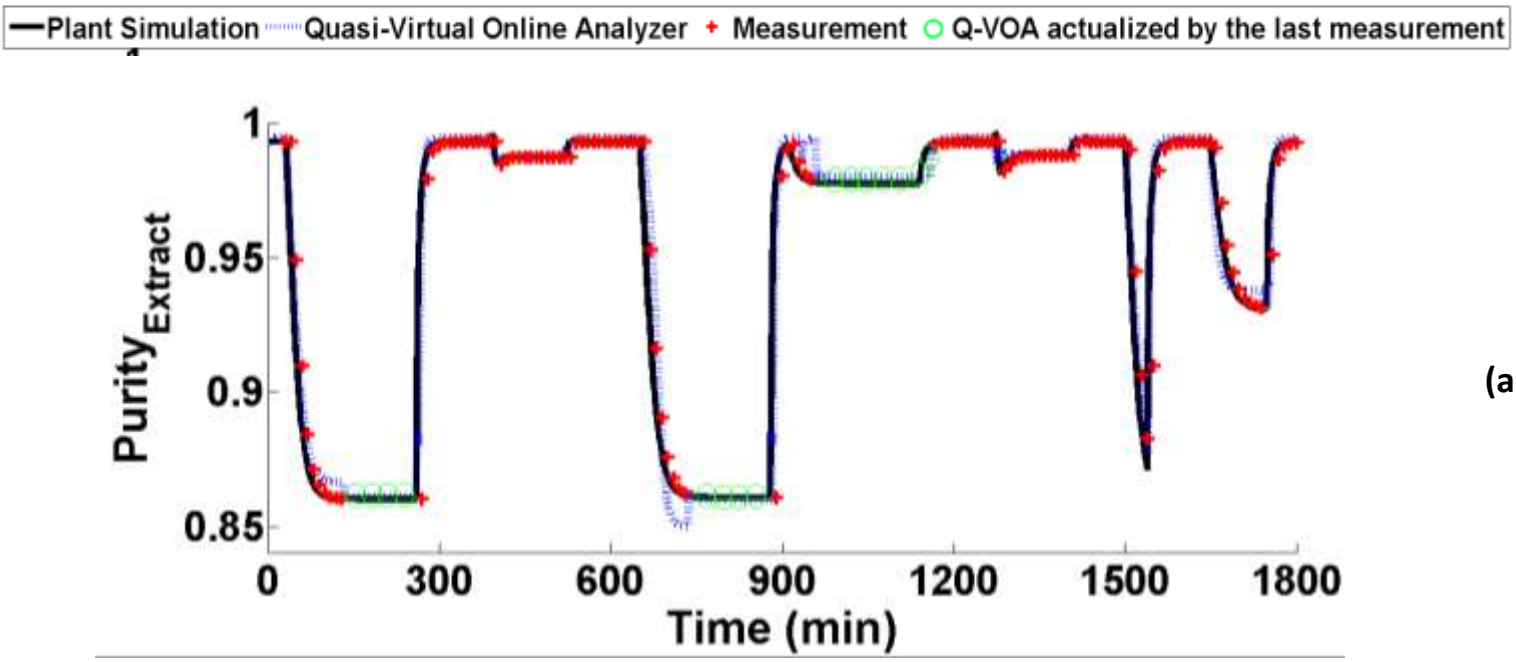

(a)

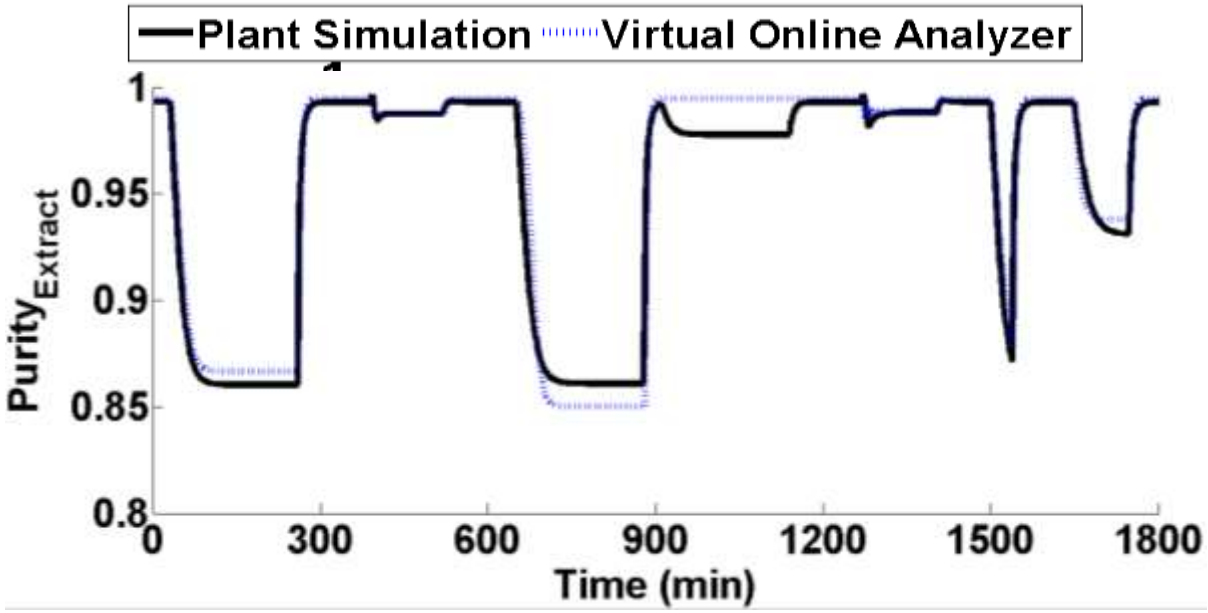

(b)

Figure 45 - Extract stream purity for the measurement system simulation: Q-VOA simulation (a); Simple VOA simulation (b).

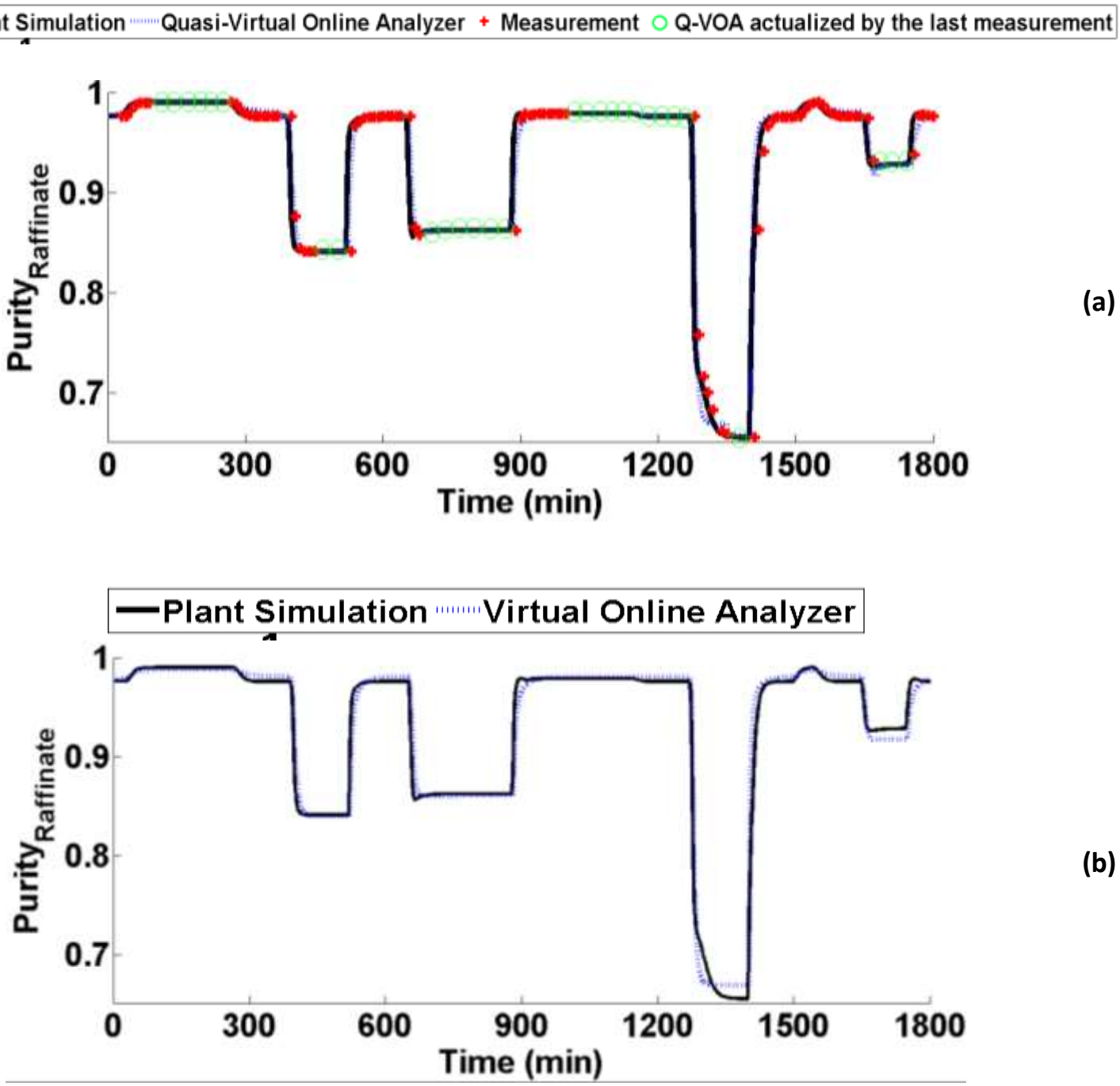

Figure 46- Raffinate stream purity for the measurement system simulation: Q-VOA simulation (a); Simple VOA simulation (b).

A further analysis can be done through the relative deviation of both systems, with and without measurement actualization. In order to evaluate the system efficiency, Figure 47 and Figure 48

show the relative deviations in the case of the purities in extract stream and in raffinate stream respectively. In those figures, the predictions of the Q-VOA and VOA are evaluated in terms of deviation from the phenomenological model predictions. Since the model was previously validated through experiments, it can be a reliable source of information about the process behaviour in real time. Therefore, the phenomenological model dynamics is taken as reference to the analysis of the methods here proposed. Hence, as closer as to the zero deviation for longer time, the better is the performance of the methods here evaluated. This information can be verified graphically in Figure 47 and Figure 48.

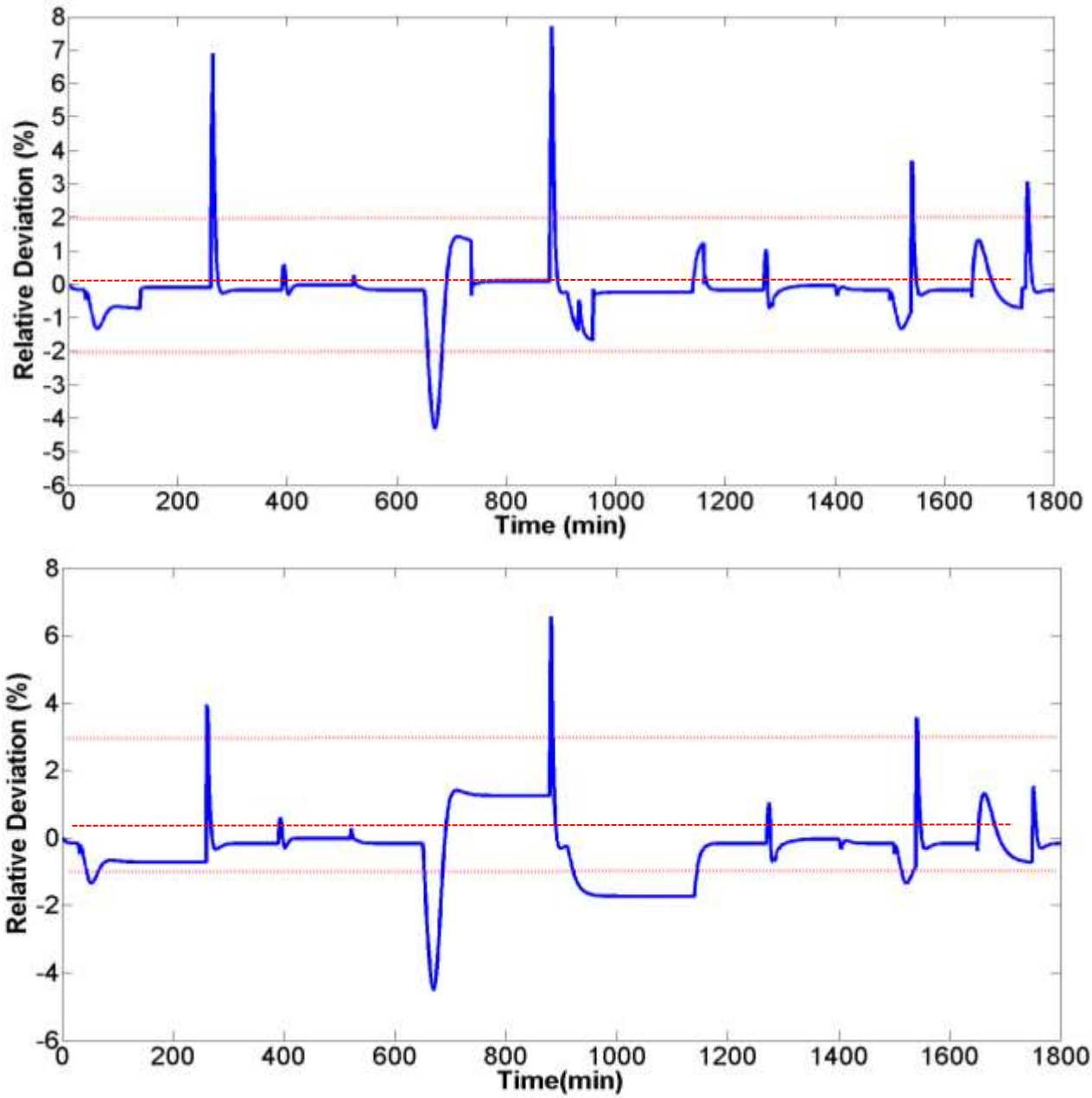

Figure 47 - Relative deviation of the purity in extract between the system prediction and the process response over the simulation time: Q-VOA (a); simple VOA (b).

From Figure 47 it is possible to note that the Q-VOA is capable of keeping the process prediction closer to the process response for longer than the simple VOA case. This shows the reliability of

the measurement system and the improvement achieved by the Q-VOA when compared to the simple VOA.

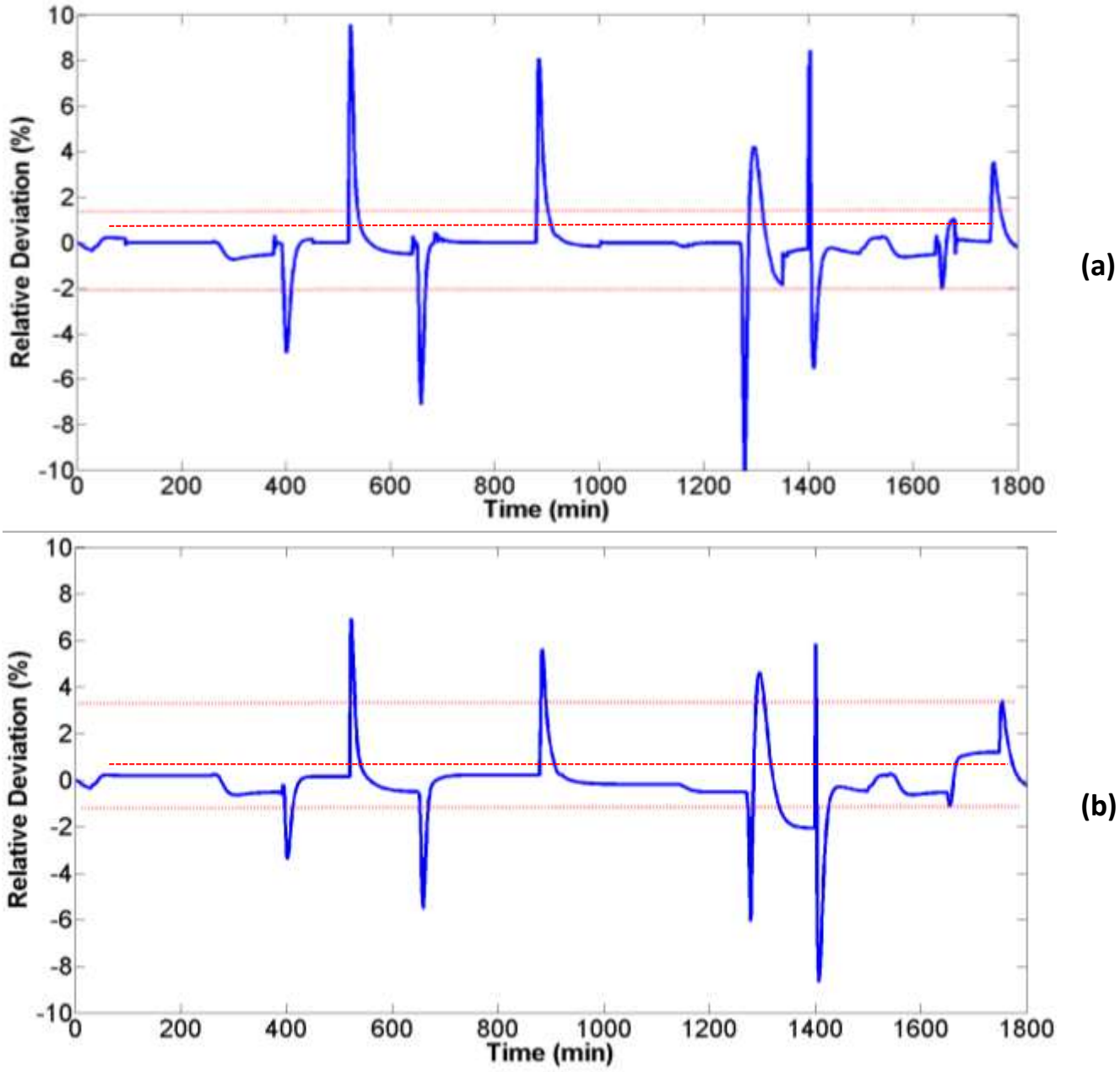

Figure 48- Relative deviation of the purity in raffinate between the system prediction and the process response over the simulation time: Q-VOA (a); simple VOA case (b).

From Figure 48 it is also possible to note that the Q-VOA can keep the process prediction closer to the process response for longer than the simple VOA case. In this case, the differences are smaller than the previous ones, but the Q-VOA still has a better prediction than the simple VOA. The greater error observed in the simple VOA structure is due to its wrong application, since that it was developed as a NARX model and employed as a predictor. However, it is the usual approach in the literature, and in some cases the error can be neglected.

P1-3.5. TMB design, optimization and determination of operational confidence regions through HPSO-TVAC-MSR

P1-3.5.1. HPSO-TVAC-MSR method validation: Benchmark functions tests

In this section, it is presented a series of tests that were done with benchmark functions in order to evaluate the efficiency of the improved HPSO-TVAC and compare its results with the previous techniques presented in the literature. In all the cases, the evaluation of the confidence region was done considering a confidence interval equal to 95%, $\alpha = 0.95$, and the method was ran 10 times for each case and the average result is presented. The HPSO-TVAC parameters were set equal to $c_{1i} = 2.5$, $c_{1f} = 0.5$, $c_{2i} = 0.5$ and $c_{2f} = 2.5$. The numbers of particles and iterations were set in accordance with each case in order to do a fair comparison with the literature.

The first two cases deal with parameter estimation problems and evaluation of the parameters confidence regions. These two cases were applied by Schwaab et al., (2008) to test the method

presented in their work. Here, those two functions were used with the same goal. The results obtained through the method here proposed and the results of Schwaab et al. (2008) were compared in order to verify the consistence of the present method. For this purpose, the same objective function used by the referred authors was used, which is the well-known least-squares function.

The first function tested is a linear model with two parameters, a very simple case of parameter estimation, expressed as:

$$y = \theta_1 x + \theta_2 \tag{82}$$

This first step was taken in order to evaluate the confidence region construction by the method here presented. The data used to estimate the parameters are presented in Table 14.

Table 14 - Parameter estimation data for Equation (82).

x	1.0	2.0	3.0	4.0	5.0	6.0	7.0	8.0	9.0	10.0
y	9.92	16.89	17.12	26.03	30.71	33.28	39.83	42.44	50.44	53.63

Figure 49 - Confidence region and objective function surface for Equation (82).Figure 49 presents the parameters confidence region and objective function surface. From the objective function surface, it is possible to note that the PSO was capable of evaluating a vast region and finding the minimum value of the objective function while its results provide important information to draw the parameters confidence region in an efficient way.

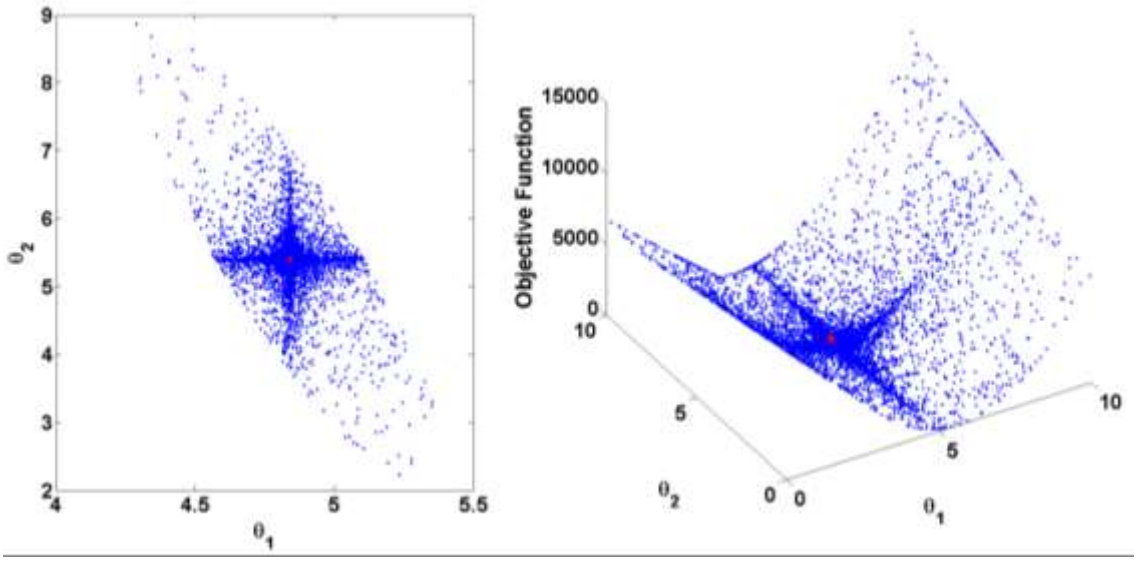

Figure 49 - Confidence region and objective function surface for Equation (82).

The second function is a nonlinear model that represents a first-order irreversible reaction in a batch stirred tank. This model represents the variation of oxygen demand through time in a biochemical system. This function is expressed as:

$$y = \theta_1(1 - e^{-\theta_2 x}) \tag{83}$$

The data used to estimate the parameters are presented in Table 15.

Table 15 - Parameter estimation data for equation (83).

x	1.0	2.0	3.0	4.0	5.0	7.0
y	8.3	10.3	19.0	16.0	15.6	19.8

Figure 50 presents the parameters confidence region and objective function surface. From the objective function surface it is again possible to note that the PSO was capable of evaluating a vast region and finding the minimum value of the objective function. In this case, the confidence region presents an unusual shape, as it represents a nonlinear model.

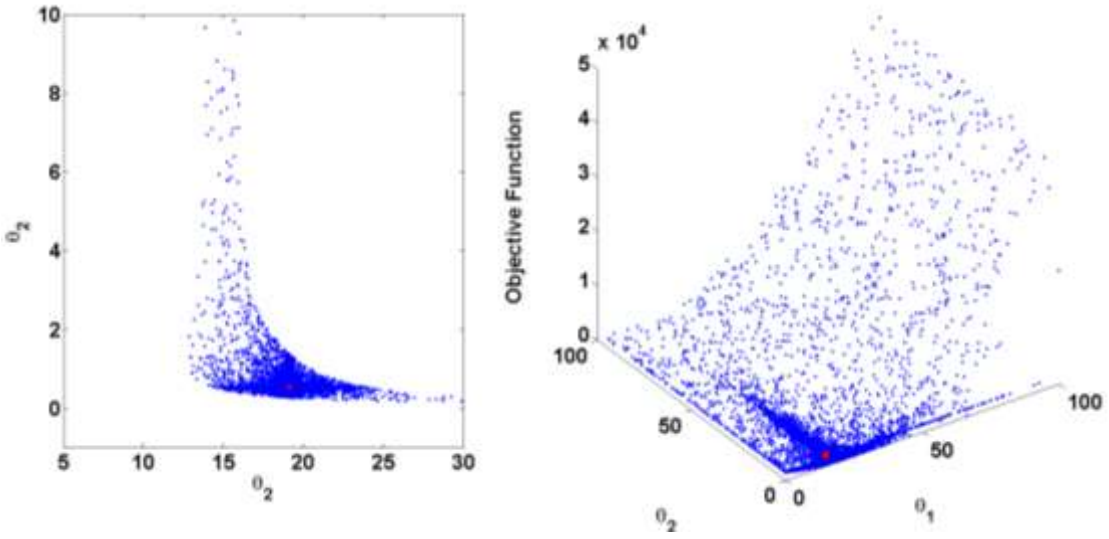

Figure 50 - Confidence region and objective function surface for Equation (83).

Table 16 presents the values of the functions parameters (θ_1 and θ_2), for each case previously presented (Equation 82 and Equation 83) and also the value obtained for the minimum of the objective function in each case.

Table 16 - Comparison between the results obtained with the method here presented and by Schwaab et al. (2008).

		Schwaab et al., (2008) $(k = 100, p = 20)$	Improved HPSO- TVAC $(k = 100, p = 20, R = 1)$
$y = \theta_1 x + \theta_2$	θ_1	4.85	4. 84
	θ_2	5.28	5.40
	fob	20.80	20.75
$y = \theta_1(1 - e^{-\theta_2 x})$	θ_1	19.15	19.14
	θ_2	0.5273	0.5311
	fob	26.00	26.00

From Table 16 it is possible to note that the improved PSO-TVAC was able to find results very close to the ones found by Schwaab et al. (2008); for the first case, the method was able to find a slightly better value of the objective function.

Then, two more benchmark functions were employed in order to evaluate the efficiency of the method here proposed with the objective of evaluating the performance of the method dealing with dynamic multimodal landscapes and confidence region estimation for multiple minima. The same functions were employed by Koduru et al. (2007) to evaluate their proposed method.

The next equation represents a model of a biological organism, which depends on two independent variables. This case is again a parameter estimation case and the model can be expressed as:

$$y = \frac{1}{(1 + (x_1 - \theta_1)^2)(1 + (x_2 - \theta_2)^2)} \quad (84)$$

The data used to estimate the parameters are presented in Table 17.

Table 17 - Parameter estimation data for Equation (84).

x_1	15	15	20	20
x_2	15	20	15	20
y	0.6	0.7	0.7	0.8

Figure 51 presents the parameters confidence region and objective function surface. From the objective function surface, it is possible to note a very irregular region. The PSO was able to cover a vast region and all the minimum points of the objective function, including the global minimum, were found. Comparing these results with the C-PSO presented by Koduru et al. (2007), it is possible to note that the searching region mutation here proposed is an efficient improvement in the method, as it was capable of identifying all the minimum points of the function, which was not achieved in the referred work with the PSO. However, the method needs to be better tuned in order to improve the drawing of the confidence region, which is not the focus of the present evaluation. The initial search region was defined within $R_{1,min} = [13\ 13]$ and $R_{1,max} = [16\ 16]$ and expanded ten times until $R_{f,min} = [13\ 13]$ and $R_{f,max} = [25.6\ 26.6]$ with $k = 200$ and $p = 40$.

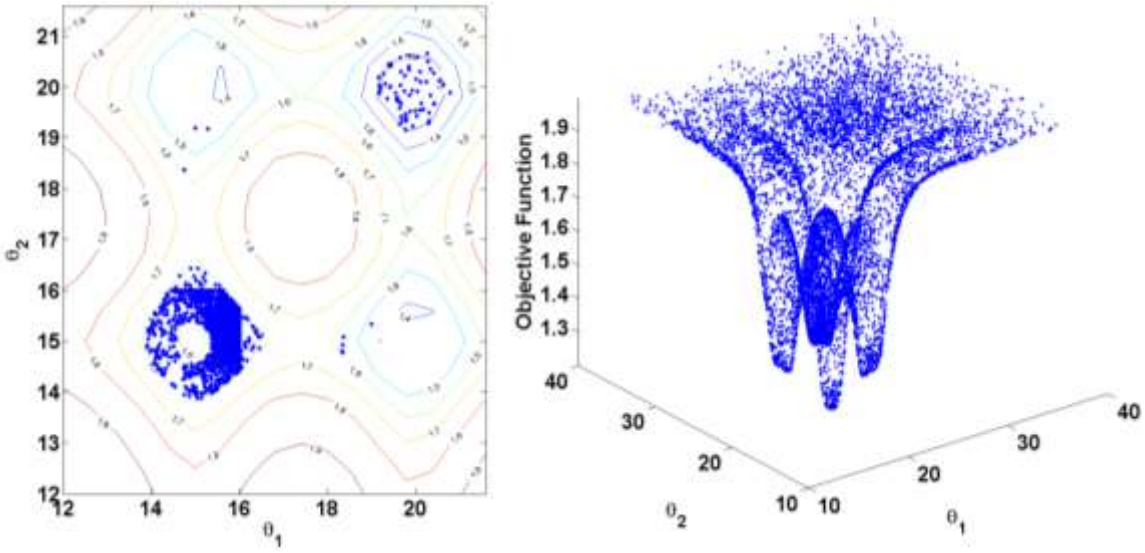

Figure 51 - Confidence region and objective function surface for Equation (84).

The last benchmark equation represents another model of a biological organism. This case is again a parameter estimation case and the model can be expressed as:

$$y = \frac{e^{\theta_1} x}{(e^{\theta_2} + x)} \tag{85}$$

The data used to estimate the parameters are presented in Table 18.

Table 18 - Parameter estimation data for Equation (85).

x	0.9	0.9	1	1
y	0.4	0.55	0.4	0.6

Figure 52 presents the parameters confidence region and objective function surface. Once again, the objective function surface is very irregular. In this case, the improved HPSO-TVAC presents an even more efficient result. It was able to cover a vast region and identify the minimum points of the objective function, including the global minimum. Furthermore, the method was able to draw all the confidence regions of each minimum with significant precision. Comparing these results with the C-PSO presented by Koduru et al. (2007), again it is possible to note that the searching region mutation here proposed is an efficient improvement in the method. The initial search region employed was $R_{1,min} = [0\ 0]$ and $R_{1,max} = [0.5\ 0.5]$ which was expanded ten times until $R_{f,min} = [0\ 0]$ and $R_{f,max} = [4.875\ 4.875\ ]$. In this case, it is possible to see in the centre of the figure a very dense zone ($0.5 < \theta_1 < 1.5$ and $0.5 < \theta_2 < 1.5$); this is one effect of the search region expansion, that was slow at the beginning to ensure that the method could describe well the surface and confidence region.

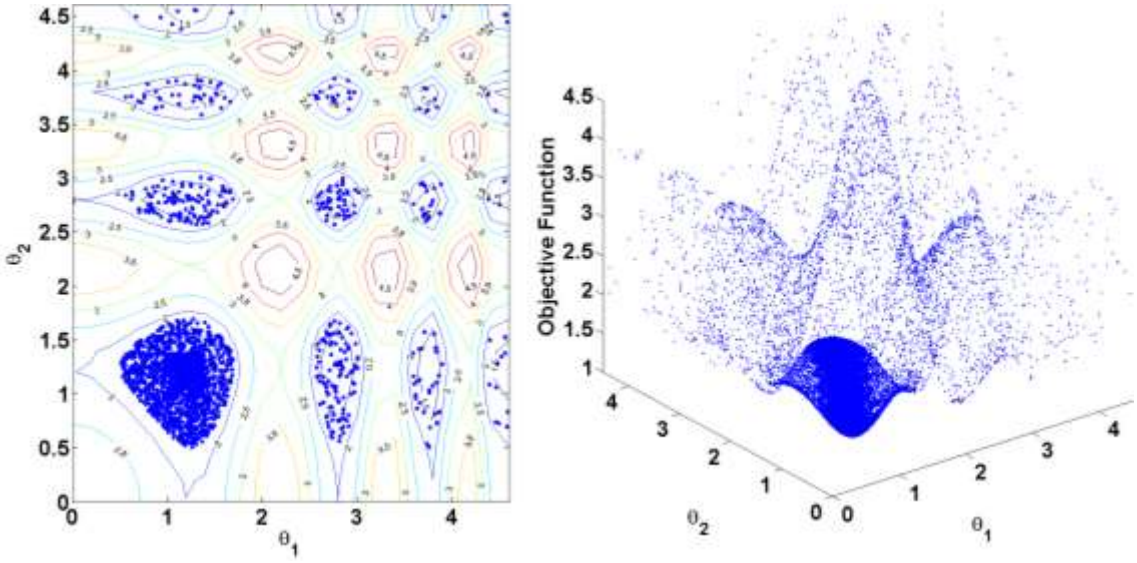

Figure 52 - Confidence region and objective function surface for Equation (85).

P1-3.5.2. TMB optimal design

In this section, the methodologies previously presented are applied in order to identify the optimal designs of the TMB unit and evaluate the operating confidence regions. The design of a TMB unit consists in the definition of a set of flow rates which will lead to the desired separation. Thus, the HPSO-TVAC with the proposed modification was applied in order to identify the set of recycle flow rate (Q_{IV}), extract flow rate (Q_X), feed flow rate (Q_F), eluent flow rate (Q_E) and solid flow rate (Q_S), that will lead to minimum points of the objective function presented in Section P1-2.5.1 and the requirements described in the next subsections where different scenarios are considered.

The confidence regions and objective function surfaces for all scenarios for a confidence level of 99%, the likelihood confidence region, are also presented. Those regions are drawn from the particles population after the optimization and following the methodology presented in Section P1-2.5.2. This can be an important tool for the process operation, making the process control and management more flexible. Concomitantly, the elliptical confidence regions were drawn through statistical test with 99% of confidence interval.

In the following subsections three different scenarios of design and optimization are presented. The first one refers to a classical approach, where the goal is to find the process optimal operating conditions under the desirable conditions of purities and recoveries. Then, the second case, presents a multi-optimal points optimization, where the goal is to find the set of different operating conditions in which the process can operate, providing different values of purities and recoveries. Finally, in the last scenario, physical limitations are introduced in the process design.

In this last case, limitations in the operating regions of the pumps are considered in order to find the process optimal operating points.

P1-3.5.2.1. First scenario – Process design for minimum purities and recoveries of 95%

The present scenario has the objective of finding the process optimal operating conditions for a minimum requirement in the purities and recoveries of 95%. This scenario follows a similar goal as when these types of units are designed through the triangle theory.

In order to gradually verify a different range of operating conditions (recycle flow rate(Q_{IV}), extract flow rate (Q_X), feed flow rate (Q_F), eluent flow rate (Q_E) and solid flow rate (Q_S), respectively) the initial search region was set equal to $R_{1,min} = [1, 1, 1, 1, 1]$ and $R_{1,max} = [18, 15, 5, 10, 16]$ and expanded until $R_{f,max} = [36, 30, 10, 20, 32]$. A number of 100 particles and a maximum of 600 iterations were used in this optimization.

Table 19 and Table 20 present the results of the optimal point found by the improved HPSO-TVAC; this result corresponds to the smallest local minimum found. Those tables also present the value obtained previously in the literature for the design of the same system with the triangle theory (Pais et al. 1998).

From Table 19 and Table 20, it is possible to note that the operating point found by the method here proposed corresponds to a productivity of approximately two times more than the value of Pais work (Pais et al. 1998), while the optimal eluent consumption is approximately half of the value provided by the triangle theory. Furthermore, from the range of values (maximum and

minimum) obtained by the 99% confidence interval, it can be seen that the productivity and eluent consumption are over and below the triangle theory values respectively. On the other hand, for the optimal point, the obtained purities are lower than the values obtained by the triangle theory. This is because 95% was the minimum value imposed in the fob constraints for the purity. This was also the value used to design the separation region in Pais et al. work (Pais et al. 1997, 1998).

Table 19 - Optimal unit design comparison, between the present work and the Triangle theory approach by Pais et al. (1998).

	Optimal Point		
	Value	**Standard Deviation**	**Triangle theory Pais et al. (1998)**
Q_{IV} (ml/min)	22.821	0.979	27.950
Q_X (ml/min)	14.332	0.382	17.980
Q_F (ml/min)	6.994	0.172	3.640
Q_E (ml/min)	14.585	1.135	21.450
Q_S (ml/min)	9.653	0.118	11.150
fob	0.931	0.001	-

Table 20 - Optimal unit performance parameters, comparison between the present work and Triangle theory approach by Pais et al. (1998).

	Optimal Point			
	Value	**99% confidence region**		**Triangle theory Pais et al. (1998)**
		Maximum	**Minimum**	**Value**
Pur (%)	95.000	99.700	95.000	99.300
Pux (%)	95.000	99.100	95.000	97.600
$Recr$ (%)	95.100	99.600	95.000	97.600
$Recx$ (%)	95.400	100.000	95.400	99.300
Pr (g/day l of bed)	126.011	126.836	71.416	61.200
Ec (l/g)	0.540	0.864	0.528	1.190

Figure 53 and Figure 54 present the confidence regions and objective function map for the operating variables Q_S/Q_e, Q_S/Q_f and Q_S/Q_X, Q_S/Q_{IV} respectively surface for a confidence level of 99%. The regions were drawn from the particles population after the optimization and following the methodology presented in Section P1-2.5.2. The method was able to identify the local minimum points and define the confidence region. Hence, for the operating point presented in Table 19, the confidence region will present the set of operating variables that will keep the process in conditions of purity and recovery over 95% and inside the intervals of productivity and eluent consumption presented in Table 20. One limitation of the present method is that the objective function with penalties, defined in Section P1-2.5.1, leads to a loss of a considerable

number of particles, as can be noted in the 3D graphics. This happens because slight changes around the optimal point will lead to conditions where the purity requirements are not met.

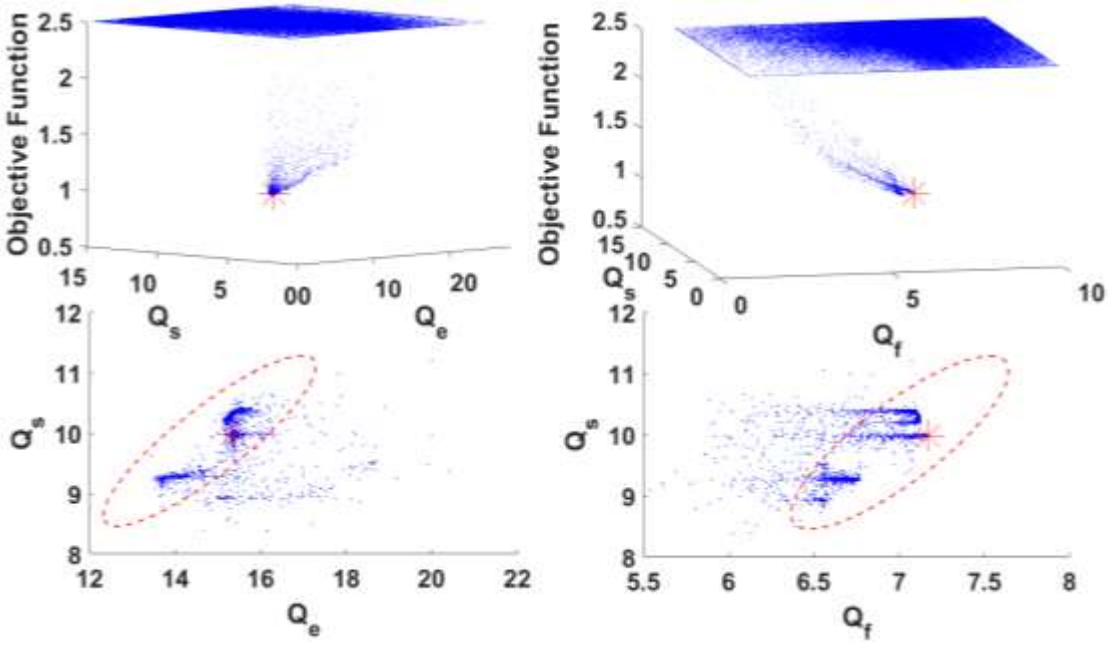

Figure 53 - Scenario 1: Likelihood confidence regions, elliptical confidence region (dashed lines) and objective function map for the operating variables Q_S/Q_e *and* Q_S/Q_f.

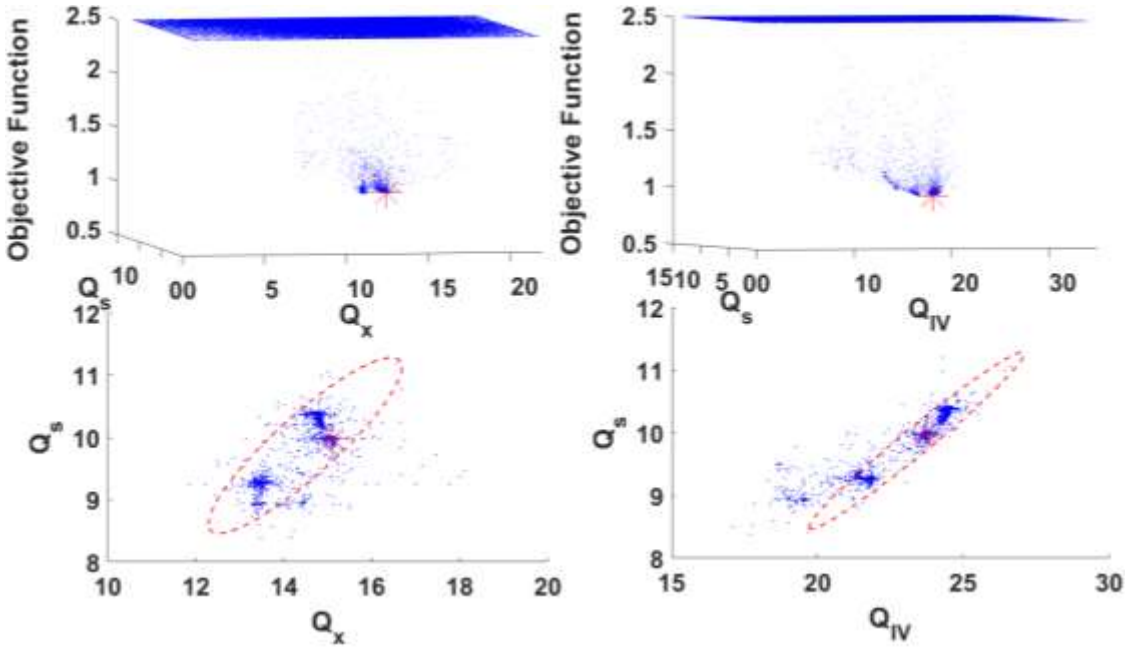

Figure 54 - Scenario 1: Likelihood confidence regions, elliptical confidence region (dashed lines) and objective function map for the operating variables Q_S/Q_X *and* Q_S/Q_{IV}.

From Figure 53 and Figure 54 it is possible to note that the elliptical confidence region does not represent the likelihood confidence region with precision. This happens due to the nonlinear nature of the model leading to a poor representation of the confidence region through the elliptical representation based on statistics test. Through the shape of the confidence regions it is possible to verify the nonlinearities and strong correlation between the solid flow rate, Q_s, and the flow rate in the section 4, Q_{IV}, and the extract flow rate, Q_X, which can be verified by the model equations in Section P1-2.1.

Finally, through Figure 53 and Figure 54 it is possible to define a set of operating conditions which obey the purities and recoveries restrictions. To do this, first it is necessary to choose a pair of flow rates inside of a confidence region; for example, choosing in Figure 54 a pair of Q_S/Q_e, in

this way with a value of Q_S fixed, it is possible to define the other variables through the remaining regions presented in the other graphics, which leads to the final set of operating conditions inside the group of possible sets. This is one of the main advantages of this method, the capacity of drawing the possible region of operating conditions, by mapping all process operating conditions that meet the imposed constraints.

P1-3.5.2.2. Second scenario – Process design for 95%, 97% and 99% of purities and recoveries

The present scenario has as objective to find the process optimal operating conditions for different minimum requirements in the purities and recoveries, 95%, 97% and 99% respectively. This will lead to different local minimum values of the objective function during the optimization step, which as previously shown the modified PSO is capable of identifying. This scenario has the goal of providing information about the different zones in which the process can be operated to produce products with different requirements.

For this case, in order to gradually verify a different range of operating conditions (recycle flow rate(Q_{IV}), extract flow rate (Q_X), feed flow rate (Q_F), eluent flow rate (Q_E) and solid flow rate (Q_S), respectively) the initial search region was set equal to $R_{1,min} = [1, 1, 1, 1, 1]$ and $R_{1,max} = [18, 15, 5, 10, 16]$ and expanded until $R_{f,max} = [36, 30, 10, 20, 32]$. A number of 100 particles and a maximum of 600 iterations were used in this optimization. Table 21 and Table 22 present the results of the optimal point found by the improved HPSO-TVAC; this result corresponds to the smallest local minimum found.

Table 21 - Optimal unit design for different requirements of purities and recoveries.

	Purity 95%		**Purity 97%**		**Purity 99%**	
	Value	**Standard Deviation**	**Value**	**Standard Deviation**	**Value**	**Standard Deviation**
Q_{IV}(ml/min)	23.749	0.347	19.813	0.509	16.831	0.541
Q_X(ml/min)	14.551	0.233	12.814	0.327	11.074	0.341
Q_F(ml/min)	7.060	0.317	5.679	0.444	4.180	0.479
Q_E(ml/min)	14.908	0.296	13.397	0.412	12.117	0.432
Q_S(ml/min)	10.024	0.130	8.341	0.188	7.014	0.199
fob	0.933	0.004	1.072	0.009	1.339	0.121

Table 22 - Optimal unit performance parameters for different requirements of purities and recoveries.

	Purity 95%			**Purity 97%**			**Purity 99%**			
	Optimal Point	**Max.**	**Min.**	**Optimal Point**	**Max.**	**Min.**	**Optimal Point**	**Max.**	**Min.**	**Triangle theory (Pais et . al; 1998)**
Pur (%)	95.000	99.300	95.000	97.000	99.600	97.000	99.000	99.300	99.000	99.300
Pux (%)	95.000	99.100	95.000	97.000	99.300	97.000	99.000	99.200	99.000	97.600
$Recr$ (%)	95.100	99.300	95.000	97.200	97.900	97.000	99.300	99.800	99.200	97.600
$Recx$ (%)	95.500	100.000	95.500	97.700	99.800	97.000	100.00	100.000	100.000	99.300
Pr (g/day l of bed)	123.012	123.181	77.099	100.539	100.541	74.468	74.009	74.010	70.995	61.200
Ec (l/g)	0.528	0.910	0.528	0.579	0.801	0.577	0.672	0.801	0.577	1.190

From Table 21 and Table 22 it is possible to note that the optimizer leads the process to operating zones where the flow rates are smaller while the minimum requirements are increased.

Furthermore, those regions are stricter as higher are the purities and recoveries, as it would be expected. Figure 55 and Figure 56 present the confidence regions and objective function map for the operating variables Q_S/Q_e, Q_S/Q_f and Q_S/Q_X, Q_S/Q_{IV} respectively.

In the objective function maps, it is possible to note that the particles flow towards a direction where the feed flow rate is always progressively increased, the eluent flow rate decreased, but the extract and the recycling flow rates start with dispersed values and converge to the optimal zone. Those movements are related with the objective function and the process model, since the goal is to maximize the productivity and minimize the eluent consumption, while keeping the process over the minimum requirements of purities and recoveries. Hence, as expressed in Table 21, the increase in the feed flow rate and the decrease in the eluent flow rate are related to the increase in the production rate and the reduction in the eluent consumption, respectively.

Finally, in this case scenario, the elliptical confidence regions become an interesting tool. As previously stated, the elliptical regions do not represent well the true process confidence regions obtained by the likelihood. However, elliptical regions represent a region within the likelihood region which respect all the process requirements. In this way, the ellipticals can be used as a simplified representation of the operating regions for the different requirements of purities and recoveries.

For the analysis in this point, it is important to remember that the 95% regions include all the purities and recoveries above this value, by its turn the 97% includes all values above it and in the same way the 99%, which can be verified in the Table 21 and Table 22. The main difference of the present case to the one presented in the previous section is that, further than just

providing the operating region for values above 95%, now it is possible to identify the operating regions which will lead to a product with higher purities and recoveries. This is important for processes where the final product type is related to its purities, which is usual in the fine chemicals and pharmaceutical industries.

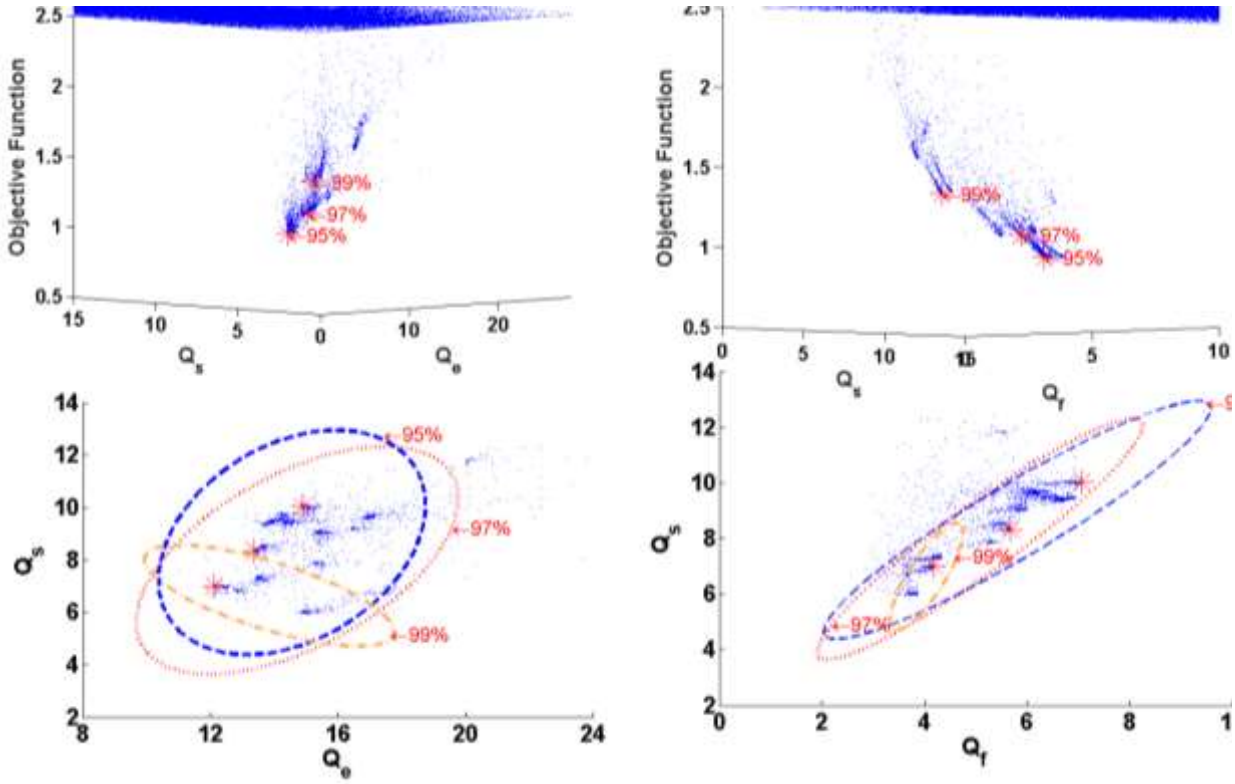

Figure 55 – Scenario 2: Likelihood confidence regions, elliptical confidence region (dashed lines) and objective function map for the operating variables Q_S/Q_e and Q_S/Q_f.

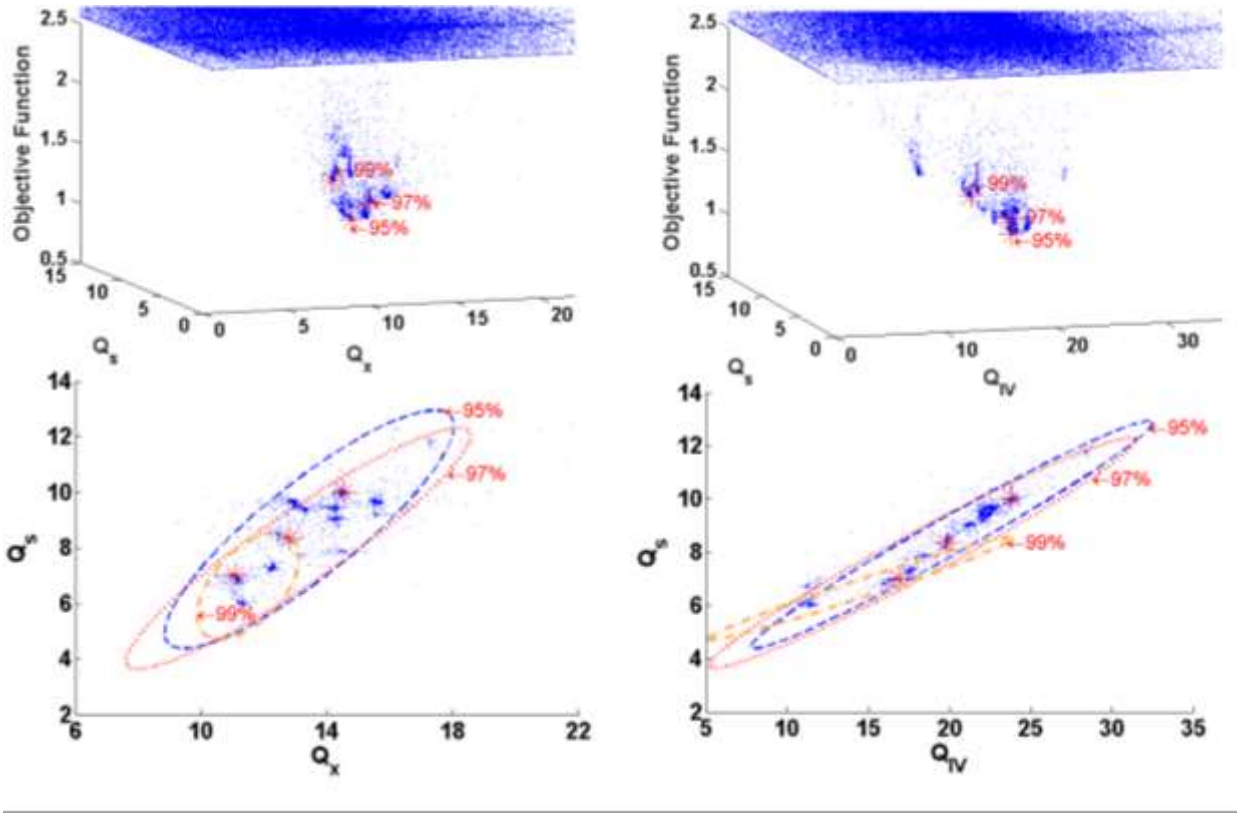

Figure 56 - Scenario 2: Likelihood confidence regions, elliptical confidence region (dashed lines) and objective function map for the operating variables Q_S/Q_X and Q_S/Q_{IV}.

P1-3.5.2.3. Third scenario – Process design for a minimum of 95% in the purities and recoveries with pumps limitations

The present scenario has the objective of finding the process optimal operating conditions in the presence of limitations in the operating region of the pumps. In this case, it is considered that the process pumps can operate only inside of specific regions, which are defined by the search regions bellow. This will lead to different local minimum values of the objective function inside each operating region of the pump.

During the optimization, in order to simulate the aforementioned process limitation, four different set of searching regions limited by R_{min} and R_{max} were considered, which are: $R_{1,min} =$

$[1, 1, 1, 1, 1]$ and $R_{1,max} = [28, 20, 10, 20, 25]$; $R_{2,min} = [14, 10, 5, 10, 12.5]$ and $R_{2,max} = [32, 23, 11, 23, 29]$; $R_{3,min} = [16.5, 12.5, 5.5, 12.5, 14.5]$ and $R_{3,max} = [37, 26,13, 26, 33]$]; $R_{4,min} = [18.5, 13,6.5, 13, 16.5]$ and $R_{4,max} = [42, 30,15, 30, 40]$, where each element of the region vector is recycle flow rate(Q_{IV}), extract flow rate (Q_X), feed flow rate (Q_F), eluent flow rate (Q_E) and solid flow rate (Q_S), respectively. A number of 100 particles and a maximum of 400 iterations were used in this optimization.

Table 23 and Table 24 present the results of the optimal point found by the improved HPSO-TVAC; these results correspond to the smallest local minimum found.

Table 23 - Optimal unit design for the different operating regions.

	Operating region 1		**Operating region 2**		**Operating region 3**	
	Value	**Standard Deviation**	**Value**	**Standard Deviation**	**Value**	**Standard Deviation**
Q_{IV}(ml/min)	22.821	0.609	28.953	0.488	32.815	0.076
Q_X(ml/min)	14.333	0.200	19.740	0.268	21.751	0.046
Q_F(ml/min)	6.995	0.206	8.066	0.192	7.846	0.139
Q_E(ml/min)	14.586	0.240	21.707	0.376	26.216	0.066
Q_S(ml/min)	9.653	0.192	12.513	0.048	14.566	0.057
fob	0.932	0.004	0.984	0.009	1.106	0.099

Table 24 - Optimal unit performance parameters for the different operating regions.

		Operating region 1			Operating region 2			Operating region 3	
	Optimal Point	**Max.**	**Min.**	**Optimal Point**	**Max.**	**Min.**	**Optimal Point**	**Max.**	**Min.**
Pur (%)	95.000	99.800	95.000	95.000	98.100	95.000	95.000	95.800	95.000
Pux (%)	95.000	99.200	95.000	96.000	97.800	95.000	95.000	95.800	95.000
$Recr$ (%)	95.100	99.600	95.000	95.000	97.900	95.000	95.000	95.800	95.000
$Recx$ (%)	95.500	100.900	95.400	95.500	98.800	95.000	95.500	96.300	95.500
Pr (g/day l of bed)	123.012	123.836	71.416	142.798	142.798	102.516	138.907	138.907	129.415
Ec (l/g)	0.528	0.864	0.528	0.636	0.853	0.532	0.749	0.853	0.532

Figure 57 and Figure 58 present the confidence regions and objective function map for the operating variables Q_S/Q_e, Q_S/Q_f and Q_S/Q_X, Q_S/Q_{IV} respectively. In the present case, discontinuities in the production are simulated. In this way, it were expected different operating points for each operating region. As presented in the following figures and previous tables, the optimization method found three optimal points. Within the three first regions R_1, R_2 and R_3. However, there was no minimum point found inside of the region R_4. This happens due to the fact that for the high flow rate regions, for the present case, it is not possible to meet the minimum requirements for purities and recoveries. Furthermore, over those regions the process eluent consumption starts to be significantly high. This can be verified in Figure 57 and Figure 58, where the feasible operating regions are reduced as the processes approximate high values of flow rates.

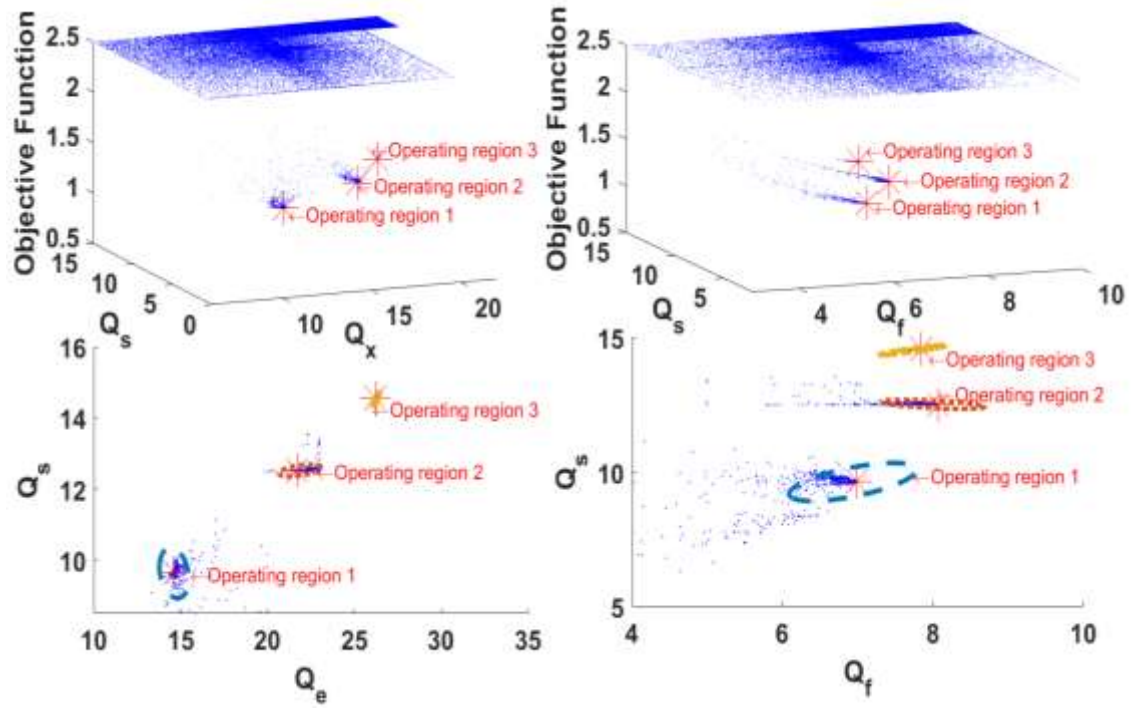

Figure 57 – Scenario 3: Likelihood confidence regions, elliptical confidence region (dashed lines) and objective function map for the operating variables Q_S/Q_e and Q_S/Q_f.

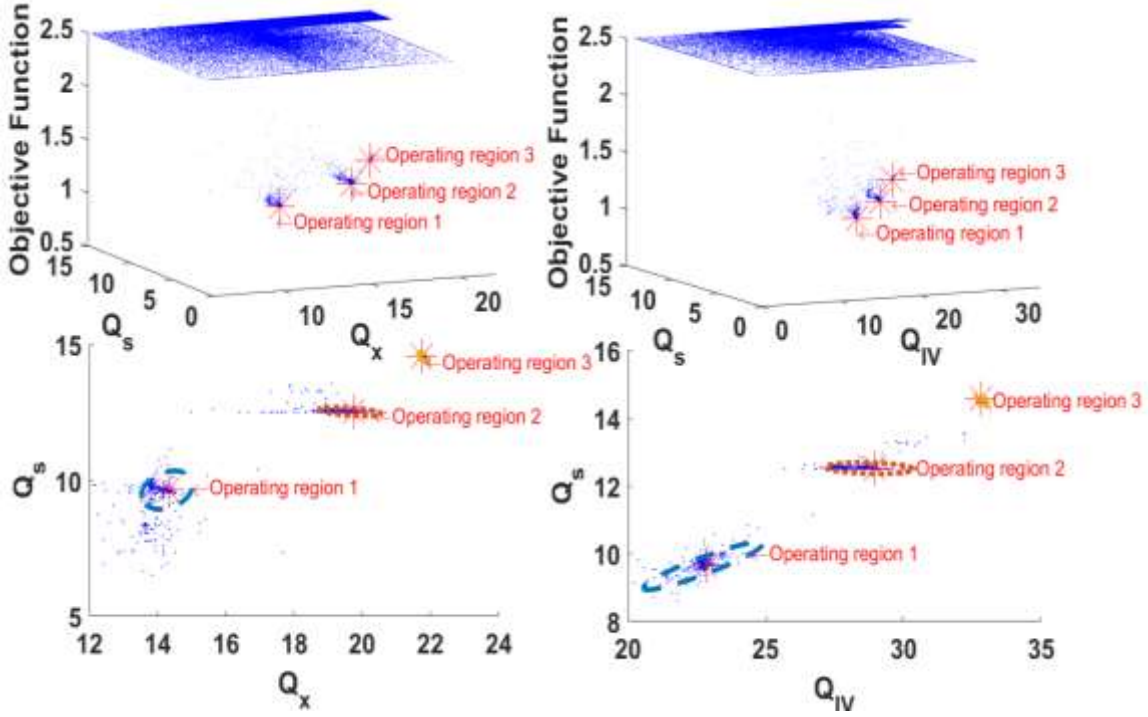

Figure 58 - Scenario 3: Likelihood confidence regions, elliptical confidence region (dashed lines) and objective function map for the operating variables Q_S/Q_X and Q_S/Q_{IV}.

P1-4. Conclusions

This part of the present thesis had the focus on the mathematical aspects of the systems in study, TMB and SMB units. Firstly, a method based on the Gram-Schmidt Orthogonalization was applied to a True Moving Bed system in order to analyze the influence of its operating variables in the process response. This method was able to take in consideration the dynamics of the system and indicate the most important process operating variable. The method also used the recovery and the eluent consumption as performance indicators besides the purity. The results obtained for the case study considered showed the following order from the most to the less important operating variable: recycling flow rate (Q_{IV}), solid flow rate (Q_s), eluent flow rate (Q_E), extract flow rate (Q_x), feed flow rate (Q_F), and feed concentration (C_F). This characterization is an essential step towards the development of further works in the SMB research field, such as processes design, optimization and control.

A step perturbation analysis was conducted in the TMB system in order to check the orthogonalization method response. The graphical analysis demonstrated that the variables indicated by the orthogonalization method as having the greatest impact in the process were the ones for which higher deviation in the products purity and recovery were observed. Furthermore, significant changes in the separation region and operating points position were also observed for these variables. The graphical analysis revealed an interesting case about the dynamic behavior of the TMB system. Through the step perturbation it was possible to see that perturbations in some process variables result in a system inverse response in recovery. These results also show the consistence of the orthogonalization based method.

It was also observed that, even for perturbations of lower magnitude for which, at steady state, only minor deviations are observed, the system still presents the same dynamic behavior and, for some instances, it presents strong deviations from its steady state, of the order of 10%. This means that the dynamics of this system cannot be ignored.

Since this method is based on the sensitivity Matrix, which depends only on the variations of the process operating variables and on the observed variation of the process responses, it is possible to apply it even without a mathematical model of the system. For example, the analysis can be done directly in the plant by performing perturbations on the operating variables and measuring the process responses. The sensitivity matrix can be constructed and the system analysis can be done. The method is capable of making an overall analysis of the system taking in consideration not only the purity, but all desired performance parameters over its dynamic behavior. The method is therefore a powerful tool to analyze efficiently the system behavior and provide consistent information about the process operating variables. This can be easily employed in more complex systems to develop studies in the field of system optimal design, control and optimization.

Afterwards, the orthogonalization method was employed to analyse two SMB units, one with 4 and another with 8 columns, simultaneously with a step perturbation analysis. Analysing the impact of the switching time it was observed that, after the orthogonalization around this variable, there was a divergence in results of the SMB-8 unit compared to the TMB and SMB-4 units. For the SMB-8 a small correlation between this variable and the remaining was found while for the TMB and SMB-4 large correlations were found. The results indicate that the correlation

between the switching time and the remaining operating variables decreases with the decrease of the switching time value. From this point of view, the SMB-4 resembles more the TMB unit than the SMB-8. These conclusions were confirmed by the graphical analysis of the simulation results of perturbations induced in several operating variables.

Furthermore, analysing the processes responses to the other operating variables, it was possible to observe, for some cases, a large inverse response of the SMB processes. This indicates that, for a period of time, the SMB processes have different dynamic behaviour when compared to the TMB.

It is therefore possible to conclude that TMB/SMB approximation is valid only for restricted conditions for which the regeneration and separation regions are not violated and also that the approximation is not valid in the dynamic regime.

However, industrial operation of these units are subject to perturbations, which can momentarily lead the process to regions outside the regeneration/separation zones.

After evaluating the efficiency of the orthogonalization method, the method was applied in the identification of the process manipulated variables of a control system strategy of a TMB unit. The method proved to be suitable to be applied in this case, since it takes in consideration the possible correlations between the operating variables, and it is capable of ranking those variables in descending order of their influence in the process controlled variables.

A control system was developed with the objective of controlling the purities and recoveries of an SMB unit used for the separation of a bi-naphthol enantiomers mixture using a 5-dinitrobenzoyl phenylglycine bonded to silica gel as adsorbent. The objective was to apply an

advanced control technique based on a linear model. However, it was found that the process presents an unusual dynamic behaviour becoming more complex as the process gets closer to its optimal point. At the optimal point, it is not possible to identify a process transfer function through the traditional way, using the process reaction curve. It was then proposed the division of the process response in two local points, one corresponding to the process response to a perturbation equal to an increase in its operating variables and another corresponding to a decrease in its operating variables.

In order to validate the approach here proposed for the identification of the global transfer function, the process was simulated when operating in a non-optimal point and three matrices of transfer functions were identified. One matrix using the traditional way, and two other using the method here proposed. After the identification, two control systems based on a model predictive control were developed and the process real time control was simulated using the phenomenological model as the plant simulator. Both control systems showed to be capable of controlling the process efficiently. Furthermore, the two controllers presented a very similar behaviour and, consequently, it was possible to conclude that the methodology proposed for the identification of the process transfer function was validated.

Finally, a set of transfer functions was identified at the optimal point through the alternative methodology proposed in this work. The transfer functions were identified to the specific system in study; however, the strategy here proposed can be applied in the transfer function identification of different configurations of TMB/SMB units. A control system was built and the controller was applied in a real time simulation. The control system showed efficient results in all

simulated scenarios. It was possible to conclude that, with this methodology, it is possible to control the process at its optimal operating conditions through a process transfer function, which cannot be done with the traditional methodology. In order to evaluate the strategy here proposed, a final simulation was performed, where a model of an SMB with four columns were used as plant and the transfer function identified for the optimal condition of the TMB unit as prediction model in the MPC. It was possible to conclude that, under the optimal conditions, the controller was able to keep the SMB under the setpoint. Furthermore, it was possible to conclude that the orthogonalization method is a powerful tool for process control when applied in the identification of the set of process manipulated variables.

Then, the development of a Virtual Online Analyzer was presented to make real time predictions of the purities in the raffinate and extract streams of an equivalent True Moving Bed unit, and an extension of a virtual on-line analyser (VOA) is proposed in order to improve the analysis system. This extension consists in the implementation of a system that uses two artificial neural network (ANN) models concomitantly with an offline measurement system. The system proposed in this work was named Quasi-Virtual Online Analyser because of its mixed nature, offline measurement, and online prediction.

The two ANN models that compose the Q-VOA system were developed based on the process data generated with the phenomenological model previously validated. A MISO system of Artificial Neural Networks was proposed to build the VOA analyser. The main structure of the neural model was based on a NARX approach to keep the system dynamics in the empirical model. The system inputs were chosen through a dynamic analysis done with the

orthogonalization method. This analysis indicated four process operating variables as the main variables with most influence on the purities response.

The Q-VOA system here proposed is composed by three parameters that were tuned to obtain the best system representation. The results show that the Q-VOA can predict with reasonable accuracy the SMB system dynamics and steady behaviour as simulated by the phenomenological model. The results of the Q-VOA were compared with the simple VOA results. Through this comparison, it was possible to conclude that the Q-VOA can reduce the system errors and keep the prediction closer to the process real response that, in this case, was the phenomenological model response. Finally, this work shows that the Q-VOA presents efficiency even under the presence of non-measured perturbations.

Finally, an improved Self-Organizing Hierarchical Particle Swarm Optimizer with Time-Varying Acceleration Coefficients and Mutable Searching Region concomitantly with an adapted method to define the operating variables confidence region were introduced. Those methods were applied in the design and optimization of a True Moving Bed unit where a chiral separation of a bi-naphthol enantiomers mixture using a 5-dinitrobenzoyl phenylglycine bonded to silica gel as adsorbent is processed.

First, the proposed methodology was applied in a series of standard cases in order to evaluate the efficiency of this approach. The method showed good results when applied to the benchmark functions and compared with traditional methods found in the literature. Once the consistence of the method was tested, it was possible to apply it to the case in study, the design and optimization of a TMB unit.

Three different scenarios were simulated here in order to verify the consistency and efficiency of the method. In the first case, a traditional TMB unit design was tackled and its results were compared to the ones obtained by the triangle theory, the traditional design method for these types of units. The method was capable of identifying an operating region in which the process can be operated with purities and recoveries above 95%, productivity two times higher and a solvent consumption 30% lower than the operating point provided by the triangle theory.

In the second case, a further discretization of the operating regions was performed, through the variation of the minimum requirements of purities and recoveries during the optimization. In this point, the method proved to be able to identify the sub regions, within the 99% confidence operating regions where the process can be operated producing purities above the minimum products requirements. This is important for processes where the final product type is related to its purity, which is usual in the fine chemicals and pharmaceutical industries.

Finally, it was simulated the situation where the unit design is constrained by instruments limitations. In this case, the pumps capacities were limited and the process was designed for four different possible operating regions. In this last scenario, the method was able to identify all the feasible operating regions where the process can be operated meeting the minimum recoveries and purities requirements.

It is possible to conclude that the method can efficiently solve the problem of the optimal design of TMB units while providing a map of the process possible operating regions, which is a useful tool for the process control and operation.

One of the main advantages of this method is the possibility of tracking all possible operating regimes of the unit that meet a given process requirement. The main limitation of this method is that the objective function here defined lead to losses of a considerable number of particles during the simulation, since it makes use of penalties and when the particles fly over the penalty region they are eliminated from the iteration. This limitation must be deeper studied, which can lead to improvements in the method computational effort.

By its turn, the present method is suitable for different types of objective functions, which can include economic factors, such as the cost of the eluent and price of the product, leading to a robust and efficient unit design and optimization. Furthermore, the method can be applied to different and more complex separation systems and it is independent of the process characteristics such as the mass transfer resistance.

Part 2 – N-Propyl Propionate experimental studies and process modelling

P2-1. Introduction

This part of the work is dedicated to the study of the n-Propyl Propionate reaction system, leading to its production in a True Moving Bed Reactor unit. In this chapter a brief introduction of the main topics covered in this part of the work is presented.

P2-1.1. N-Propyl Propionate

The use in large scale of readily biodegradable and environmentally friendly solvents is limited by the high cost of these products in comparison with the common solvents. Their high cost is normally associated with their production that is usually done through traditional routes which are expensive and generate several ecological impacts. The research about alternative routes of production of these solvents is an important challenge to be addressed in order to make them more prone to large scale use in industry.

As pointed out in the Introduction of this thesis, in the field of industrial solvents, n-Propyl Propionate (ProPro) can be considered an alternative solvent with environmental advantages. The ProPro can be produced by esterification, which is a reversible reaction in which 1-Propanol (POH) reacts with Propionic Acid (AcidPro) producing water as a by-product. This reaction system presents a complex Vapor Liquid Equilibrium with four azeotropes; among those, two are homogeneous azeotropes (Water/1-Propanol and Water/Propionic Acid) and two are heterogeneous azeotropes (Water/n-Propyl Propionate and Water/1-Propanol/n-Propyl Propionate). The reaction system can be represented as follows:

$$C_3H_8O + C_3H_6O_2 \leftrightarrow C_6H_{12}O_2 + H_2O$$

n-Propyl Propionate is normally produced through a catalytic reaction in liquid phase in a Plug Flow Reactor (PFR) which is followed by a separation step in a distillation column. With the objective of improving the production process, several works in the literature reported the study of the ProPro production through an alternative route applying a multifunctional unit, the Reactive Distillation (RD) (Duarte 2006; Altman et al. 2010; Cruz-Díaz et al. 2012; Xu et al. 2014).

However, the RD route presents some limitations, as the aforementioned system complexity in the liquid vapor equilibrium. Furthermore, in those units the outlet streams are composed by a mixture of the main product and the non-converted reactants. Thus, those processes present difficulty to achieve high purity products. In order to obtain a higher conversion and purity in a RD system it is necessary to employ auxiliary units, which increase even more the complexity and energy consumption of the process (Altman et al. 2010; Cruz-Díaz et al. 2012; Xu et al. 2014).

In this way, alternative improvements for ProPro production could be the employment of chromatographic separation in the downstream purification step of the Reactive Distillation production or in the traditional production route. A further improvement in this process could be performing the reaction and separation simultaneously in a continuous chromatographic unit like a Simulated Moving Bed Reactor (SMBR). However, there isn´t any work in the literature with the focus on the behaviour of this system in a chromatographic unit. This is why the study of the chromatographic separation of the compounds of this reaction system could be an important contribution.

P2-1.2. Chromatographic separation

Chromatographic separations are considered as one of the most important and powerful techniques for continuous separation of complex multicomponent mixtures, and have been employed with success in pharmaceutical, food and petrochemical industries (Faria et al. 2014). These processes are based on the difference of affinities between the chemical compounds of a given fluid mobile phase and a solid stationary phase. The compounds which have higher affinity with the solid phase will be more retained than the components with weaker affinity. This results in that the different components travel at different velocities along the column. Thus, the components separation is promoted, since components are obtained at the column outlet stream in increasing order of their affinity to the adsorbent solid phase. Several possible combinations of mobile and stationary phases, together with simple configuration, operation and scale-up procedures make this technology very versatile, which is one of its major advantages (Faria et al. 2014).

Hence, the employment of chromatographic units seems to be an important point to be explored in the field of ProPro production. However, deeper experimental studies and modelling developments are necessary to evaluate the eventual benefits that such units may bring to this process. One of the objectives of the present work is to study the separation of the non-reactive pairs of the compounds involved in the n-Propyl Propionate formation in a fixed bed adsorptive column packed with Amberlyst-46 resin, a typical catalyst used in the ProPro synthesis, and in this way determine the adsorption equilibrium isotherms.

Several papers have been published investigating the application of chromatographic separation as an alternative to the synthesis or separation of traditional compounds (Ziyang et al. 2001; Pereira et al. 2009a; Faria et al. 2014; Regufe et al. 2016). Thus, there is a consolidated methodology in the literature for the validation of chromatographic separation models through laboratory experiments. However, it was not found any report about the evaluation of the performance of the optimization method used in the parameters estimation step. Furthermore, it was also not found any deeper study about the uncertainties evaluation in both laboratory experiments and model prediction. As it will be demonstrated in this work, those are important points to be addressed as they can have a significant impact in the final results of this procedure.

Therefore, in parallel to the studies about the ProPro reaction system adsorptive separation, it is also objective of the present work to evaluate the efficiency of the optimization method in the parameters estimation step, which will be done based on the HPSO-TVAC-MSR presented and applied in the first part of this work (Sections P1-2.5 and P1-3.5.1), and to evaluate the uncertainties associated with the experiments and model parameters, which are also important contributions to the field as it will be shown in the next Section.

P2-1.3. Uncertainties Evaluation in Chromatography

Based on the principle that there is no measurement which can provide an absolute and true value, the uncertainty is an inherent characteristic of any measurement performed. The Guide to the Expression of Uncertainty in Measurement (GUM) defines uncertainty as: “parameter, associated with the result of a measurement, that characterizes the dispersion of the values that could reasonably be attributed to the measurand” (International Organisation for

Standardisation 2008). In this definition, the measurand is an unknown property which is to be determined by the measurement; it is composed by a value and a respective character that gives meaning to the measurand.

As mentioned by Konieczka and Namieśnik (2010) there are only a few original papers on the metrological characterization of analytical procedures that use chromatographic techniques. In the present work the chromatographic analysis is an essential step in the determination of the experimental results. Furthermore, there are even fewer works in the literature that perform the uncertainty evaluation of chromatographic separation experiments and models. Usually, these works are limited to the calculation of the standard deviation (SD) or the relative deviation (RSD) (Konieczka and Namieśnik 2010a).

The evaluation of the uncertainty is a crucial step to characterize properly the experiments and model predictions. Furthermore, it leads to a better understanding about the experimental results increasing the confidence while applying the experimental data. Hence, it allows reducing the number of experiments performed, which are usually done in excessive number in order to reduce the experimental error. Normally, each experiment is associated with a long period of time mainly related with analytical procedures, with reactants cost and with generation of waste. Those factors, with the knowledge of the experiments uncertainties, can be reduced generating benefits to the laboratory, researcher and research quality. Moreover, it should be a good practice to represent an analytical result according to the values of a continuous random variable, as a confidence interval, i.e., the interval likely to include the expected value (Konieczka and Namieśnik 2010a).

Hence, this work has one of its focus on the uncertainty evaluation of the experimental data and the model parameters. The parameters uncertainty is determined through the parameters confidence region.

P2-1.4. True Moving Bed Reactor

Similar to the chromatographical separations units True Moving Bed, presented in the Part 1 of this thesis, and based on the same concept, the True Moving Bed Reactor (TMBR) system consists in the countercurrent flow of liquid (eluent) and solid phases (adsorbent) that plays the role of adsorbent and catalyst at the same time. The countercurrent movement promotes the separation of the components based on their affinity to the phases in play. The liquid phase becomes richer in the less retained compound while the more retained compound will be dragged by the solid phase, as in the TMB. However, as the solid has also the function of catalyst, the contact with it will promote the reaction. Hence, while being produced, the products are carried by the phase for which they have more affinity. As the products are being adsorbed, i.e. being removed from the reaction medium, it is possible to overcome the equilibrium conversion.

Considering a simple reversible reaction $A + B \leftrightarrow C + D$, where C is the most retained compound and D the less retained one, Figure 59 presents a schematic representation of a generic TMBR unit. It is possible to observe in Figure 59 that each section of the column must accomplish a different role in the separation system. Sections II and III are responsible for the reaction and simultaneous separation of the products, while sections I and IV are responsible for the regeneration of the adsorbent and eluent respectively. Hence, the Raffinate stream will be composed mainly by the compound D and the Extract stream by the compound C.

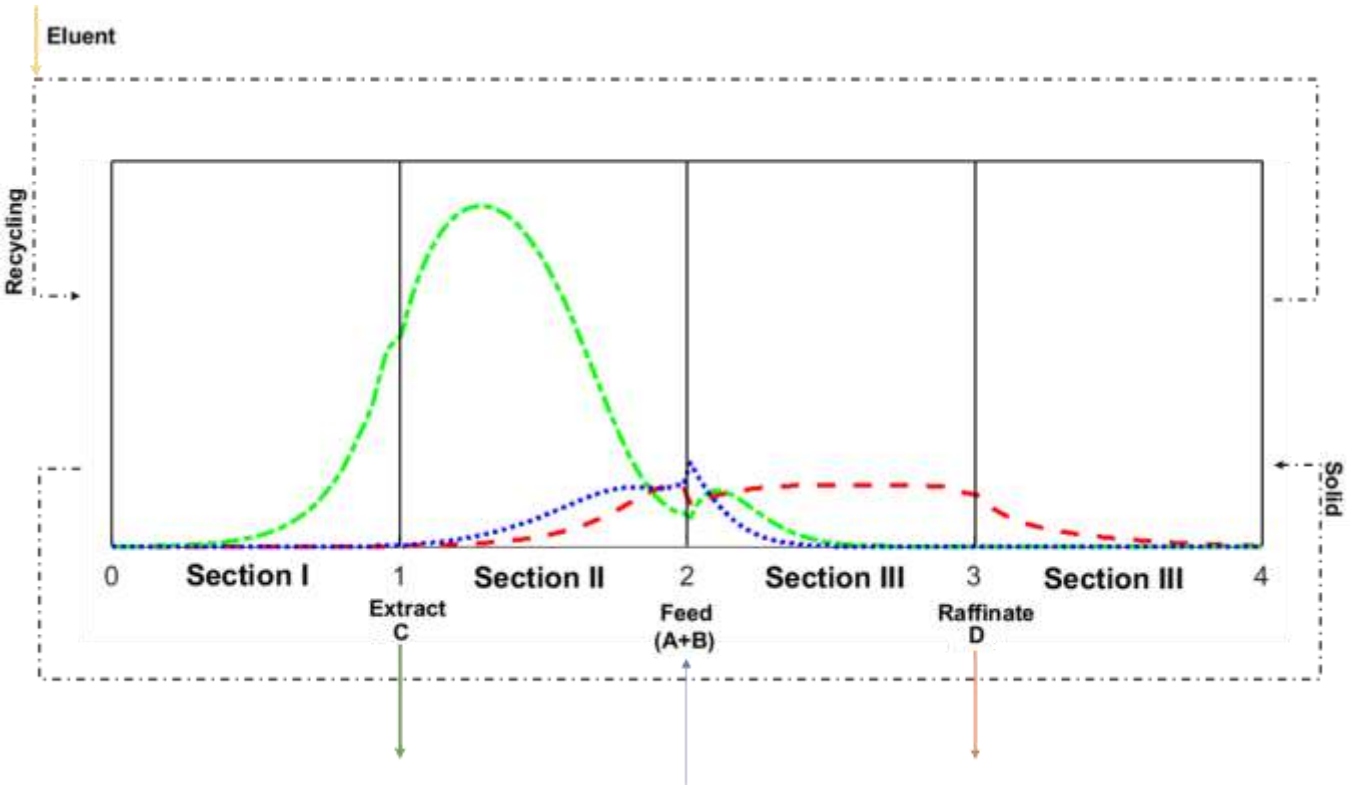

Figure 59 - True Moving Bed Reactor unit representation

As in the TMB case, the movement of the solid phase is not simple to perform. Therefore, the Simulated Moving Bed Reactor (SMBR) is presented as a feasible application of the TMBR concept. The SMBR, as the Simulated Moving Bed units, is operated through the synchronized changing of the positions of the inlet and outlet ports at predefined times, the switching time, which simulates the solid phase movement.

The relationship between the TMBR and SMBR is established through the correlation of the solid flow rate and the switching time, which is defined as: $u_s = \frac{L}{t}$, where L is the bed length. Several works make use of this relation to apply the TMBR phenomenological model in order to characterize a SMBR system (Minceva and Rodrigues 2005; Minceva et al. 2008; Pereira et al. 2008; Graça et al. 2012; Santos et al. 2015). Furthermore, several studies have been published

addressing the application of TMBR/SMBR units to systems characterized by equilibrium-limited reactions (Son et al. 2011; Faria et al. 2014; Constantino et al. 2015a; Regufe et al. 2016).

Thus, one of the main objectives of this work is to study the production of the n-Propyl Propionate through a True Moving Bed Reactor, presenting this route as one novel alternative to the ProPro synthesis. Therefore, a proper design and optimization of the TMBR are the main steps to accomplish the aforementioned objective, as previously demonstrated in Part 1. However, there is a lack of studies addressing this point for those units. In this way, it is also proposed the application of the design method presented in P1-3.5.1 as an alternative method for the design of the TMBR unit for the ProPro production, comparing the proposed method with the traditional one employed in the literature.

P2-2. Methods

As mentioned before, there are no studies about the production of n-Propyl Propionate using an adsorption system. In order to study the production of n-Propyl Propionate by a SMBR unit, it is first necessary to assess the following points:

i. Adsorption equilibrium isotherms determination.
ii. Reaction kinetics study.
iii. Fixed-bed adsorption and reaction system tests.
iv. TMBR design and optimization.

The methodologies used to address the different points of the problem in study are described in this chapter. Those are the experimental tests that should be performed in order to characterize the ProPro synthesis system, the modelling of the different units in study, i.e. the fixed bed chromatographic unit, the fixed bed chromatographic reactor and the TMBR. The results obtained from the application of those methods are presented at the end of this part in the results chapter.

P2-2.1. Reaction system

P2-2.1.1. Reaction kinetics

As aforementioned, the n-Propyl Propionate is formed by a reversible reaction that can be represented as follows:

$$POH + ProAc \xrightarrow{k_1} ProPro + H_2O \quad (86)$$

$$ProPro + H_2O \xrightarrow{k_{-1}} POH + ProAc \quad (87)$$

where k_1 is the rate constant of the formation of n-Propyl Propionate and k_{-1} is the rate constant of the consumption of n-Propyl Propionate. Considering the non-ideality of the liquid phase and considering a pseudo-homogeneous model, which leads to the assumption that the behaviour of the reactive mixture in presence of a heterogeneous catalyst is equivalent to the behaviour in the presence of a homogeneous catalyst, and from Equations (86) and Equation (87), the reaction rate of formation of ProPro can be written, in terms of activity (a), as follows:

$$r_{ProPro} = k_1 a_{POH} a_{ProAc} - k_{-1} a_{ProPro} a_{H_2O} \quad (88)$$

Considering reaction equilibrium, the equilibrium constant (K_{eq}) of this reaction can be defined as:

$$K_{eq} = \frac{k_1}{k_{-1}} = \frac{a_{ProPro} a_{H_2O}}{a_{POH} a_{ProAc}} \quad (89)$$

Finally, rearranging Equation (88) with Equation (89), the reaction rate law for n-Propyl Propionate can be described as:

$$r_{ProPro} = k_1 \left(a_{POH} a_{ProAc} - \frac{a_{ProPro} a_{H_2O}}{K_{eq}} \right) \quad (90)$$

The relation between a rate constant and temperature can be described by the Arrhenius equation:

$$k_1 = k_0 e^{-\frac{E}{RT}} \quad (91)$$

Where, k_0 is the pre-exponential factor and E is the activation energy.

The Van´t Hoff equation expresses the relation between the equilibrium constant and the temperature:

$$K_{eq} = K_{\infty} e^{-\frac{\Delta H}{RT}} \quad (92)$$

Where, K_{∞} is the pre-exponential factor and ΔH is the reaction enthalpy. Duarte (2006) studied this reaction through experiments in a batch reactor.

P2-2.1.2. Catalyst/Adsorbent

Several works in the literature employ heterogeneous catalysis in the production of ProPro using catalysts with strong acidic functional group (Duarte 2006; Keller et al. 2011; Cruz-Díaz et al. 2012; Xu et al. 2014). As mentioned above, ProPro can be produced by esterification of 1-Propanol (POH) with Propionic Acid (AcidPro). However, this system can lead to several secondary reactions, as the production of di-n-Propyl Ether (DPE) by etherification of two Propanol molecules or production of Propene (Pro) by the dehydration of 1-Proponol (Cruz-Díaz et al. 2012). Not only because of economic questions but also because of safety questions (propene is a highly flammable gas), the presence of these compounds in the reaction system is undesirable (Duarte 2006). Figure 60 presents the reaction path of the synthesis of the ProPro.

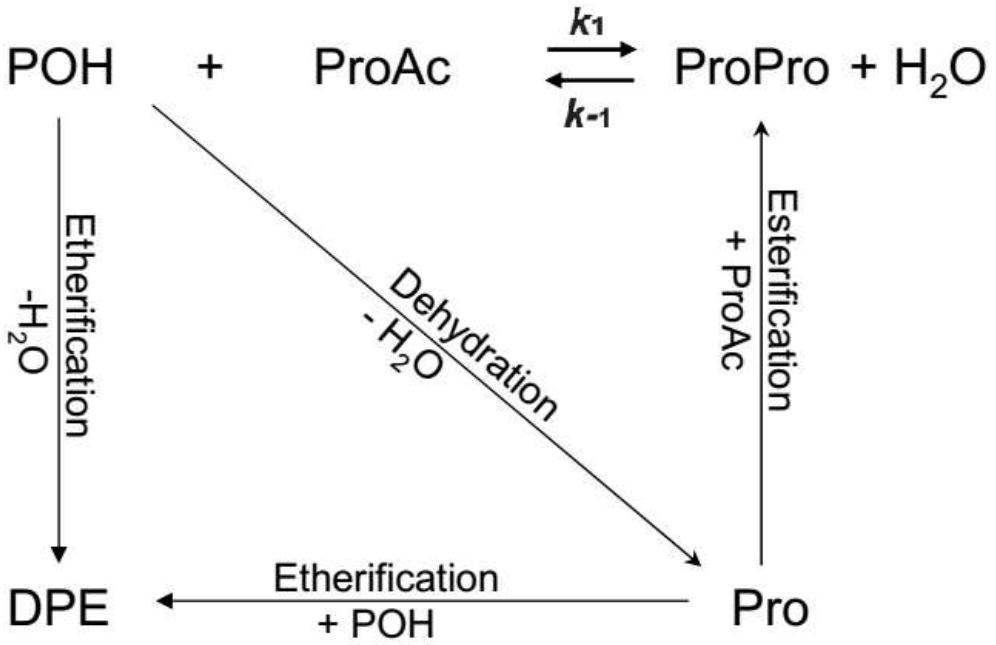

Figure 60 - Reaction routes for the formation of the n-Propyl Propionate (Adapted from: (Duarte 2006)*).*

In order to overcome these problems, Amberlyst 46 catalyst was developed (Lundquist 1995).

In that work, mass transfer effects inside the Amberlyst 46 resin were studied and this resin showed to be capable of catalyzing the ester production, while at the same time reducing or eliminating the secondary products formation (Lundquist 1995). The author´s study indicates that the production of secondary products in ester formation is directly proportional to the functionalized groups position in the catalyst. When the active sites are located further from the catalyst surface more ether is produced during the esterification reaction. In this way, Lundquist proposed the functionalization of the catalyst only in the beads surfaces, leaving the inner surface inactivated.

Furthermore, an advantage presented by Amberlyst 46 is that the esterification reaction occurs at low temperatures. Another is its selectivity to preferably adsorb water in presence of the ProPro reaction system compounds, which is ideal to its simultaneous application as catalyst and adsorbent. Hence, Amberlyst 46 presents all the necessary characteristics to be applied in the present work. Therefore, Amberlyst 46 was adopted as Catalyst/Adsorbent in this study. Table 25 presents the main properties of this resin, which was gently provided by The Dow Company for the experimental developments of this work.

Table 25 - Catalyst characterization, Amberlyst 46 physical properties (Duarte 2006; The Dow Chemical Company 2014).

	Value	**Standard Deviation**
Maximum Operating Temperature (°C)	120	-
Water Content (%)	21	0.1
Concentration of active Sites ($eq.kg^{-1}$)	0.95	0.01
Surface area (m^2g^{-1})	75	-
Average particle diameter (mm)	2.450	-

Duarte (2006) studied the reaction equilibrium and kinetics of this system and estimated the respective parameters as presented in Equation (91) and Equation (92) of the previous section. These values are presented in Table 26. In that work, the UNIQUAC thermodynamic model was employed for the calculation of the activity coefficients.

Table 26 - Reaction equilibrium and kinetic constants (Duarte 2006).

	$k_0\ (mol.s^{-1}.eq^{-1})$	$E\ (J.mol^{-1})$	K_∞	$\Delta H(J.mol^{-1})$
k_1	6.848×10^7	5.918×10^4	-	-
K_{eq}	-	-	7.504	-4.161×10^3

P2-2.1.3. Thermodynamic model

In order to develop a rigorous model of the reaction system, the liquid phase activity coefficients must be calculated through a thermodynamic model developed using realistic liquid-liquid equilibrium (LLE) determinations. The liquid phase non-idealities for the n-Propyl Propionate system is usually addressed in the literature through the UNIQUAC model (Duarte 2006; Keller et al. 2011; Cruz-Díaz et al. 2012). However, in Samarov et al. (2016) a complete liquid-liquid equilibrium study is presented for the quaternary system and ternary subsystems composed by 1-Propanol, Propionic Acid, Water and n-Propyl Propionate, in which the NRTL model parameters are estimated and validated. The referred work carried out the study at three different temperatures (293.15 K, 313.15 K and 333.15 K) and atmospheric pressure. The authors demonstrated that the NRTL model can describe well the LLE systems. Furthermore, the referred work provided enough experimental data to allow the estimation of the NRTL parameters uncertainty in the present work, and respective propagation of these uncertainties to the activity coefficients. In this way, the NRTL model was here used to describe the liquid-liquid equilibrium. The activity coefficients, γ_i, in the solution of n_c components can be described by the NRTL model as:

$$\ln(\gamma_i) = \frac{\sum_{j=1}^{n_c} x_j \tau_{ji} G_{ij}}{\sum_{j=1}^{n_c} x_j G_{ji}} + \sum_{j=1}^{n_c} \frac{x_j G_{ij}}{\sum_{l=1}^{n_c} x_l G_{lj}} \left(\tau_{ij} - \frac{\sum_{l=1}^{n_c} x_l \tau_{lj} G_{lj}}{\sum_{l=1}^{n_c} x_l G_{lj}} \right) \quad (93)$$

where:

$$\tau_{ji} = \frac{g_{ij} - g_{ii}}{RT} = \frac{\Delta g_{ij}}{RT} \quad (94)$$

$$G_{ij} = \exp(-\alpha_{ij} \tau_{ji}) \quad (95)$$

$$\alpha_{ij} = \alpha_{ji} \quad (96)$$

where, g_{ij} is an energy parameter that characterizes the interaction of components i and j, α_{ij} is related to the non-randomness in the systems.

The NRTL binary parameters determined in the work of Samarov et al. (2016) are given in Table 27. This model was implemented in the gPROMS modelling builder (Process Systems Enterprise 2015).

Table 27 - NRTL binary parameters (Samarov et al. 2016).

	Propionic Acid	Propionic Acid	Propionic Acid
	1-Propanol	Water	n-Propyl Propionate
Δg_{ij} (J mol^{-1})	1120.8	1631.9	590.0
Δg_{ji} (J mol^{-1})	1754.0	-182.3	32.1
α_{ij}	0.3	0.3	0.3
	1-Propanol	1-Propanol	n-Propyl Propionate
	Water	n-Propyl Propionate	Water
Δg_{ij} (J mol^{-1})	1744.7	566.0	3505.0
Δg_{ji} (J mol^{-1})	-93.5	236.9	1142.5
α_{ij}	0.06	0.3	0.3

P2-2.2. Experimental setup and analytical method

The experiments here presented were done in a Fixed Bed unit, composed by a jacketed column of 12.1 cm of length and 2.6 cm of diameter packed with the resin Amberlyst-46 wet, pre-treated in 1-Propanol. The complete experimental unit has the column; a thermostatic bath (Julabo, Model F12), which was responsible for keeping the column and the feed at a constant temperature (313 K); a sample collector, responsible for performing the periodic and automatized sampling of the column outlet stream; a liquid chromatographic pump (Gilson, Model 302), responsible for feeding the solutions at a constant and pre-defined flow rate. The described experimental set-up is presented schematically in Figure 61.

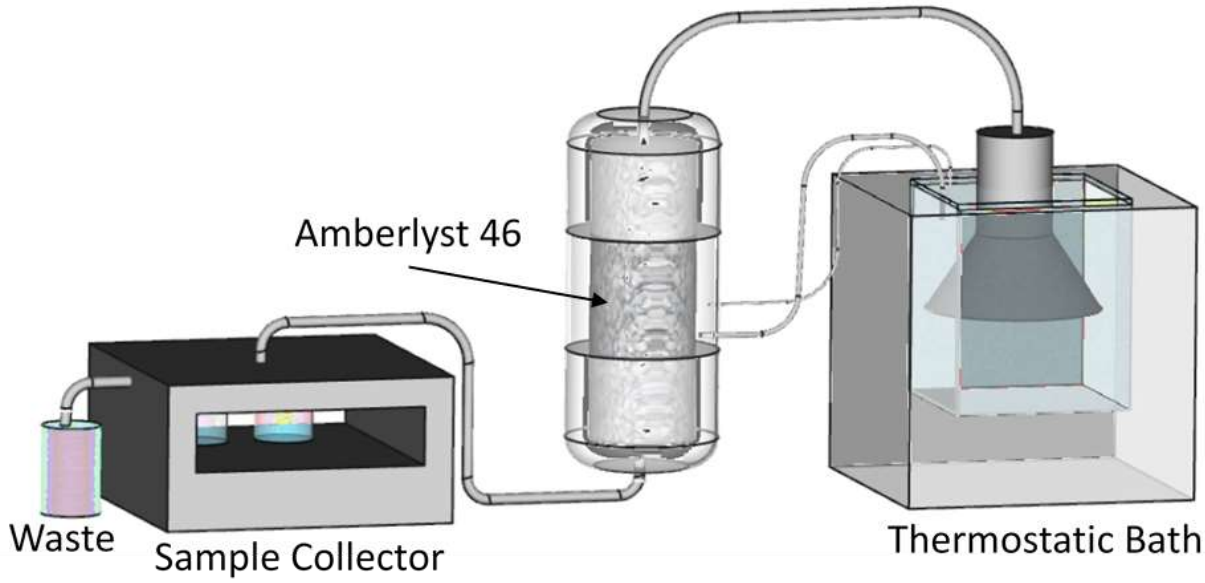

Figure 61 - Experimental setup.

All the collected samples were analyzed in a gas chromatograph (Master GC Dani) using a fused silica capillary column (PoraBOND Q 12 m x 12 µm) to separate the compounds and a thermal conductivity detector (TCD) to quantify the samples. For the analysis, the GC column temperature was initially at 323 K during 3.0 min, then the temperature was increased up to 393K using a ramp of 7 K min^{-1} and this temperature was held for 10.0 min. The TCD temperature was 473 K. The carrier gas was helium. The analyses were done by injecting 1µL of the collected sample.

Two types of experiments were performed. The first one was breakthrough curve adsorption tests with non-reactive pairs for the determination of the adsorption equilibrium isotherms which are presented in Section P2-2.3.2. The second one was sorption enhanced fixed bed tests for mathematical model validation that are presented in Section P2-2.3.4.

P2-2.3. Fixed bed hydrodynamics

The characterization of the fixed-bed column hydrodynamics was done through tracer experiments. In this way, the bed porosity, ε_b and axial dispersion coefficient, measured by the Peclet number, Pe were determined. The experiments consisted in the injection of an inert compound (tracer) in the column and the measurement of the column outlet concentration. The tracer used was the Blue Dextran because it is a substance that does not enter the pores of the Amberlyst 46 resin. Through the experimental data and the following equations, it is possible to characterize the fixed-bed column:

$$E(t) = \frac{C_{out}(t)}{\int_0^\infty C_{out}(t)dt} \tag{97}$$

$$\bar{t_r} = \int_0^\infty tE(t)dt \tag{98}$$

$$\sigma^2 = \int_0^\infty (t - \bar{t_r})^2 E(t)dt = \frac{2}{Pe}\bar{t_r}^2 \tag{99}$$

where $E(t)$ represents the residence time distribution, C_{out} the tracer concentration in the column outlet stream and $\bar{t_r}$ the mean residence time.

P2-2.4. Langmuir competitive adsorption parameters estimation

Once the fixed bed hydrodynamics is characterized, adsorption tests with the non-reactive pairs were performed. In order to do it, a series of breakthrough experiments was done. This

methodology is based on the successive change in the feed concentration of the column with it in equilibrium with a previous concentration. After each change, the concentration is kept until a new steady state is reached. When the new steady state is reached, the column will in equilibrium with the feed concentration and the composition of the liquid and solid phases are a new point in the adsorption equilibrium isotherm. Then, through the experimental data it is possible to determine the solid composition in each equilibrium. This is done through a global mass balance to the system which corresponds to:

$$\Delta n_i = Q \int_0^{t_{exp}} (c_{in} - c_{out})\, dt \tag{100}$$

$$\frac{\Delta n_i}{V} = \left[\varepsilon_b + (1-\varepsilon_b)\varepsilon_p\right]\left(c_{in,i} - c_{out,i}\right) + (1-\varepsilon_b)\left(1-\varepsilon_p\right) \times \left[q_i\left(c_{in,i}\right) - q_i\left(c_{0,i}\right)\right] \tag{101}$$

whereΔn_i is the change in number of moles of the compound i in the empty space between the particles and in the solid phase from the previous steady state to the new one, $c_{in,i}$, $c_{out,i}$ and $c_{0,i}$ are the concentrations of the compound i in the liquid phase of the new feed stream, of the outlet stream of the column and of the previous steady state (initial concentration), respectively and q_i is the adsorbed concentration of the compound i in equilibrium with the liquid phase.

Hence, through Equations (100) and (101) and the breakthrough experiments it was possible to determine the value of the adsorbed concentration (q) in equilibrium with the liquid phase concentration (c).

The Langmuir competitive adsorption model was adopted to represent the liquid phase adsorption equilibrium. This was done following previous works in the literature where similar

systems were addressed and the Langmuir model was indicated as the most suitable to describe this phenomenon (Faria et al. 2014; Constantino et al. 2015a; Regufe et al. 2016). The Langmuir competitive adsorption model is represented as:

$$q_i = \frac{Q_{max,i} K_i c_i}{1 + \sum_i^{n_c} K_i c_i} \tag{102}$$

where $Q_{max,i}$ is the equilibrium adsorption capacity and K_i is the Langmuir adsorption constant for component i.

The parameters of the Langmuir isotherm model were estimated through the same PSO approach presented in Section P1-2.5.

As previously mentioned, the Particle Swarm Optimization method has been applied successfully in the literature to solve parameters estimation problems (Ratnaweera et al., 2004; Schwaab et al., 2008). This method presents as its main advantages the easy implementation, the easy improvement of the computational performance through parallelization and, moreover, its results can be directly applied in the evaluation of the parameters confidence region and uncertainty (Schwaab et al. 2008).

In P1-2.5 it was proposed a Self-Organizing Hierarchical Particle Swarm Optimizer with Time-Varying Acceleration Coefficients and mutable searching region, HPSO-TVAC-MSR, in order to verify the local minimums of the objective function. The results presented in section P1-3.5.1 demonstrated that it is possible for the PSO to find the local minima of several benchmark functions that were tested. Thus, in this part the proposed PSO was employed in order to avoid that only a possible local minimum is found during the parameter estimation.

In this way, this optimization method is here applied to determine the set of parameters that composes the Langmuir model for the system here in study. The system has a total of 8 parameters. The optimization will minimize the objective function, $J(\theta)$, that accounts for the least-squares function described by the difference between the model predictions and the values obtained in the breakthrough experiments, Equation (103). The method evaluates a vast range of parameters values and indicates the optimal value and the possible local minima, in case they exist. Through the particle swarm results it is possible to define the parameters confidence region, as described in the next Section.

$$J(\theta) = \sum_{i=1}^{n_c} \sum_{j=1}^{n_e} ({q_{ij}}^* - {q_{ij}}^e)^2 \quad (103)$$

In Equation (103), n_c is the number of compounds and NE the number of experiments.

The HPSO-TVAC-MSR, objective function and Langmuir model were implemented in the MatLab software. Thus, it was possible to perform the parameters estimation.

P2-2.5. Parameters confidence region evaluation

The parameters confidence region was determined in a different way than the process confidence region described in the Part 1 of this thesis. In this Section an approach similar to the one described in Section P1-2.5.2 is presented. However, in the present case new considerations were necessary to be introduced, because now a parameter estimation problem is being addressed. In this way, the new deduction is presented.

As described by Benyahia et al. (2013), the evaluation of the confidence regions of the parameters is a useful tool to verify the estimation accuracy (Benyahia et al. 2013). A poor evaluation of the true confidence regions can mislead the reliability of a mathematical model. The referred authors indicate that the high nonlinearity of the parameters, which is normaly found in pratical cases as the present one, is the main limitation to an accurate evaluation of the true confidence region of the parameters. Furthermore, those cases, particulary when the number of measurements is too low, present a non-normal distribution of the measurements errors which makes the evaluation of the paramters confidence region a complex task (Schwaab et al., 2008). In this way, Benyahia et al. (2013) and Schwaab et al. (2008) presented a methodology to define the parameters confidence region taking in consideration the aforementioned peculiarities of these systems. A similar method is here adopted with the same goal.

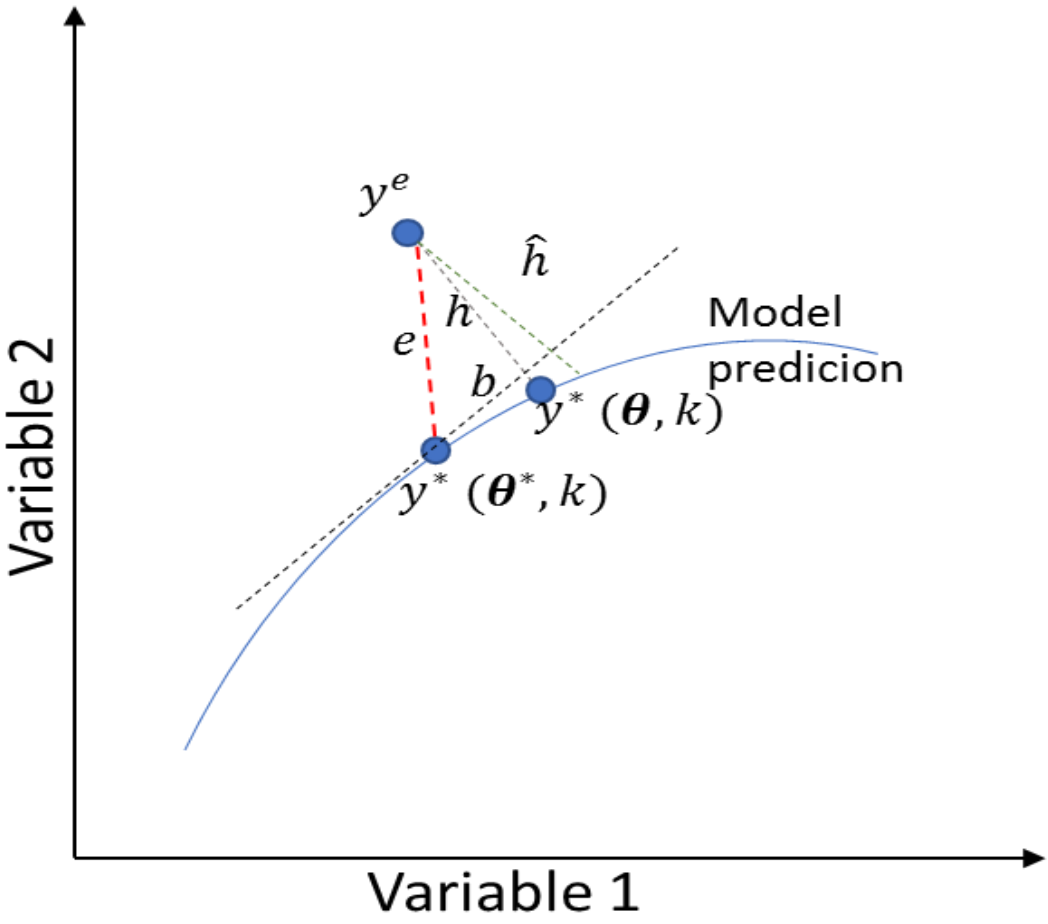

Figure 62 - Simplified representation of the experimental measurements and the model predictions in the parameters space, adapted from Benyahia et al. (2013).

Considering the optimization problem presented in Equation (103) and the optimization space given in Figure 62, e corresponds to the difference between the value of the measured variable y^e and the model prediction $y^*(\boldsymbol{\theta}^*, k)$ where $\boldsymbol{\theta}^*$ is the vector of the best parameters values found in a given optimization instant, k (in the present case it means that θ^* corresponds to the best position found by the particles inside of a given search zone). On the other hand, h corresponds to the difference between the measured variable y^e and the value of the process performance parameters $y^*(\boldsymbol{\theta}, k)$ where $\boldsymbol{\theta}$ is the vector of parameters values evaluated in a given instant k of

the optimization. Thus, in a given iteration k, the squared error between the value of the measured variable and the model prediction with the optimal set of parameters, $\boldsymbol{\theta}^*$ is:

$$e^2{}_k = (y^e - y^*(\boldsymbol{\theta}^*|k))^2 \tag{104}$$

This error can be normalized with respect to the variance of the measured variable i in a measurement j as:

$$e^2{}_{ijk} = \frac{\left(y^e{}_{ij} - y^*{}_{ijk}(\boldsymbol{\theta}^*, k)\right)^2}{V_i} \tag{105}$$

From Equation (105) and following a similar approach to the one used by Benyahia et al. (2013), the error can be generalized to all instants n_k considered in the optimization as:

$$e^2 = \sum_{k=1}^{n_k}\sum_{i=1}^{n_c}\sum_{j=1}^{n_e} e^2{}_{ijk} = \sum_{k=1}^{n_k}\sum_{i=1}^{n_c}\sum_{j=1}^{n_e} \frac{(y^e{}_{ij} - y^*{}_{ij}(\boldsymbol{\theta}^*, k))^2\ )}{V_i} \tag{106}$$

Considering the variance of a measured variable with respect to the vector of estimated parameters ($V_i(\boldsymbol{\theta})$) as:

$$V_i(\boldsymbol{\theta}) = \frac{1}{NE}\sum_{j=1}^{n_e}\left(y^e{}_j - y^*{}_j(\boldsymbol{\theta}, k)\right)^2 \tag{107}$$

Thus, from Equation (106) and Equation (107) the error can be presented as:

$$e^2 = \sum_{k=1}^{n_k}\sum_{i=1}^{n_c} NE\,\frac{V_{ik}(\boldsymbol{\theta}^*)}{V_i} \tag{108}$$

Considering the assumption that the error e follows a Gaussian distribution with zero mean and that there is only one possible set of parameters values which will compose the vector $\boldsymbol{\theta}^*$, then e^2 has a chi square distribution, χ^2 given by:

$$e^2 \rightarrow \chi^2(n_k + n_e - 1) \tag{109}$$

Also, the squared error of the value of the measured variable and the model prediction through a given set of parameters $\boldsymbol{\theta}$ is expressed as:

$$h^2{}_i = (y^e - y^*(\boldsymbol{\theta}|k))^2 \tag{110}$$

$$h^2 = \sum_{k=1}^{n_k} \sum_{i=1}^{n_c} n_e \frac{V_i(\boldsymbol{\theta})}{V_i} \tag{111}$$

Identical assumptions to the ones considered for e can be employed for h. Then, h^2 has a chi square distribution with $n_k + n_e - (n_\theta + 1)$ degrees of freedom. In this way, it is finally obtained the approximation:

$$h^2 \rightarrow \chi^2(n_k + n_e - n_\theta + 1) \tag{112}$$

Where n_θ is the length of the vector $\boldsymbol{\theta}$ which corresponds to the number of model parameters; hence:

$$e^2 - h^2 \rightarrow \chi^2(n_\theta) \tag{113}$$

From Figure 62, it is possible to define an approximation, which is proposed by Benyahia et al. (2013), represented as:

$$\frac{b^2}{\hat{h}^2} = \frac{e^2 - h^2}{\hat{h}^2} \cong \frac{e^2 - h^2}{h^2} \tag{114}$$

Equation (114) presents the ratio between two independent chi square distributions, $e^2 - h^2$ with n_θ degrees of freedom, and h^2 with $n_k + n_e - n_\theta + 1$ degrees of freedom; therefore, it can be represented as a Fisher-Snedecor distribution, given by:

$$\frac{\frac{e^2 - h^2}{n_\theta}}{\frac{h^2}{n_k + n_e - n_\theta + 1}} \rightarrow F_\alpha(n_\theta, n_k + n_e - n_\theta + 1) \tag{115}$$

Moreover, from Equation (108), Equation (111) and Equation (115) the following is obtained:

$$\begin{aligned} &\frac{\sum_{k=1}^{n_k}\sum_{i=1}^{n_c} n_e \frac{V_{ik}(\boldsymbol{\theta}^*)}{V_i} - \sum_{k=1}^{n_k}\sum_{i=1}^{n_c} n_e \frac{V_i(\boldsymbol{\theta})}{V_i}}{\sum_{k=1}^{n_k}\sum_{i=1}^{n_c} n_e \frac{V_i(\boldsymbol{\theta})}{V_i}} \rightarrow \\ &\rightarrow \frac{n_\theta}{n_k + NE - n_\theta + 1} F_\alpha(n_\theta, n_k + n_e - n_\theta + 1) \end{aligned} \tag{116}$$

where α is the confidence level to be taken in consideration. The objective function at the optimal point $J(\theta)$ can be expanded in a second-order Taylor expansion around a given point found in the optimization, θ^* (Schwaab et al., 2008):

$$J(\theta^*) = J(\theta) + (\theta^* - \theta)\nabla S_\theta + \frac{1}{2}(\theta^* - \theta)^T \boldsymbol{H}_\theta (\theta^* - \theta) \tag{117}$$

where ∇J_θ is the gradient vector and $\boldsymbol{H}_\theta$ the Hessian matrix of the objective function; this matrix is related to the covariance matrix of the model parameters (Bard 1974; Schwaab et al. 2008) by:

$$\boldsymbol{H}_\theta = 2V_\theta^{-1} \tag{118}$$

Considering Equation (117), Equation (118) can be rewritten as:

$$J(\theta^*) - J(\theta) = (\theta^* - \theta)^T V_\theta^{-1}(\theta^* - \theta) \equiv \chi^2(n_\theta) \tag{119}$$

and consequently, Equation (116) can be rewritten as:

$$J(\theta^*) - J(\theta) \to \sum_i^{n_y} \frac{n_k V_i(\theta)}{V_i} \frac{n_\theta}{n_k - n_\theta - n_y + 1} F_\alpha(n_\theta, n_k + n_e - n_\theta + 1) \tag{120}$$

Given that V_i provides a good approximation to $V_i(\theta)$, the parameter confidence region may be assessed by:

$$J(\theta^*) \leq J(\theta) + \frac{n_\theta}{n_k - n_\theta - n_y + 1} F_\alpha(n_\theta, n_k + n_e - n_\theta + 1) \tag{121}$$

The criterion above is the Fisher–Snedecor test that is used here to draw the confidence regions and also to verify if local minima exist. The Fisher–Snedecor test was implemented in the MatLab software. The test was done after the PSO optimization using its final results.

P2-2.6. Uncertainties evaluation

The uncertainty of an experimental procedure can be originated by errors of the method, the instrument or personal error. Those factors are found in all the steps that compose an experimental analysis. The Guide to the Expression of Uncertainty in Measurement (GUM) indicates a series of factors which must be satisfied in order to determine the analytical uncertainty (International Organisation for Standardisation, 2008). Those factors can be listed as:

- A defined measurand and its measurement procedure;
- The analytical results must be able to be calculated through a model and the measured parameters;
- All the possible parameters that can affect the final results must have their values and uncertainties determined;
- The principles of uncertainty propagation must be applied when the standard uncertainty of an analytical result is being calculated;
- The result of the analysis is presented as a value and its parameters, which express the dispersion of the quantity values, attributed to a measurand.

By its turn, Konieczka and Namieśnik (2010) listed the main sources of uncertainties in a chromatographic analysis and their respective procedure to compute as:

- The amount of sample used for a determination;
    - This source of uncertainty is very often not taken into account since it has a small impact in the uncertainty of the measurement. It is associated with the measurement of the weight of a sample and it is inherent to the measurement

procedure. Hence, in the present work, this source was approximated to the uncertainty of the measurement equipment.

- The recovery value of the analytical procedure;

  The recovery, R, is normally defined by the ratio between c_{obs}, the observed concentration of the sample and c_{ref}, the true concentration in the reference material. Thus, it is desirable that the recovery is equal to the unity. However, if the recovery deviates from the unity, the uncertainty associated is included in the uncertainty budget of results. While addressing the sample recovery, or trueness, there is always a probability to evaluate incorrectly its influence. In order to cope with this uncertainty source, a sample pre-treatment is normally done in the chromatographic analysis which tries to ensure that the trueness will be as close as possible to the unity and consequently the uncertainty is negligible. This component can be computed through the average value obtained from a large set of test results and an accepted reference value (Vanatta and Coleman 2007), as given by:

$$R = \frac{c_{obs}}{c_{ref}} \tag{122}$$

  For the relative standard deviation Std of the n results obtained when analysing, this uncertainty component, u_{true}, can be calculated as:

$$u_{true} = \frac{1}{R}\frac{Std}{\sqrt{n}} \tag{123}$$

- The repeatability;
    - It is associated with the measurements repeatability for true samples. This is usually the main source of uncertainty and can be calculated according to Equation (124), where SD is the standard deviation, n is the number of repetitions and δ is the coverage factor:

$$u_{rep} = \delta \frac{Std}{\sqrt{n}} \quad (124)$$

- The concentration associated with the upper detection limit;
    - The limit of detection is a property of the equipment used to perform the analysis. In this case, the uncertainty has a proportional relationship with the limit of detection (LOD) and the measured concentration (c) which can be expressed as:

$$u_{LOD} = \frac{LOD}{c} \quad (125)$$

- Calibration.
    - The procedure to determine the uncertainty of this step is more complex and it will be detailed in the next sub-section.

P2-2.6.1. Uncertainty associated with calibration

This is a step done in the majority of the analytical measurements, normally with support of linear regression to establish a relationship between the chromatographic signal and the amount of

measurand, the calibration curve. Again, Konieczka and Namieśnik (2010) enumerate the main sources of uncertainties which can be listed and evaluated as:

- The repeatability with which the value of a signal is read, both for standard samples (based on measurements for which the calibration curve is determined) and for study samples, $u_{sample,cal}$;
- The determination of the reference value for the standard samples, $u_{sample,std}$;
- The method to prepare the standard samples;
- The incorrect approximation of measurement points using a regression curve.

The uncertainty due to the calibration and linear regression method, u_{sample} is determined by the linear regression parameters through:

$$u_{sample,cal} = \frac{SD_{xy}}{b}\sqrt{\frac{1}{p}+\frac{1}{n}+\frac{\left(x_{sample}-x_m\right)^2}{Q_{xx}}} \quad (126)$$

where x_{sample} is the signal value of the sample, b the coefficient of the calibration curve, p is the number of repetitions made for one sample, n is the total number of standard samples used for plotting the calibration, x_m is the average of the signals value for all samples used to plot the regression curve. Thus, considering x_i as the signal value of the standard i, Q_{xx} is calculated as:

$$Q_{xx} = \sum_{i=1}^{n}(x_i - x_m)^2 \quad (127)$$

This component of the uncertainty in the calibration step is the main source of uncertainty; in this way, the following approximation can be done (Konieczka and Namieśnik 2010b):

$$u_{cal} \cong u_{sample,cal} \quad (128)$$

P2-2.6.2. Combined and expanded uncertainty for chromatographic analysis

Finally, the combined uncertainty for the chromatographic analysis (U) can be computed by the previously mentioned elements through the following equation:

$$U = \delta\sqrt{\left(u_{sample}\right)^2 + (u_{true})^2 + \left(u_{rep}\right)^2 + (u_{LOD})^2 + (u_{cal})^2} \quad (129)$$

where δ is the coverage factor, usually equal to 2.

P2-2.7. Fixed-bed chromatographic separation model

A phenomenological model that describes the dynamic behavior of the internal concentration profile of a chromatographic adsorptive column was developed. It is expected that the model is capable of representing with precision the breakthrough experiments done in this work. This model is based on a series of assumptions which are listed below:

- Isothermal process;
- Plug flow model of the fluid phase with axial dispersion;
- Negligible radial dispersion;
- Constant bed porosity and length;
- External mass transfer resistance to the particle;

- Internal mass transfer resistance negligible due to the Amberlyst 46 properties (only the particles surface is functionalized);
- Velocity variation along the bed due to composition variation.

Hence, the mass balances to the liquid and adsorbed phases can be described as:

$$\frac{\partial c_i}{\partial t} = D_{ax}\frac{\partial}{\partial z}\left(C_T \cdot \frac{\partial y_i}{\partial z}\right) - \frac{\partial (u c_i)}{\partial z} - \frac{(1-\varepsilon)}{\varepsilon}\frac{3}{R_p}k_{L,i}(q_i^* - q_i) \tag{130}$$

$$\frac{\partial q_i}{\partial t} = \frac{3}{R_p}k_{L,i}(q_i^* - q_i) \tag{131}$$

Where, z is the axial coordinate, t is the time, D_{ax}, is the axial dispersion coefficient, c_i is the liquid phase molar concentration of compound i, q_i is the adsorbed phase concentration of compound i, q_i^* is the adsorbed concentration of compound i in equilibrium with c_i, y_i is the molar fraction of the compound i in the liquid phase, u is the interstitial fluid velocity, R_p is the particle radius, $k_{L,i}$ is the external mass transfer coefficient and C_T is the total molar concentration in the liquid phase which is related with the molar volume $V_{M,i}$ of each compound and can be calculated as:

$$C_T = \frac{1}{\sum y_i V_{M,i}} \tag{132}$$

The boundary and initial conditions are described as:

$$z = 0:\ uc_{i,z=0} - D_{ax}C_T\left.\frac{\partial y_i}{\partial z}\right|_{z=0} = uc_{i,f} \tag{133}$$

$$z = L:\ \left.\frac{\partial y_i}{\partial z}\right|_{z=L} = 0 \tag{134}$$

$$t = 0: c_i = c_{i,0} \quad (135)$$

where L is the column length, $c_{i,f}$ is the feed concentration and $c_{i,0}$ is the initial concentration. As described above, one of the assumptions of this model is that the (particle) internal resistance to mass transfer is negligible. This is due to the characteristics of the resin Amberlyst 46, which was developed in order to avoid side reactions as explained in Section P2-2.1.2. Therefore, internal mass transfer resistances can be neglected and only the external mass transfer kinetics should be accounted for. The external mass transfer coefficient can be calculated through the correlation of Wilson and Geankoplis (Glueckauf and Coates 1947) as:

$$Sh_p = \frac{1.09}{\varepsilon}(Re_p Sc)^{0.33} \quad (136)$$

where Sh_p, Re_p and Sc are respectively the Sherwood, Reynolds and Schmidt numbers and they can be calculated as:

$$Sh_p = \frac{k_{L,i} d_p}{D_{i,mix}} \quad (137)$$

$$Re_p = \frac{\rho u d_p}{\eta} \quad (138)$$

$$Sc = \frac{\eta}{\rho D_{i,mix}} \quad (139)$$

where ρ is the fluid density, η is the fluid viscosity, d_p is the particle diameter $D_{i,mix}$ is the diffusivity coefficient of compound i in the mixture. The diffusivity coefficient can be calculated by the correlation of Perkins and Geankoplis (Ruthven 1984). For a compound A in a multi-component mixture, this correlation is presented as:

$$D_{A,m}\eta_m^{0.8} = \sum_{\substack{i=1 \\ i\neq A}}^{n} y_i D_{A,i}^0 \, \eta_i^{0.8} \tag{140}$$

where η_i is the viscosity of the pure compound i, η_m is the mixture viscosity, $D_{A,i}^0$ is the diffusion coefficient of the compound A diluted in the compound i. The diffusivity coefficient for a solution of two compounds A and B can be determined through the infinite diffusivity coefficients (Scheibel 1954), as:

$$D_{A,B} = D_{B,A} = (D_{A,B}^0)^{y_B}(D_{B,A}^0)^{y_A} \tag{141}$$

And the infinite diffusion coefficient for a mixture $D_{A,B}^0$, with A diluted in the solvent B, can be calculated through the Scheibel correlation (Scheibel 1954), as:

$$D_{A,B}^0 = \frac{8.2 \times 10^{-8} T}{\eta_B V_{M,A}^{1/3}} \left[1 + \left(\frac{3V_{M,B}}{V_{M,A}}\right)^{2/3}\right] \tag{142}$$

Finally, the variation of the internal velocity due to the composition changes can be represented as:

$$\frac{\partial u}{\partial z} = -\frac{1-\varepsilon}{\varepsilon}\frac{3}{R_p}\sum_{1=1}^{NC} k_{L,i} V_{M,i} \, (q_i^* - q_i) \tag{143}$$

where NC is the total number of compounds, and the boundary condition for Equation (143) can be represented as:

$$z = 0: \forall t \rightarrow u = u|_{z=0} \tag{144}$$

The Langmuir competitive adsorption model, Equation (102), as described in section P2-2.4, was used to represent the adsorption equilibrium.

The fixed-bed chromatographic separation model was implemented in gPROMS, where it can be ran externally by MatLab, using the go:MATLAB extension (Process Systems Enterprise 2015).

P2-2.8. Batch Reactor Model

As presented in Section P2-2.1, the reaction rate model here employed was based on the work of Duarte (2006); however, in the referred work, the model was developed considering the UNIQUAC model in the calculation of the activity coefficients while here it is proposed to apply the NRTL thermodynamic model, as presented in Section P2-2.1.3. Therefore, a batch reactor model was developed and simulated in order to verify the validity of the proposed modification in the reaction rate model through Duarte's experimental data. This model was simulated based on the reaction rate here presented and compared with the experimental results for the ProPro production in a batch reactor, presented by Duarte (2006).

Considering the mass balance to a batch reactor operated in a time interval varying from t to $t + \Delta t$ presented as:

$$n_{i,t+\Delta t} = n_{i,t} + \vartheta_i r_{ProPro} A m_{cat}^{dry} \Delta t \tag{145}$$

where ϑ_i is the stoichiometric coefficient of component i, r_{ProPro} is the reaction rate given by Equation (88), expressed in [$mol.s^{-1}.eq^{-1}$], A is the concentration of active sites in $[eq.(kg_{cat}^{dry})^{-1}]$ and m_{cat}^{dry} is the mass of dried catalyst. The dry mass of catalyst is calculated through the water content, presented in Table 25, which is given by: $m_{cat}^{dry} = m_{cat}[1 - Water(\%)]$.

Equation (145) can be rewritten as:

$$\frac{n_{i,t+\Delta t} - n_{i,t}}{\Delta t} = \vartheta_i r_{ProPro} Am_{cat}^{dry} \quad (146)$$

And at the limit when $\Delta t \to 0$ the differential form is written as:

$$\frac{dn_i}{dt} = \vartheta_i r_{ProPro} Am_{cat}^{dry} \quad (147)$$

Therefore, knowing that n_i can be presented as the molar fraction x_i times the total number of moles in the system, N_t (which is taken as constant in the present case), the final representation is obtained:

$$\frac{dx_i}{dt} = \vartheta_i r_{ProPro} \frac{Am_{cat}^{dry}}{N_t} \quad (148)$$

where N_t is the total number of moles in the system, which is taken as constant in the present case.

Initial condition:

$$t = 0;\ x_i = x_{i,0} \quad (149)$$

This model was simulated based on the reaction rate here presented and compared with the experimental results for the ProPro production in a batch reactor, presented by Duarte (2006). The present batch reactor model was implemented in gPROMS.

P2-2.9. Fixed bed chromatographic reactor model

A detailed phenomenological model was developed to describe the dynamic behaviour of the internal concentration profile of a fixed-bed adsorptive reactor. Similar assumptions, as the ones presented in P2-2.7 for the fixed-bed chromatographic separation model, were used here:

- Pseudo-homogeneous reaction system;
- Isothermal system;
- Constant length and bed porosity;
- Axial dispersed plug flow model;
- No radial dispersion;
- Negligible internal mass transfer resistance;
- External mass transfer resistance;
- Langmuir isotherm model for multicomponent adsorption;
- Velocity variation along the bed due to the composition variation.

Hence, the model for the fixed-bed reactor unit is similar to the one already presented in P2-2.7. The main different in the present case is the reaction term, which is added to the solid phase balance and variation of the internal velocity due to the composition changes, as:

$$\frac{\partial q_i}{\partial t} = \frac{3}{R_p} k_{L,i}(q_i^* - q_i) - \vartheta_i \frac{\rho_b}{1-\varepsilon} r_{ProPro} \tag{150}$$

$$\frac{\partial u}{\partial z} = -\frac{1-\varepsilon}{\varepsilon}\frac{3}{R_p}\sum_{i=1}^{NC} k_{L,i} V_{M,i}\,(q_i^* - q_i) + \frac{\rho_b}{1-\varepsilon} r_{ProPro} A \sum_{1=1}^{NC} \vartheta_i V_{M,i} \tag{151}$$

In this way, the mathematical model is composed by equations (131) to (142), (144), (150) and (151). The model was implemented in gPROMS.

P2-2.10. True Moving Bed Reactor model

Finally, based on the models presented in P2-2.3, P2-2.7 and P2-2.9, a detailed phenomenological model was developed in other to describe the concentration profiles of the production of n-Propyl Propionate in a TMBR unit. This model is based on a series of considerations previously described in Section P2-2.9. For each section k of a TMBR unit, the mass balances to the liquid and adsorbed phases can be described as:

$$\frac{\partial c_{i,k}}{\partial t} = D_{ax}\frac{\partial}{\partial z}\left(C_T \cdot \frac{\partial x_{i,k}}{\partial z}\right) - \frac{\partial u_k c_{i,k}}{\partial z} - \frac{(1-\varepsilon)}{\varepsilon}\frac{3}{R_p}k_{L,i}(q^*_{i,k} - q_{i,k}) \tag{152}$$

$$\frac{\partial q_{i,k}}{\partial t} = \frac{3}{R_p}k_{L,ik}\left(q^*_{i,k} - q_{i,k}\right) + \mathrm{u}_s\frac{\partial q_{i,k}}{\partial z} - \vartheta_i\frac{\rho_b}{1-\varepsilon}r_{ProPro}A \tag{153}$$

where, u_s, is the solid velocity, z, is the position in the section, t is the time, ϑ_i is the stoichiometric coefficient of component i, r_{ProPro} is the reaction rate given by Equation (90), A is the concentration of active sites, ρ_b is the solid bulk density, D_{ax}, is the axial dispersion coefficient, $q^*_{i,k}$ is the adsorbed concentration (based on the Langmuir competitive adsorption model presented in Equation (102)) of a determined i compound in equilibrium with $c_{i,k}$ in section k, $q_{i,k}$ is the adsorbed phase concentration of compound i in section k, $x_{i,k}$ is the molar fraction of the compound i in the liquid phase in the section k, u_k is the section interstitial velocity, R_p is the particle radius, $k_{L,ik}$ is the external mass transfer coefficient calculated as described in P2-2.7 and C_T is the total molar concentration in the liquid phase which is related with the molar volume $V_{M,i}$ of each compound and can be calculated as:

$$C_T = \frac{1}{\sum x_{i,k} V_{M,i}} \tag{154}$$

The variation of each section internal velocity due to the composition changes can be represented as:

$$\frac{\partial u_k}{\partial z} = -\frac{1-\varepsilon}{\varepsilon}\frac{3}{R_p}\sum_{i=1}^{NC} K_{L,i} V_{M,i}\,(q_i^* - q_i) + \frac{\rho_b}{1-\varepsilon} r_{ProPro} A \sum_{1=1}^{NC} \vartheta_i V_{M,i} \tag{155}$$

The boundary and initial conditions for each section of the TMBR unit can be expressed as:

$$t = 0:\ \ c_{i(i\neq eluent)k} = q_{ik} = 0;\ \ c_{i(i=eluent)k} = {c_i}^e;\ \ q_{i(i=eluent)k} = q({c_i}^e) \tag{156}$$

$$z = 0:\ c_{ik} - \frac{D_{Lk}}{v_k} C_T \frac{\partial x_{i,k}}{\partial z} = c_{ij,0} \tag{157}$$

$z = L$:

$$\left.\frac{\partial x_{i,k}}{\partial z}\right|_L = 0 \tag{158}$$

$$\left.c_{i,IV}\right|_L = \frac{u_I}{u_{IV}}\left.c_{i,I}\right|_0 - \frac{u_e}{u_{IV}}{c_i}^e \tag{159}$$

$$\left.c_{i,I}\right|_L = \left.c_{i,II}\right|_0 \tag{160}$$

$$\left.c_{i,II}\right|_L = \frac{u_{III}}{u_{II}}\left.c_{i,III}\right|_0 - \frac{u_F}{u_{II}}{c_i}^f \tag{161}$$

$$\left.c_{i,III}\right|_L = \left.c_{i,IV}\right|_0 \tag{162}$$

$$q_{i,IV}\big|_L = q_{i,I}\big|_0, \qquad q_{i,I}\big|_L = q_{i,II}\big|_0,$$
$$q_{i,II}\big|_L = q_{i,III}\big|_0, \qquad q_{i,III}\big|_L = q_{i,IV}\big|_0, \tag{163}$$

The global node balances of the unit are expressed as:

$$u_I = u_{IV} + u_e \tag{164}$$

$$u_{II} = u_I - u_x \tag{165}$$

$$u_{III} = u_{II} + u_f \tag{166}$$

$$u_{IV} = u_{III} - u_r \tag{167}$$

$$c_i{}^e u_e + c_i{}^f u_f = c_i{}^x u_x + c_i{}^r u_r \tag{168}$$

where u_e is the eluent, u_x the extract, u_f the feed, and u_r the raffinate velocities.

The performance indicators are:

$$Pur_r = \frac{c_{ProPro}{}^r}{\sum_{i=1}^{n_c} c_i{}^r} \tag{169}$$

$$Pur_x = \frac{c_{Water}{}^x}{\sum_{i=1}^{n_c} c_i{}^x} \tag{170}$$

$$Conv = 100\,\frac{c_{AcidPro}{}^f u_f - (c_{AcidPro}{}^x u_x + c_{AcidPro}{}^r u_r)}{c_{AcidPro}{}^f u_f} \tag{171}$$

$$EC = \frac{c_{POH}{}^e u_e - u_f(c_{POH}{}^f - c_{POH}{}^f \frac{Conv}{100})}{c_{ProPro}{}^r u_r} \tag{172}$$

$$Pr = \frac{{c_{ProPro}}^{r} u_r}{V_T} \quad (173)$$

where Pur_x, is the extract purity, Pur_r, is the raffinate purity, ${c_i}^x$, is the concentration of the component i in the extract stream, ${c_i}^r$, is the concentration of the component i in the raffinate stream, ${c_i}^e$, is the concentration of the component i in the eluent stream and ${c_i}^f$, is the concentration of the component i in the feed stream, V_T, is the volume of the bed, *EC,* is the eluent consumption and Pr is the unit productivity. This model was implemented in the gPROMS modelling builder (Process Systems Enterprise 2015).

P2-2.11. TMBR design and optimization

The PSO-TVAC-MSR algorithm previously developed and validated in the Part 1 (P1-2.5 and P1-3.5) of this thesis was here applied in order to define the set of optimal operating conditions for the production of ProPro in a TMBR unit.

It is expected that the methodology previously proposed is able to deal with the TMBR design problem. However, it is necessary first to define an objective function that computes the main goals of the optimization problem. In this way, the definition of the optimization objective function is an essential step for the optimization problem solution. The main goal of this work is to design and optimize a TMBR unit. Therefore, in those type of processes, the main design variables are the set of external operating flow rates (Q_f, Q_e, Q_{IV}, Q_x and Q_s) and consequently the internal flow rates. The optimal set of those variables is the one which will lead to the maximization of the unit productivity and conversion while the eluent consumption is minimized

attending to the minimum quality requirement of the final product (streams purity), P_{st}. Hence, considering a general optimization problem:

$$\min_{\theta} J(\boldsymbol{y}) \tag{174}$$

where $\boldsymbol{y}$ is the vector of process performance parameters and θ is the set of process variables to be optimized, the objective function for the present case can be defined as:

$$\mathrm{J} = \sum_{1}^{n_k} \left((P_{st} - Pur_k)^2 + (P_{st} - Pux_k)^2 + \frac{1}{Conv_k} + \frac{1}{Pr_k} + Ec_k \right) \tag{175}$$

where, P_{st} is the minimum requirement for the purities, n_k is the total number of instants of evaluation of the performance parameters. Hence, the objective function presented was employed with the methodology defined in Part 1 to design the TMBR unit.

P2-2.12. Confidence region evaluation

The final result of the HHPSO-TVAC-MSR optimization provides a matrix containing all the evaluated positions by the particles during the sworn flight over the search region. In this way, as it was previously demonstrated in P1-2.5 and P1-3.5, it is possible to draw the unit operating variables confidence regions through the statistical verification of the optimization results as function of the optimal point found in the complete optimization, as shown in:

$$J(\theta) \leq J(\theta^*) + \frac{n_k n_\theta}{n_k - n_\theta - n_y + 1} F_\alpha(n_\theta, n_k - n_\theta - n_y + 1) \tag{176}$$

The above equation represents the Fisher–Snedecor test, which relates the minimum point found in the optimization, θ^*, and its corresponding value of objective function, $J(\theta^*)$, with a determined position θ with objective function value of $J(\theta)$, evaluating if this condition respects the Fisher-Snedecor distribution F_α, with confidence level of α and $n_k - n_\theta - n_y + 1$ degrees of freedom, where n_y is the total number of process performance parameters considered, n_k is the number of iterations considered in the optimization and n_θ is the number of optimized operating variables. In Section P1-2.5.2 the full deduction of the above test, Equation (176), is presented. Here the test is employed in the same way as in P1-3.5, to perform the robust design of the TMBR unit.

The HPSO-TVAC-MSR, objective function and Fisher–Snedecor test here presented were implemented in the MatLab software. To run the optimization, a communication between gPROMS, where the process models were written, and MatLab was used through the go:MATLAB extension (Process Systems Enterprise 2015). It was possible for MatLab to run externally the model and collect the responses of the process simulation.

P2-3. Results

In this chapter all the results obtained from the application of the methodologies presented in chapter P2-2 are presented.

P2-3.1. Fixed bed adsorptive unit hydrodynamics

In order to characterize the fixed-bed chromatographic column, a series of tracer experiments was performed. Thus, pulses of 200 µL of Blue Dextran solution were injected in the fixed bed previously in equilibrium with water. The Blue Dextran is a substance of high molecular size which prevents its access to the pores of the Amberlyst 46 resin. The flow rates ranged from 1.0 to 7.9 mL min^{-1} using water as eluent and the temperature was kept constant at 313 K. While the concentration of the outlet stream was online monitored with a UV-Vis detector at 300 nm.

This first step had as objective the determination of the column porosity, ε_b, and axial dispersion coefficient, evaluated by the Peclet number, Pe. Through the experimental data and the equations described in Section P2-2.3. The results obtained are shown in Table 3.

Table 28 - Tracer experiments results.

Experiment	Q (mL/min)	$\bar{t}_r$ (min)	ε	Pe
1	2.00 ± 0.03	13.05 ± 0.20	0.042 ± 0.014	218 ± 10
2	4.96 ± 0.07	5.29 ± 0.08	0.041 ± 0.014	181± 9
3	7.88 ± 0.12	3.35 ± 0.05	0.042 ± 0.014	163± 8

In order to verify the parameters estimated through the experiments, a mathematical model was proposed to represent the fixed bed adsorptive unit hydrodynamics. This model is based on the mass balance to the system taking in consideration the dispersive effect in the bed. The mass balance is represented by:

$$\frac{\partial C_{b,i}}{\partial t} + u\frac{\partial C_{b,i}}{\partial z} = D_{ax}\frac{\partial^2 C_{b,i}}{\partial z^2} \tag{177}$$

where $C_{b,i}$, is the concentration of the compound i, u is the interstitial velocity and D_{ax} is the axial dispersion coefficient determined through $D_{ax} = \frac{uL}{Pe}$.

The previous model was simulated for the same conditions in which the tracer experiments were performed. Figure 63 presents the tracer residence time distribution curves, experimental points and model predictions. It is possible to conclude that the model is able to predict with precision the fixed bed adsorptive unit hydrodynamics.

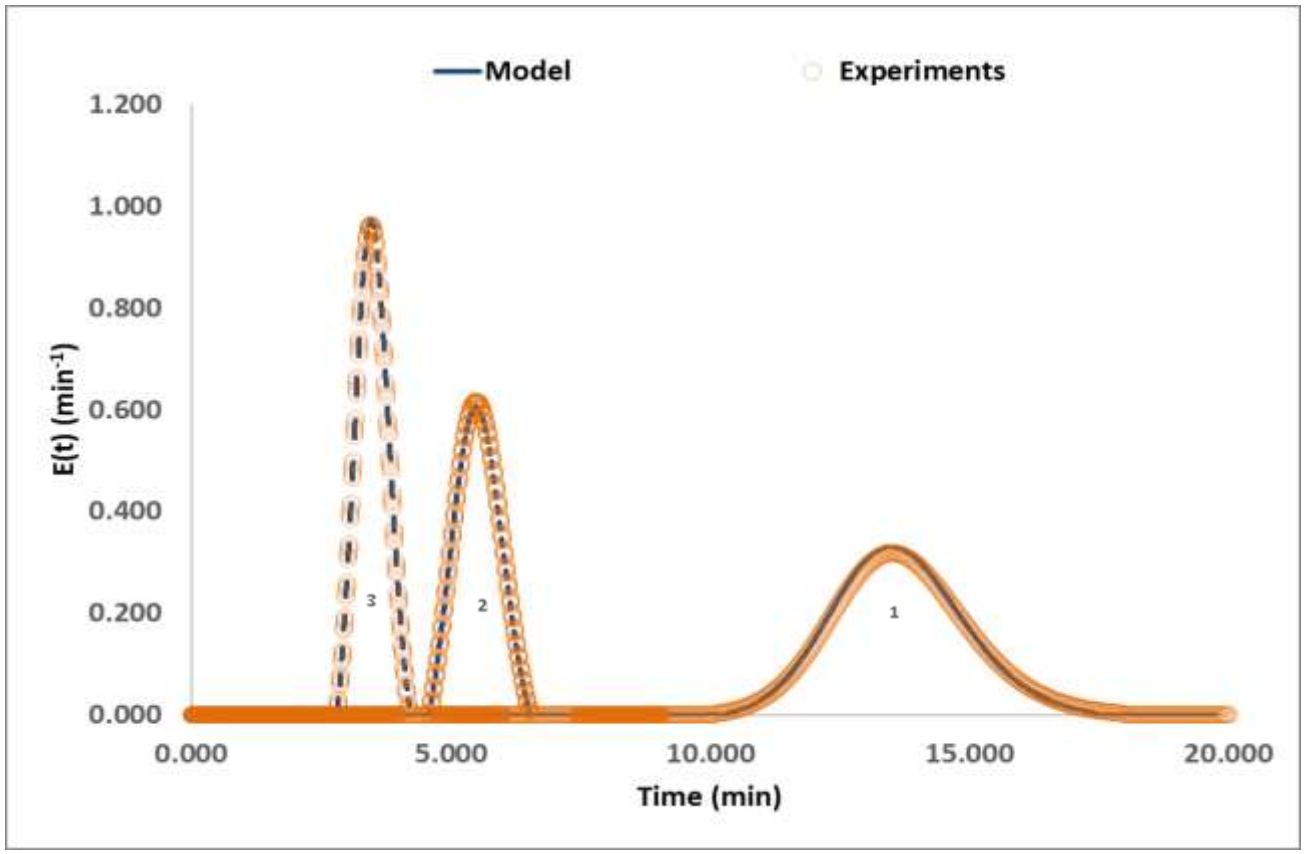

Figure 63 - Tracer residence time distribution curves, for the experiments presented in Table 28.

P2-3.2. Adsorption equilibrium isotherms

After the fixed bed column hydrodynamics characterization, adsorption experiments with the non-reactive pairs were performed. The first step is to determine the uncertainty of the concentration measurement through the methodology presented in Section P2-2.6. The results of the uncertainty evaluation of the concentration measurement are presented in Table 29.

Table 29 - Calculated values of relative standard uncertainties, combined standard uncertainties and expanded uncertainties for the determination of the experimental concentrations.

Parameter	Value
Q_{xx}	133.222
n	11.000
p	3.000
b	0.163
SD_{xy}	0.031
SD_{rrf}	0.024
u_{cal}	0.002
u_{rep}	0.010
u_{LOD}	0.011
u_{sample}	0.002
u_{rec}	0.028
U	0.064

Then, a series of breakthrough experiments was done using the methodology described in section P2-2.4 and multicomponent adsorption equilibrium points were calculated.

The first experiment was done with the column in equilibrium with 1-Propanol (POH) and successive increases of the feed concentration of n-Propyl Propionate (ProPro) and at the end the column was fed with pure POH. In the second experiment, the same procedure was applied, but in this case the column was first filled with Propanoic Acid (AcidPro) and fed with different concentrations of ProPro. Finally, the column was filled with Water and fed with different concentration of AcidPro. This experimental data can be used to estimate the parameters of the Langmuir competitive adsorption isotherm and finally to validate the model proposed in Section P2-2.7. The isotherm parameters values and uncertainties are presented in Table 30.

Table 30- Langmuir competitive adsorption parameters over Amberlyst-46 and their uncertainties, calculated from the parameters confidence regions and HPSO-TVAC-MSR, with Q in ($mol\ L_{ads}^{-1}$) and K in ($L\ mol^{-1}$).

	HPSO-TVAC-MSR							
	$Q_{max,POH}$	$Q_{max,AcidPro}$	$Q_{max,Water}$	$Q_{max,ProPro}$	K_{POH}	$K_{AcidPro}$	K_{Water}	K_{ProPro}
Value	9.13	10.06	43.07	5.11	11.66	9.04	2.35	5.08
Mean	9.13	10.07	43.07	5.11	11.67	9.06	2.36	5.10
Std.	0.10	0.06	0.23	0.16	0.96	1.24	0.63	1.06
Uncert.	0.19	0.12	0.47	0.33	1.92	2.47	1.25	2.12
	Objective function	18.83						

Figure 64 presents the parameters confidence regions. In the parameter estimation step, the PSO was applied to the system in study with a c_1 varying from 0.5 to 2.5, c_2 varying from 2.5 to 0.5, number of particles p equal to 200, number of iterations k_{total} equal to 400 and finally the searching region starting from $R_{1,min} = 10^{-5} \times [1, 1, 1, 1, 1, 1, 1, 1]$ and $R_{1,max} = 10 \times [1.2, 1, 1.4, 5, 1.4, 1.2, 1, 1]$ to $R_{i,max} = 1.05 \times R_{i-1,max}, i = 2, \dots, 5$, where $R_i = [Q_{max,POH}, Q_{max,AcidPro}, Q_{max,Water}, Q_{max,ProPro}, K_{POH}, K_{AcidPro}, K_{Water}, K_{ProPro}]$. From Figure 64 it is possible to see that an elliptical approximation of the confidence region is close to the likelihood confidence region, which is an indication that the optimal point follows a normal distribution. In Figure 64, it is also possible to note that the axes of the ellipses shape are parallel to the parameter axes which means that there are no correlations between the parameters. This is coherent with the phenomenological knowledge of the system, since each parameter presents a property of a given compound, which are not correlated with each other.

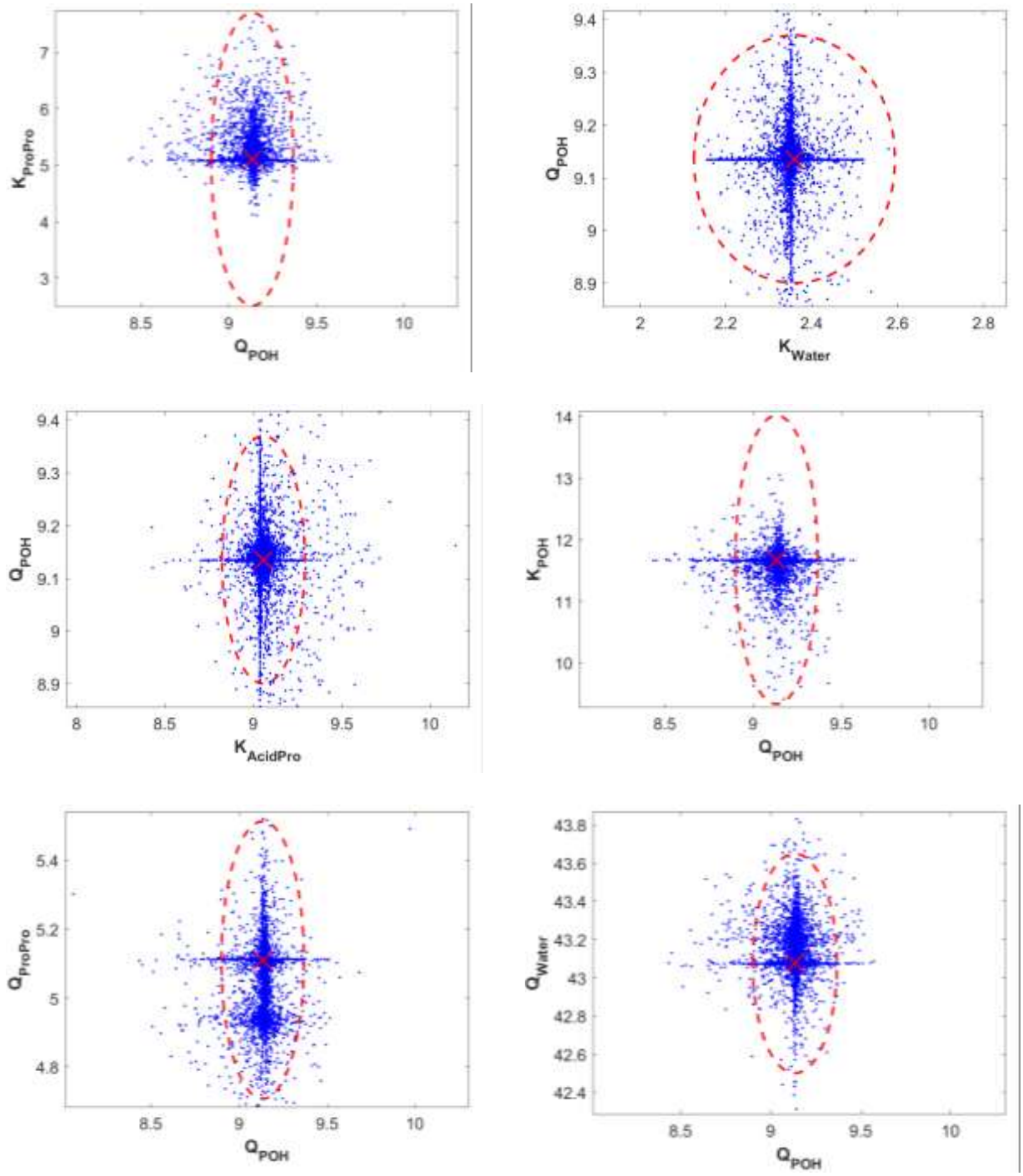

Figure 64 - Parameters confidence regions, elliptical confidence region (dashed line) and optimal point (cross), with Q in ($mol\ L_{ads}^{-1}$) and K in ($L\ mol^{-1}$).

Traditionally in the literature, the estimation of the Langmuir parameters is done through the simple solution of the optimization problem employing a gradient based method. The parameters uncertainty assessment is rarely done; in some few cases, the error of the parameters is calculated, as for example in Faria et al. (2014) where the Jack Knife method is applied in the parameter estimation and the parameters error is computed for the synthesis of glycerol ethyl acetal in a chromatographic column. In order to compare with the results presented in Table 30, a Generalized Reduced Gradient (GRG) algorithm was applied to solve the same optimization problem solved by the PSO. Table 31 presents the results obtained through the method, where it is possible to note that the minimum value of the objective function found by the HHPSO-TVAC-MSR is significantly lower than the GRG algorithm.

Table 31 - Langmuir adsorption competitive parameters over Amberlyst 46 estimated by the Generalized Reduced Gradient algorithm.

	GRG algorithm							
	$Q_{max,POH}$	$Q_{max,AcidPro}$	$Q_{max,Water}$	$Q_{max,ProPro}$	K_{POH}	$K_{AcidPro}$	K_{Water}	K_{ProPro}
Value	8.99	9.94	42.86	5.70	8.61	10.06	2.48	5.18
	Objective function		24.05					

From the results presented in Table 30 and Table 31 it is possible to see that, as expected, the water is the most retained compound in the resin Amberlyst 46, while the ProPro is the compound with less affinity to the resin. Figure 65, Figure 66 and Figure 67 present the Langmuir model predictions with the parameters presented in Table 30 and their uncertainties; the experimental points with their uncertainty intervals are also presented.

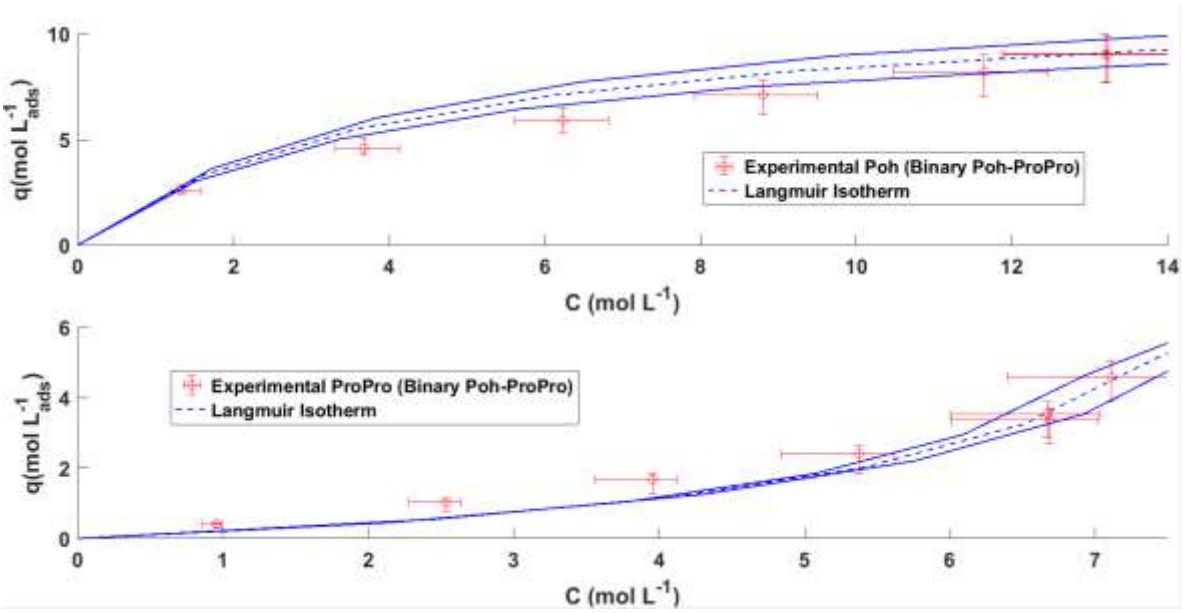

Figure 65 - Langmuir competitive adsorption isotherm for the binary 1-Propanol (a) – n-Propyl Propionate (b) over Amberlyst-46 at 313 K. The lines represent the theoretical adsorption isotherm considering the parameters presented in Table 30.

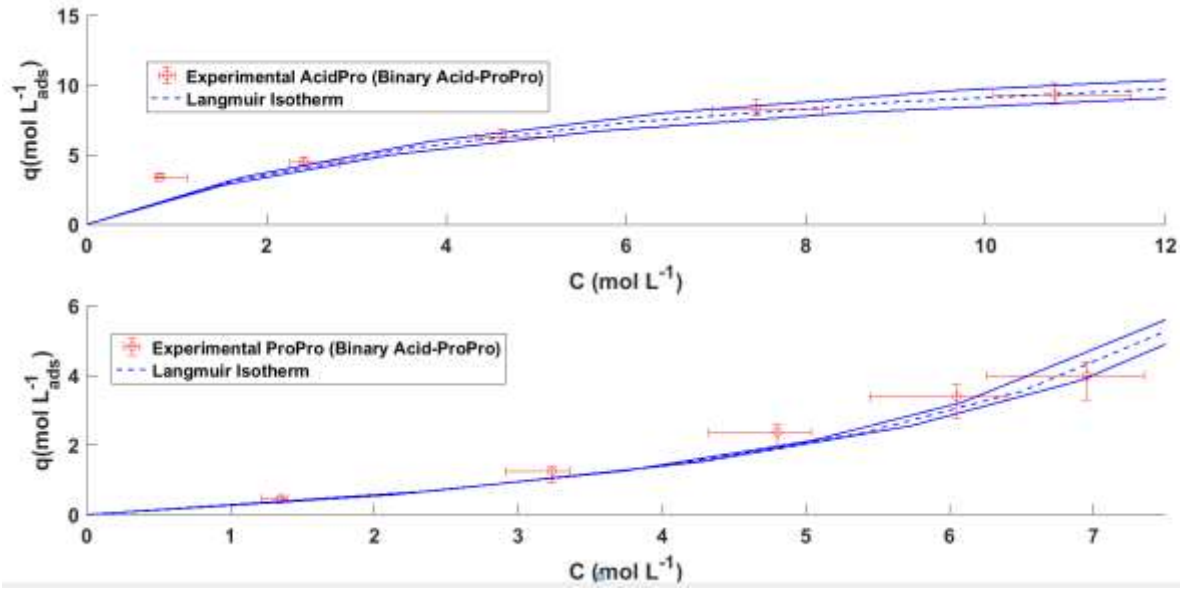

Figure 66 - Langmuir competitive adsorption isotherm for the binary Propionic Acid (a) – n-Propyl Propionate (b) over Amberlyst-46 at 313 K. The lines represent the theoretical adsorption isotherm considering the parameters presented in Table 30.

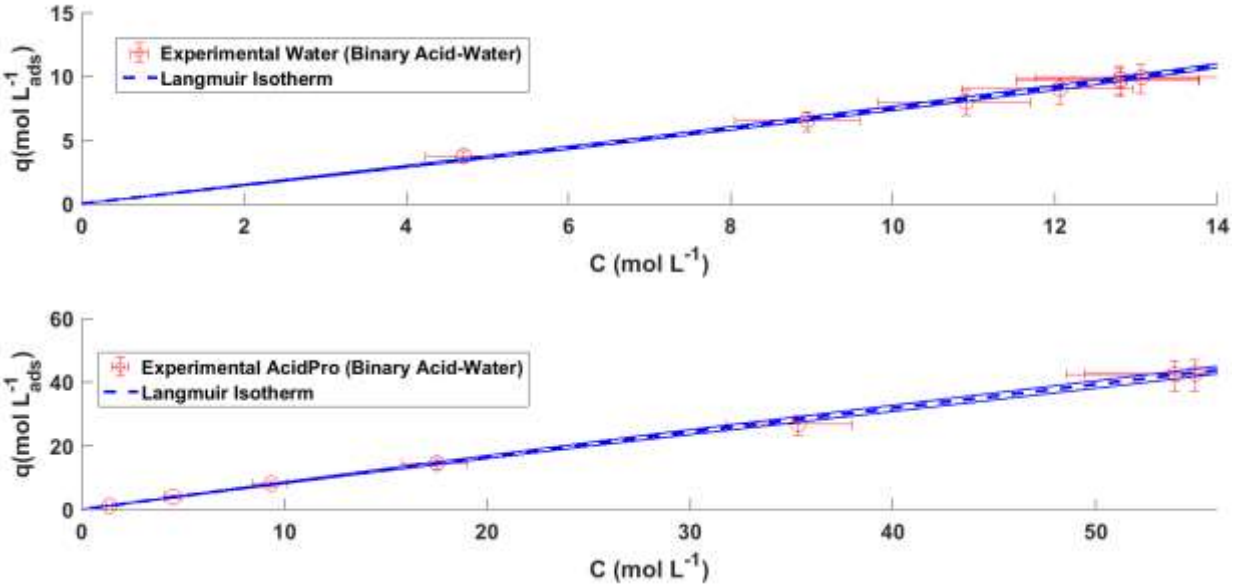

Figure 67 - Langmuir competitive adsorption isotherm for the binary Propionic Acid (a) – Water (b) over Amberlyst-46 at 313 K. The lines represent the theoretical adsorption isotherm considering the parameters presented in Table 30.

Finally, the model here proposed for the fixed bed unit was used to simulate the breakthrough experiments. The methodology here proposed allows the evaluation of the uncertainties of the model prediction, based on the uncertainties of the model parameters and measurements. Figure 68, Figure 69 and Figure 70 present both model predictions and experimental data, as well as their uncertainties for the performed breakthrough experiments.

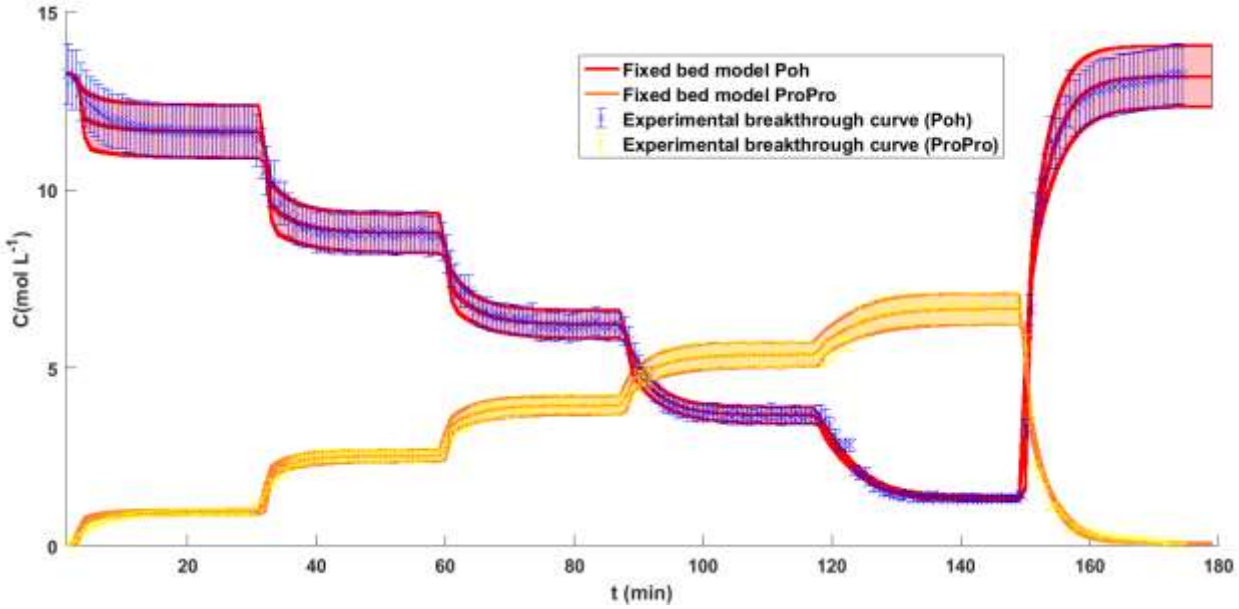

Figure 68 - Experimental and predicted breakthrough curves for the binary 1-Propanol– n-Propyl Propionate and the respective uncertainties at 313 K and a flowrate of 7.88 mL/min^{-1}. The lines represent the breakthrough curves predicted by the model while the dots represent the experimental data.

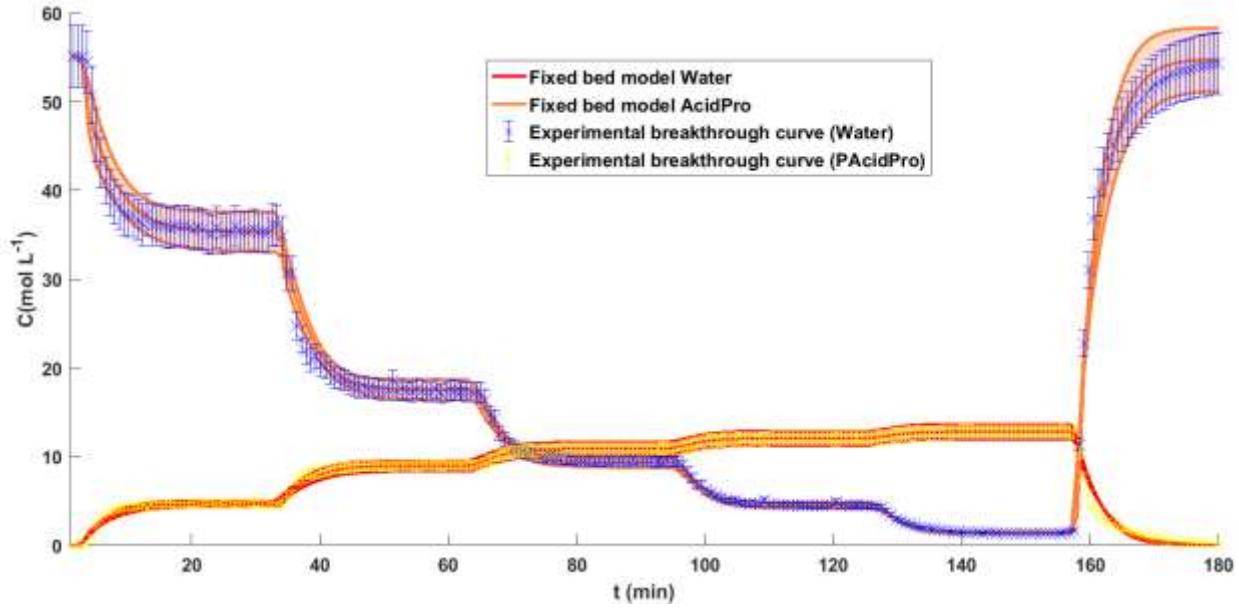

Figure 69 - Experimental and predicted breakthrough curves for the binary Acid Propanoic – Water and the respective uncertainties at 313 K and a flowrate of 7.88 mL/min^{-1}. The lines represent the breakthrough curves predicted by the model while the dots represent the experimental data.

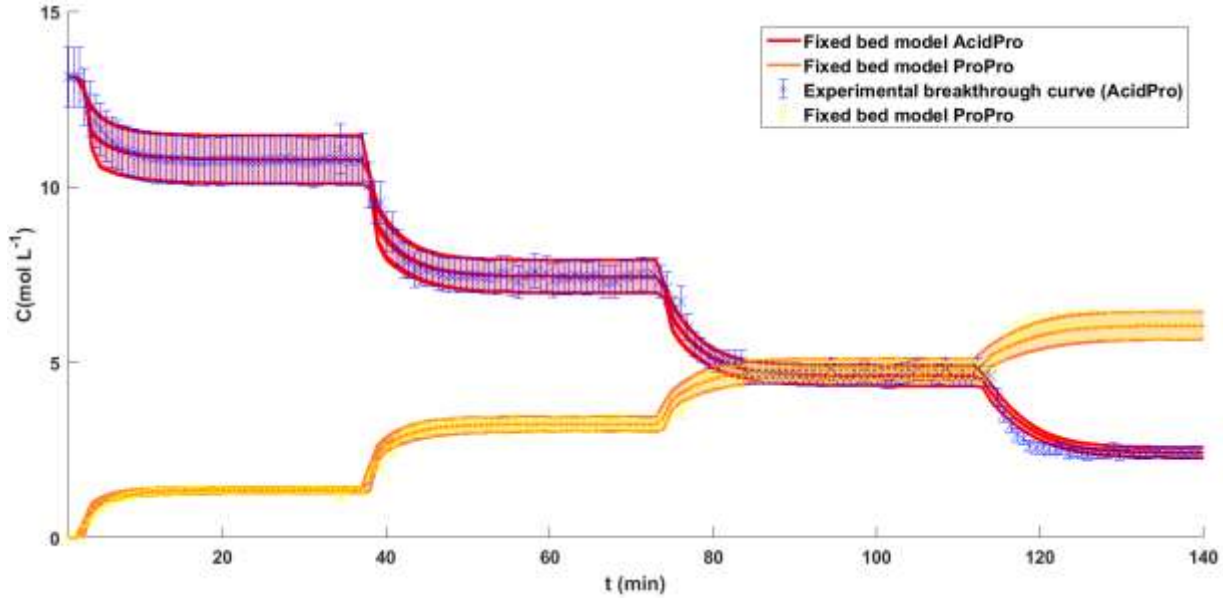

Figure 70 - Experimental and predicted breakthrough curves for the binary Acid Propanoic – n-Propyl Propionate and the respective uncertainties at 313 K and a flowrate of approximately 7.88 mL/min^{-1}. The lines represent the breakthrough curves predicted by the model while the dots represent the experimental data.

From the previous figures, it is possible to verify that the model predictions range overlaps the experimental points range. This leads to a more reliable model prediction, even under a reduced number of experiments. In terms of number of experiments, the present work performed a total of 16 breakthrough experiments in order to estimate the necessary parameters. While in the literature it can be found reports where it were performed for example: 32 breakthrough experiments (Faria et al. 2014); 20 experiments (Regufe et al. 2016); 21 experiments (Pereira et al. 2009a). It is also important to highlight that each experiment produces several samples to be analysed which have a significant analysis time associated.

Therefore, the experimental work was performed through a faster methodology and with a reduced number of experiments, when compared with other works in the literature. This enables the verification of the consistency of the method here proposed.

P2-3.3. Reaction rate model validation: Batch Reactor

As previously mentioned, the reaction rate presented in Section P2-2.1 was originally proposed by Duarte (2006) considering the UNIQUAC model. However, the present work proposes to apply a different thermodynamic model for the calculation of the activity coefficients. Therefore, in order to verify the validity of these modifications, a batch reactor model, presented in Section P2-2.8, was used to simulate experimental data reported in Duarte's work (Duarte 2006) considering the reaction rate and the thermodynamic model presented in Section P2-2.1.1 and Section P2-2.1.3. Table 32 presents the conditions in which the experiments were done and the model simulated.

Table 32 - Experimental and batch model simulation conditions of Duarte (2006).

	POH:AcidPro	**Temperature (K)**	m_{cat}	N_t
Experiment 1	1:1	333.15	10.00	10.00
Experiment 2	1:1	343.15	10.03	6.75

Figure 71.a) and Figure 71.b) present the experimental points and model predictions respectively for experiment 1 and experiment 2. From these graphics it is possible to note that the present model can represent with precision the experimental data. Hence, it is possible to conclude that the reaction rate model based on the NRTL and its kinetic parameters are suitable for the present case.

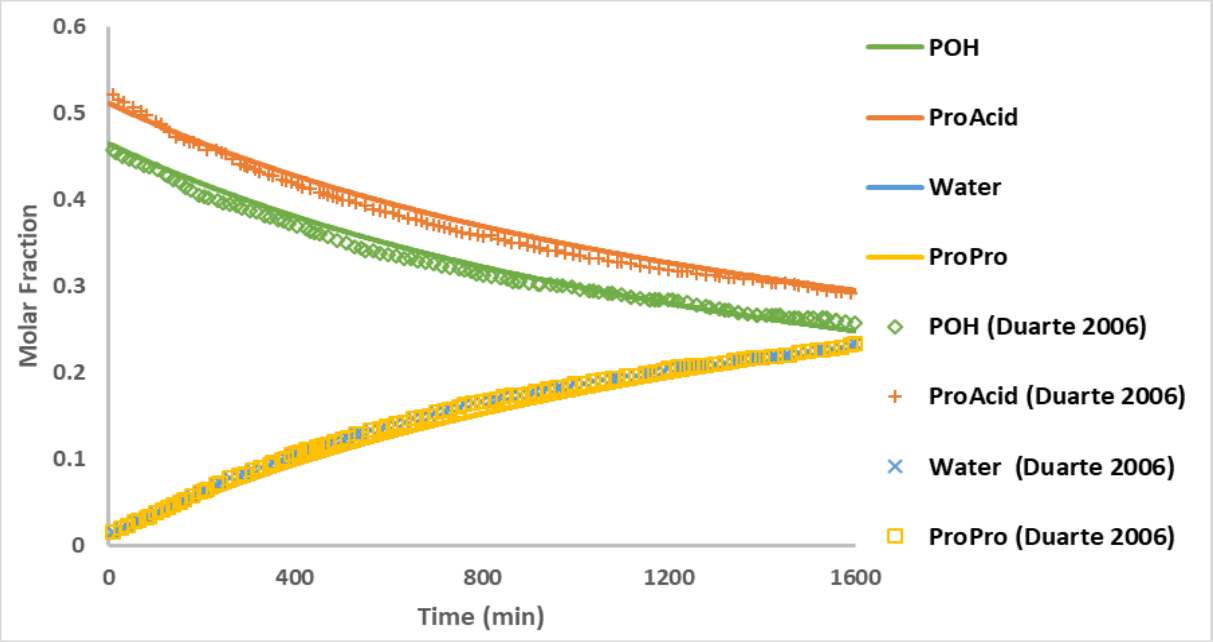

(a)

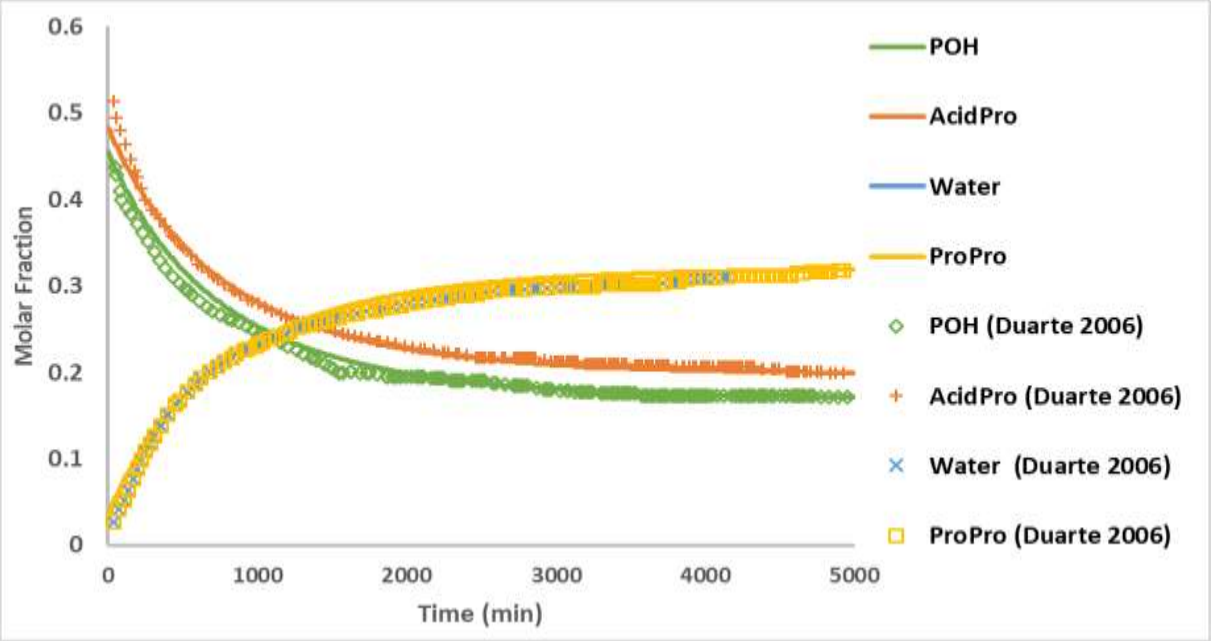

(b)

Figure 71 - Experimental and simulation results for the production of ProPro in a batch reactor, (a) Experiment 1; (b) Experiment 2 of Table 5.

P2-3.4. Fixed-bed reactor model validation

In order to validate the fixed-bed reactor model presented in section P2-2.9, a series of experiments was done in the experimental unit described in Section P2-2.2. First, a stream composed by 100% of Propanoic Acid was fed to the column in equilibrium with 1-Propanol (experiment 1). Following the first experiment, a stream composed by 100% of 1-Propanol was fed to the column in order to regenerate it to its initial state (experiment 2). Then, two experiments with binary feed mixtures, starting with the column filled with 100% of 1-Propanol, were performed with different feed compositions (experiments 3 and 4). The experimental conditions used are presented in Table 33. All experiments were done at a constant temperature of 313.15 K.

Table 33 - Fixed bed reactor experimental conditions.

	Compound	x_0	x_{feed}	Q_{feed} (ml min^{-1})
Exp. 1	**POH**	1	0	2
	AcidPro	0	1	
Exp. 2	**POH**	0	1	1.2
	AcidPro	1	0	
Exp. 3	**POH**	1	0.6	1.8
	AcidPro	0	0.4	
Exp. 4	**POH**	1	0.76	1.8
	AcidPro	0	0.24	

The model here proposed for the production of the ProPro through a fixed bed reactor was used to simulate these experiments. The experimental results together with the model predictions and its uncertainty are presented in Figure 72 and Figure 73.

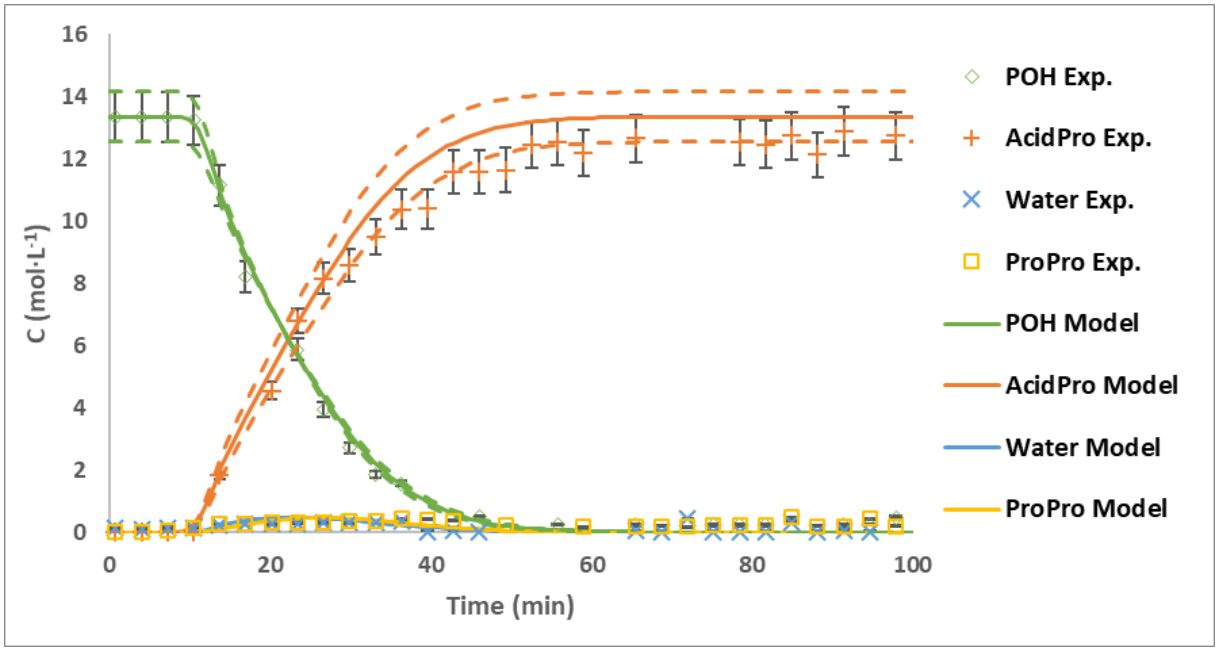

Exp. 1

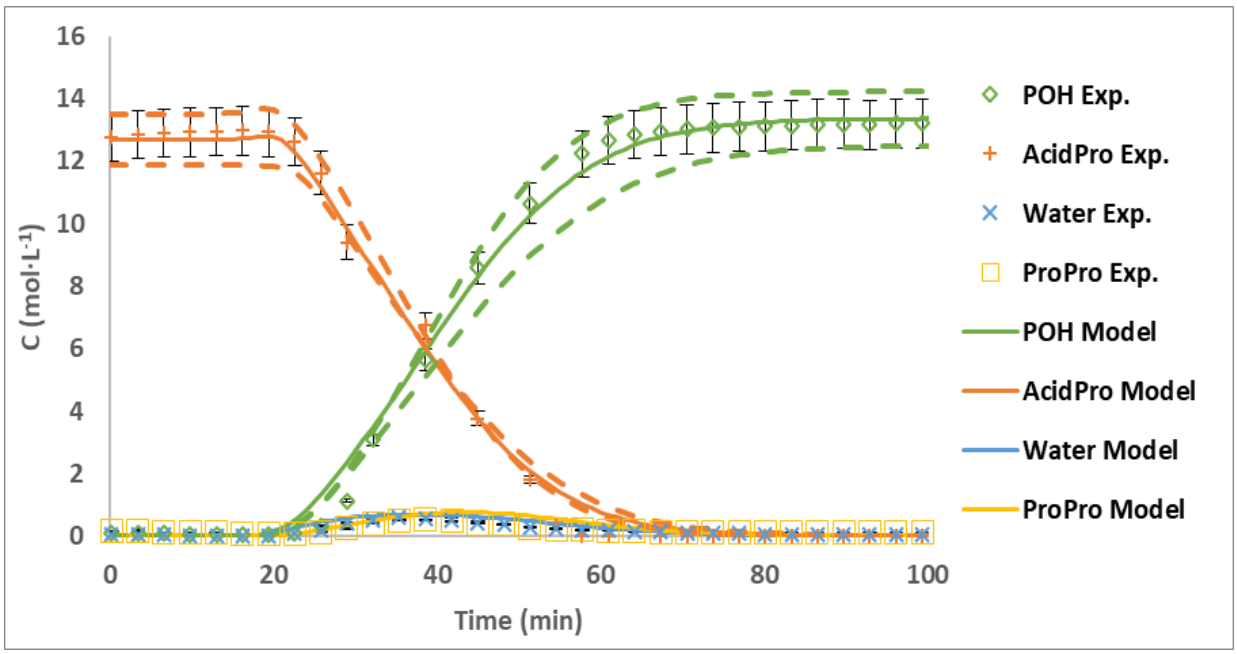

Exp. 2

Figure 72 - Synthesis of ProPro in a fixed bed adsorptive reactor at 313 K under the conditions presented in Table 33.

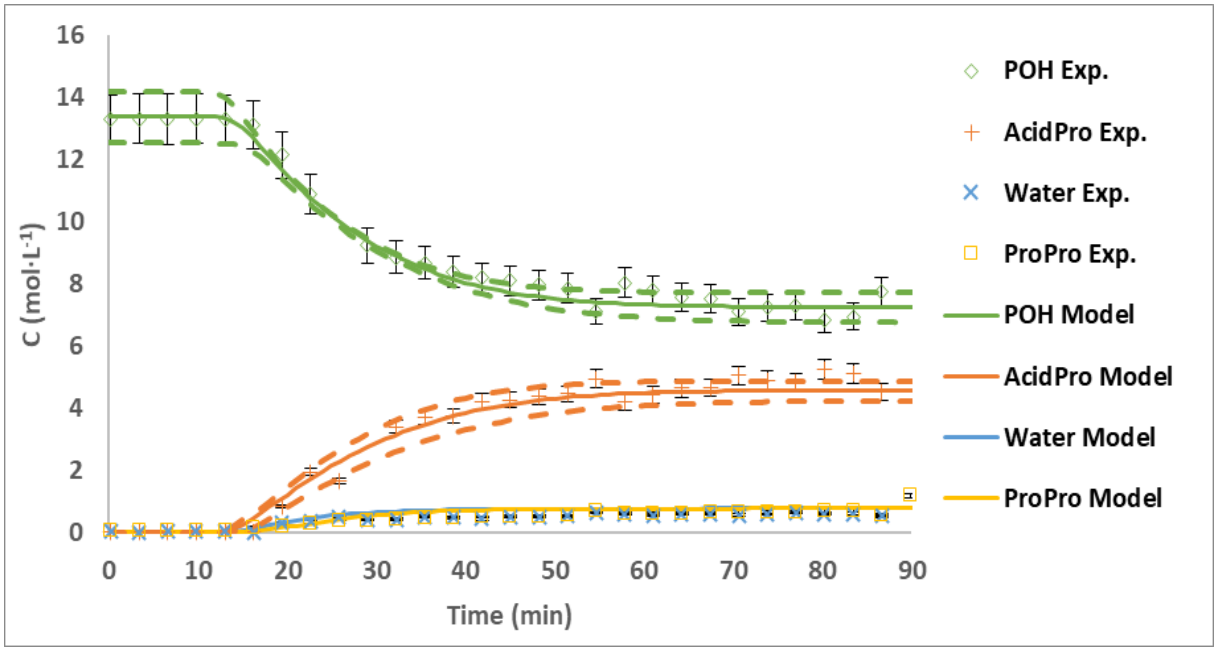

Exp. 3

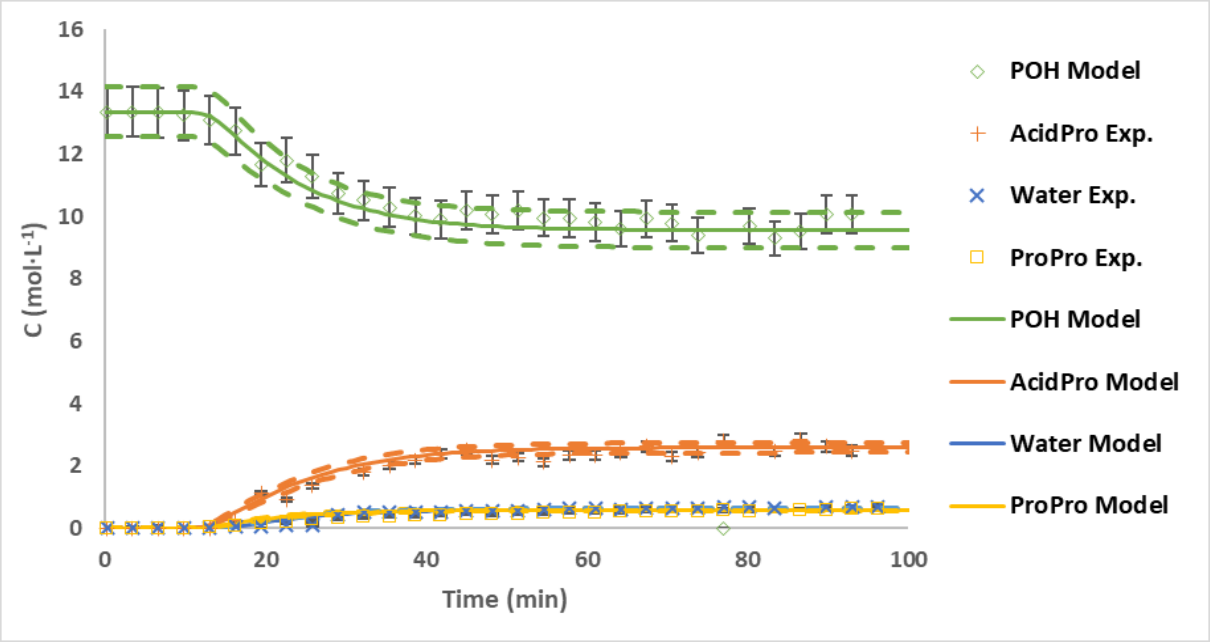

Exp. 4

Figure 73 - Synthesis of ProPro in a fixed bed adsorptive reactor at 313 K under the conditions presented in Table 33.

From the previous figures, it is possible to note that the predictions curves are in agreement with the experimental data. Hence, the mathematical model here proposed was capable of predicting with precision the concentration histories for the synthesis of n-Propyl Propionate in a fixed bed adsorptive reactor. Furthermore, the predictions are presented with their uncertainties which gives a more complete information about the system behaviour. From Figure 72 and Figure 73 it is possible to note that the Propanoic Acid was the first species to elute from the column. As the reactants contact with the resin active sites, the esterification reaction is promoted and consequent production of n-Propyl Propionate and Water. As the ProPro presents a lower affinity to the resin, it elutes first than water, at 16.23 min and 17.00 min respectively. The evolution of the concentration history proceeds until the resin is in equilibrium with water. Afterwards, the outlet stream composition remains constant, where is found a maximum concentration of ProPro

equal to 0.81 mol.L^{-1} in experiment 4 and 1.03 mol.L^{-1} in experiment 3.

P2-3.5. True Moving Bed Reactor design and optimization

The system here presented was simulated taking in consideration a pilot scale SMBR unit located in the Laboratory of Separation and Reaction Engineering. The unit model is a LICOSEP1 12–26 unit by Novasep, which can be operated up to 332 K and 60 bar and where 12 Superformance SP columns with 2.3 dm of length and 0.26 dm of diameter are installed. The columns are considered to be packed with the resin Amberlyst 46. For the simulation of the TMBR process, a unit with four sections of equal size, corresponding to two LICOSEP columns, that is 4.6 dm in length, was assumed. The operating conditions considered are presented in Table 34. It was also considered that pure 1-Propanol was used as process eluent.

Table 34 – Conditions considered in the simulations of the TMBR unit.

Section length	4.6 dm
Column diameter	0.23 dm
Operating temperature	313 K
Bed porosity	0.4
Peclet number	166
Particle diameter	245.5 µm
Feed composition	60% AcidPro -40% POH

P2-3.5.1. Triangle Theory

The design and optimization of a TMBR unit is a complex task because it must assure the separation and reaction simultaneously and efficiently. Some studies in the literature propose a two steps approach for this problem based on the Equilibrium Theory, which is usually applied in the design and optimization of TMB/SMB units. This approach consists in starting with the determination of the necessary conditions that guarantee the regeneration of the liquid and solid recycling streams. That means to specify the conditions for which pure eluent/solid are obtained at the outlet streams of sections IV and I respectively. Those conditions can be determined setting the limits of the ratio between the fluid internal flow rates and solid flow rate as:

$$\gamma_I = \frac{u_I}{u_s} > \frac{(1-\varepsilon)}{\varepsilon}\frac{q_{Water,I}(c_{Water}{}^x)}{c_{Water}{}^x} \tag{178}$$

$$\gamma_{IV} = \frac{u_{IV}}{u_s} < \frac{(1-\varepsilon)}{\varepsilon}\frac{q_{ProPro,I}(c_{ProPro}{}^r)}{c_{ProPro}{}^r} \tag{179}$$

Hence, the values of the ratio between the fluid interstitial velocity and solid velocity for sections I and section IV were calculated for the system in study based on the previously presented results, $\gamma_I > 0.9693$ and $\gamma_{IV} < 0.2484$. It is important to note that the ratio values for sections I and IV mentioned above are obtained based on the Equilibrium theory. However, as mass transfer resistance is present in the system it is necessary to add a safety factor (SF) to the values obtained above. The next step of the approach is to fix a value for the switching time, which consequently fixes the values of solid, section IV and section I flow rates. After that, the reactive separation region can be defined for a specific requirement of purity. This is done by simulating the process for different values of γ_{II} and γ_{III}. That means, starting with a low value of the feed

stream flow rate and a low value of the extract flow rate, the process is simulated and the performance parameters determined. Then, the extract flow rate is gradually increased until the two limits of the reactive separation region that obey the purity restriction are found. Afterwards, the value of the feed flow rate is increased and the simulation procedure with different values of extract flow rate repeated. This is done until the separation region is closed, that is, the maximum feed flow rate for which it is possible to obtain the required purity is found.

Table 35 - Operating conditions and performance parameters obtained through the triangle theory.

Operating Conditions	Q_f**(ml/min)**	Q_e**(ml/min)**	Q_{IV}**(ml/min)**	Q_x**(ml/min)**	Q_s**(ml/min)**
Value	0.14	2.56	0.12	0.90	2.45
Performance Parameters	Pur **(%)**	Pux **(%)**	$Conv$ **(%)**	Pr **(mol/day l of bed)**	EC **(l/g)**
Value	96.55	96.72	97.10	26.12	10.54

In the present case, after a preliminary analysis, the SF was fixed to a value equal to 1.7. After an analysis of the influence of the switching time, which is presented in the next section, it was fixed at 60 minutes. Figure 74 presents the reactive separation region evaluated through the aforementioned procedure for different purity values of 80%, 90% and 95% in both extract and raffinate streams. Those simulations are based on the process conditions described in Table 34. The considered operating point on the regeneration region (γ_I and γ_{IV}) is also shown in the Figure. An operating point within the 95% region was selected. Table 35 presents the

corresponding operating conditions and its performance parameters obtained through the Triangle Theory. From the results it is possible to note that a conversion of 97.1% was obtained, which is significantly higher than the equilibrium conversion for the same initial conditions, which is 51.7%. As previously mentioned, the moving bed reactor unit, as other multifunctional units, presents the advantage of overtaking the equilibrium limitation due to the continuous removal of the products from the reaction medium. This can be clearly seen from the results presented in Table 35 and, later on this section, it will be demonstrated that applying these units for the production of ProPro it is possible to achieve a conversion over 99%.

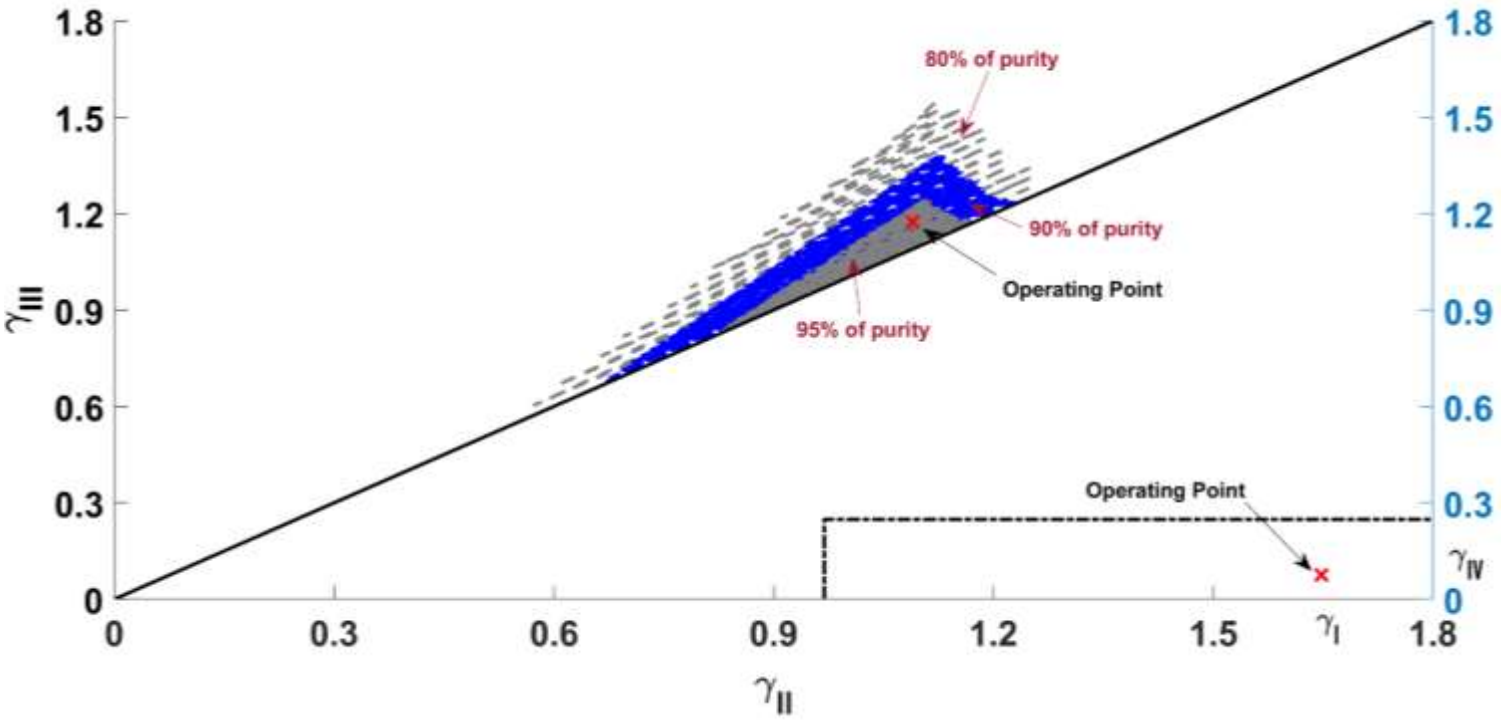

Figure 74 - Reactive separation regions with $\boldsymbol{t^* = 60}$ min and $\boldsymbol{SF = 1.7}$ for purities of 80%, 90% and 95%.

P2-3.5.1.1. Influence of the switching time

This Section is dedicated to the evaluation of the influence of the switching time on the process performance parameters. To do this, the values of γ_i were kept constant and equal to the ones that are obtained by the operating conditions presented in Table 35 while the solid flow rate is changed within a range of switching time from 3 minutes to 120 minutes.

Figure 75 presents the influence of the solid velocity (switching time) on the process purities, conversion, productivity and internal concentration profiles. The change of the switching time affects different phenomena within the process. Higher switching times result in lower solid flow rates. For the same γ values, this means lower feed flow rates and lower internal flow rates. Therefore, higher residence times within each section are obtained which consequently increases the conversion and decreases the mass transfer effects. Looking at Figure 75, it is possible to see that for low switching times (for example 40 min), the raffinate and extract purities are low. This happens because the lower conversion results in lower ProPro concentration and contamination of the raffinate stream with water, which spread through the column due to the mass transfer effects and unreacted AcidPro. The extract stream is also contaminated with unreacted AcidPro and a small amount of ProPro, which also spreads through the column due to the mass transfer effect. On the other hand, if the switching time is increased to 120 min, as previously mentioned, the feed flow rate tends to decrease and the reaction conversion to increase. As presented in Section P2-2.10, Equation (173), the productivity is proportional to the feed flow rate, thus the productivity tends to decrease while the switching time increases. Hence, at a switching time of 60 minutes it is possible to obtain purities and conversion over 95%.

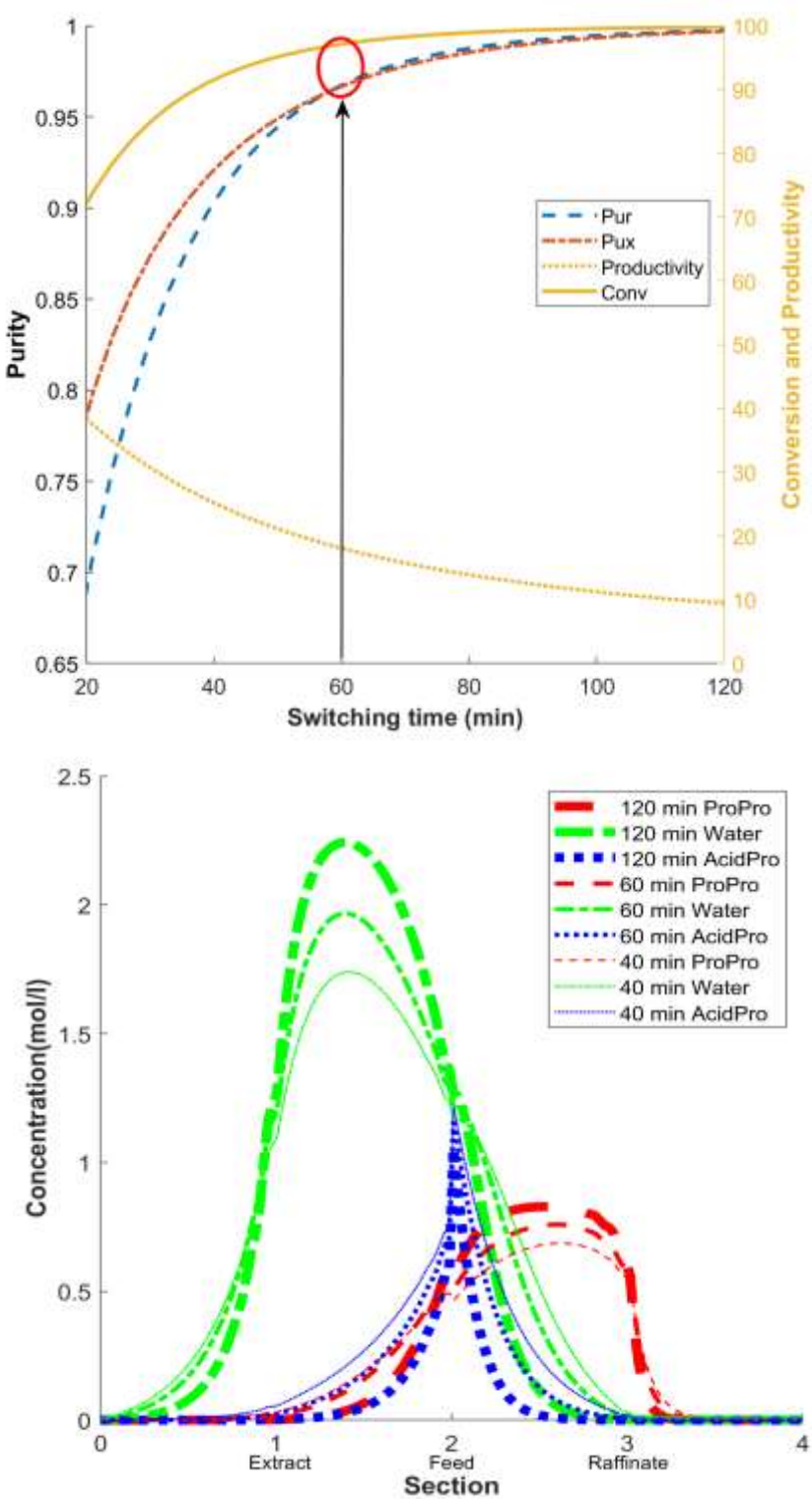

Figure 75 - Influence of the switching time on the performance parameters and internal concentration profiles of the TMBR unit.

In order to better visualize the aforementioned effects, Figure 76 presents the 3D concentration profiles and heat map graphics of ProPro, AcidPro and Water inside the TMBR where it is possible to note the behaviour of the profile waves as function of the different switching times.

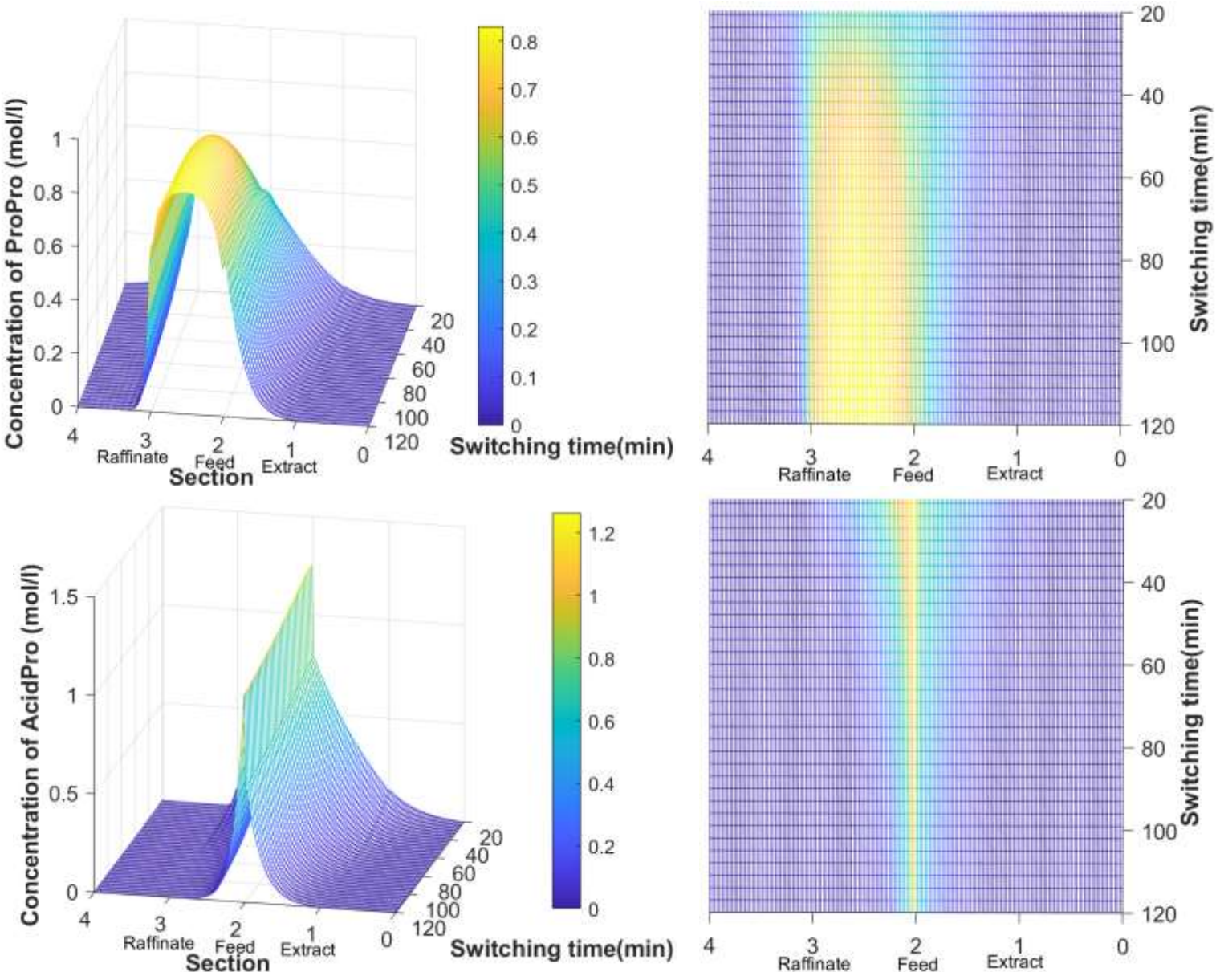

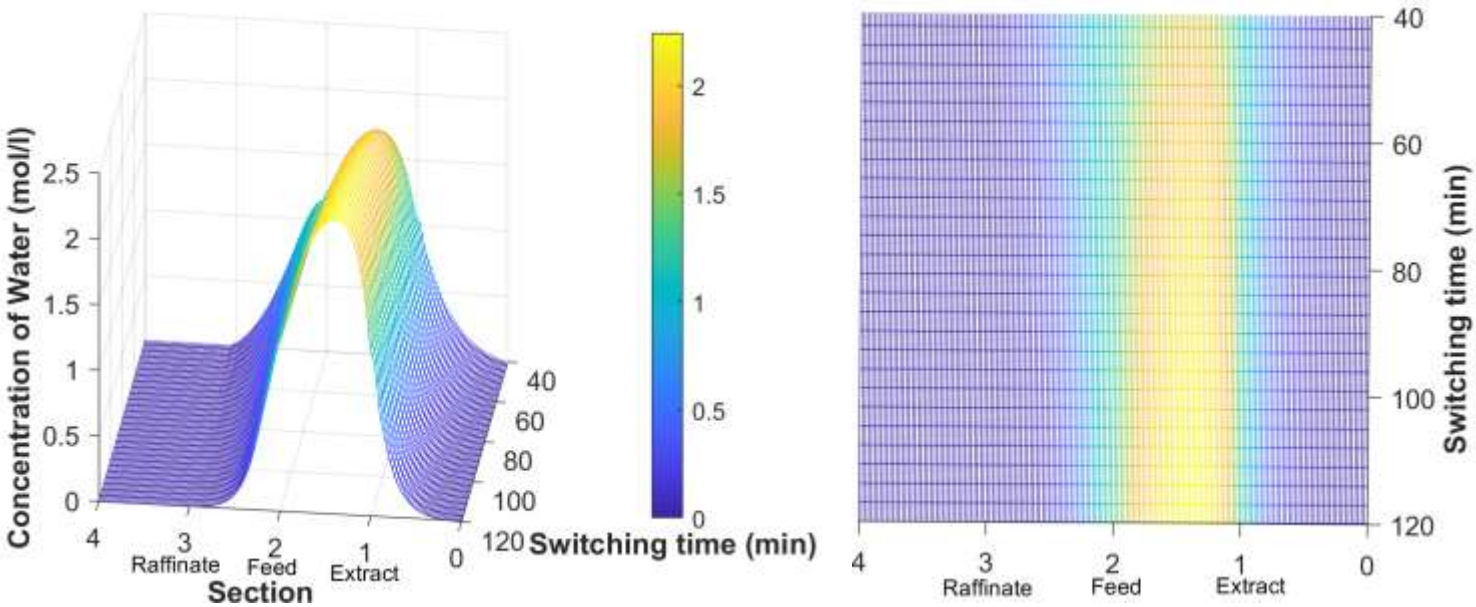

Figure 76 - TMBR internal concentration profiles as function of the switching time, 3D and heat map graphics.

P2-3.5.1.2. Influence of the feed concentration

The influence of the feed concentration on the process performance was also analysed in order to better describe the system behaviour through the Equilibrium Theory. A switching time of 60 min was used.

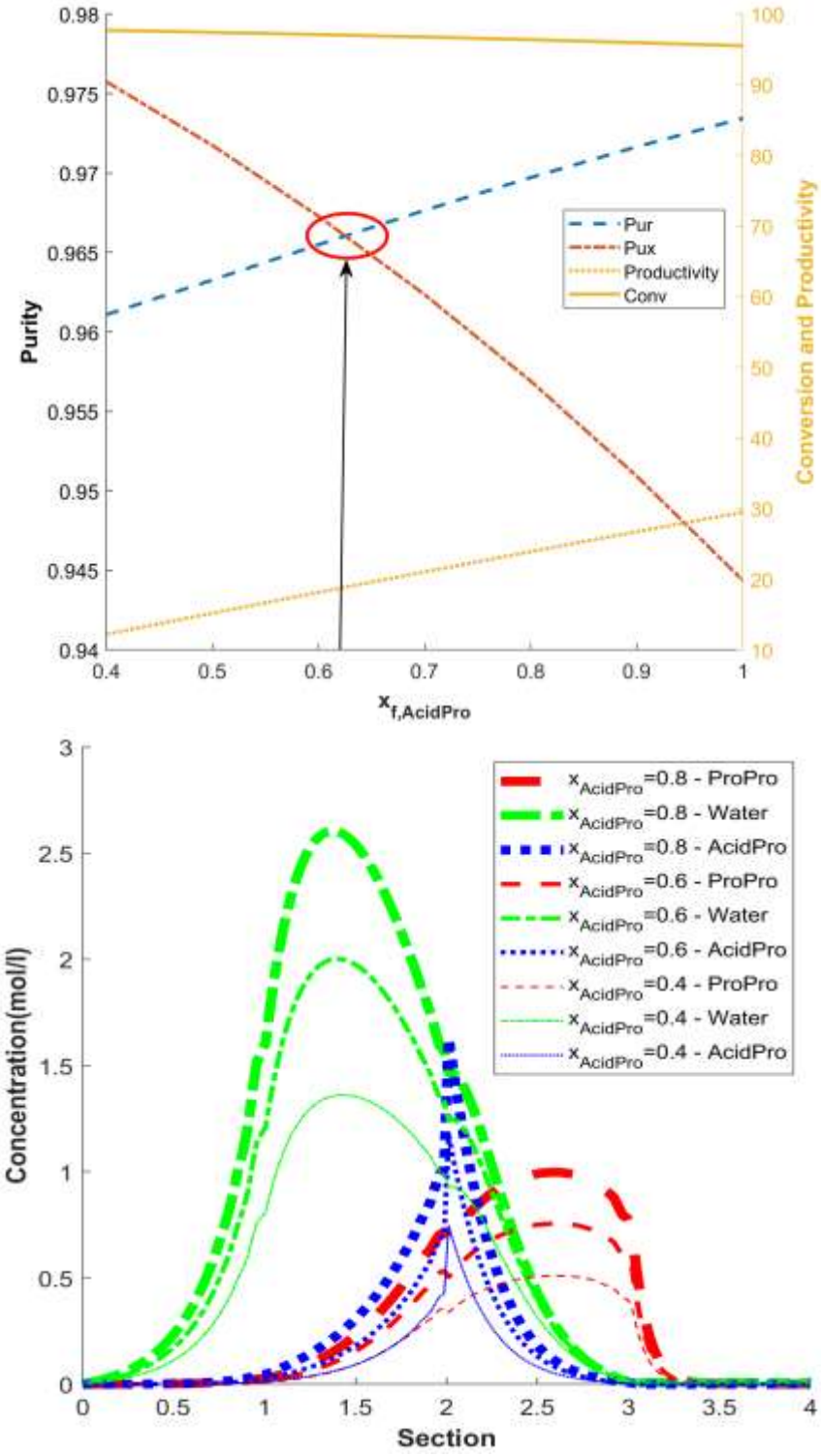

Figure 77 - Influence of the molar fraction of AcidPro in the feed stream on the performance parameters and internal concentration profiles.

Figure 77 presents the influence of the molar fraction of Propanoic Acid in the feed stream on the process performance parameters and internal concentration profile. It is possible to note that a better compromise is obtained when the molar fraction of the acid in the feed stream is around 0.6. It can be seen that an increase in AcidPro molar fraction results in a decrease of extract purity and an increase on raffinate purity. This is because higher concentrations are obtained within the bed as the AcidPro molar fraction increases. And although more water reached the raffinate port, the increase in ProPro concentration over compensates this effect and higher raffinate purities are obtained. However, in the extract port the amount of AcidPro that reaches that port is enough to cause a decrease in purity.

These effects can be better verified in the 3D concentrations profiles and heat maps presented in Figure 78.

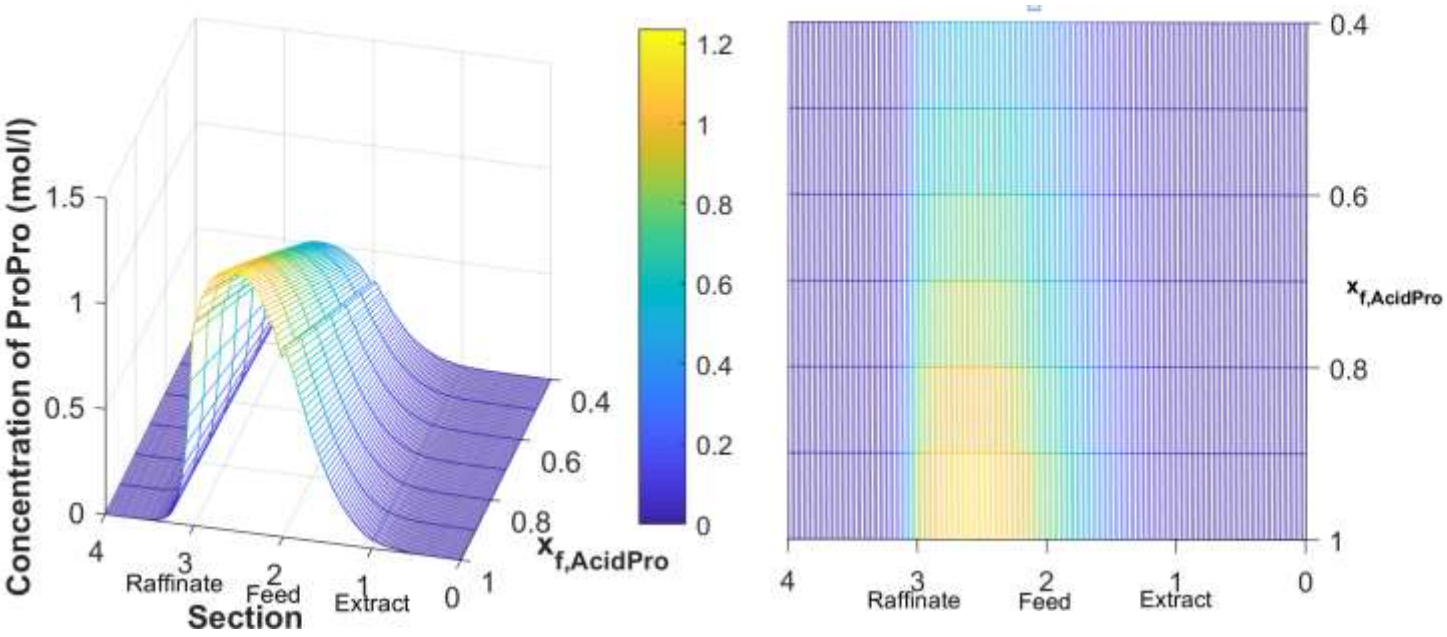

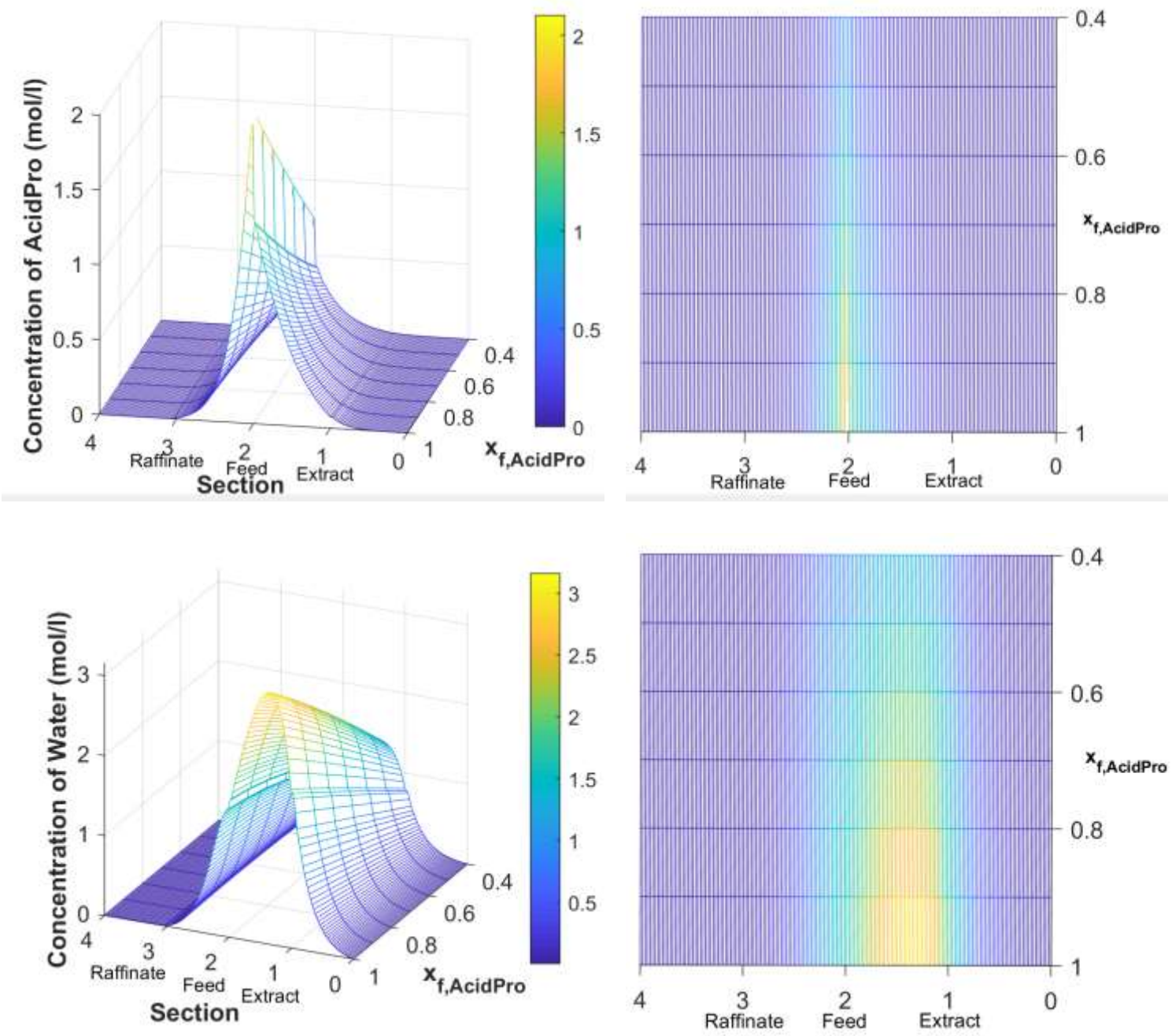

Figure 78 - TMBR internal concentration profiles as function of the molar fraction of AcidPro on the feed stream, 3D and heat map graphics.

P2-3.5.2. HPSO-TVAC-MSR

P2-3.5.2.1. Optimal design for 95% of purities requirement

First, the HPSO-TVAC-MSR was applied in order to solve the optimization problem described in Equation (176) for a 95% of minimum requirement of purities. This was done to compare the TMBR design and optimization through both methodologies here described. In this way, the PSO was applied to the system in study with a c_1 varying from 0.5 to 2.5, c_2 varying from 2.5 to 0.5, number of particles p equal to 60, number of iterations k_{total} equal to 120 and finally the searching region (where $R_i = [Q_f, Q_e, Q_{IV}, Q_x, Q_s]$) starting from $R_{1,min} = [0.050,\ 0.20,\ 0.070,\ 0.070, 0.080]$ and $R_{1,max} = [0.80, 7.00,\ 0.700,\ 2.00,\ 3.00]$ to $R_{2,max} = 1.05 \times R_{1,max}$, considering the $R_{i,min}$ constant and that the search region was enlarged twice. Under those conditions the algorithm was able to find one optimal minimum; the set of operating variables and performance parameters corresponding to the minimum found are presented in Table 36; the same table presents the values obtained through the Equilibrium Theory in order to compare both results. For both cases the feed composition was 60% of AcidPro and 40% of POH.

Table 36 - Operating conditions and performance parameters obtained through the HHPSO-TVAC-MSR and triangle theory.

Operating Conditions	Q_f**(ml/min)**	Q_e**(ml/min)**	Q_{IV}**(ml/min)**	Q_x**(ml/min)**	Q_s**(ml/min)**
Equilibrium Theory	0.14	2.56	0.12	0.90	2.45
HHPSO-TVAC-MSR	0.26	0.77	0.30	0.21	1.1
Performance Parameters	Pur **(%)**	Pux **(%)**	$Conv$ **(%)**	Pr **(mol/day l of bed)**	EC **(l/g)**
Equilibrium Theory	96.55	96.72	97.10	26.12	10.54
HHPSO-TVAC-MSR	95.47	95.50	97.17	48.76	2.48

From Table 36 it is possible to note that the PSO could lead to a set of operating conditions for which the process presents two times higher productivity and approximately five times lower eluent consumption comparing with the Equilibrium Theory values. An analysis of the TMBR internal concentration profiles obtained from both methods is presented by Figure 79. From this figure, it is possible to note that the unit design through the PSO leads to a better usage of sections I and IV of the TMBR. This happens since there are no restrictions for the PSO algorithm, while the Equilibrium Theory is restricted by its own nature, as previously described. Hence, the PSO optimal design provides a significant higher productivity and lower eluent consumption, while keeping the process in its minimal requirements of purities.

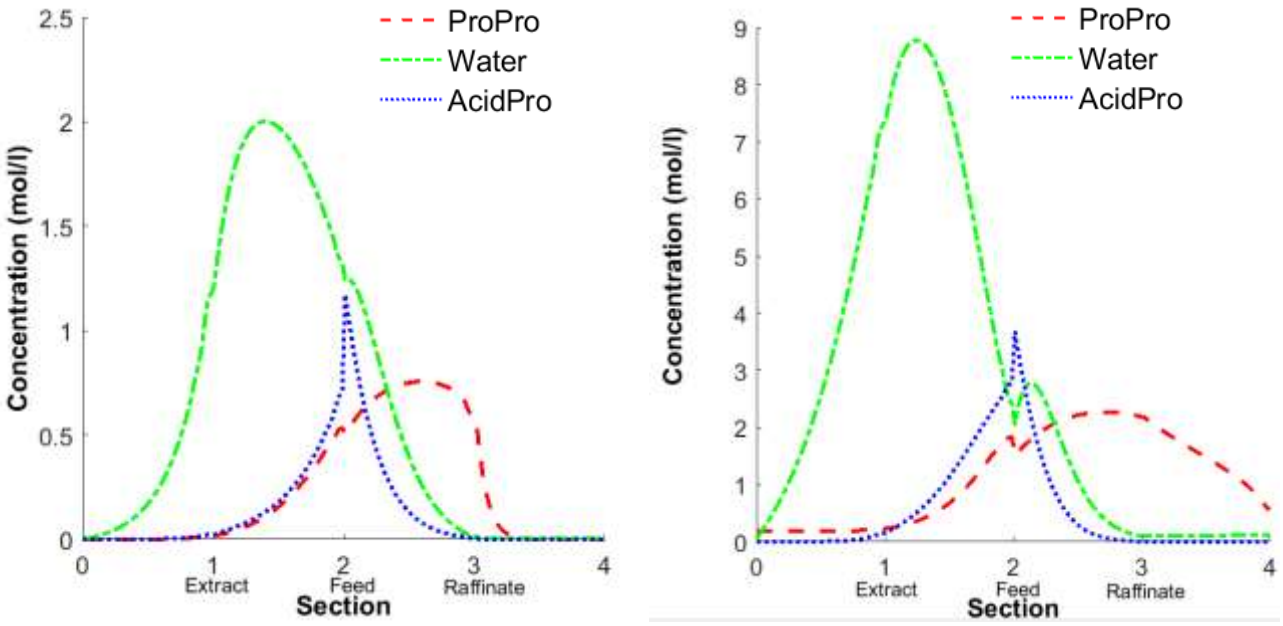

Equilibrium Theory operating conditions ***HHPSO-TVAC-MSR operating conditions***

Figure 79 - Internal concentration profiles for a TMBR unit designed through the equilibrium theory, left side and a TMBR unit designed through the HHPSO-TVAC-MSR, right.

P2-3.5.2.2. Optimal design for 99% of purities requirement

As presented in P1-2.5 the HPSO-TVAC-MSR leaded to a better TMBR design than the Equilibrium theory. Furthermore, this method presents the flexibility to evaluate all possible operating conditions inside of the search area. Moreover, through this technique it is possible to map all the operating conditions which respect the process performance parameters optimal conditions. Hence, in this Section the TMBR unit is redesigned in order to attend to a 99% purities requirement and the confidence regions for the optimal operating condition are drawn.

Therefore, the PSO was applied to the system in study with a c_1 varying from 0.5 to 2.5, c_2 varying

from 2.5 to 0.5, number of particles p equal to 60, number of iterations k_{total} equal to 180 and finally the searching region (where $R_i = [Q_f, Q_e, Q_{IV}, Q_x, Q_s]$) starting from $R_{1,min} = [0.050,\ 0.20,\ 0.070,\ 0.070, 0.080]$ and $R_{1,max} = [0.80, 7.00,\ 0.700,\ 2.00,\ 3.00]$ to $R_{2,max} = 1.05 \times R_{1,max}$, considering the $R_{i,min}$ constant and that the search region was enlarged twice. Under those conditions the algorithm was able to find the optimal minimum; the set of operating variables and performance parameters corresponding to the minimum found are present in Table 37. Here it should be highlighted that a conversion over 99% was obtained. The corresponding concentration profiles are presented in Figure 80.

Table 37 - Operating conditions and performance parameters obtained through HHPSO-TVAC-MSR for 99% of purities.

Operating Conditions	Q_f**(ml/min)**	Q_e**(ml/min)**	Q_{IV}**(ml/min)**	Q_x**(ml/min)**	Q_s**(ml/min)**
HHPSO-TVAC-MSR99%	0.14	0.35	0.087	0.097	0.41
Performance Parameters	Pur **(%)**	Pux **(%)**	$Conv$ **(%)**	Pr **(mol/day l of bed)**	EC **(l/g)**
HHPSO-TVAC-MSR99%	99.93	99.27	99.49	27.40	1.34

In Figure 80 is possible to note how the optimization led the process to a condition of 99% purities. A comparison between the 99% purities profile and the 95% one indicates that the sections I and IV are performing a better purification of the solid and liquid streams respectively. This leads to a higher purity while costing a reduction in the productivity, since that it was

necessary to reduce the solid and feed flow rates. However, this productivity is of the same order of magnitude of the one found in the Equilibrium theory design.

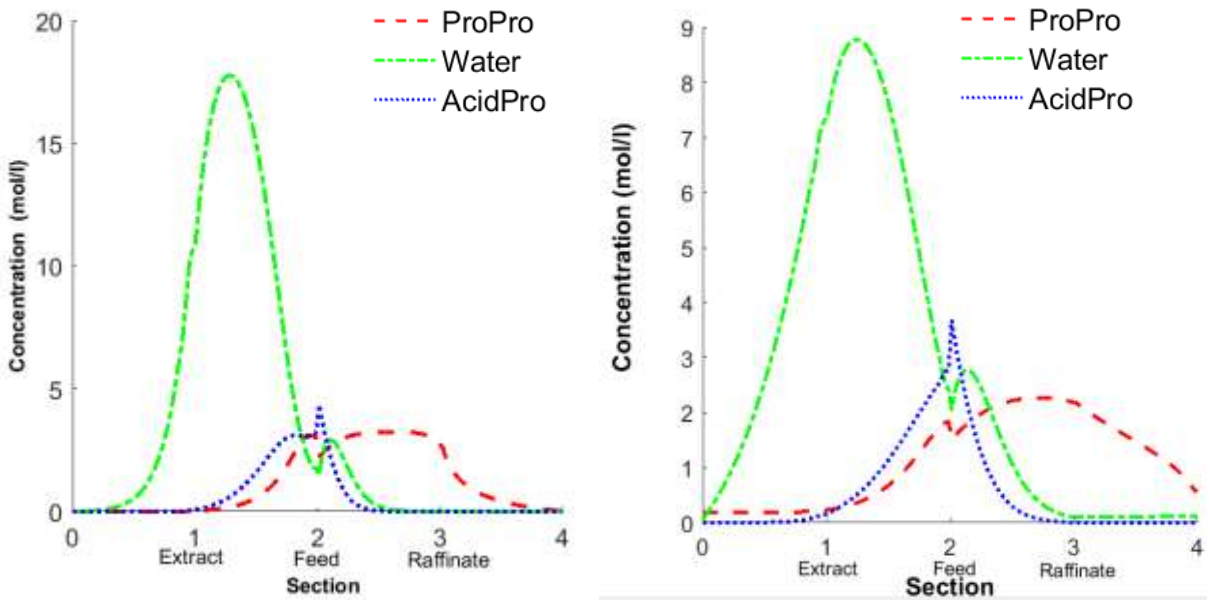

99% purities concentration profiles ***95% purities concentration profiles***

Figure 80 - Internal concentration profiles for TMBR optimal design through the HPSO-MMSR with 99% vs 95% of purities requirements.

P2-3.5.2.3. Confidence region evaluation

The Fisher–Snedecor test described in Section P2-2.12 was here applied. The optimization results can be also evaluated in terms of the ratios between the interstitial velocities and the solid velocity, providing a tool for direct comparison with the results as they are commonly presented for Equilibrium theory. Thus, Figure 81 provides the values of the ratios evaluated during the PSO optimization that obey the Fisher–Snedecor test, for a 99% purity requirement, and the respective optimal point, where in the left side is presented a two dimensions graphic containing

the information about all values of γ_{II} vs γ_{III} and γ_{I} vs γ_{IV} that were evaluated. On the right side of Figure 81 it is presented a 3 dimensions graphic, with the values of γ_{II} vs γ_{III} as function of the fob, where it is possible to observe the general behavior of the system through the optimization. It is also possible to note that, under the conditions evaluated, the system presents only one minimum point. Comparing the optimal values of interstitial velocities ratio, the PSO found $\gamma_{II} = 0.55$, $\gamma_{III} = 0.78$, $\gamma_{I} = 0.70$ and $\gamma_{IV} = 0.14$ for a minimal requirement of purity equal to 99%. This optimization has more freedom to search the best process operating point than the triangle theory, since it has no restrictions such as the fixed value of solid flow rate or the safety factor.

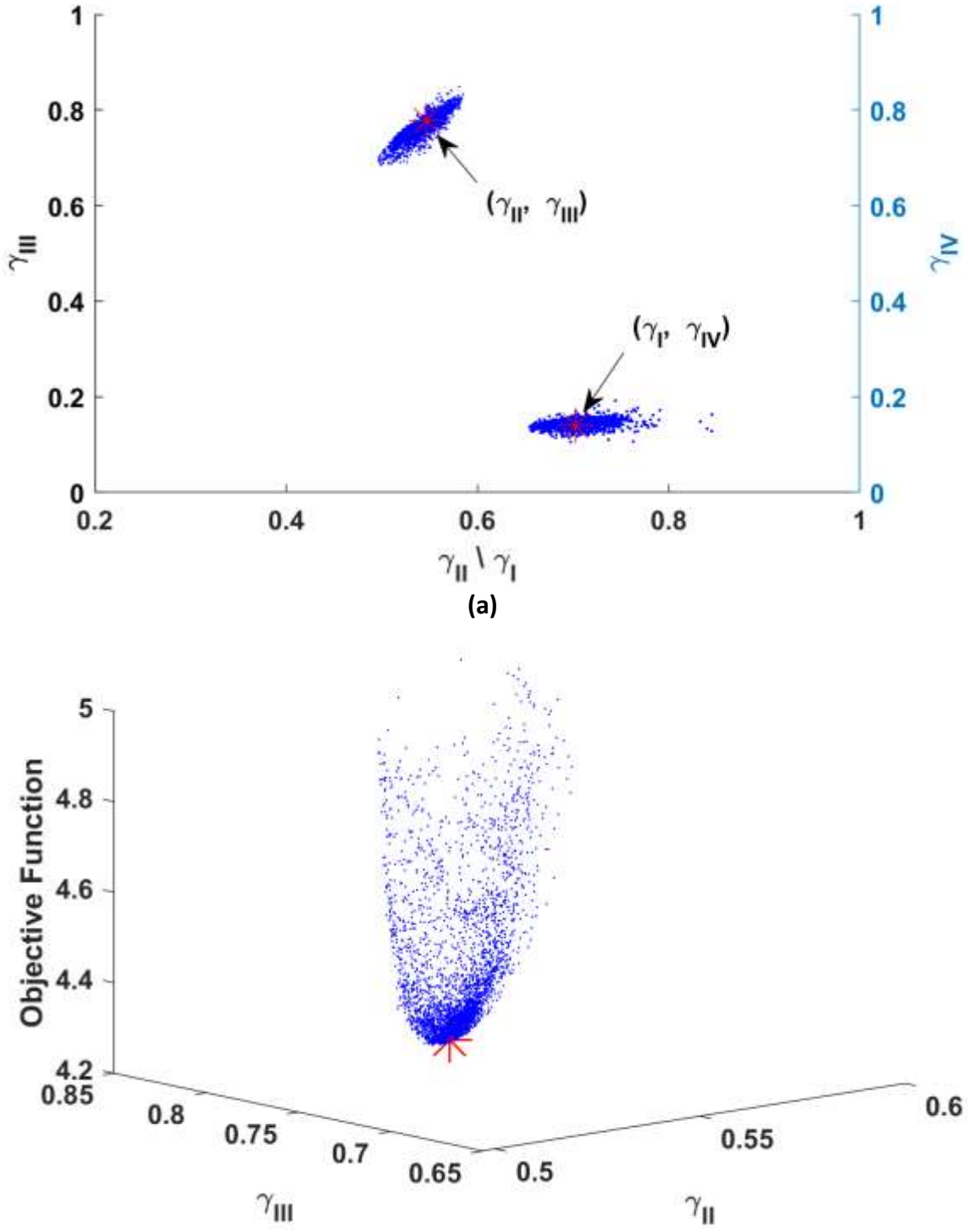

Figure 81 – Confidence regions for the interstitial velocities ratios and objective function vs the values of interstitial velocities ratios in sections II and III.

Figure 82 presents the confidence regions for the process operating variables as function of the

solid flow rate for a confidence level of 99%. The confidence regions are obtained through the evaluation of the Fisher–Snedecor test. In the parameters estimation, a usual approach is to simplify the problem of confidence regions drawing, through the consideration that the parameter estimates follow a normal distribution, leading to the well-known elliptical regions. However, it was demonstrated in the literature that this can be a poor simplification when applied to non-linear systems (Schwaab et al. 2008). In this way, as a comparison tool, Figure 82 also presents the elliptical regions, and as can be noted, for the present case, those regions can be a good approximation; thus, the simplification can be employed for the determination of the confidence regions. This can also be considered a verification that the PSO results can be efficiently employed to draw the operating variables confidence region. Finally, it is possible to verify, through the orientation of the ellipses, a strong and positive correlation between the operating variables. This correlation is related to the influence of the solid flow rate and the other flow rates on the performance parameters. The strength of the influence can also be evaluated by the form of the ellipse, that is the more elongated the shape, the bigger is the correlation. In this way, from Figure 82, it is possible to see that the correlation strength increases from graphic a to d.

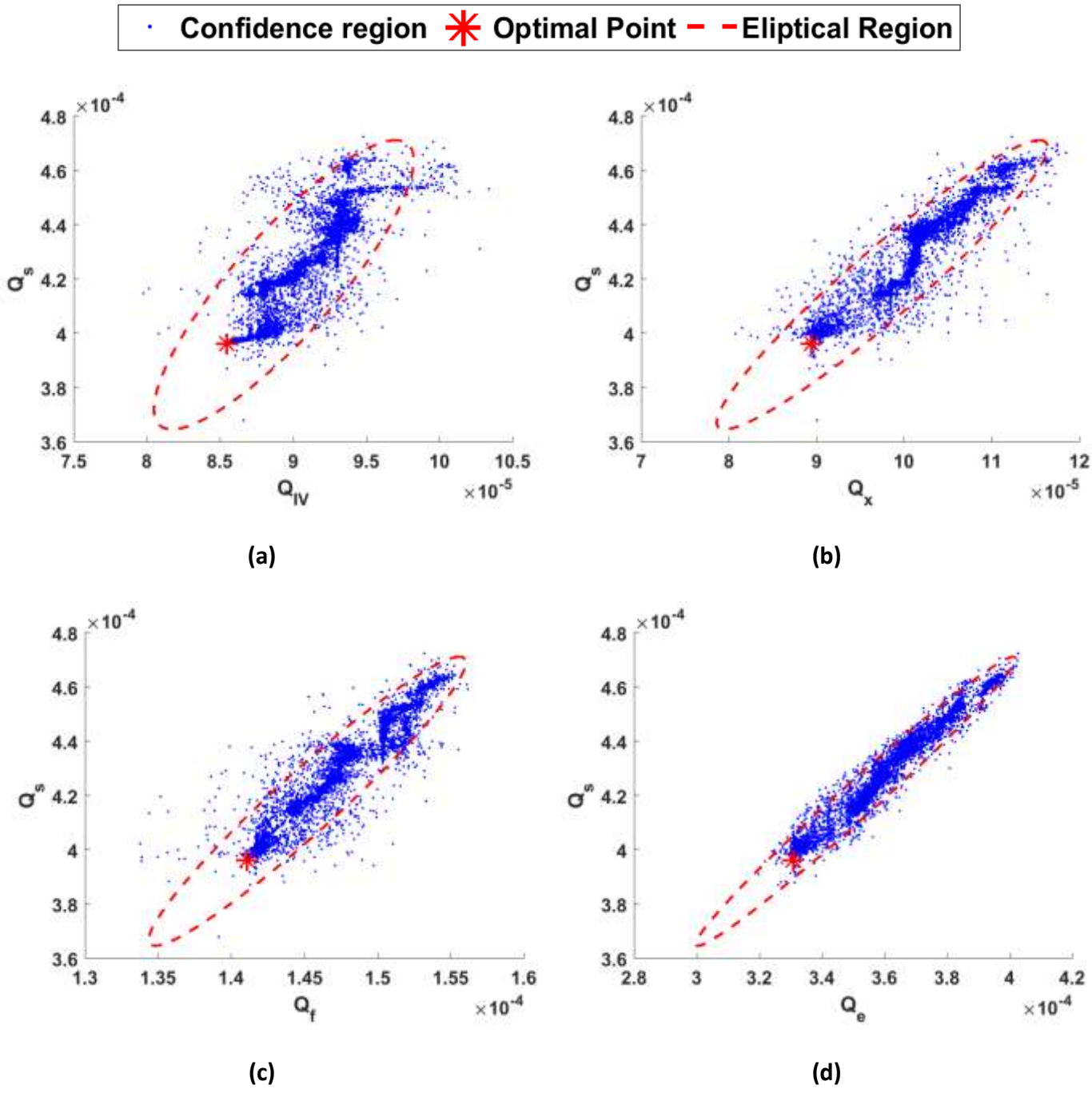

Figure 82 – Optimal points, elliptical confidence regions and confidence regions for the operating variables.

Finally, the method here proposed to design and optimize the TMBR unit employs the confidence region as a process operating map, containing all the possible operating conditions which will

comply with the pre-established requirements. From the confidence regions, Figure 82, the definition of an operating condition with 99% purities can be done by setting first a desirable value of solid flow rate in Figure 82.a, and selecting the corresponding value of recycling flow rate; doing the same for the remaining graphics it is possible to obtain a set of operating conditions that, even though not optimal, are inside the process performance requirements. Table 38 presents the maximum and minimum values of the performance parameters that can be obtained through this procedure.

Table 38 - Performance variables limits for the previously presented operating confidence regions.

Performance Parameters	Pur (%)	Pux (%)	$Conv$ (%)	Pr (mol/day l of bed)	EC (l/g)
Maximum	99.93	99.42	99.61	28.45	1.36
Minimum	99.93	98.99	99.27	26.52	1.32

P2-3.6. Comparison between the Chromatographic Reactor and Distillation Reactor

A detailed comparison between the SMBR and Distillation Reactor production routes should be the focus of future studies, since this analysis requires the scale up design of the SMBR unit and addressing the problem including economic concerns. However, a straight comparison based on the performance parameters can be done in order to evaluate if the chromatographic unit

appears to be a viable alternative worth of further investigation. Therefore, using the available information in the literature, it is possible to note that reactive distillation (RD) processes present a complex operation and purities and conversion under 90% (Altman et al. 2010; Keller et al. 2011). Significant higher reaction conversion and purities were obtained here, over 99%. In order to obtain a higher conversion and purity in a RD system it is necessary the employment of auxiliary units, which increases even more the complexity and energy consumption of the process (Altman et al. 2010; Cruz-Díaz et al. 2012; Xu et al. 2014). However, those systems present a high productivity, which is not certain to be attained with a SMBR unit. However, the actual productivity, associated with low eluent consumption and operation at significant lower temperature, gives enough evidence that the SMBR can be an efficient and competitive route for the production of the n-Propyl Propionate.

P2-4. Conclusions

The separation of the compounds involved in the n-Propyl Propionate production was studied in a chromatographic separation unit packed with Amberlyst 46 resin. Through a series of breakthrough experiments, it was possible to determine the Langmuir adsorption equilibrium model parameters for the system in study, where it was verified that the water is the most retained compound in the resin Amberlyst 46, while the ProPro is the compound with less affinity to the resin. The uncertainty evaluation of the experimental work was conducted. Also, a phenomenological model to describe the adsorption system was proposed. A modified PSO algorithm was applied to perform the model parameters estimation successfully, allowing to draw the parameters confidence regions. Through the parameters confidence regions, it was possible to evaluate the parameters uncertainty and concomitantly with the experimental uncertainty, the evaluation of the extended uncertainty of the model predictions.

The results showed that the model was capable of predicting the experiments accurately. Furthermore, it was possible to estimate the model parameters with a reduced number of experiments, when compared with other reports in the literature; nevertheless, the final results lead to a statistically more reliable model. In this way, it was possible to reduce the costs associated with the experiments. Therefore, the main contributions of this work are the methodology for the parameters estimation with uncertainty evaluation, the Langmuir isotherms parameters for the n-Propyl Propionate reaction system and the validated model for the Fixed Bed adsorptive separation.

Then, the synthesis of n-Propyl Propionate in a fixed bed adsorptive reactor packed with

Amberlyst 46 resign was investigated. A series of experiments were done in an experimental fixed bed unit in order to characterize the system; concomitantly, a phenomenological model was proposed. The proposed model includes the liquid-liquid non-linearities and the most suitable thermodynamic model to represent the system was investigated. Finally, the uncertainties evaluations were carried out and extended to the model predictions.

The simulation of a batch reactor for the production of the ProPro and comparison with experimental data demonstrated that the thermodynamic and the reaction rate models were suitable for the case in study. Then, the model for the fixed bed adsorptive reactor was simulated and compared with the experimental data. It is possible to conclude that the model is capable of describing the system dynamic behaviour with precision, providing simultaneously a characterization of its uncertainties.

The results obtained allow the characterization of the synthesis of the n-Propyl Propionate through a novel route, leading to the possibility of the application of a more complex chromatographic process which may lead to a more efficient production of this compound.

Finally, the synthesis of n-Propyl Propionate through a True Moving Bed reactor packed with Amberlyst 46 resin, simultaneously with the proposal of a method for the design and optimization of a TMBR unit, was studied.

The TMBR unit design parameters, the external flow rates, were firstly defined through the traditional method based on the Equilibrium Theory, demonstrating that the unit is capable of producing ProPro with high purity and conversion, over 95%. The system was also designed through a Particle Swarm Optimization algorithm which provided better results than the Equilibrium Theory. However, it is important to note that the Equilibrium Theory is an important

tool providing initial notion about the system behaviour, information that can be used to improve the swarm optimization.

Finally, the HPSO-TVAC-MSR was applied in order to design and optimize the process for high purity conditions, over 99%. The method identified successfully the set of operating conditions which lead to the required purity. Moreover, the method provided a data base which was used to draw the operating confidence region. Hence, a map with all the possible operating conditions that meet the minimum purity requirement is also provided, in which the process can be operated with a high productivity, small eluent consumption and conversion above 99%.

The present work demonstrated that the HPSO-TVAC-MSR can be a powerful tool to optimize and simultaneously provide deep information about the TMBR operation. Furthermore, the results of the present report provide evidences that the SMBR can be an efficient and competitive route to produce n-Propyl Propionate. However, deeper studies are necessary in order to take in consideration the scale of the systems and their economic factors.

General conclusions

This thesis presented a series of mathematical and experimental developments with focus on chromatographic units. The present work was divided in two parts, each one with different but complementary objectives. Part 1 had the focus on methods development addressing the control, inference and design problems of TMB and SMB units and performing a dynamics analysis of the processes. Part 2 presented the experimental studies about the n-Propyl Propionate production in chromatographic units concomitantly with the parameters estimation, uncertainties evaluation, models validation and the application of the design and optimization methods, developed in Part 1, in the design of a True Moving Bed Reactor to produce n-Propyl Propionate with high purity.

Through Part 1 developments, it was possible to propose a tool to assess the influence of the processes operating conditions on their performance parameters based on the Orthogonalization method. The method was capable of ranking all process variables in order or their influence on predefined process performance parameters. Due to its simplicity and efficiency, the Orthogonalization method can be employed to analyze any type of process if there is a model available, or it is even possible to do small perturbation in the operating variables of the actual process. This method was used as a basis for the other developments presented in Part 1.

Therefore, in Part 1 it was also discussed a different point of view for the comparison between the dynamics of a TMB and a SMB unit, concluding that, in some specific cases, the representation of a SMB process by a TMB model is not the best approach.

The work presented in the first part of this thesis continued by proposing a new methodology to address the control problem of these units. A novel approach based on the identification of multiple transfer functions for different types of process perturbations was presented. The proposed strategy was compared with the traditional one and tested for different scenarios. The results showed that the method can efficiently control the process on its optimal operating condition, which could not be done employing a traditional model predictive control.

Then, the inference problem was addressed, which is related to the real-time measurement of the unit purities and consequently its main performance parameters. In this way, a hybrid system called Quasi-Virtual Analyzer was proposed which makes use of an Artificial Neural Network model and laboratory measurements. The Quasi-VOA was tested through simulations and the approach was successfully validated allowing a real-time estimation of the process purities.

Part 1 finished with a study about the robust design of TMB units. To address this problem a novel PSO algorithm was proposed, based on previous developments presented in the literature. Futhermore, a methodology to draw the confidence regions of the operating variables was also developed. The combination of those two methodologies provided an efficient tool to perform the robust design of the unit, giving better results than the traditional method used in the field.

Thus, it is possible to conclude that Part 1 contributes to the growing discussions about the control, inference and optimization of Moving Bed units. The methods and their results showed that it is possible to deal with some of the key points in this field, making use of the computer power available nowadays. Therefore, further investigations should be conducted in order to deeper evaluate the methodologies potentialities.

On the other hand, Part 2 of this thesis addressed the problem of the production of n-Propyl Propionate on a TMBR unit. Hence, a series of experimental studies was done in order to characterize the reaction system adsorption parameters, which were estimated concomitantly with their uncertainties. For the parameters estimation, the PSO algorithm developed in Part 1 was used, while a modified version of the confidence region test was applied to draw the parameters confidence region and define their uncertainties. Then, a model for the separation of the non-reactive pairs in a chromatographic unit was presented and validated through the experimental work. The uncertainties were expanded to the model predictions and it was shown that the uncertainty evaluation can be an important tool in order to reduce the number of experiments necessary to study the system. Furthermore, it is part of the contributions of this step of the work the determination of the Langmuir isotherm parameters for the system at the temperature of 313 K.

Moreover, the synthesis of the ProPro in a chromatographic fixed bed reactor was studied. A series of experiments were done and a phenomenological model of the process was presented. Thus, the phenomenological model was validated and its prediction uncertainty evaluated based on the previous development of this part. The results showed that the model predicted with precision the synthesis of the n-Propyl Propionate in the fixed bed reactive column.

Hence, the aforementioned steps of the Part 2 culminated on the development of a model for the production of the n-Propyl Propionate on a True Moving Bed Reactor. The model was based on the validated fixed bed reactor unit and in the experimental unit located in the Laboratory of Separation and Reaction Engineering. The TMBR unit optimal operating conditions was defined by the PSO-MSG and its confidence regions were drawn by the methodology presented in Part 1.

Concomitantly, the system optimal design was also defined through the Triangle Theory. Hence, both methodologies were compared and also for this case the PSO-MSG with confidence regions presented better results. Finally, it was shown that the TMBR unit presented a ProPro production with higher purity and conversion, when compared with the Reactive Distillation technology.

Hence, the second part of this thesis contributes to the solution of a problem faced by the chemical industry nowadays, namely its adaptation in order to face its environmental impacts. The results of this part showed that the production of the n-Propyl Propionate, considered a green solvent, can be done through another environmentally friendly way, the TMBR unit, providing a better conversion and purities than the other alternative, the Reactive Distillation. However, it is still necessary to study, from the economic point of view, the advantages and disadvantages of each route.

Furthermore, on one hand it was shown that part of the methodology presented in Part 1 has the potential to be applied in the design of experiments, in order to reduce the experimental costs. On the other hand, it was demonstrated that the design and optimization problem of TMBR units can be simplified by using the methodology developed in Part 1.

Future Works

The two parts of this thesis have several contributions starting with new methodologies to experimental results, as described in the general conclusions. However, this work is a very small part of what can still be done. The methods here presented should be deeper explored in the future. On one hand, all the methods presented in Part 1 can be applied to other types of cycling processes, such as Pressure Swing Adsorption units or other types of processes in which similar problems can be found. On the other hand, inside of the TMB/SMB units there are still a myriad of possibilities to be developed which will be further detailed in this section.

The control system strategy here proposed could be applied for a SMB case comparing its performance with the case here presented, TMB application. Moreover, the identification strategy here proposed allows the application of more complex MPC strategies, such as the infinite horizon model prediction control or the robust model prediction control; this last case, is very suitable for those types of units, since it considers the systems uncertainties. In the same way, the Quasi-Virtual analyzer can be applied for a SMB case and compared with the results here presented.

It is important to highlight that the previous mentioned suggestions contemplate only simulations and computational work. A further development of the works started in this thesis could be the experimental implementation/application of those methods for the dynamics evaluation, control, inference and design of an SMB pilot unit.

In the sense of True or Simulated Moving Bed Reactor units, the Orthogonalization method here presented was not applied to the TMBR case. A similar approach to the one presented here could

be done using a TMBR vs SMBR in order to verify the dynamic behavior of those units, their similarities and differences. Furthermore, the control and inference methodology could be applied also in the case of those units, since they present the same problems as the TMB/SMB cases, with deeper implication due their complexity. Moreover, the present thesis only applied the PSO-MSG to the design of the TMBR case. It could be of interest to apply all the other methods: dynamics analysis, control, inference and robust design to the TMBR and/or SMBR units also. All those points can also lead to their experimental applications on a SMBR pilot unit.

Finally, a complete evaluation considering the economic questions should be carried out for the case of the application of the TMBR to produce n-Propyl Propionate. Eventually, the application of chromatographic processes as downstream units should be also considered in order to improve the current production routes of the ProPro. Then, a comparison of all possible routes can be properly done and further conclusions could be obtained.

Bibliography

Abel S, Erdem G, Amanullah M, Morari M, Mazzotti M, Morbidelli M. Optimizing control of simulated moving beds—experimental implementation. J Chromatogr A. 2005;1092(1):2–16.

Al-Dunainawi Y, Abbod MF, Jizany A. A new MIMO ANFIS-PSO based NARMA-L2 controller for nonlinear dynamic systems. Eng Appl Artif Intell. 2017;62:265–75.

Ali MA-H, Betlem B, Weickert G, Roffel B. Non-linear model based control of a propylene polymerization reactor. Chem Eng Process Process Intensif. 2007;46(6):554–64.

Altman E, Kreis P, van Gerven T, Stefanidis GD, Stankiewicz A, Górak A. Pilot plant synthesis of n-propyl propionate via reactive distillation with decanter separator for reactant recovery. Experimental model validation and simulation studies. Chem Eng Process Process Intensif. Elsevier B.V.; 2010;49(9):965–72.

Alvarez L a., Odloak D. Optimization and control of a continuous polymerization reactor. Brazilian J Chem Eng. 2012;29(4):807–20.

Amanullah M, Grossmann C, Mazzotti M, Morari M, Morbidelli M. Experimental implementation of automatic “cycle to cycle” control of a chiral simulated moving bed separation. J Chromatogr A. 2007;1165(1–2):100–8.

Andrade Neto AS, Secchi AR, Souza MB, Barreto AG. Nonlinear model predictive control applied to the separation of praziquantel in simulated moving bed chromatography. J Chromatogr A. Elsevier B.V.; 2016;1470:42–9.

Aniceto JPS, Cardoso SP, Silva CM. General optimization strategy of simulated moving bed units through design of experiments and response surface methodologies. Comput Chem Eng. Elsevier Ltd; 2016;90:161–70.

Aniceto JPS, Silva CM. Simulated Moving Bed Strategies and Designs: From Established Systems to the Latest Developments. Sep Purif Rev. 2015;44(1):41–73.

Azevedo DCS, Rodrigues AE. Design of a simulated moving bed in the presence of mass-transfer resistances. AIChE J. 1999;45(5):956–66.

Azevedo DCS, Rodrigues AE. Fructose-glucose separation in a SMB pilot unit: Modeling, simulation, design, and operation. AIChE J. 2001;47(9):2042–51.

Badgwell TA. Robust model predictive control of stable linear systems. Int J Control. 1997;68(4):797–818.

Bard Y. Nonlinear parameter estimation. New York: Academic Press; 1974.

Behbahani RM, Jazayeri-Rad H, Hajmirzaee S. Fault Detection and Diagnosis in a Sour Gas Absorption Column Using Neural Networks. Chem Eng Technol. 2009;32(5):840–5.

Bentley J, Sloan C, Kawajiri Y. Simultaneous modeling and optimization of nonlinear simulated moving bed chromatography by the prediction-correction method. J Chromatogr A. Elsevier B.V.; 2013;1280:51–63.

Benyahia B, Latifi MA, Fonteix C, Pla F. Emulsion copolymerization of styrene and butyl acrylate in the presence of a chain transfer agent. Part 2: Parameters estimability and confidence regions. Chem Eng Sci. Elsevier; 2013;90:110–8.

Bowden GJ, Maier HR, Dandy GC. Optimal division of data for neural network models in water resources applications. Water Resour Res. 2002;38(2):2-1-2–11.

Capriglione D, Carratù M, Liguori C, Paciello V, Sommella P. A soft stroke sensor for motorcycle rear suspension. Meas J Int Meas Confed. Elsevier Ltd; 2017;106:46–52.

Choi JH, Nam HG, Mun S. Enhancement of yield and productivity in the 3-zone nonlinear SMB for succinic-acid separation under overloaded conditions. J Ind Eng Chem. The Korean Society of Industrial and Engineering Chemistry; 2017;58:222–8.

Chu KH, Hashim M a. Simulated countercurrent adsorption processes: a comparison of modelling strategies. Chem Eng J Biochem Eng J. 1995;56(2):59–65.

Constantino DSM, Pereira CSM, Faria RP V., Ferreira AFP, Loureiro JM, Rodrigues AE. Synthesis of butyl acrylate in a fixed-bed adsorptive reactor over Amberlyst 15. AIChE J. 2015a;61(4):1263–74.

Constantino DSM, Pereira CSM, Faria RPV, Loureiro JM, Rodrigues AE. Simulated moving bed reactor for butyl acrylate synthesis: From pilot to industrial scale. Chem Eng Process Process Intensif. Elsevier B.V.; 2015b;97:153–68.

Costa MCB, Jardini AL, Maciel MRW, Embiruçu M, Maciel Filho R. Empirical models for end-use properties prediction of LDPE: application in the flexible plastic packaging industry. Mater Res. 2008;11(1):23–30.

Cruz-Díaz M, Buchaly C, Kreis P, Pérez-Cisneros ES, Lobo-Oehmichen R, Górak A. Synthesis of n-propyl propionate in a pilot-plant reactive distillation column: Experimental study and

simulation. Comput Chem Eng. 2012;39:118–28.

Delnavaz M, Ayati B, Ganjidoust H. Prediction of moving bed biofilm reactor (MBBR) performance for the treatment of aniline using artificial neural networks (ANN). J Hazard Mater. Elsevier B.V.; 2010;179(1–3):769–75.

Diehl M, Amrit R, Rawlings JB. A Lyapunov function for economic optimizing model predictive control. IEEE Trans Automat Contr. 2011;56(3):703–7.

Duarte CFM. Production of TAME and n-Propyl Propionate by Reactive Distillation. University of Porto; 2006.

Engelbrecht A. Particle swarm optimization: Velocity initialization. 2012 IEEE Congr Evol Comput CEC 2012. 2012;(2):10–5.

Erdem G, Abel S, Morari M, Mazzotti M, Morbidelli M. Automatic Control of Simulated Moving Beds II: Nonlinear Isotherm. Ind Eng Chem Res. 2004;43(14):3895–907.

Faria RP V, Pereira CSM, Silva VMTM, Loureiro JM, Rodrigues AE. Sorption enhanced reactive process for the synthesis of glycerol ethyl acetal. Chem Eng J. Elsevier B.V.; 2014;258:229–39.

Fontes RM, Kalid RA, Martins MAF. Application of an optimal MPC tuning strategy in control of a nonlinaear reactor system. XX Congr Bras Eng Química. 2014.

Frank PM, Kiippen-seliger B, Kppen-seliger B. Fuzzy Logic and Neural Network Applications to Fault Diagnosis. (96):67–88.

Ghosh S, Maka S. Genetic algorithm based {NARX} model identification for evaluation of insulin

sensitivity. Appl Soft Comput. 2011;11(1):221–6.

Glueckauf E, Coates JI. Theory of Chromatography. Part IV. J Chem Soc. 1947;1315–21.

Gonzaga JCB, Meleiro L a. ., Kiang C, Maciel Filho R. ANN-based soft-sensor for real-time process monitoring and control of an industrial polymerization process. Comput Chem Eng. 2009;33(1):43–9.

Graça NS, Pais LS, Silva VMTM, Rodrigues AE. Thermal effects on the synthesis of acetals in a simulated moving bed adsorptive reactor. Chem Eng J. 2012;207–208:504–13.

Grossmann C, Amanullah M, Erdem G, Mazzotti M, Morbidelli M, Morari M. “Cycle to cycle” optimizing control of simulated moving beds. AIChE J. 2008;54(1):194–208.

Grossmann C, Langel C, Mazzotti M, Morari M, Morbidelli M. Experimental implementation of automatic “cycle to cycle” control to a nonlinear chiral simulated moving bed separation. J Chromatogr A. Elsevier B.V.; 2010;1217(13):2013–21.

Hoque S, Farouk B, Haas CN. Development of metamodels for predicting aerosol dispersion in ventilated spaces. Atmos Environ. Elsevier Ltd; 2011;45(10):1876–87.

Hu X, Eberhart R. Multiobjective optimization using dynamic neighborhood particle swarm optimization. Proc 2002 Congr Evol Comput CEC’02 (Cat No02TH8600). 2002;2:1677–81.

Huang M, Ma Y, Wan J, Chen X. A sensor-software based on a genetic algorithm-based neural fuzzy system for modeling and simulating a wastewater treatment process. Appl Soft Comput J. Elsevier B.V.; 2015;27:1–10.

Huang R, Harinath E, Biegler LT. Lyapunov stability of economically oriented NMPC for cyclic

processes. J Process Control. Elsevier Ltd; 2011;21(4):501–9.

Hunt KJ, Sbarbaro D, Żbikowski R, Gawthrop PJ. Neural networks for control systems—A survey. Automatica. 1992;28(6):1083–112.

International Organisation for Standardisation. Guide to the Expression of Uncertainty in Measurement (GUM). Geneva: International Organisation for Standardisation; 2008.

Jalee EA, Aparna K. Neuro-fuzzy Soft Sensor Estimator for Benzene Toluene Distillation Column. Procedia Technol. The Author(s); 2016;25(25):92–9.

Jiang Y, Hu T, Huang C, Wu X. An improved particle swarm optimization algorithm. Appl Math Comput. 2007;193(1):231–9.

Kaspereit M, Seidel-Morgenstern A, Kienle A. Design of simulated moving bed processes under reduced purity requirements. J Chromatogr A. 2007;1162(1):2–13.

Kawase M, Inoue Y, Araki T, Hashimoto K. The simulated moving-bed reactor for production of bisphenol A. Catal Today. 1999;48(1–4):199–209.

Keller T, Muendges J, Jantharasuk a., Gónzalez-Rugerio C a., Moritz H, Kreis P, et al. Experimental model validation for n-propyl propionate synthesis in a reactive distillation column coupled with a liquid–liquid phase separator. Chem Eng Sci. 2011;66(20):4889–900.

Kennedy J, Eberhart R. Particle swarm optimization. Proc ICNN'95 - Int Conf Neural Networks. IEEE; 1995. p. 1942–8.

Klatt KU, Hanisch F, Dünnebier G. Model-based control of a simulated moving bed

chromatographic process for the separation of fructose and glucose. J Process Control. 2002;12(2):203–19.

Klöker M, Kenig EY, Schmitt M, Althaus K, Schoenmakers H, Markusse AP, et al. Influence of Operating Conditions and Column Configuration on the Performance of Reactive Distillation Columns with Liquid - Liquid Separators. Can J Chem Eng. 2003;81(3–4):725–32.

Kloppenburg E, Gilles ED. Automatic control of the simulated moving bed process for C8 aromatics separation using asymptotically exact input/output-linearization. J. Process Control. 1999. p. 41–50.

Koduru P, Welch SM, Das S. A Particle Swarm Optimization Approach for Estimating Parameter Confidence Regions. Proc 9th Annu Conf Genet Evol Comput. 2007;70–7.

Koivisto H. A practical approach to model based neural network control. 1995;

Konieczka P, Namieśnik J. Estimating uncertainty in analytical procedures based on chromatographic techniques. J Chromatogr A. 2010a;1217(6):882–91.

Konieczka P, Namieśnik J. Estimating uncertainty in analytical procedures based on chromatographic techniques. J Chromatogr A. 2010b;1217(6):882–91.

Kravaris C, Hahn J, Chu Y. Advances and selected recent developments in state and parameter estimation. Comput Chem Eng. Elsevier Ltd; 2013;51:111–23.

Langel C, Grossmann C, Morbidelli M, Morari M, Mazzotti M. Implementation of an automated on-line high-performance liquid chromatography monitoring system for “cycle to cycle” control of simulated moving beds. J Chromatogr A. 2009;1216(50):8806–15.

Leão CP, Rodrigues AE. Transient and steady-state models for simulated moving bed processes: Numerical solutions. Comput Chem Eng. 2004;28(9):1725–41.

Lee J, Natarajan S, Lee K. A model-based predictive control approach to repetitive control of continuous processes with periodic operations. J Process Control. 2001;11:195–207.

Lee JH. Model Predictive Control. Biomol Eng. 2007;403.

Lehoucq S, Verheve D, Cavoy E. SMB Enantioseparation : Process Development , Modeling , and Operating Conditions. 2000;46(2):247–56.

Li S, Feng L, Benner P, Seidel-Morgenstern A. Using surrogate models for efficient optimization of simulated moving bed chromatography. Comput Chem Eng. Elsevier Ltd; 2014;67:121–32.

Li W, Wei S, Jiao W, Qi G, Liu Y. Modelling of adsorption in rotating packed bed using artificial neural networks (ANN). Chem Eng Res Des. Institution of Chemical Engineers; 2016;114:89–95.

Lima NMN, Manenti F, Maciel Filho R, Embiruçu M, Wolf Maciel MR. Fuzzy model-based predictive hybrid control of polymerization processes. Ind Eng Chem Res. 2009;48(18):8542–50.

Lin W, Biegler LT, Jacobson AM. Modeling and optimization of a seeded suspension polymerization process. Chem Eng Sci. Elsevier; 2010;65(15):4350–62.

Liu G, Zhou D, Xu H, Mei C. Model optimization of SVM for a fermentation soft sensor. Expert Syst Appl. Elsevier Ltd; 2010;37(4):2708–13.

Liu Z, Wang L, Zhang Y, Chen CLP. A SVM controller for the stable walking of biped robots based on small sample sizes. Appl Soft Comput. Elsevier B.V.; 2016;38:738–53.

Lode F, Mazzotti M, Morbidelli M. A New Reaction-Separation Unit: The Simulated Moving Bed Reactor. 2001;55(10):883–6.

Löfberg J. Linear model predictive control: Stability and robustness. Linkopings universitet, editor. Linkoping; 2001.

Lund BF, Foss B a. Parameter ranking by orthogonalization—Applied to nonlinear mechanistic models. Automatica. 2008;44(1):278–81.

Lundquist E. Catalyzed Esterification Process. 1995. p. 3–10.

Martins M a. F, Zanin AC, Odloak D. Robust model predictive control of an industrial partial combustion fluidized-bed catalytic cracking converter. Chem Eng Res Des. Institution of Chemical Engineers; 2014;92(5):917–30.

Martins VFD, Ribeiro AM, Plaza MG, Santos JC, Loureiro JM, Ferreira AFP, et al. Gas-phase simulated moving bed: Propane/propylene separation on 13X zeolite. J Chromatogr A. Elsevier B.V.; 2015;1423:136–48.

Mayne DQ, Rawlings JB, Rao C V, Scokaert POM. Constrained model predictive control: Stability and optimality. Automatica. 2000;36:789–814.

Menezes JMP, Barreto GA. Long-term time series prediction with the NARX network: An empirical evaluation. Neurocomputing. 2008;71(16–18):3335–43.

Minceva M, Gomes PS, Meshko V, Rodrigues AE. Simulated moving bed reactor for

isomerization and separation of p-xylene. Chem Eng J. 2008;140(1–3):305–23.

Minceva M, Pais LS, Rodrigues AE. Cyclic steady state of simulated moving bed processes for enantiomers separation. Chem Eng Process. 2003;42(2):93–104.

Minceva M, Rodrigues AE. Simulated moving-bed reactor: Reactive-separation regions. AIChE J. 2005;51(10):2737–51.

Mirsoleimani-azizi SM, Amooey AA, Ghasemi S, Salkhordeh-panbechouleh S. Modeling the Removal of Endosulfan from Aqueous Solution by Electrocoagulation Process Using Artificial Neural Network (ANN). Ind Eng Chem Res. 2015;54(40):9844–9.

Narendra KS, Parthasarathy K. Identification and Control of Dynamical Systems Using Neural Networks. Trans Neur Netw. Piscataway, NJ, USA: IEEE Press; 1990;1(1):4–27.

Nelles O. Nonlinear System Identification [Internet]. Berlin, Heidelberg: Springer Berlin Heidelberg; 2001.

Nery GA, Martins MAF, Kalid R. A PSO-based optimal tuning strategy for constrained multivariable predictive controllers with model uncertainty. ISA Trans. 2014;53(2):560–7.

Nogueira I, Fontes C, Sartori I, Pontes K, Embiruçu M. A model-based approach to quality monitoring of a polymerization process without online measurement of product specifications. Comput Ind Eng. 2017;106:123–36.

Noor R a. M, Ahmad Z, Don MM, Uzir MH. Modelling and control of different types of polymerization processes using neural networks technique: A review. Can J Chem Eng. 2010;88(6):1065–84.

Odloak D. Extended robust model predictive control. AIChE J. 2004;50(8):1824–36.

P. Menezes Jr. J, Barreto G. A New Look at Nonlinear Time Series Prediction with NARX Recurrent Neural Network. 2006 Ninth Brazilian Symp Neural Networks. 2006;28–28.

Pais LS, Loureiro J, Rodrigues AE. Separation of 1,1'-bi-2-naphthol enantiomers by continuous chromatography in simulated moving bed. Chem Eng Sci. 1997;52(2):245–57.

Pais LS, Loureiro JM, Rodrigues a E. Modeling strategies for enantiomers separation by SMB chromatography. AIChE J. 1998;44(3):561–9.

Pais LS, Loureiro JM, Rodrigues AE. Chiral separation by SMB chromatography. Sep Purif Technol. 2000;20(1):67–77.

Pannocchia G, Wright SJ, Rawlings JB. Existence and computation of infinite horizon model predictive control with active steady-state input constraints. IEEE Trans Automat Contr. 2003;48(6):1002–6.

Paredes G, Mazzotti M. Optimization of simulated moving bed and column chromatography for a plasmid DNA purification step and for a chiral separation. J Chromatogr A. 2007;1142(1):56–68.

Park C. Determination of the joint confidence region of the optimal operating conditions in robust design by the bootstrap technique. Int J Prod Res. 2013;51(15):4695–703.

Parsopoulos KE, Vrahatis MN. Particle swarm optimization method in multiobjective problems. SAC '02 Proc 2002 ACM Symp Appl Comput. 2002;3:603–7.

Pereira CSM, Gomes PS, Gandi GK, Silva VMTM, Rodrigues AE. Multifunctional Reactor for the

Synthesis of Dimethylacetal. Ind Eng Chem Res. 2008;47(10):3515–24.

Pereira CSM, Rodrigues AE. Process intensification: New technologies (SMBR and PermSMBR) for the synthesis of acetals. Catal Today. Elsevier B.V.; 2013;218–219:148–52.

Pereira CSM, Silva VMTM, Rodrigues AE. Fixed Bed Adsorptive Reactor for Ethyl Lactate Synthesis: Experiments, Modelling, and Simulation. Sep Sci Technol. 2009a;44(12):2721–49.

Pereira CSM, Zabka M, Silva VMTM, Rodrigues AE. A novel process for the ethyl lactate synthesis in a simulated moving bed reactor (SMBR). Chem Eng Sci. 2009b;64(14):3301–10.

Poli R, Kennedy J, Blackwell T. Particle Swarm Optimization : An Overview. Swarm Intell. 2007;1(October 2007):33–57.

Process Systems Enterprise. www.psenterprise.com/gproms. 2015.

Quaiser T, Mönnigmann M. Systematic identifiability testing for unambiguous mechanistic modeling--application to JAK-STAT, MAP kinase, and NF-kappaB signaling pathway models. BMC Syst Biol. 2009;3:50.

Rajendran A, Paredes G, Mazzotti M. Simulated moving bed chromatography for the separation of enantiomers. J Chromatogr A. 2009;1216(4):709–38.

Ramaiah GB, Chennaiah RY, Satyanarayanarao GK. Investigation and modeling on protective textiles using artificial neural networks for defense applications. Mater Sci Eng B. Elsevier B.V.; 2010;168(1–3):100–5.

Ratnaweera A, Halgamuge SK, Watson HC. Self-organizing hierarchical particle swarm optimizer

with time-varying acceleration coefficients. IEEE Trans Evol Comput. 2004;8(3):240–55.

Rawlings JB, Muske KR. The stability of constrained receding horizon control. IEEE Trans Automat Contr. 1993a;38(10):1512–6.

Rawlings JB, Muske KR. The stability of constrained receding horizon control. … Control IEEE Trans. 1993b;38(10):1512–6.

Regufe MJ, Faria RP V., Ribeiro AM, Loureiro JM, Rodrigues AE. Synthesis of the biofuel additive 1,1-Diethoxybutane in a fixed bed column with Amberlyst-15 wet. Chem Eng Technol. 2016;(0):1–11.

Ribeiro AE, Gomes PS, Pais LS, Rodrigues AE. Chiral separation of flurbiprofenflurbiprofen enantiomers by preparative and simulated moving bed chromatography. Chirality. 2011a;23(8):602–11.

Ribeiro AE, Gomes PS, Pais LS, Rodrigues AE. Chiral Separation of Ketoprofen Enantiomers by Preparative and Simulated Moving Bed Chromatography. Sep Sci Technol. 2011b;46(11):1726–39.

Rodrigues AE, Pereira C, Minceva M, Pais L, Ribeiro AM, Ribeiro A, et al. Simulated Moving Bed Technology. Principles, Design and Process Applications. 1st Editio. Oxford: Elsevier; 2015.

Rodrigues MA, Odloak D. An infinite horizon model predictive control for stable and integrating processes. Comput Chem Eng. 2003;27(8–9):1113–28.

Roy R, T F, P C. Advances in soft computing: engineering design and manufacturing. Springer. New York; 1999.

Ruthven DM. Principles of Adsorption and Adsorption Processes. New York: JohnWiley & Sons; 1984.

Sá Gomes P, Lamia N, Rodrigues AE. Design of a gas phase simulated moving bed for propane/propylene separation. Chem Eng Sci. 2009;64(6):1336–57.

Sá Gomes P, Rodrigues a. E. Simulated moving bed chromatography: From concept to proof-of-concept. Chem Eng Technol. 2012;35(1):17–34.

Samarov A, Toikka M, Trofimova M, Toikka A. Liquid-liquid equilibrium for the quaternary system propionic acid + n-propanol + n-propyl propionate + water at 293.15, 313.15 and 333.15 K. Fluid Phase Equilib. 2016;425:183–7.

Sánchez AS, Rodrigues DA, Fontes RM, Martins MF, Kalid R de A, Torres EA. Wave resource characterization through in-situ measurement followed by artificial neural networks' modeling. Renew Energy. 2018;115(September):1055–66.

Santos B a. V, Pereira CSM, Silva VMTM, Loureiro JM, Rodrigues a. E. Design of a true moving bed reactor for the direct synthesis of dimethyl carbonate. Chem Eng Sci. Elsevier; 2015;123:406–19.

Schaul T, Horgan D, Gregor K, Silver D. Universal Value Function Approximators. In: Bach F, Blei D, editors. Proc 32nd Int Conf Mach Learn. Lille, France: PMLR; 2015. p. 1312–20.

Scheibel EG. Correspondence. Liquid Diffusivities. Viscosity of Gases. Ind Eng Chem. American Chemical Society; 1954;46(9):2007–8.

Schenker B, Agarwal M. Cross-validated structure selection for neural networks. Comput Chem

Eng. 1996;20(2):175–86.

Schwaab M, Biscaia, EC, Monteiro JL, Pinto JC. Nonlinear parameter estimation through particle swarm optimization. Chem Eng Sci. 2008;63(6):1542–52.

Seborg DE, Mellichamp DA, Edgar TF, Doyle III FJ. Process Dynamics and Control. New York: Wiley; 2003.

Sharmin R, Sundararaj U, Shah S, Vande Griend L, Sun Y-J. Inferential sensors for estimation of polymer quality parameters: Industrial application of a PLS-based soft sensor for a LDPE plant. Chem Eng Sci. 2006;61(19):6372–84.

Son SM, Kimura H, Kusakabe K. Esterification of oleic acid in a three-phase, fixed-bed reactor packed with a cation exchange resin catalyst. Bioresour Technol. Elsevier Ltd; 2011;102(2):2130–2.

Song IH, Lee SB, Rhee HK, Mazzotti M. Identification and predictive control of a simulated moving bed process: Purity control. Chem Eng Sci. 2006;61(6):1973–86.

Sorrosal G, Irigoyen E, Borges CE, Martin C, Macarulla AM, Alonso-Vicario A. Artificial neural network modelling of the bioethanol-to-olefins process on a HZSM-5 catalyst treated with alkali. Appl Soft Comput J. Elsevier B.V.; 2017;58:648–56.

Soufi Y, Bechouat M, Kahla S. Fuzzy-PSO controller design for maximum power point tracking in photovoltaic system. Int J Hydrogen Energy. 2017;42(13):8680–8.

Storti G, Baciocchi R, Mazzotti M, Morbidelli M. Design of Optimal Operating Conditions of Simulated Moving Bed Adsorptive Separation Units. Ind Eng Chem Res. American Chemical

Society; 1995;34(1):288–301.

Storti G, Mazzotti M, Morbidelli M, Carrà S. Robust design of binary countercurrent adsorption separation processes. AIChE J. 1993;39(3):471–92.

Su H-T, McAvoy T j. Neural Model Predictive Control of Nonlinear Chemical Processes. Int Symp Intell Control. 1993.

Suvarov P, Kienle A, Nobre C, De Weireld G, Vande Wouwer A. Cycle to cycle adaptive control of simulated moving bed chromatographic separation processes. J Process Control. Elsevier Ltd; 2014a;24(2):357–67.

Suvarov P, Kienle A, Nobre C, De Weireld G, Vande Wouwer A. Cycle to cycle adaptive control of simulated moving bed chromatographic separation processes. J Process Control. Elsevier Ltd; 2014b;24(2):357–67.

Suvarov P, Wouwer A Vande, Kienle A. A simple robust obust control for simulated moving bed chromatographic hromatographic separation. 8th IFAC Symp Adv Control Chem Process. The International Federation of Automatic Control; 2012. p. 137–42.

The Dow Chemical Company. UCAR n-Propyl Propionate. 2002.

The Dow Chemical Company. Amberlyst 46 ®. 2014;(177):3028.

Tian X, Wang P, Huang D, Chen S. Offset-free multistep nonlinear model predictive control under plant-model mismatch. Int J Adapt Control Signal Process. 2014;28(3–5):444–63.

Torrecilla JS, Cancilla JC, Aroca-Santos R, Pariente ES. Neural networks to Estimate Physicochemical Properties of Choline Carboxylate Ionic Liquids. ACS Sustain Chem Eng.

American Chemical Society; 2016;4(2):536–40.

Toumi A, Engell S. Optimization-based control of a reactive simulated moving bed process for glucose isomerization. Chem Eng Sci. 2004;59(18):3777–92.

Toumi A, Engell S, Diehl M, Bock HG, Schlöder J. Efficient optimization of simulated moving bed processes. Chem Eng Process Process Intensif. 2007;46(11):1067–84.

Vanatta LE, Coleman DE. Calibration, uncertainty, and recovery in the chromatographic sciences. J Chromatogr A. 2007;1158(1–2):47–60.

Ventouras EM, Asvestas P, Karanasiou I, Matsopoulos GK. Classification of Error-Related Negativity (ERN) and Positivity (Pe) potentials using kNN and Support Vector Machines. Comput Biol Med. Elsevier; 2011;41(2):98–109.

Vignesh S V., Hariprasad K, Athawale P, Siram V, Bhartiya S. Optimal strategies for transitions in simulated moving bed chromatography. Comput Chem Eng. Elsevier Ltd; 2016;84:83–95.

Wang C, Klatt K, D G, Engell S, Hanisch F. Neural network-based identification of SMB chromatographic processes. Control Eng Pract. 2003;11:949–59.

Wang X-J, Zhao X-Y, Li Q-G, Chan TW, Wu S-Z. Artificial Neural Network Modeling and Mechanism Study for Relaxation of Deformed Rubber. Ind Eng Chem Res. 2016;55(14):4059–70.

Welch G, Bishop G. An Introduction to the Kalman Filter. In Pract. 2006;7(1):1–16.

Wu H, Cao L, Wang J. Gray-box modeling and control of polymer molecular weight distribution using orthogonal polynomial neural networks. J Process Control. Elsevier Ltd;

2012;22(9):1624–36.

Xu H, Ye Q, Zhang H, Qin J, Li N. Design and control of reactive distillation–recovery distillation flowsheet with a decanter for synthesis of N-propyl propionate. Chem Eng Process Process Intensif. Elsevier B.V.; 2014;85:38–47.

Yao KZ, Shaw BM, Kou B, McAuley KB, Bacon DW. Modeling Ethylene/Butene Copolymerization with Multi-site Catalysts: Parameter Estimability and Experimental Design. Polym React Eng. 2003;11(3):563–88.

Yap WK, Karri V. Comparative analysis of artificial neural networks and dynamic models as virtual sensors. Appl Soft Comput. Elsevier B.V.; 2013;13(1):181–8.

Yu H, Fu J, Dang L, Cheong Y, Tan H, Wei H. Prediction of the Particle Size Distribution Parameters in a High Shear Granulation Process Using a Key Parameter Definition Combined Artificial Neural Network Model. Ind Eng Chem Res. 2015;acs.iecr.5b02679.

Zenoni G, Pedeferri M, Mazzotti M, Morbidelli M. On-line monitoring of enantiomer concentration in chiral simulated moving bed chromatography. J Chromatogr A. 2000;888(1–2):73–83.

Zhang Y, Hidajat K, Ray AK. Modified reactive SMB for production of high concentrated fructose syrup by isomerization of glucose to fructose. Biochem Eng J. 2007;35(3):341–51.

Zhao Y, Stadtherr MA. Rigorous Global Optimization for Dynamic Systems Subject to Inequality Path Constraints. Ind Eng Chem Res. 2011;50(574):12678–93.

Zhao ZZZ, Ning YNY, Gao YGY. Polymer properties on-line estimation for an industrial

polyethylene process based on suboptimal strong tracking filter. 2009 7th Asian Control Conf. 2009;841–6.

Ziyang Z, Hidajat K, Ray AK. Determination of Adsorption and Kinetic Parameters for Methyl tert-Butyl Ether Synthesis from tert-Butyl Alcohol and Methanol. J Catal. 2001;200(2):209–21.